CHEMICAL ENGINEERING SCIENCE
GENIE CHIMIQUE

VOL. 7 1957 Nos. 1/2

VOL.
7
1957/58

An approximate method of predicting composition response of a fractionating column

W. L. WILKINSON and W. D. ARMSTRONG

(*Received* 30 *April* 1957)

Abstract—The response of a plate type distillation column to changes in the feed composition is considered and an approximate mathematical solution of the simplified equations is given. This solution gives a satisfactory prediction of the early part of the response, which is of importance in the application of automatic control. The theoretical curves are compared with those obtained experimentally on a laboratory scale column using a two component system.

Résumé—Les auteurs considèrent la réponse d'une colonne à distillation à plateaux quand la composition de l'alimentation varie. Ils donnent une solution mathématique approchée des équations simplifiées. Cette solution donne une précision satisfaisante de la première partie de la réponse, ce qui est important dans l'application du contrôle automatique. Les courbes théoriques sont comparées aux courbes expérimentales obtenues avec une colonne de laboratoire, pour des mélanges binaires.

Zusammenfassung—Es wird das Verhalten einer Boden-Destillationskolonne bei Änderung der Zulaufzusammensetzung betrachtet und eine angenäherte mathematische Lösung der vereinfachten Gleichungen gegeben. Diese Lösung erlaubt eine ausreichende Vorausberechnung des Verhaltens unmittelbar nach der Änderung, das für die Anwendung bei automatischer Regelung wichtig ist. Die theoretischen Kurven sind mit solchen verglichen, die experimentell an einer Laboratoriumskolonne unter Verwendung eines Zweistoffsystems erhalten wurden.

1. INTRODUCTION

IN DESIGNING control equipment for chemical processes it is essential that the dynamic characteristics of the plant should be known. At present these characteristics are largely based on experimental analyses of existing plants under operating conditions, the response of the plant being obtained by studying the result of the injection of a known disturbance on some operating variable. This type of experimental technique provides a considerable amount of useful information but it is increasingly evident that it is necessary to be able to derive from first principles the dynamic response equations which govern any particular unit of the process.

The present investigation is concerned with the unit process of distillation in a plate tower. In a previous paper [1] a simple unit operating at total reflux was analysed and the transient response corresponding to a step change in the composition of the vapour entering the column from the reboiler was obtained both theoretically and experimentally. A similar investigation has also been reported by VOETTER [2].

It is the more realistic problem of a fractionating column having both enriching and stripping sections and a continuous feed near the middle of the column which is considered here. A number of authors, notably ACRIVOS and AMUNDSON [3], ROSE and WILLIAMS [4], WILLIAMS, HARNETT, and ROSE [5] and VOETTER [2], have obtained various types of solutions of the problem. In some

cases the computational work involved is considerable and the solution is obtained using an analogue computer [4, 5].

The transient response discussed in this paper is that corresponding to a step change in the composition of the feed to the column, all flow rates being maintained constant. An attempt is made to obtain a reasonably simple analytical solution which will enable the transients to be calculated quickly.

2. Theoretical Analysis

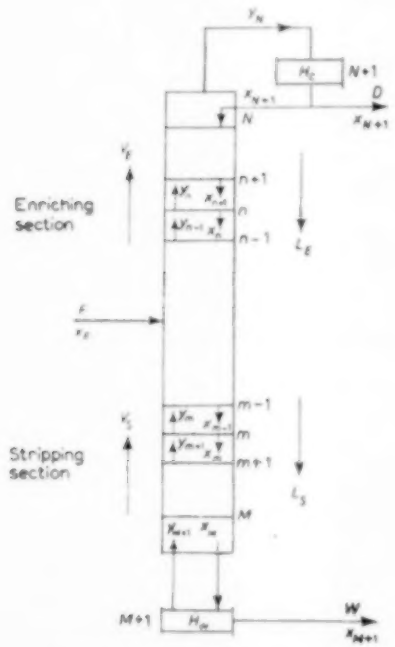

Fig. 1. Fractionating column.

2·1 *Assumed operating conditions.* A fractionating column working with a binary mixture is shown diagrammatically in Fig. 1. For the problem considered the following operating conditions have been assumed.

(i) The liquid hold-up on each tray, H moles, is assumed to be constant and perfectly mixed.

(ii) Vapour hold-up is neglected.

(iii) Plate efficiency is independent of composition.

(iv) The column operates adiabatically.

(v) The time to attain fluid dynamic equilibrium is small compared with that for mass transfer. This is justified for the case under consideration, i.e. changes of composition at constant flow. It would not apply if the flow changed appreciably, e.g. by changing reflux return rate or the throughput.

The mixture being distilled is assumed to have

(a) constant molal latent heat
(b) constant molal volume
(c) a vapour-liquid equilibrium relationship which can be approximated by two straight lines of slopes α_E and α_S as in Fig. 2.

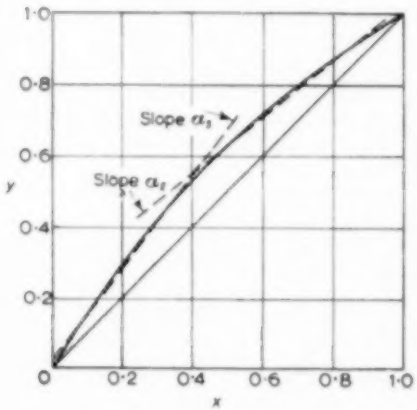

Fig. 2. Linearized approximation for equilibrium curve.

2·2 *Derivation of the basic equation.* A material balance around a typical plate n in the enriching section of Fig. 1 leads to the equation,

$$\frac{H}{L_E}\cdot\frac{dx_n}{dt} = x_{n+1} - x_n(1+\mu) + \mu x_{n-1} \qquad (1)$$

where $\mu = V_E\,\alpha_E/L_E = (1+R)\,\alpha_E/R$

and similarly for the condenser,

$$H_c\frac{dx_{N+1}}{dt} = V_E(y_N - x_{N+1}) \qquad (2)$$

where H_c is the condenser hold-up.

For the stripping section and the reboiler the analogous equations are, from Fig. 1, with $\lambda = \frac{V_S \alpha_S}{L_S}$,

$$\frac{H}{\alpha_S V_S} \cdot \frac{dx_m}{dt} = x_{m+1} - x_m \left(1 + \frac{1}{\lambda}\right) + \frac{1}{\lambda} x_{m-1} \quad (3)$$

together with the reboiler end condition,

$$H_W \frac{dx_{M+1}}{dt} = L_S x_M - V_S y_{M+1} - (L_S - V_S) x_{M+1} \quad (4)$$

where H_W is the reboiler hold-up.

The above equations express the dynamics of the mass transfer process. In cases where the fluid dynamic effects cannot be neglected, e.g. when the reflux ratio is changed, then the relations between V_n and V_{n-1} and also between L_n and L_{n+1} would be involved.

VOL. 7 1957/58

2·3 *Reduction to partial differential equations.* For N and M large, equations (1—4) may be reduced to equivalent partial differential equations.

For the enriching section let Z_{N+1} correspond to $N+1$, the total number of plates plus condenser and z_n correspond to n so that

$$\frac{n}{N+1} = \frac{z_n}{Z_{N+1}} \text{ then } \delta z_n = \frac{Z_{N+1}}{N+1} \text{ for } n \text{ changing by unity.}$$

Similarly we can take $\frac{Z_{M+1}}{M+1} = 1$ as the unit of length for the stripping section.

By Taylor's theorem

$$f(x \pm h) = f(x) \pm hf'(x) + \frac{h^2}{2!} f''(x) \pm \ldots$$

$$\text{i.e. } x_{n\pm1} = x_n \pm \frac{\partial x_n}{\partial z_n} \delta z_n + \frac{\partial^2 x_n}{\partial z_n^2} \cdot \frac{\delta z_n^2}{2!} \pm \quad (5)$$

Putting $\delta z_n = \frac{Z_{N+1}}{N+1} = 1$ and substituting in (1) we get

$$\frac{H}{L_E} \frac{\partial x_n}{\partial t} = (1-\mu) \frac{\partial x_n}{\partial z_n} + \frac{(1+\mu)}{2!} \frac{\partial^2 x_n}{\partial z_n^2} + \frac{(1-\mu)}{3!} \frac{\partial^3 x_n}{\partial z_n^3} + \ldots \quad (6)$$

In the steady state x_n may be expressed in the form $x_n = l\mu^n + m$ where l and m are constants, then successive derivatives of x_n with respect to z_n are in the ratio $\log \mu$ and when $\mu \approx 1$, third, and higher order terms may be neglected.

Since for small changes we may write δx_n in place of x_n equation (6) becomes,

$$\frac{2H}{L_E(1+\mu)} \frac{\partial(\delta x_n)}{dt} = \frac{\partial^2(\delta x_n)}{\partial z_n^2} + 2\left(\frac{1-\mu}{1+\mu}\right) \frac{\partial(\delta x_n)}{\partial z_n}. \quad (7)$$

The condenser boundary condition may be similarly reduced to give

$$\frac{H_c}{V_E} \frac{\partial}{\partial t}(\delta x_{N+1}) = (\alpha_E - 1)\,\delta x_{N+1} - \alpha_E \frac{\partial}{\partial z_n}(\delta x_{N+1}) \quad (8)$$

and further if $H_c \approx 0$

$$\alpha_E \frac{\partial}{\partial z_n}(\delta x_{N+1}) = (\alpha_E - 1)\,\delta x_{N+1};\ z_n = Z_{N+1} \quad (9)$$

2·4 *Solution of the governing equations.* A solution of (7) may be effected by considering a small cyclic oscillation in x_n about the mean, due to a sinusoidal signal imposed at $z = 0$.

i.e. put $\delta x_n = \delta x_{z_n} = X_{z_n} e^{i\omega t}$ where X_{z_n} is complex.

Substitution in (7) and (9) gives

$$\frac{d^2X}{dz^2} + A\frac{dX}{dz} - BX = 0 \quad (10)$$

together with $X = X_0$ at $z_n = 0$ i.e. feed section (11)

and $\frac{dX}{dz} - CX = 0$ at $z_n = Z_{N+1}$ i.e. top of column (12)

where
$$\left.\begin{aligned} A &= 2(1-\mu)/(1+\mu) \\ B &= 2H\, i\omega / L_E(1+\mu) \\ C &= (\alpha_E - 1)/\alpha_E : H_c = 0. \end{aligned}\right\} \quad (13)$$

Similarly for the stripping section the equations are

$$\frac{d^2X}{dz^2} + A'\frac{dX}{dz} - B'X = 0 \quad (14)$$

$X = X_0$ at $z_m = 0$ i.e. feed section

and $\frac{dX}{dz} - C'X = 0$ at $z_m = Z_{M+1}$ i.e. bottom of column (15)

where
$$\left.\begin{aligned} A' &= 2(\lambda-1)/(\lambda+1) \\ B' &= 2H\lambda i\omega/\alpha_S V_S(\lambda-1) \\ C' &= (1-\alpha_S)\,V_S/L_S - i\omega H_W/L_S \end{aligned}\right\} \quad (16)$$

The complex frequency dependent transfer functions which are the solutions of these equations may be written in the form

$$\frac{X_z}{X_0} = \exp(a_2 z)\,\frac{1-\{(a_2-C)/(a_1-C)\}\exp\{(a_2-a_1)(Z-z)\}}{1-\{(a_2-C)/(a_1-C)\}\exp\{(a_2-a_1)Z\}} \quad (17)$$

where $a_{1,2} = -\frac{A}{2}\left[1 \pm \sqrt{(1+4B/A^2)}\right]$ (18)

The ratio $\frac{X_z}{X_0}$ will be written $F(i\omega) = \alpha e^{i\phi}$ (19)

A similar solution has been reported by Croockewit, Honig, and Kramers [6] for the case of a diffusion equation.

2·5 *Mathematical coupling of the enriching and stripping sections.* With reference to Fig. 3, for the enriching section alone define

$$F_E(i\omega) = \frac{\delta x_0}{\delta y_0}(i\omega)$$

i.e. $$F_E(i\omega) = \frac{L_E}{\alpha_E(F+L_E)}\left(\frac{X_1}{X_0}\right)_E \quad (20)$$

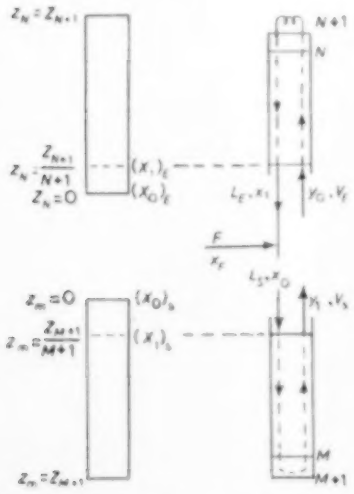

Fig. 3. Mathematical coupling of stripping and enriching sections.

since $\delta x_0 = \left(\frac{L_E}{F+L_E}\right)\delta x_1$,

$$\alpha_E \delta x_0 = \delta y_0 \text{ and } \left(\frac{X_1}{X_0}\right)_E = \frac{\delta x_1}{\delta x_0}(i\omega)$$

and similarly for the stripping section.

Assuming now that $N \gg 1$; $\frac{N}{N+1} \approx 1$ and $(1-\mu) \ll 1$. Also $\frac{2H(1+\mu)}{L_E(1-\mu)^2} \gg 1$ since $\frac{H}{L_E} = 0$ (1).

It may then be shown that

$$F_E(i\omega) = a_E e^{-k_1\sqrt{i\omega}} \quad (21)$$

and
$$F_S(i\omega) = a_S e^{-k_1\sqrt{i\omega}} \quad (22)$$

where
$$\left.\begin{aligned} a_E &= \frac{L_E}{\alpha_E(F+L_E)}\exp\left(\frac{\mu-1}{\mu+1}\right) \\ a_S &= \alpha_S \exp\left(\frac{1-\lambda}{1+\lambda}\right) \\ k_1 &= \frac{1-\lambda}{1+\lambda}\sqrt{2H\lambda(\lambda+1)/\alpha_S V_S(\lambda-1)^2} \\ k_2 &= \frac{\mu-1}{\mu+1}\sqrt{2H(1+\mu)/L_E(1-\mu)^2}. \end{aligned}\right\} \quad (23)$$

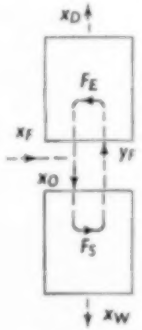

On coupling the two sections the response of y_F, the vapour leaving the feed plate, to a step change in x_0 to $x_0 + \Delta x_0$ is given as

$$\delta y_F(p) = \frac{\Delta x_0}{p}\,\frac{F_S(p)}{1-F_S(p)F_E(p)} \quad (24)$$

following Brown and Campbell [7] and using the Laplace transform notation.

Substituting for $F_S(p)$ and $F_E(p)$ into (24) from (21) and (22) gives

$$\delta y_F(p) = \frac{a_S\,\Delta x_0}{p}\,\frac{e^{-k_1\sqrt{p}}}{1-a_E a_S e^{-(k_1+k_2)\sqrt{p}}} \quad (25)$$

the inverse transform of which is

$$\frac{F+L_E}{F\Delta x_F}\,\delta y_F(t) = a_S \sum_{n=0}^{\infty}(a_E a_S)^n \operatorname{erfc}\frac{n(k_1+k_2)+k_1}{2\sqrt{t}} \quad (26)$$

since $(F+L_E)\,\Delta x_0 = F\,\Delta x_F$.

VOL. 7 1957/58

2·6 *Response of distillate composition.* If $\frac{\delta x_D}{\delta y_F}(i\omega) = \frac{1}{\alpha_E}\frac{X_{Z_{N+1}}}{X_0}$ is written $F_D(i\omega)$ then from (17) with $z_n = Z_{N+1}$ we have

$$F_D(i\omega) = \frac{1}{\alpha_E}\exp(a_2 Z_{N+1}) \frac{1-\{(a_2-C)/(a_1-C)\}}{1-\{(a_2-C)/(a_1-C)\}\exp(a_2-a_1)Z_{N+1}} \quad (27)$$

which may be written, putting $p = i\omega$

$$F_D(i\omega) = K\left(\frac{\sqrt{p}\exp\{-k\sqrt{p}\}}{a+\sqrt{p}}\right)\Big/ \left(1-\left\{\frac{a-\sqrt{p}}{a+\sqrt{p}}\right\}\exp\{-2k\sqrt{p}\}\right) \quad (28)$$

$$\left.\begin{aligned} \text{where } K &= \frac{2}{\alpha_E}\exp\left[Z_{N+1}\left(\frac{\mu-1}{\mu+1}\right)\right] \\ k &= Z_{N+1}\sqrt{2H/L_E(1+\mu)} \end{aligned}\right\} \quad (29)$$

$$\text{and } a = \left(\frac{\mu-1}{\mu+1} - \frac{\alpha_E - 1}{\alpha_E}\right)\Big/\sqrt{2H/L_E(1+\mu)}$$

where p is not small.

The indicial response of the distillate $\phi_D(t)$ i.e. the response of the distillate x_D to a unit step change in y_F is given by $\frac{F_D(p)}{p}$ which may then be expanded and transformed back into the time domain to give

$$\left.\begin{aligned} \phi_D(t) = {} & K\exp(ak+a^2t)\operatorname{erfc}\left(a\sqrt{t}+\frac{k}{2\sqrt{t}}\right) \\ & + 4aK\sqrt{\frac{t}{\pi}}\exp(-9k^2)/(4t) \\ & - K(1+6ak+4a^2t)\exp(3ak+a^2t) \\ & \operatorname{erfc}\left(a\sqrt{t}+\frac{3k}{2\sqrt{t}}\right)+\cdots \end{aligned}\right\} \quad (30)$$

Except for large values of t the second and third terms are negligible.

For the special case of $L = V$ and $\alpha = 1$ i.e. $a = 0$ the series reduces to

$$\phi_D(T) = 2\sum_{n=0}^{\infty}\frac{(-1)^n}{n!}\operatorname{erfc}\frac{(2n+1)(N+1)}{2\sqrt{T}}$$

where $T = \{(L_E t)/H\}$. This was checked against the accurate analysis given in [1] for $N = 5$ and the agreement was good (within 5 per cent. for $T = 60$). For $N > 5$ the agreement would be much better.

Finally the response of the product composition to a step change in feed composition is found using DUHAMEL's integral.

$$\delta x_D(t) = \frac{d}{dt}\int_0^t \phi_D(t-\xi)\,\delta y_F(\xi)\,d\xi \quad (31)$$

where $\delta x_D(t)$ is the response of x_D to a step change in x_F.

Substituting for δy_F from (26) and differentiating under the integral sign gives

$$\left.\begin{aligned} \frac{\delta x_D(t)}{\Delta x_F} = {} & \frac{Fa_S}{F+L_E}\cdot\frac{2}{\sqrt{\pi}}\int_0^t \phi_D(t-\xi)\times \\ & \times\sum_{n=0}^{\infty}\left[\frac{(a_E a_S)^n[n(k_1+k_2)+k_1]}{4\xi^{3/2}}\times\right. \\ & \left.\times\exp\left(\frac{-[n(k_1+k_2)+k_1]^2}{4\xi}\right)\right]d\xi \end{aligned}\right\} \quad (32)$$

where ϕ_D is given by the first term of (30).

2·7 *Extension to other cases.* The transfer function and hence the indicial response of any other plate in the column could be obtained by inserting the appropriate value of z in (17) and, using DUHAMEL's integral, the response to a step change in feed composition could be determined exactly as in the case of the top product.

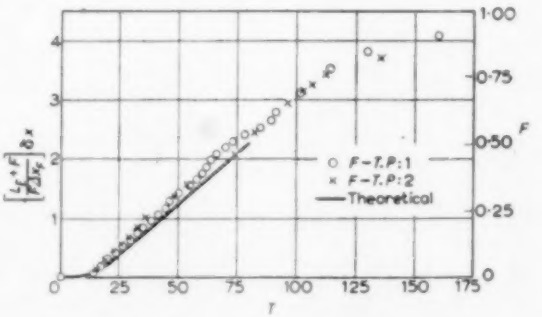

FIG. 4. Feed change.
O $F - T.\ P:1$
X $F - T.\ P:2$
— Theoretical

2·8 *Experimental correlation.* The transient composition response of a laboratory distillation column following a step disturbance in the feed composition, enthalpies and flows remaining constant, has been measured and the work is reported elsewhere [8]. The experimental distillate composition change is compared with that given by equation (32) in Fig. 4.

CONCLUSION

The approximate mathematical method presented in sections 2·3 to 2·6 gives a satisfactory prediction of the early part of the response of a distillation column to changes in the feed composition. It is primarily of use in demonstrating the form of the response and the effect of the column variables. Further elaboration or refinement of the method and approximations would be possible but these would probably involve the use of digital computers in deriving a solution.

Acknowledgements—The authors wish to thank Prof. T. R. C. Fox and Dr. J. F. DAVIDSON of the Cambridge University Department of Chemical Engineering for their encouragement and advice.

The first author is grateful to the Directors of the Salters' Institute of Industrial Chemistry for the award of a Scholarship which enabled this work to be carried out.

APPENDIX A

Computation of equation (32). Equation (32) may be written in the form

$$\left(\frac{F+L}{F\,\Delta x_F}\right).\,\delta x_D(T) = \int_0^T \phi(T-\xi) f(\xi)\,d\xi \qquad \text{(A.1)}$$

Since $f(\xi)$ changes rapidly near $\xi = 0$ split the integral into two parts

$$\left(\frac{F+L}{F\Delta x_F}\right)\delta x_D(T) = \int_0^\tau \phi(T-\xi) f(\xi)\,d\xi + \int_\tau^T \phi(T-\xi) f(\xi)\,d\xi \qquad \text{(A.2)}$$

where τ is small c.f. T.

ϕ does not change rapidly and since τ is small (A.2) can be rewritten to give

$$\left(\frac{F+L}{F\,\Delta x_F}\right)\delta x_D(T) = \phi\left(T-\frac{\tau}{2}\right)\int_0^\tau f(\xi)\,d\xi + \int_\tau^T \phi(T-\xi) f(\xi)\,d\xi \qquad \text{(A.3)}$$

where $\phi\left(T-\frac{\tau}{2}\right)$ is taken as the mean value of $\phi(T-\xi)$ from $\xi = 0 \to \tau$

Comparing (A.1) with equation (31) it is seen that

$$\frac{F\,\Delta x_F}{F+L} f(\xi) = \frac{\partial}{\partial \xi}.\,\delta y_F(\xi)$$

i.e. $$\int_0^\tau f(\xi)\,d\xi = \left(\frac{F+L}{F\,\Delta x_F}\right)\delta y_F(\tau).$$

and (A.3) becomes

$$\left(\frac{F+L}{F\,\Delta x_F}\right)\delta x_D(T) = \underbrace{\left(\frac{F+L}{F\,\Delta x_F}\right)\phi\left(T-\frac{\tau}{2}\right)\delta y_F(\tau)}_{\text{(a)}} + \underbrace{\int_\tau^T \phi(T-\xi) f(\xi)\,d\xi}_{\text{(b)}}$$

Term (a) may be obtained directly and (b) by graphical integration for each value of T.

For the experimental results quoted $\alpha_E = \alpha_S = 1$ and the reflux ratio was 10:1 i.e. $\frac{V_E}{L_E} = \frac{11}{10}$ and $\frac{V_S}{L_S} = \frac{11}{12}$ taking a saturated liquid feed and $F = 2D$.

$\phi_D(T)$ was calculated from (27) and $f(T)$ from (26). The value of τ was chosen as 2·5.

NOTATION

- α = slope of equilibrium line
- $\mu = V_E\alpha_E/L_E$
- $\lambda = V_S\alpha_S/L_S$
- ω = angular frequency
- ϕ = indicial response
- τ = time
- a = defined by (29)
- $a_{1,2}$ = defined by (18)
- $a_{E,S}$ = defined by (23)
- k = defined by (29)
- $k_{1,2}$ = defined by (23)
- m = plate number (stripping section)
- n = plate number (enriching section)
- p = Laplace variable
- t = time
- x = mole fraction of more volatile component in the liquid
- y = mole fraction of more volatile component in the vapour

z_n = a length defined by $z_n = nZ_{N+1}/N + 1$
z_m = a length defined by $z_m = mZ_{M+1}/M + 1$
A,B,C = defined by (13)
A',B',C' = defined by (16)
F = molal feed rate
$F(i\omega)$ = complex frequency dependent transfer function
H = hold-up per plate (moles)
H_C = condenser hold up
H_W = reboiler hold up
K = defined by (29)
L = molal liquid overflow rate
M = total number of plates in the stripping section
N = total number of plates in the enriching section
R = reflux ratio
T = dimensionless time = Lt/H
V = molal vapour flow rate
X_z = defined by $\delta x_n = X_{Z_n} e^{i\omega t}$
Z_{N+1} = total length of enriching section
Z_{M+1} = total length of stripping section

Subscripts :

c = condenser
m = plate number (stripping section)
n = plate number (enriching section)
w = reboiler
D = top product
E = enriching section
F = feed
S = stripping section.

References

[1] Wilkinson, W. L. and Armstrong, W. D. *Proc. Conference on Plant and Process Dynamic Characteristics.* Cambridge, 1956.

[2] Voetter H. *Proc. Conference on Plant and Process Dynamic Characteristics.* Cambridge, 1956.

[3] Acrivos A. and Amundson N. R. *Industr. Engng. Chem.* (*Industr.*) 1955 **47** 1533.

[4] Rose A. and Williams T. J. *Industr. Engng. Chem.* (*Industr.*) 1955 **47** 2284.

[5] Williams T. J., Harnett R. T. and Rose A. *Industr. Engng. Chem.* (*Industr.*) 1956 **48** 1008.

[6] Croockewit P., Honig C. C. and Kramers H. *Chem. Engng. Sci.* 1955 **4** 111.

[7] Brown G. S. and Campbell D. P. *Principles of Servomechanisms* 1948.

[8] Armstrong W. D. and Wilkinson W. L. *Trans. Instn. Chem. Engng. Lond.* 1957.

VOL. 7 1957/58

Chemical Engineering Science, 1957, Vol. 7, pp. 8 to 14. Pergamon Press Ltd.

On shape factors for irregular particles—II.*

The transient problem. Heat transfer to a packed bed

R. ARIS

The Mathematical Institute, 16 Chambers Street, Edinburgh 1

(*Received* 20 *January* 1957)

Abstract—In the transient heat or matter transfer problem it is shown that taking the ratio v_p/s_x, the volume of the particle to its external surface area, as the characteristic dimension does not reconcile the results for different particle shapes. However a new shape factor can be introduced from which the contribution of internal diffusion to the dispersion of heat or matter in the direction of flow may be calculated for a particle of any shape. The relation between the two problems and AMUNDSON's solution for spherical particles is discussed in conclusion.

Résumé—Dans le problème de transfert de masse ou de chaleur pendant la période transitoire, l'auteur montre que le choix, comme grandeur caractéristique du rapport v_p/s_x (rapport du volume de la particule à sa surface externe) ne convient pas étant donné que les résultats sont différents suivant la forme des particules. L'introduction d'un nouveau facteur : facteur de forme, permet de calculer, pour une particule de forme quelconque, la contribution de la diffusion interne à la dispersion de matière ou de chaleur dans le sens de l'écoulement. En conclusion l'auteur établit la relation entre les deux problèmes et discute la solution d'AMUNDSON pour des particules sphériques.

Zusammenfassung—Bei Problemen der nichtstationären Wärme - oder Stoffübertragung reicht, wie gezeigt wird, der Quotient v_p/s_x, das Verhältnis des Partikelvolumens zu seiner äusseren Oberfläche, als kennzeichnende Länge nicht aus, um die Ergebnisse für verschiedene Partikelformen in Übereinstimmung zu bringen. Man kann aber einen neuen Formfaktor einführen, der den Anteil der inneren Diffusion an der Ausbreitung von Wärme und Stoff in Strömungsrichtung für beliebige Partikelformen zu berechnen gestattet. Die Beziehung zwischen den beiden Problemen und der Lösung von AMUNDSON für kugelförmige Teilchen wird abschliessend diskutiert.

6. SHAPE FACTORS FOR PARTICLES IN AN EXCHANGE COLUMN

It is well-known that the equations of matter and heat transfer in a packed bed, such as a heat exchanger or ion exchange column, are similar; see, for example GOLDSTEIN [3] or KLINKENBERG [5]. Considerable work has been done by AMUNDSON [1] and others on the system for spherical particles and it is of interest to see how far their work may be carried over for particles of arbitrary shape. To avoid considerable repetition we shall follow AMUNDSON's notation, the relevant part of which is given in the index of notation at the end of this paper.

The problem of a hot fluid flowing through a bed of spherical particles is considered by AMUNDSON. The temperature $t = t(s, x, \eta)$ within the particle and the temperature $T = T(u, x, \eta)$ in the fluid are given by the set of equations

$$\left.\begin{aligned}
&\frac{\partial^2 t}{\partial s^2} + \frac{2}{s}\frac{\partial t}{\partial s} + \bar{t} + \Delta t = \alpha \frac{\partial t}{\partial \eta} \\
&\quad - \epsilon \left(\frac{\partial t}{\partial s}\right)_{s=1} = t - T \\
&t = t_i(s, u, x), \quad \eta = 0 \\
&-\sigma \frac{\partial T}{\partial u} + \frac{\partial^2 T}{\partial u^2} + \frac{1}{u}\frac{\partial T}{\partial u} - \mu \left(\frac{\partial t}{\partial s}\right)_{s=1} = 0 \\
&\qquad \left(\frac{\partial T}{\partial u}\right)_{u=1} + BT = 0 \\
&T = T_0(u), \quad x = 0
\end{aligned}\right\} \quad (22)$$

*Part I of this paper was published in *Chem. Engng. Sci.* 1957 **6** No. 6, 262.

VOL. 7 1957/58

A sequence of integral transforms is used to reduce these equations to three readily soluble. The sequence is

(i) a finite Bessel transform on u, the radius in the bed; transform variable ξ_m; $T \to Y$; $t \to y$;

(ii) a Laplace transform on η, the time; transform variable p_1; $Y \to W$; $y \to w$;

(iii) a Laplace transform on x, the bed length; transform variable p_2; $W \to V$; $w \to v$;

giving the equations

$$\frac{d^2v}{ds^2} + \frac{2}{s}\frac{dv}{ds} + \frac{\tilde{\imath}\, J_1(\xi)_m}{p_1 p_2\, \xi_m} + \Delta v = \alpha\left[p_1 v - \frac{t_i J_1(\xi_m)}{p_2\, \xi_m}\right] \quad (23)$$

$$-\epsilon\left(\frac{dv}{ds}\right)_{s=1} = v - V \quad (24)$$

$$-\sigma\left[p_2 V - \frac{T_0 J_1(\xi_m)}{p_1\, \xi_m}\right] - \xi_m^2 V - \mu\left(\frac{dv}{ds}\right)_{s=1} = 0 \quad (25)$$

In modifying these equations for a particle of general shape we will from the outset render the co-ordinates within the particle dimensionless by multiplying them by the ratio s_x/v_p. If dv is the element of volume in these reduced co ordinates and as before R denotes the region occupied by the particle $\iiint_R dv = s_x^3/v_p^2$. Equations (22) then remain valid if we replace

$\frac{\partial^2 t}{\partial s^2} + \frac{2}{s}\frac{\partial t}{\partial s}$ by $\nabla^2 t$ in the second and $\left(\frac{\partial t}{\partial s}\right)_{s=1}$ by $\iint_S \frac{\partial t}{\partial n}\, ds$ in the fifth and if

$$\left.\begin{aligned} \tilde{\imath} &= \frac{a\, v_p^2}{k_s\, s_x^2},\ \Delta = \frac{b v_p^2}{k_s\, s_x^2},\ \alpha = \frac{V_f\, c_s\, \rho_s\, v_p^2}{l k_s\, s_x^2} \\ \epsilon &= \frac{k_s s_x}{h_f v_p},\ \mu = \frac{(1-\alpha')P^2 k_s}{s_x\, k_{fr}},\ \sigma = \frac{V_f \alpha' c_f \rho_f P^2}{l k_{fr}} \end{aligned}\right\} \quad (26)$$

If now we write $\lambda^2 = \alpha p_1 - \Delta$

$$F = \frac{J_1(\xi_m)}{p_2 \xi_m}\Big|(\alpha t_i + \tilde{\imath}/p_1),\ G = \frac{J_1(\xi_m)}{p_1 \xi_m}\,\sigma\, T_0 \quad (27)$$

equations (23)-(25) become in the general case

$$\nabla^2 v = \lambda^2 v - F \quad \text{in } R \quad (28)$$

$$\epsilon\frac{\partial v}{\partial n} + v = V \quad \text{on } S \quad (29)$$

$$(\sigma p_2 + \xi_m^2)\, V = G - \mu \iint_S \frac{\partial v}{\partial n}\, ds \quad (30)$$

These equations we can relate to the set previously considered as follows. Let χ_ϵ (where we shall drop the subscript ϵ when it is not necessary) be defined by

$$\left.\begin{aligned} \nabla^2 \chi &= \lambda^2 \chi \quad \text{in } R \\ \epsilon\frac{\partial \chi}{\partial n} + \chi &= 1 \quad \text{on } S \end{aligned}\right\} \quad (31)$$

Then clearly when $\epsilon = 0$ we have the function χ considered before in equation (14). Equations (28)-(30) are satisfied by putting

$$v = V\chi_\epsilon + F(1 - \chi_\epsilon)/\lambda^2 \quad (32)$$

$$V\left[\sigma p_2 + \xi_m^2 + \mu B^*(\lambda, \epsilon)\right] = G + \mu F B^*(\lambda, \epsilon)/\lambda^2 \quad (33)$$

The function $B^*(\lambda, \epsilon)$ is the analogue of AMUNDSON's $B(\omega)$. It is defined as $B^*(\lambda, \epsilon) = \iint_S \frac{\partial \chi}{\partial n}\, ds$ and using GREEN's theorem and the equation (31) we have

$$\left.\begin{aligned} B^*(\lambda, \epsilon) &= \iint_S \frac{\partial \chi}{\partial n}\, ds = \iiint_R \nabla^2 \chi\, dv \\ &= \lambda^2 \iiint_R \chi\, dv = \lambda^2 \frac{s_x^3}{v_p^2}\bar{\chi} \end{aligned}\right\} \quad (34)$$

where $\bar{\chi}$ is the mean value of the function χ throughout the region R of the particle. This last form is the most convenient and might indeed have been introduced from the outset by writing the fourth of equations (22) as a heat balance over both solid and fluid elements in a layer of the bed rather than over the fluid element only. Since B^* always occurs in conjunction with μ we can absorb the factor s_x^3/v_p^2 into μ and write $\mu B^* = \mu' \lambda^2 \bar{\chi}$ where

$$\mu' = (1 - \alpha')\, P^2 k_s\, s_x^2/k_{fr}\, v_p^2.$$

For a sphere we have

$$\lambda^2 \bar{\chi} = \frac{(3\lambda \coth 3\lambda - 1)/3\lambda^2}{\lambda^{-2} + \epsilon\,(3\lambda \coth 3\lambda - 1)/3\lambda^2} \qquad (35)$$

and substituting in equation (33) gives the function V in agreement with Amundson's equation (64). For the long cylinder, with heat flow across the ends negligible, we have

$$\lambda^2 \bar{\chi} = \frac{I_1(2\lambda)/\lambda I_0(2\lambda)}{\lambda^{-2} + \epsilon I_1(2\lambda)/\lambda I_0(2\lambda)} \qquad (36)$$

and for thin flat plates

$$\lambda^2 \bar{\chi} = \frac{\tanh \lambda/\lambda}{\lambda^{-2} + \epsilon \tanh \lambda/\lambda} \qquad (37)$$

The analogy between equations (15)-(17) and (35)-(37) is evident : in each case we may write

$$(\lambda^2 \bar{\chi})^{-1} = (\lambda^2 \eta)^{-1} + \epsilon \qquad (38)$$

and comparing (38) with (21) we have $\epsilon = (\lambda^2 \eta_f)^{-1}$ in accord with its nature as a film resistance. More significantly, we know that the three functions (15)-(17) lie close to one another so that this also is true of the functions (35)-(37).

From this circumstance we might be inclined to think that the use of v_p/s_x as the linear dimension, and the taking of the equivalent spherical radius to be $\phi\,(3\,v_p/4\pi)^{\frac{1}{3}}$ would be entirely satisfactory. However this is not the case for the following reason. The earlier problem is a steady state problem and the parameter A was a constant of the system and the effectiveness factor η determined by A was reasonably consistent for all shapes ; a mean error of approximately 0·05 might be committed but the value of A where this might occur was known. In the present problem $\lambda = (\alpha\, p_1 - \Delta)^{\frac{1}{2}}$ is a function of the transform variable p_1 as well as the constants of the system. In the inversion of the transform with respect to the time η an integration with respect to p_1 is involved and so the argument λ of the function $\bar{\chi}$ will vary throughout its range and in addition will be complex. Thus the inverse transforms will have no reason to lie close to one another. Moreover the behaviour of the inverse transform (i.e. the solution of the problem) for large times depends on the behaviour of the transform V for small values of p_1, and we shall do much to reconcile the results for different shapes if we make the behaviour of $\bar{\chi}$ for different shapes agree for small λ.

The method of doing this may be most simply demonstrated by taking a special case of Amundson's analysis. We consider an adiabatic bed with no heat generation initially at zero temperature ; then $E = \bar{\imath} = \Delta = t_i = 0$. For the inlet conditions we consider a short burst of very hot fluid. This solution is of basic importance for if $T_\delta(x, \tau)$ is the solution of this problem the solution to the more general problem when the inlet temperature is specified as a function of time $T_0(\tau)$ is $T = \int_0^\tau T_0(\tau')\, T_\delta(x, \tau - \tau')\, d\tau'$. In particular the warming of the bed by a steady stream of inlet temperature T_0 is given by $T_0 \int_0^\tau T_\delta(x, \tau')\, d\tau'$. As this "sharp burst" of temperature travels down the bed it broadens out into a bell-like distribution of temperature. It has been shown elsewhere [2] that this distribution rapidly tends toward a normal distribution

$$N(x, t) = \frac{1}{\sqrt{2\pi\, m_2(x)}} \exp - \frac{(\tau - m_1(x))^2}{2m_2(x)}. \qquad (39)$$

This means that observations of the temperature at a reasonable distance x down the bed would fall on a normal curve, the mean time or time for the peak temperature being $m_1(x)$ and the variance or spread of temperature being $m_2(x)$. The variance thus represents the "softening" of the sharp burst of temperature. In the case of the warming of the bed by a warm stream of constant temperature T_0 the temperature at a distant point x does not suddenly rise to T_0 as the temperature wave reaches that point. The initially sharp front of temperature has by then softened and $m_2(x)$ is a measure of this softening, whilst $m_1(x)$ is approximately the time at which $T = \frac{1}{2} T_0$. We shall show that $m_1(x) = m_1 x$ and $m_2(x) = m_2 x$ are both proportional to x. In the first case the constant of proportionality m_1 is the speed of the temperature wave or what Lighthill [7] terms the kinematic wave velocity and this is independent of the shape of the particles. In the second case the constant of proportionality

m_2 is a function of the shape of the particle and the constants of the system and it is by identifying the constants m_2 for all shapes that we can find a shape factor which will bring together all the results.

The particular solution we wish to consider is obtained by putting $E = \xi_m = \bar{t} = \Delta = t_i = 0$ and $T_0/p_1 = 2$ so that $F = 0$ and $G = \sigma$. Then by equation (33)

$$V = \left\{ p_2 + \frac{\mu}{\sigma} B^* (\lambda, \epsilon) \right\}^{-1}$$

The inversion of this with respect to p_2 is easily performed giving

$$W = \exp - \mu x \, B^*/\sigma = \exp - \frac{\mu' \alpha}{\sigma} x \, p_1 \, \bar{X} (\lambda)$$

$$\text{and } \lambda^2 = \alpha \, p_1 \qquad (40)$$

As is shown elsewhere this tends towards the transform of the normal distribution (39) and by comparison we find the values of m_1 and m_2

$$m_1 = 1 + \frac{\mu' \alpha}{\sigma} \bar{X} (0) \qquad (41)$$

$$m_2 = - \frac{\mu' \alpha}{\sigma} 2 \eta \, \bar{X}' (0) \qquad (42)$$

where $\bar{X}' (0)$ denotes $\left[\frac{d}{d\lambda^2} \bar{X} (\lambda) \right]_{\lambda = 0}$

But $\bar{X} (0) = 1$ independently of all particle shapes so that

$$m_1 (x) = m_1 x = \left(1 + \frac{\mu' \alpha}{\sigma} \right) x$$

$$= \frac{(1 - \alpha') c_s \rho_s + \alpha' c_f \rho_f}{\alpha' c_f \rho_f} x.$$

Now $\tau = (V_f/l) \theta$ where θ is the actual time and $x = z/l$ where z is the actual distance in the bed, hence the actual speed of the temperature wave is

$$\frac{x}{m_1 (x)} V_f = \frac{V_f}{m_1} = \frac{\alpha' c_f \rho_f}{\alpha' c_f \rho_f + (1 - \alpha') c_s \rho_s} V_f \qquad (43)$$

i.e. its ratio to the fluid speed is the ratio of the heat content of the fluid to the total heat content. This may be deduced from a heat balance the bed as a whole for when the hot front has reached a point x sufficient heat must have been introduced by the hot fluid to raise the temperature of both solid and fluid elements of the bed.

It is in the coefficient m_2 that the influence of shape is seen. We have

$$m_2/m_1 = - 2\alpha \, \bar{X}' (0) = 2\alpha \left(\tfrac{2}{3} + \epsilon \right) \text{ for spheres}$$

$$= 2\alpha \left(\tfrac{1}{2} + \epsilon \right) \text{ for cylinders}$$

$$= 2\alpha \left(\tfrac{1}{3} + \epsilon \right) \text{ for plates}$$

and $\alpha = V_f v_p^2 / l \, D_s s_x^2$ where $D_s = k_s/c_s \rho_s$ is the diffusivity within the particle. The contribution of the surface effect to the ratio m_2/m_1, in all cases

$$2 \alpha\epsilon = 2 \frac{V_f}{l} \frac{c_s \rho_s}{h_f} \frac{v_p}{s_x} \qquad (44)$$

The contribution due to internal diffusion is dependent on the shape but additive as was the case in § 5. It may be written in all cases as

$$\frac{2}{3} \kappa\alpha = \frac{2}{3} \frac{V_f}{l D_s} \kappa \frac{v_p^2}{s_x^2}, \qquad (45)$$

where κ is a shape factor, $= 1$ for flat plates, $= 1{\cdot}5$ for cylinders, $= 1{\cdot}8$ for spheres.

Before determining this shape factor for a variety of shapes we may mention another interpretation of the equations which gives an extra boundary condition in equations (31). If we consider the exchange of matter instead of heat the problem we are considering may be regarded as the problem of chromatography. We write C and c in place of T and t, as the concentrations of a given solute in the mobile phase and in a stationary held in the pores of a particle. The short burst of heat corresponds to the putting of a sample on to the column in a narrow and concentrated band, and the bell-like distribution of concentration is the so-called chromatographic peak which emerges from the column. $m_1 (x)$ is the time of emergence of the peak and in the terminology of chromatography the speed given in equation (43) is $R_f \, V_f$ where R_f is the so-called R_f number of the solute. $m_2 (x)$ is a measure of the breadth of the peak and the knowledge of this is vital for good chromatographic separations. To transform the equations to this interpretation we replace $c_s \rho_s/c_f \rho_f$, the ratio of the heat capacities of the two phases, by ζ, the partition coefficient or ratio of the capacities of the two phases to absorb the solute, and $D_s = k_s/c_s \rho_s$ the diffusivity of heat in the solid by D_s, the

VOL. 7 1957/58

diffusivity of the solute in the stationary phase. Then

$$R_f = \left(1 + \frac{1-\alpha'}{\alpha'}\,\zeta\right)^{-1}$$

as is well known, and the contribution of internal diffusion to the spread of the peak is again given by (45).

The stationary phase is usually a non-volatile liquid held on a porous particle of some shape, and the particle need not be completely saturated with the liquid. If it occupies the region R between the external surface S and an internal surface S' we have an additional boundary condition for equation (31) namely

$$\frac{\partial \chi}{\partial n} = 0 \quad \text{on } S' \tag{46}$$

where $\partial/\partial n$ denotes differentiation along the normal to S'.

7. The Calculation of the Shape Factor κ

Assembling equations (31) and (46) and comparing (42) and (45) we have the following definition of the shape factor i.e.

$$\kappa = -3\left[\bar{\chi}_\epsilon'(0) + \epsilon\right] \tag{47}$$

$$\text{where } \bar{\chi}_\epsilon(0) = \left[\frac{d}{d\lambda^2}\left\{\frac{1}{v_p}\int\!\!\int\!\!\int_R \chi\, dv\right\}\right] \tag{48}$$

$$\nabla^2 \chi_\epsilon = \lambda^2 \chi_\epsilon \qquad \text{in } R \tag{49}$$

$$\epsilon\frac{\partial \chi_\epsilon}{\partial n} + \chi_\epsilon = 1 \qquad \text{on } S \tag{50}$$

$$\frac{\partial \chi_\epsilon}{\partial n} = 0 \qquad \text{on } S' \tag{51}$$

The evaluation of κ may be simplified if we expand χ as a series in λ^2, $\chi = \chi_0 - \lambda^2\chi_1 + \lambda^4\chi_2$. Then $\nabla^2\chi_0 = 0$ and χ_0 satisfies the boundary conditions (50) and (51) so that $\chi_0 \equiv 1$. χ_1 satisfies

$$\nabla^2\chi_1 = -1 \quad \text{in } R \tag{52}$$

$$\epsilon\frac{\partial\chi_1}{\partial n} + \chi_1 = 0 \qquad \text{on } S \tag{53}$$

and condition (51) on S'. It may be shown that if $\partial\chi/\partial n$ is constant over the surface of the particle then the shape factor κ is independent of ϵ. In the general case this will not be quite true, though it is in the case of the sphere, cylinder and plate. However the dependence may in general be shown to be small, for putting

$$\chi_1 = \chi_1^* + \epsilon + \psi$$

χ_1^* satisfies $\nabla^2\chi_1^* = -1$ in R, $\chi_1^* = 0$ on s, and ψ satisfies $\nabla^2\psi = 0$ in R, $t\dfrac{\partial\psi}{\partial n} + \psi = 1 + \dfrac{\partial\chi_1^*}{\partial n}$ on s and both satisfy (51). If $\partial\chi_1^*/\partial n$ were constant it would equal $\dfrac{1}{s_\alpha}\displaystyle\int\!\!\int_S \frac{\partial\chi_1^*}{\partial n}\,ds = \frac{1}{v_p}\int\!\!\int\!\!\int_R \nabla^2\chi^*\,dv = -1$ and so the function ψ would vanish identically. Assuming $\epsilon\psi$ to be negligible we have the simplest definition of κ as follows;

$$\left.\begin{aligned} \kappa &= 3\left[\frac{1}{v_p}\int\!\!\int\!\!\int_R \chi^*\,dv\right] \\ \text{where}\quad \nabla^2\chi^* &= -1 \text{ in } R \\ \chi^* &= 0 \quad \text{on } S \\ \partial\chi^*/\partial n &= 0 \quad \text{on } S' \end{aligned}\right\} \tag{54}$$

The shape factor κ is said to be a functional of the solution of the equations (54) in the region R. It depends only on the geometry of the region. It may be calculated by purely numerical methods should the need arise for a region R for which no analytic solution of (54) is available. We give it below for a number of common shapes. They are shown in Fig. 3.

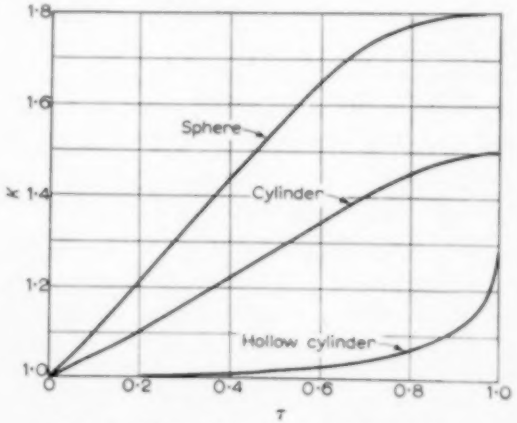

Fig. 3. Shape factor κ for various shapes.

Sphere: S is the outer surface and S' a concentric spherical surface the distance between S and S' being a fraction τ of the radius.

$$\kappa = \left(1 - 2\tau + \frac{7}{5}\tau^2 - \frac{1}{3}\tau^3\right) \Big/ \left(1 - \tau + \frac{1}{3}\tau^2\right)^3.$$

Cylinder, sufficiently long for the transfer across the flat ends to be neglected: S is the outer cylindrical surface, S' a coaxial one and the distance between them a fraction τ of the radius

$$\kappa = \frac{3}{16} \frac{1 - 4(1-\tau)^2 + 3(1-\tau)^4 - 4(1-\tau)^4 \log(1-\tau)}{\{\tau(1 - \frac{1}{2}\tau)\}^3}.$$

Hollow cylinder, again long but transfer can take place over both inner and outer surfaces, S is thus both surfaces and S' vanishes; the thickness is a fraction τ of the mean of the inner and outer radii.

$$\kappa = \frac{3}{4}\left\{(1 + \tau^2)\log\frac{1+\tau}{1-\tau} - 2\tau\right\} \Big/ \left\{\tau^2 \log\frac{1+\tau}{1-\tau}\right\}.$$

Finite cylinder, S the outer surface and S' vanishes with p = ratio radius : length,

$$\kappa = 384(p+1)^2 \sum_{n=0}^{\infty} \sum_{m=1}^{\infty} [j_m^2 (2n+1)^2 \pi^2 \{j_m^2 + (2n+1)^2 \pi^2 p^2\}]^{-1}.$$

This is shown in Fig. 4, where clearly $\kappa \to 1$ as $p \to \infty$ and $\kappa \to 1{\cdot}5$ as $p \to 0$. A finite cylinder of height and diameter comparable is a much more compact object than the flat disc or long thin cylinder so that we should expect κ to be greatest in this region.

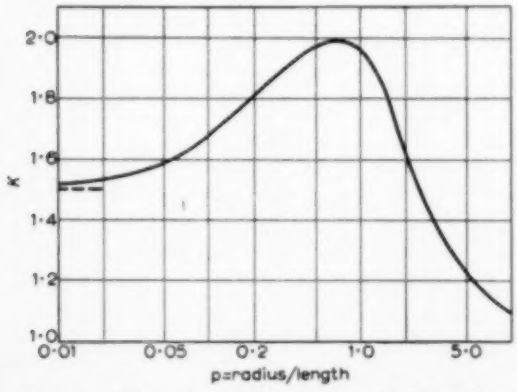

FIG. 4. κ For a finite cylinder p = radius/length.

8. DISCUSSION

The two problems we have considered here are essentially specializations of the problem which AMUNDSON has solved completely for spherical particles. Our first problem is obtained by considering the matter flow problem analogous to his heat flow presentation making the changes outlined in § 6 and taking the steady state solution (C. p. 88 of [1]). In this case we let $p_1 \to 0$ and so $\lambda^2 = -\Delta$, but in the analogue to AMUNDSON's Δ we have $b/k_s = -k\sigma/D$ so that $\lambda^2 = k\sigma v_p^2/D s_x^2 = \Lambda^2$ of § 3. As we have remarked our $B^*(\lambda)$ is the analogue for a particle of general shape of AMUNDSON's function B for spheres. In the second problem we have been considering the transient case with no heat generation $\Delta = 0$ (D p. 88 of [1]). Our method of treating this problem may be readily extended to the case of axial diffusion; see [2].

We have seen that the introduction of a suitable shape factor is by no means straightforward. In the first (steady state) problem the error committed by using v_p/s_x as the characteristic dimension for all shapes was seen to be small. The second (transient) problem however requires a different treatment. The use of v_p/s_x does indeed reduce the error from a factor of 5 or more to within a factor of 2, but for more accurate results a new factor must be defined and calculated. The introduction of a shape factor must therefore be carefully considered in relation to the particular aspect of the problem for which it is required.

NOMENCLATURE

(Notation used only in § 6 to concur with AMUNDSON's is shown marked*)

* a = constant in heat generating function
B^* = function defined in (34)
* b = constant in heat generating function
C = concentration in fluid
c_f = specific heat of fluid
c_s = specific heat of solid
E = modified Nusselt number
F = function defined in (27)
G = function defined in (27)
I_0, I_1 = modified Bessel functions
J_0, J_1 = Bessel functions
j_m = m^{th} root of $J_0(x) = 0$
k = reaction rate constant
* k_s = conductivity of heat in solid

- k_f = conductivity of heat in fluid
- k_{fr} = conductivity of heat in fluid, radially
- l = length of bed
- m_1 = mean of normal distribution
- m_2 = variance of normal distribution
- N = normal distribution [39]
- p = ratio radius : length of cylinder
- p_1, p_2 = transform variables
- R = region occupied by particle
- R = radius of spherical particle
- R_f = R_f value of solute (§ 6).
- r = particle radius variable = sR
- S, S' = outer and inner surfaces of R
- s = dimensionless particle radius variable
- s_x = external surface area of particle
- T = temperature of fluid
- T_0 = temperature of incoming fluid
- T_δ = solution for burst of hot fluid
- t = temperature in particle
- t_i = initial temperature of particles
- $\tilde{t} = aR^2/k_s$, $av_p^2/k_s s_x^2$
- u = dimensionless axial variable
- V = transform of W
- V_f = interstitial fluid velocity
- v = transform of w
- v_f = volume rate of fluid
- W = transform of Y
- w = transform of y
- x = length coordinate
- Y = transform of T
- y = transform of t
- z = length coordinate
- α' = voidage of bed
- $\alpha = V_f c_s \rho_s R^2/lk_s$, also by (26)
- $\Delta = b R^2/k_s$, also by (26)
- $\epsilon = k_s R/k_f$, also by (26)
- ζ = partition coefficient
- η = dimensionless corrected time variable
- κ = shape factor defined by (47)
- $\lambda = (k\alpha/D)^{\frac{1}{2}}$
- $\Lambda = v_p \lambda/s_x$
- $\mu = 3(1 - \alpha') P^2 k_s/R k_{fr}$, also by (26)
- ξ_m = transform variable
- P = radius of bed
- ρ_s = density of solid
- ρ_f = density of fluid
- $\sigma = V_f \alpha' c_f \rho_f P^2/l k_{fr}$, also by (26)
- τ = fractional thickness of layers § 7
- τ = dimensionless time
- ϕ = shape factor = $(36\pi v_p^2)^{\frac{1}{2}}/s_x$
- χ = solution of (9)
- χ_s = solution of (31)

REFERENCES

[1] AMUNDSON N. R. *Industr. Engng. Chem.* (*Industr.*) 1956 **48** 26-42.

[2] ARIS R. in preparation.

[3] GOLDSTEIN S. *Proc. Roy. Soc.* 1953 A **219** 151-185.

[4] HOUGEN O. A. and WATSON K. M. *Chemical Process Principles* Vol. III.

[5] KLINKENBERG A, *Industr. Engng. Chem.* (*Industr.*) 1954 **46** 2285-2289.

[6] LEVA M. *Chem. Engng.* 1949 **56** 115.

[7] LIGHTHILL M. J. and WHITHAM G. B. *Proc. Roy. Soc.* 1955 A **229** 281.

[8] THIELE E. W. *Industr. Engng. Chem.* (*Industr.*) 1939 **31** 916.

[9] WHEELER A. *Advances in Catalysis* 1951 Vol. II.

Chemical Engineering Science, 1957, Vol. 7, pp. 15 to 25. Pergamon Press Ltd.

On the instability and inhomogeneity of filter-cakes

P. M. Heertjes and J. Nijman

Chemical Engineering Laboratory, Technical University, Delft, Holland

(*Received* 19 *March* 1957)

Abstract—Experimental proof is given that cakes formed by filtration or by sedimentation in planes perpendicular to the direction of flow are not homogeneous.

Moreover it is demonstrated that by flow and through the arising cake pressures the instable cakes are consolidated. Even small cake pressures are sufficient to ensure this consolidation.

Résumé—On démontre expérimentalement que les gâteux formés par filtration ou par sédimentation dans des plans perpendiculaires au sens du courant ne sont pas homogènes.

On démontre ensuite que les gâteaux instables sont consolidés sous l'influence du courant et de la pression augmentante dans de gâteau. Même de faibles pressions dans le gâteau suffisent à provoquer la dite consolidation.

Zusammenfassung—Es wird experimentell nachgewiesen, dass durch Filtration oder Sedimentation gebildete Kuchen in zur Strömungsrichtung senkrechten Ebenen nicht homogen sind.

Weiterhin wird gezeigt dass, durch die Strömung und die steigenden Kuchendrücke die instabilen Kuchen verfestigt werden, sogar schon bei kleinen Kuchendrücken.

VOL. 7 1957/58

Introduction

It can be found in the literature that beds of particles occuring in nature or formed by man made operations, in general are not homogeneous, nor will they show a stable structure especially if fluids are moving through these beds.

A few examples cited from the literature on rather different subjects may elucidate this.

From Harting [1] it is known that consolidation of the soil, when percolated with water, is a time function. The velocity of consolidation depends on the system, on the particle size, on the size spectrum and on the particle shape. The time needed for complete consolidation, that is the time needed to reach equilibrium between particle pressure and liquid pressure [2], varies from a couple of hours for sand to some months for clay.

Forchheimer [3], in the same field of soil mechanics, observes an increase as well as a decrease of the liquid flow rate through sand and clay, especially in the first period of consolidation.

Applying a mechanical pressure on beds of dry metal powders, Duwes and Zwell [4] observe large differences in pressure in different parts of the bed.

From measurements of the transport of heat by air flowing through dumped beds of granular materials (seeds) Businger [5] concludes that the beds are not homogeneous, moreover there is as usual a strong wall effect.

As a cake will not be deposited in the densest packing the possibility that it departs from its original packing is always present. The departure may e.g. be caused by the fact that the cake is not immediately in equilibrium with the conditions of flow, or that some outside force is applied. Cakes therefore are not stable and must show the same consolidation as soils. Proof of this instability is the well known influence of the cake pressure on the resistance of the cake to flow, is the swelling of a cake after the filtration pressure has been released, is the retarded packing compressibility as found by Rietema [6] and is the consolidation of a cake of crushed limestone with time as described by Tiller [7].

From the above it can be concluded that it is very likely that filter cakes perpendicular to the

direction of flow are not homogeneous. The contrary is nearly always assumed in the literature. Moreover the consequences of the instability of the cake are not too well known. If anything is to be expected from a closer study of the behaviour of filtercakes e.g. by porosity measurements and by researches on the influence of particle shape and particle spectrum, more must be known about the instability and the inhomogeneity of these cakes. This is the more true if, as is necessary more use will be made of the rather considerable amount of knowledge available from the field of fluid flow through porous masses [8].

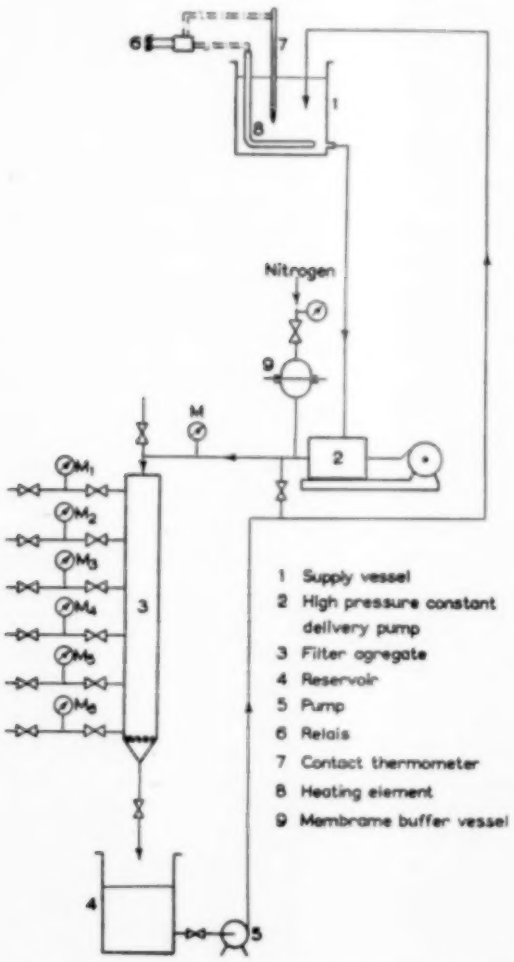

FIG. 1. Set up for the percolation of cakes at a high pressure difference.

As an introduction to a more systematic investigation, some phenomena pertaining to the subject mentioned, will be presented in this paper.

EXPERIMENTAL
(with T. FRIELING and A. P. VERVAART)

The information on the inhomogeneity and instability of cakes formed of different substances by filtration and by sedimentation has been obtained in small scale experiments by percolation with water under changing conditions of time, pressure difference and cake thickness.

The substances used were : calcium carbonate ($< 40\ \mu$) calcium sulphate 2 aq. ($< 75\ \mu$), hydrated aluminium oxide, norit ($< 75\ \mu$), quartz ($< 90\ \mu$) and polyvinylchloride ($< 50\ \mu$).

The three substances mentioned first were obtained by precipitation from corresponding soluble salts, aged for several weeks and stored under water. The percolation water was saturated with the substance under investigation.

Two set-ups in which the cakes were formed and percolated, were employed.

The first set-up used for experiments at relatively high pressures (Fig. 1) consisted of a metal cylinder of inside diameter of 8 cm and height of 36 cm, provided at the bottom with a nylon filtercloth supported by a perforated brass plate. In a few cases twillfill cloth has been used.

In the wall at 1·6 (M_6), 7·6 (M_5), 12·6 (M_4), 17·6 (M_3), 22·6 (M_2) and 27·6 (M_1) cm from the filter, manometer connexions were constructed which enabled to measure the liquid pressure in the apparatus at different places in the cake viz. at 0, 1, 2, 3, and 4 cm from the wall with the aid of oval metal tubes sealed with a thin sieve. With a piston-pump with adjustable stroke, liquid could be forced through the filter cake from top to bottom. A membrane buffer vessel with a nitrogen counter-pressure equalized pressure variations, caused by the pump, to one atmosphere.

The second set-up was rather simple and was used to measure at relatively low pressure differences. It consisted (Fig. 2) of a supported nylon filter with a cylindrical container (brass or plastic) of inside diameter of 11 cm, open to the air, with an overflow at about 25 cm from the

VOL. 7 1957/58

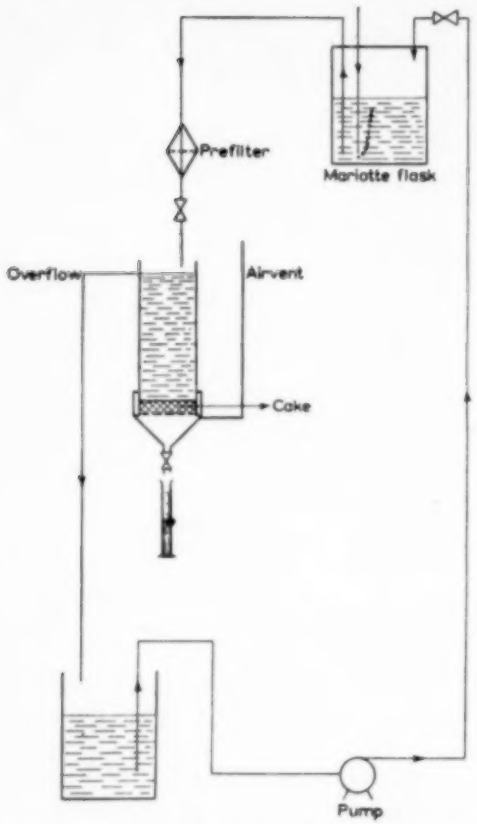

FIG. 2. Set up for the percolation of cakes at a low pressure difference.

filter. This enabled to maintain a head of ~ 25 cm of water over the filter. The filter could be shut off by means of a stopcock, so that the cake could be kept in water if it was not percolated. In some cases an upward bended tube was inserted just under the filter, as an airvent. Water was admitted to the container at a constant rate by means of a Mariotte flask.

In all experiments prefiltered water was used and the grow of algea was prevented by adding a disinfectant.

RESULTS AND DISCUSSIONS

A. *The Stability of a Cake**

Both the influence of the time and of the cake pressure have been investigated as to their effect on the stability of cakes which are percolated.

The experiments are most conveniently divided into those carried out at a low percolation pressure (equal to a head of 25 cm water = 1/40 atm, (1)) and those carried out at a high percolation pressure (10 – 100 atm, (2)). In both cases as a parameter for the behaviour of the cake the percolation rate θ_v is taken. The results will be presented in graphical form. The percolations have been carried out continuously and discontinuously.

(1) *Percolations at a low pressure difference over the cake*

Experimental results. In order to make ϕ_v not too small, rather thin cakes (1 – 3 cm) were used here.

In Fig. 3 two experiments, I and II, with a cake of calcium carbonate of 2 cm thick, which has been formed by rapid filtration and percolated

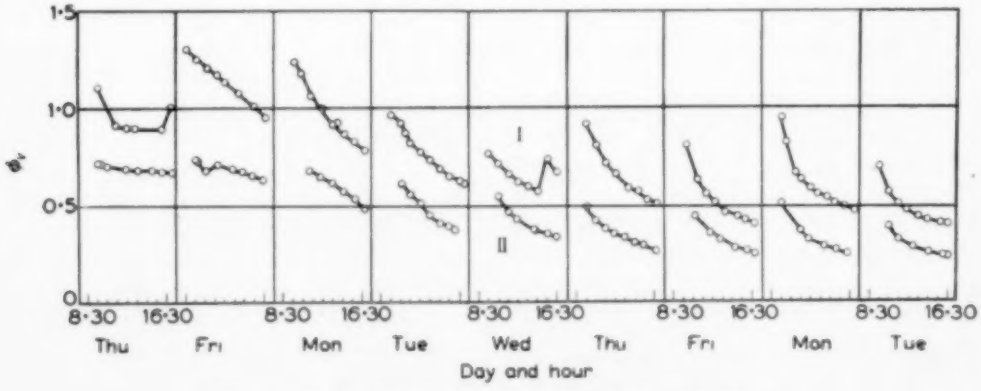

FIG. 3. Discontinuous percolation of 2 cm layers of $CaCO_3$.

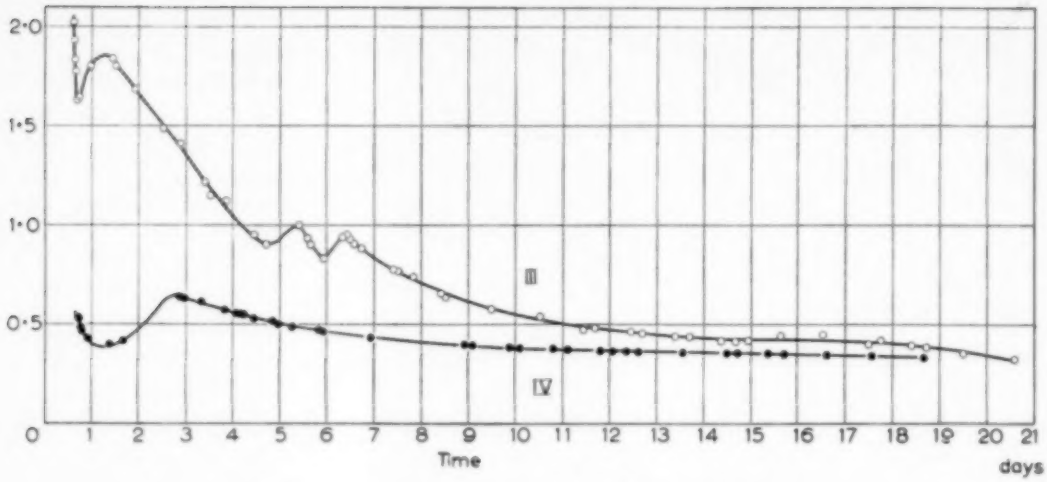

Fig. 4. Continuous percolation of 2 cm layers of $CaCO_3$.

discontinuously are given. In Fig. 4 two experiments for continuous flow one cake formed by sedimentation (II) the other by filtration (IV) both again of calcium carbonate and of 2 cm thickness are shown.

If 1 cm layers of calcium carbonate-cakes and of calcium sulphate-cakes were percolated discontinuously, the same effects were observed as with the 2 cm layers although the period of increase of ϕ_v with time was much longer and in some cases calcium carbonate after more than 14 percolation days, even did not show a tendency to decrease. Air under the filter results in an increase of flow, but does not change the phenomena. By microscopical analysis no scouring effects have been found. The facts presented having been chosen from a larger amount of experimental material are representative for the type of cakes investigated.

Discussion. The following conclusions can be drawn. By liquid flow cakes change the packing of the particles. If flow is applied to a cake consolidation sets in immediately. This does not necessarily imply that ϕ_v will decrease at once. If the cake is not homogeneous in planes perpendicular to flow parts of the cake may consolidate at the cost of other parts, causing e.g. crack formation as will be shown in paragraph B. The width of the cracks may be such that the total flow may increase.

With time however in the long run also the regions of lesser packing density will consolidate and finally ϕ_c will decrease. It is remarkable that with freshly formed cakes an alternating increase and decrease of flow has been observed in some cases. The same behaviour has been found by Forchheimer for soils. The density of packing can be temporarily increased in this sense, that if flow is interrupted the cake will restore itself somewhat toward its original porosity. This effect is more pronounced if the influence of the filtercloth in which the first layers are embedded, rather strongly diminishes, that is for relatively thick cakes. The denser the packing, the less is the restorative power, in other words the less resilient is the cake.

The behaviour of thin cakes of calcium carbonate where even after a long period of flow no decrease in flow has been found seems abnormal. It is however possible that the crack formation mentioned before for thin cakes obscures the results, because the cracks can reach the filtercloth. This abnormal behaviour has only been found for calcium carbonate cakes of about 1 cm. The 1 cm cakes of calcium sulphate did not show this phenomenon so markedly.

Also no essential difference has been found

*The cakes investigated have been formed either by filtration or by sedimentation. If no distinction is necessary they will simply be called cakes in this paper.

VOL. 7 1957/58

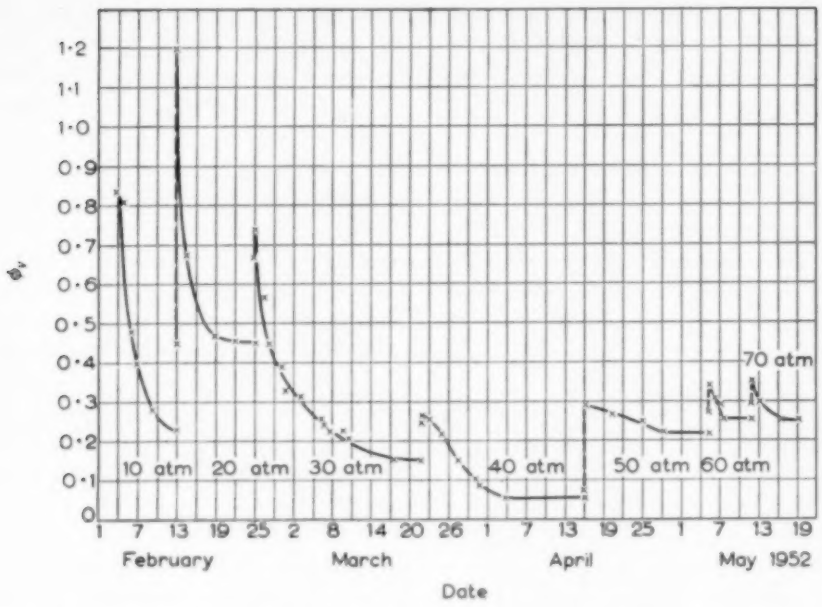

FIG. 5. The ϕ_v – time curves of cakes of P.V.C. power at different pressures.

between cakes formed by sedimentation or by filtration. In general the cakes formed by filtration were more homogeneous and had a denser packing than the cakes formed by sedimentation.

(2) *Percolations at high pressure differences*

The experiments using a high pressure difference over the cake have been carried out to amplify the cake pressure effect and in order to be able to work with thicker cakes.

Experimental results. It has again been found that ϕ_v at constant pressure decreased with time. Most often after each start a time period, —changing for different substances from some minutes to 4 – 6 hr—of rapid and rapidly changing flow, preceeded the continuous decrease of flow. As an example of the decrease of ϕ_v with time in Fig. 5, the results obtained with layers of polyvinylchloride-powder, 2 – 3 cm thick, for constant pressures, measured in increasing order, are given. The very first part of each series has not been measured because of the too rapid nature of the phenomena.

A marked change occurs when after consolidation at a certain pressure, this pressure is increased. A much higher flow rate than calculated from the pressure increase—the flow is laminar—occurs.

Quite the same effect has been found for cakes of calcium carbonate of about 20 cm thick.

To establish a constant pressure needed continuous manual adjustment of the delivery of the pump, which was cumbersome, especially at the start of each run.

Therefore the technique of measuring has been changed for the next experiments. The layers were percolated at a constant rate, which could be more easily adjusted. The corresponding percolation pressure was arbitrarily chosen as follows. After each increase in flow rate, the pressure as indicated by M increased with time. As soon as the increase was less than 0·3 atm/45 min, or oscillated less than 0·3 atm around a certain value, this value was used to establish the percolation pressure. It has to be observed that the percolation pressures used ranged from 10 – 100 atm.

Norit was now percolated in the following way. A run was started at a certain flow rate and as soon as the arbitrarily chosen equilibrium

pressure was reached, the velocity was increased. This was repeated several times until a certain final pressure was reached. Then a second run was started at about the same initial rate as chosen in the first run and the measurements carried out in the same way. This was continued for weeks on end.

Five succesive runs, taken at the end of the total period are given in Fig. 6 together with the corresponding time (θ) necessary to reach equilibrium after each change for each point measured.

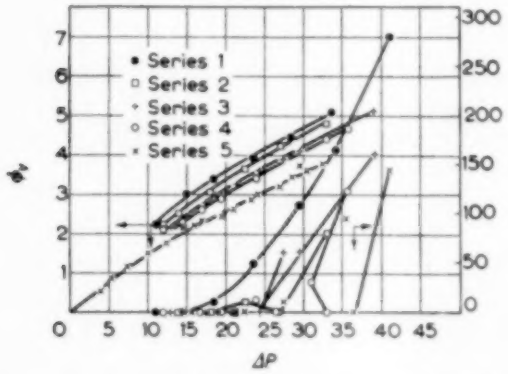

Fig. 6. Five succesive percolation runs for a thick norit cake with the corresponding times (θ) to reach equilibrium.

The final height of the cake (after expansion) was 30·5 cm. From pressure measurements at the wall the impression had been gained that the resistance against flow was mainly offered by the part of the cake near the filter. To investigate this, after the experiments just described had been finished, by means of a sharp horizontal knife, rotating along a vertical axis, the cake was pealed off carefully to a certain depth and the percolation measured again over the range of the pressure differences used before. The results are represented in Fig. 7. The observation has to be included that an extremely thin layer of iron oxide had been deposited on the top of the cake.

The $\phi_v - \Delta P$ line of the consolidated cake of norit is not a straight line, but slightly curved, although the flow is laminar.

For calcium carbonate cakes the same phenomena as described for norit were encountered, with the exception that after a few runs, even before the equilibrium consolidation was reached, the $\phi_v - \Delta P$ lines were straight and passed the origin. Apparently these cakes are not reversibly compressible.

The behaviour of hydrated aluminium oxide was very erratic. It may suffice to say that the time to reach equilibrium was much longer under the same conditions than with other substances. Even with cakes of a few centimetres thick this took weeks. Also the consistency of the cake in the direction of flow differed more than with the other cakes described. For a cake of an original height of 30 cm, which height after consolidation at 70 atm had decreased to 6 cm, the first layer of

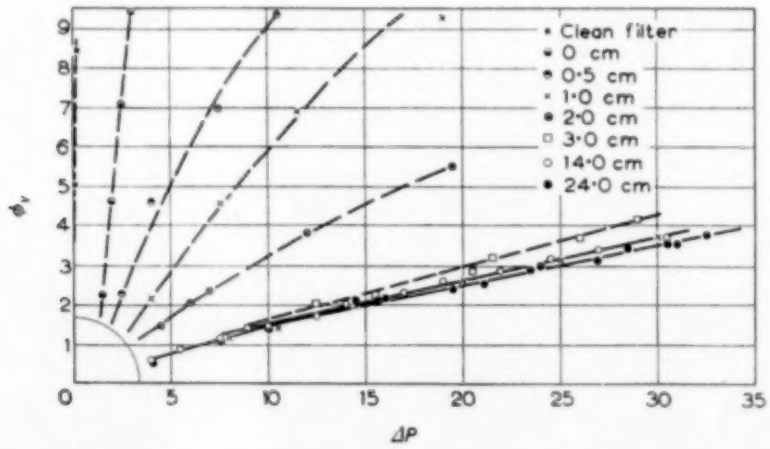

Fig. 7. Percolation runs for the pealed off cake of norit at different heights.

VOL. 7 1957/58

1 cm, measured from the top had the consistency of the original cake. The substance near the filter having been subjected to the highest cake pressure resembled candle wax, the cake in between had a granular structure. If these granules were brought in a humid atmosphere for weeks they showed no alteration and remained quite different from the original somewhat slimy substance.

The measurements given so far have been carried out along gradual lines. A more erratic picture is obtained if this pattern is left. This is shown in Fig. 8 for experiments with norit where the ratio of the pressure difference at the wall measured with manometer M_6 (1·6 cm from the filter) to the total pressure difference over the filter is given as a function of the total ΔP in the sequence as measured.

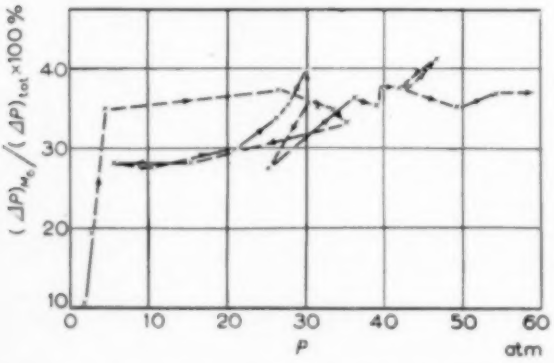

FIG. 8. The ratio of pressure differences in the norit cake at the wall 1·6 cm above the filter to the total pressure difference as a function of the total pressure difference.

The sequence is indicated by means of arrows. A dotted line signifies that the flow between the two points connected has been interrupted for one night or longer, a full line signifies uninterrupted flow. For the same cake, after the last percolation experiment, the porosity ϵ measured at three places, in the centre of the cake, near the wall and a mean value over every horizontal layer is presented in Fig. 9 as a function of the height of the cake. The porosities have been calculated from the loss of weight of 1 cm^3 samples on drying and corrected for the amount of water taken up by the dry substance from air with a relative humidity of 100 per cent. In Fig. 9 are also plotted the cake pressure (assumed to be equal to the total pressure on top of the cake minus the liquid pressure measured at a certain height) measured in the centre of the cake versus the height of the cake, as found in the last percolation experiment of the series. The "cake" pressure at the wall was almost zero up to the last manometer M_6.

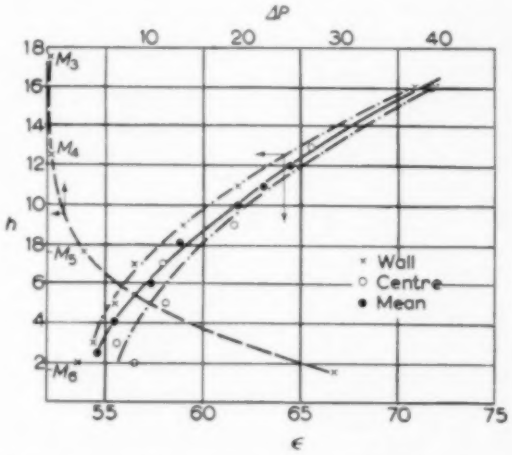

FIG. 9. The porosity of a norit cake and the cake pressure in the centre of the cake as a function of the height of the cake.

The experiments described show that the decrease of ϕ_v by flow takes place slowly. The process can be speeded up considerably by applying different and rapidly changing pressures on the cake, which will be called pulsating. For the thick cakes in the metal apparatus this could most conveniently be done by changing the nitrogen pressure on the buffer vessel rapidly.

Vibrations can have the same effect but could not be used in the metal apparatus with the thick walls.

Norit on pulsation gave a relatively rapid consolidation in which under the same conditions the same final $\phi_v - \Delta P$ relation was obtained as with flow only.

However with a quartz-flour fraction of $10-90\,\mu$ a different behaviour has been found. This fraction was obtained by sieving, giving a fraction of $0-90\,\mu$, followed by elutriation with water

to remove the particles smaller than 10 μ. A sedimentated cake of this flour was subjected to consolidation by flow and behaved normally, although the process was slow. The results showed straight $\phi_v - \Delta P$ lines from the start, which passed the origin. As soon as the cake was stable under the conditions chosen the pulsating technique (using pressures between 0 and 100 atm) was applied. Contrary to the experience with norit, a displacement of the $\phi_v - \Delta P$ lines towards higher values of ϕ_v was found after pulsation. Normal flow thereafter caused a normal decrease of ϕ_v. Pulsating again reversed the phenomenon. This could be repeated several times. Some of the results are given in Fig. 10. The runs are numbered in the sequence as carried out. Pulsating (full arrows) took place between the runs I and II and VI and VII.

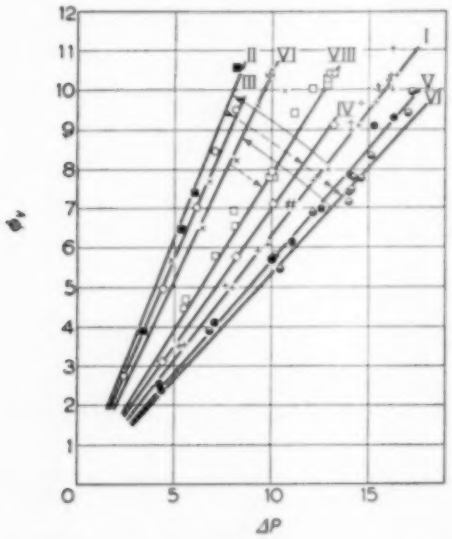

Fig. 10. Influence of pulsating and flow on a cake of quartz-flour (10 – 90μ).

The lines representing the liquid pressure in the centre of the cake as a function of the height of the cake were of the same type, before and after pulsating. Two examples are given in Fig. 11, line (*a*) before pulsating ($\Delta P \sim 12$ and $\phi_v = 7{\cdot}2$) and line (*b*) after pulsating ($\Delta P \sim 12$ and $\phi_v = 9{\cdot}2$).

When carrying out the same experiments with the same weight of quartz-flour of 0 – 90 μ, again straight $\phi_v - \Delta P$ lines were obtained for each run and again the consolidating effect of flow was found.

However pulsating here had the same effect as found for norit, showing a further consolidation. Repeated pulsation created a definite endstage where further pulsation caused no change.

The pressure distribution showed larger differences than in the former case as can be seen from line (*c*) in Fig. 11, obtained for $\Delta P \sim 41$ $\phi_v = 2{\cdot}73$, before pulsating and line (*d*) obtained for $\Delta P \sim 45$, $\phi_v = 1{\cdot}78$, after pulsating.

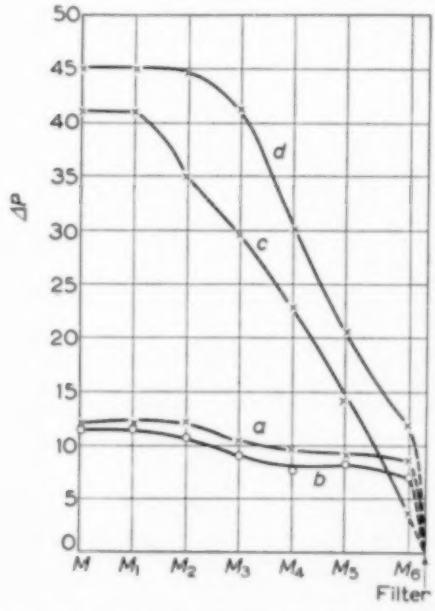

Fig. 11. The liquid pressure in cakes of quartz-flour as a function of the height.

Porosities have been measured in 1 cm^3 samples as before. The porosity of the 10 – 90 μ quartz cake was about 44 per cent varying from top to bottom near the wall from 43·0 – 45·2 per cent and in the centre from 42·8 – 46·5 per cent. Total height of the cake 29 cm. The porosity of the 0 – 90 μ cake was about 38 per cent, varying near the wall from 36·4 – 39·2 per cent in the centre

VOL. 7 1957/58

from 36·4 – 39·4 per cent. Total height of the cake was 26 cm. The heights tally with the porosities found. The distribution of the porosities was random. If anything can be said about the differences in porosity it is that the porosity seems to be largest about 3 – 5 cm from the filter.

Although no large differences in porosity in horizontal planes have been found with the quartz-flour cakes, preference channels of flow have also been found here. Such a preference channel was e.g. found in the 10 – 90 μ cake, in which in the centre iron oxide from the container had penetrated to a few centimetres above the filter, whereas in the rest of the cake no iron oxide could be detected.

The cake pressure, combined with the displacement of the cake during consolidation has a strong influence on the manometer tubes with the non-resilient quartz cake. A photograph of the six 4 cm tubes is given in Fig. 12 after the experiments with the 0 – 90 μ quartz flour had been taken. As the cake pressure increases from top to bottom, it is not surprising that the force exerted on the tubes and therefore their distortion will show a maximum near the middle of the cake, that is for tube M_4, as found.

Discussion. Both low and high cake pressures result in a decrease of ϕ_v with time of flow, after a period of uncertainty in the beginning. The decrease in ϕ_v is less if the cake has already been consolidated beforehand. Consolidation is larger if the pressure and the rate of flow are increased.

If a cake has been consolidated at a certain maximum pressure difference the cake is stable at pressures below this value, is however unstable for higher pressures at which a further consolidation occurs.

There appears to be a time lag with regard to the effect of flow rate and pressure difference. The time necessary to reach equilibrium is shorter if the cake is more consolidated.

The liquid pressure distribution in the cake and the porosity measurements demonstrate that the layers of the cake near the filter of the consolidated cakes, which have been subjected to the highest cake pressures, show the greatest resistance against flow. It has also been found that it is indeed the cake and not the filter which causes this high resistance. For norit, also in a more consolidated state curved $\phi_v - \Delta P$ lines have been found; for quartz and calcium carbonate already in an early stage of consolidation, straight lines, passing the origin, have been obtained. This proves that norit forms a reversible compressible cake.

In layers parallel to the filter the consolidated cakes are not homogeneous, as has clearly been shown for quartz and especially for norit.
The influence of pulsation of a cake seems to depend on the size spectrum. If many small particles were present, pulsation caused a consolidation.

B. *The Homogeneity of a Cake*

Indications on the inhomogeneity of cakes have been obtained by percolation experiments of cakes with a solution of potassium permanganate, and from visual observation of the surface of cakes during periods of percolation and periods of rest.

Experimental results. Cakes from different substances always kept under water varying in thickness from 2 – 30 cm and of quite different origin as far as the treatment to which they had been subjected is concerned (percolation for long and short periods of time, at low and at high pressures), have been percolated with a potassium permanganate solution until colour appeared in the filtrate.

Thereafter the flow pattern was studied by carefully pealing off the cake layer by layer parallel to the filter and comparing the coloured and not coloured patches.

The percolation time was 15 min at a maximum, so displacement by diffusion can be neglected.

It was found in all cases that only part of the cake was coloured, showing marked preference regions of flow of a rather erratic nature. In most cases a wall effect was observed. No essential difference could be found between cakes formed by sedimentation or by filtration nor between cakes consolidated at low or high pressures, although the cakes brought in by filtration showed a somewhat more regular flow pattern.

Another phenomenon was obtained by visual observation of cakes during flow. As an example one experiment will be described, which is

qualitatively typical of the phenomena encountered.

A cake of calcium carbonate (2–3 cm thick) was formed in the apparatus of Fig. 2 and percolated with water. If the flow was interrupted for a few hours, at the end of that period a star shaped crack had appeared in the centre. If flow was then resumed again, the crack slowly filled up and either a new crack appeared about 1 cm from the wall, or—diminishing from the top of the cake to the filter—the cake detached itself from the wall.

When the flow was again interrupted for some time, the original crack reappeared, the crack near the wall, if present, disappeared. This could be repeated several times. If air is trapped under the filter the effect is intensified.

No appreciable difference in porosity measured from 1 cm^3 samples was found between places near the wall and in the centre of the cake.

Discussion. If in view of the magnitude of the observed phenomena and of the system used a homogeneous cake will be defined as a cake in which each volume-element of $\sim 0{\cdot}1$ cm^3 contains an equal number of particles. It must be concluded from the experiments given that a cake in general is inhomogeneous, also in the direction perpendicular to flow.

The crack formation as described for rather thin cakes, is caused by the consolidation effect described in the preceding paragraph. If a cake is inhomogeneous the velocity of flow and the resulting cake pressure will not be the same in each part, causing local consolidation at the cost of other parts, which may result in the formation of cracks or channels.

Conclusions

From the results and the discussions presented in the foregoing paragraphs the following qualitative conclusions can be drawn. A cake formed by sedimentation or by filtration in or perpendicular to the direction of flow is not homogeneous.

Each newly formed cake will be built up in such a way that it is more or less far removed from the state of the densest packing possible. Therefore any cake has the possibility to depart from its original type of packing to a more denser packing. The magnitude of the change in density can be more or less pronounced, depending on the size and size spectrum of the substance, on the form of the particles, on the lubricating action of the fluids and on the magnitude of the cake-pressure, and of the stabilizing forces caused by flow; it is always present nevertheless. Therefore every newly formed cake will consolidate and is compressible. In the literature a compressible cake has been defined as a cake in which the porosity depends on the cake pressure. In view of the foregoing it is necessary to distinguish compressibility from consolidation; who both cause a smaller porosity. Cake compressibility will be defined as a reversible influence of the cake pressure on the porosity of the cake. The cake returns to its original higher porosity as soon as the cake pressure is released. Consolidation is a permanent decrease in porosity.

Consolidation in principle will set in immediately after the cake has been formed, it is accelerated by flow and the resulting cake pressure. Consolidation increases with cake pressure. It may also be accelerated by a change in the relative magnitude of the cake pressures and of the stabilizing forces caused by flow.

Consolidation may also be caused by disturbance of the state of equilibrium established between cake and liquid under the conditions of flow chosen, e.g. by pulsating of the pressure or by mechanical vibrations.

The more a cake is homogeneous, the more consolidation will occur homogeneous in the layers perpendicular to the direction of flow. In inhomogeneous cakes as discussed, consolidation will occur locally, owing to an unequal distribution of flow and of the cake pressures. Consolidation in the beginning will increase the inhomogeneity. Therefore the decrease in volume of the cake caused by consolidation will not always cause a decrease in height of the cake alone, cracks may be formed, the cake can detach itself from the wall.

In other words the displacement of the particles will not always be in the direction of flow. Moreover this displacement is local. Again it is not necessary that consolidation results in the beginning in an increase of the overall packing

VOL.
7
1957/58

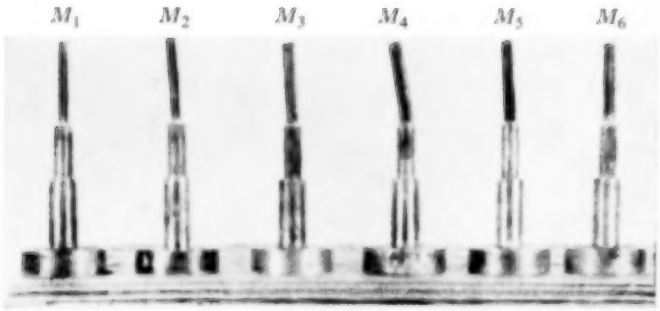

FIG. 12. The distortion of the manometer tubes.

density of the cake. It is possible that increase in overall permeability occurs e.g. because the influence of consolidation in the denser parts will be overruled by the increase in porosity in the less dense parts.

If the influence of the filter is not very strong, the overall permeability will decrease with time for relatively thick cakes. The inhomogeneity of the cake, formed even when homogeneous slurries are filtered, must partly be attributed to the inhomogeneous flow through the filter. It will therefore be a function of the type of filter, of the regularity of the weave pattern, the amount of pores per unit of surface, regularity of the distribution and of the pore size distribution. Consolidation proper may often be preceeded by a temporarily elastic displacement of the particles.

The qualitative conclusions drawn permit to say that it is necessary to enlarge the knowledge on the inhomogneity and instability of cakes by a more systematic investigation. The somewhat confusing multitude of effects have to be broken down in a simpler pattern and each effect studied separately.

Nomenclature

ΔP = pressure difference over the cake and the filter (atm)

ϵ = porosity of the cake, volume of liquid on total volume of liquid + solid substance (no dimension)

ϕ_v = overall flow rate through cake (1/hr)

VOL. 7 1957/58

References

[1] Harting P. *Verhandel. Koninklijk. Akad. Ned. Wetenschap. Afdeel. Natuurk.* (2e reeks) Vol. 13, p. 228, 1878 In Dutch.

[2] Terzaghi K. and Peck R. B. *Soil Mechanics in Engineering Practice.* John Wiley, New York, 1948.

[3] Forchheimer Ph. Z. *Ver. Disch. Ing.* 1901 **45** No. 2, 1786.

[4] Duwes P. and Zwell L. *J. Metals* 1947 **1** 137.

[5] Businger J. A. *Ingenieur* 1956 **68** *O.* 87.

[6] Rietema K. Thesis, Delft, 1952.

[7] Tiller F. M. *Chem. Engng. Progr.* 1953 **49** 467.

[8] Eisenklam P. *Chemical Engineering Practice* Vol. II. Chap. 9. p. 342. Buttersworth, London, 1956; see also Dallavalle J. M. *Micromeretics* (Second Impression) Pitman, New York, 1948.

Chemical Engineering Science, 1957, Vol. 7, pp. 26 to 39. Pergamon Press Ltd.

Absorption of carbon dioxide in water under pressure using a gas-bubble column

G. Houghton, A. M. McLean and P. D. Ritchie

Technical Chemistry Department, Royal College of Science and Technology, Glasgow, C.1.

(*Received* 3 *September* 1956)

Abstract—A bubble-type water scrubber has been studied with special reference to the absorption of large quantities of carbon dioxide from gas mixtures consisting mainly of this substance. The effect of various operating variables has been determined ; and it is shown that this type of scrubber is superior to the packed-tower type.

Résumé—Les auteurs ont étudié un laveur à eau à barbottage pour l'absorption de grandes quantités de CO_2 dans des mélanges de gaz en contenant une grande partie. Ils ont déterminé l'effet de différentes variables dans les expériences. Ils ont montré que le type de laveur est supérieur à la colonne à garnissage.

Zusammenfassung—Ein Gaswäscher von Blasentyp wurde unter besonderer Berücksichtigung der Absorption grosser CO_2-Mengen aus einem Gasgemisch hoger CO_2-Konzentration untersucht. Die Wirkung der verschiedenen Veränderlichen wurde bestimmt ; es zeigte sich, dass dieser Gaswäschertyp dem Füllkörperturm überlegen ist.

Introduction

Various industrial processes give rise to gaseous mixtures containing up to *ca.* 90 per cent of carbon dioxide ; and much work has been done on the removal of the carbon dioxide, leading to the recovery of the often more valuable minor components. There are several possible methods for removing carbon dioxide from such mixtures:

(a) Absorption in caustic alkali or ammonia to form the carbonates or bicarbonates ;

(b) Absorption in a base such as ethanolamine, followed by regeneration of the base ;

(c) Absorption in water.

Water scrubbing of such mixtures presents interesting possibilities, especially at pressures greater than atmospheric. Increase in pressure decreases the amount of scrubbing water required, and reduces the volume of gas handled, which is especially important on the large scale, since it will decrease the dimensions of the absorber, possibly to a size comparable with or less than that of a chemical scrubber. Consequently, the relative advantages of water and chemical absorption are closely linked with the relative costs of the gas compression in case (c), as compared with the cost and availability of caustic alkali or ammonia solutions, in case (a), and the cost of heat for the regeneration of ethanolamine, in case (b).

Carbon dioxide is moderately soluble (1 ft^3 at n.t.p. per ft^3 water at 15°C) and most evidence indicates that its rate of absorption in water is controlled by the liquid-film resistance. It might therefore be expected that bubble-type absorbers would here be more efficient than spray or packed towers ; for, as the bubbles rise, the liquid-film around them is continually renewed by flow of liquid over the bubble surface, from front to back. Shulman and Molstad [1] investigated the rates of absorption and desorption of carbon dioxide and hydrogen from water in a bubble-type absorber, and concluded that bubble columns are superior to spray and packed towers where high liquid-rates are required, and where the liquid-film resistance controls. However, most of their experiments were at atmospheric pressures, and were largely concerned with desorption. In addition, the gases contained only small percentages of carbon dioxide, so that gas velocity did not change appreciably during absorption or desorption.

The absorption of carbon dioxide in water by a bubble-type absorber under pressure has been discussed by Howard [2] ; the carbon dioxide content of a burner gas was here reduced from 12 per cent to 1 per cent by absorption in water at 75 lb/in^2 gauge. The water was

VOL. 7 1957/58

regenerated under vacuum at 27·5 in. of mercury. For this particular burner gas, HOWARD used three bubble-type absorbers in series to accomplish the stripping, and concluded that a continuous bubble-type ethanolamine scrubber was preferable to water scrubbing.

Very little work has been published on the effect of pressure on the rate of absorption of carbon dioxide in water, or on the rate of absorption from concentrated mixtures, where the gas velocities change considerably and the operating line is curved. For the present work a counter-current bubble-type absorber has been designed suitable for high pressures and concentrations of carbon dioxide. The results are of direct theoretical and practical importance in the design of large-scale carbon dioxide scrubbers using water.

EQUIPMENT AND OPERATION

The equipment (Fig. 1) consisted essentially of an absorber column (3 in. nominal-bore class *C* pipe, 8 ft long and flanged at both ends) provided with sight-glasses, and with ten pet-cocks for removing liquid samples at various heights. The completed column was pressure-tested to 1,200 lb/in^2 gauge. Water (from the Glasgow city water-mains) was pumped in at the top from a 300 gal storage tank by a treble-cylinder plunger pump capable of delivering 6 gal/min of water at pressures up to 450 lb/in^2 gauge. The flow rate could be continuously adjusted during operations; the exit-water rate from the column was measured by a rotameter.

Carbon dioxide was generated from a "Penguin" liquefier; and after mixing it with nitrogen (from a cylinder), the gas stream was forced into the base of the column via some type of gas distributor. Both gases were metered through orifices obtained by drilling small holes (diam. *ca.* 0·063 in.) through brass blocks. Bourdon gauges at each end of the block gave the pressure drop corresponding to the desired flow rate; different flow ranges could be obtained by partially filling the orifices with wires of various diameters. Before and after each run the orifices were calibrated by by-passing the gas stream to a dry gas-meter to measure the flow rates at atmospheric pressure. The same meter measured the exit-gas rate from the column after absorption, so that all gas-flow rates were obtained on the same basis. A preheater on the carbon dioxide line prevented freezing in the orifice. The inlet-gas compositions normally used were in the range 80–90 per cent carbon dioxide, the rest being nitrogen.

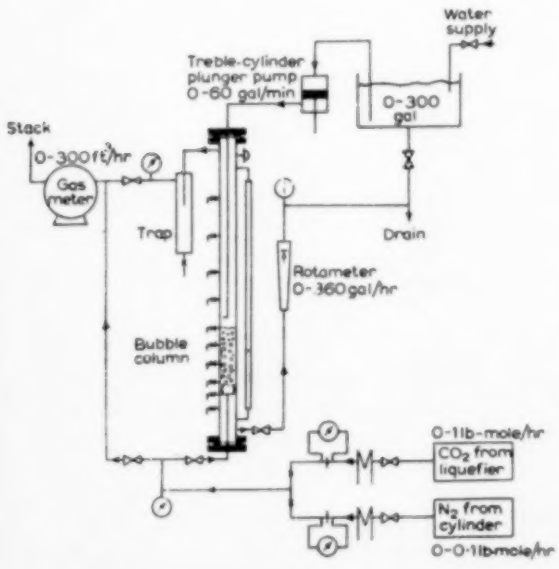

FIG. 1. Diagram of equipment.

The absorber pressure could be adjusted within the range 10–450 lb/in^2 by throttling back the exit-gas and water valves, while keeping the liquid level in the sight-glass constant. During operations, there was a small pressure drop (5–10 lb/in^2) across the bubble or gas distributor.

When the plant had reached steady state, the exit-gas rate after absorption was measured on the gas meter. Samples of inlet and exit gas were analysed in a Macfarlane gas-analysis unit. Samples of the liquid phase could be taken from the column at various levels by using the pet-cocks. The procedure was to release a known volume of sample under a measured volume of standard caustic soda solution; the carbon dioxide in the sample was then obtained by measuring the carbonate content of the caustic solution. By analysing the inlet water for carbon dioxide, a complete material balance, based on carbon dioxide, was obtained. The accuracy of the procedure is confirmed by the consistency of the material balances (average 99·4 per cent for 50 runs; average deviation 1·3 per cent).

A trap was included in the exit line to collect any moisture carried over; but in practice the exit-gas velocities were so small (0·012–0·12 ft/sec) that no liquid was ever collected.

GAS DISTRIBUTORS

The main type of gas distributor used was a sintered-bronze porous disc in a cylindrical holder. Its porosity was measured by determining the pressure drop across each disc under water at various gas-flows, and extrapolating to give the back pressure at zero-flow. This pressure drop is then equal to the maximum bubble-pressure required for the formation of single bubbles: and the average pore-diameter is then calculated from the expression:

$$d = 4\gamma'/\Delta P_0 \qquad (1)$$

(γ' = surface tension of liquid;
ΔP_0 = maximum bubble pressure at zero gas-flow).

Another type of gas distributor was constructed from indented nickel strip, 1 in. wide with indentations every

0·078 in. (2 mm) along its length on one side only. These strips were packed into a square brass holder, either with the indentations of alternate strips facing each other or alternatively with the indentations of one strip facing the plain surface of the next strip.

Table 1. *Properties of porous discs*

Distributor	*Thickness* (in.)	*Surface area* (ft^2)	*No. of holes*	*Porosity* (μ)
Fine bronze	0·123	0·0307	—	72
Medium bronze	0·126	0·0307	—	408
Coarse bronze	0·121	0·0307	—	634
Indented strip *A*	1·0	0·0214	441	1150
Indented strip *B*	1·0	0·0214	903	810

Table 1 summarizes the size and measured porosity of various distributors of the foregoing types. Other gas distributors investigated were an open pipe (i.d. $\frac{3}{4}$ in.) and a brass plate (area 0·030 ft^2) drilled with four holes (diam. $\frac{1}{4}$ in.).

Almost all the measurements on the effect of gas velocity, liquid velocity, pressure, bed height, and temperature were made using the finest of the sintered bronze discs.

Densities of "Fluidized Bubble-Beds"

The gas is bubbled counter-current to the liquid. At any instant the liquid holds a certain volume of gas, so that the density of the bubble-bed is less than that of pure water; hence, the liquid level registered by the sight-glass is always less than the bed level inside the column. To estimate the bed level inside the absorber, experiments were conducted in a glass column (diam. 3 in.) to find the bed levels inside the column at various sight-glass levels for different gas and liquid velocities. The locations of bubbler and sight-glass were the same in the glass unit as in the metal pressure-column.

Results for the fine porous disc are shown in Fig. 2. In calculating bed densities it has been assumed that liquid and gas velocities are so low that frictional and contractional effects can be neglected, so that bed density (ρ_B) is expressed by:

$$\rho_B = h_L \rho_L / h \qquad (2)$$

(h and h_L = bed and sight-glass heights, respectively, above surface of disc; ρ_L = density of water).

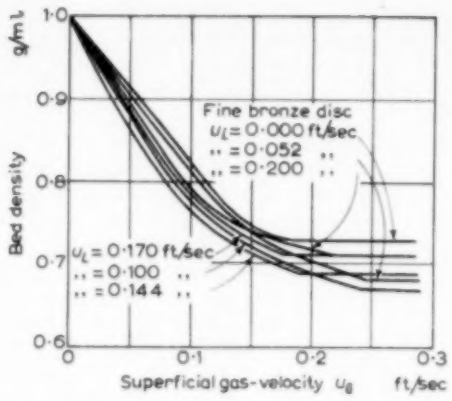

Fig. 2. Effect of liquid and gas velocities on bed density.

The results from the glass column were confirmed with the metal pressure-column (where the bed was not visible) under high pressure by using the pet-cocks to locate the bed level inside the unit.

The bed-density curves for the other types of gas distributor are not shown; but all curves show that bed density decreases with increase in gas velocity until an approximately constant average value is obtained. Similar characteristics are well known in the fluidization of solid particles by gases and liquids. At low gas-velocities the bubbles rise independently of one another; but as the velocity increases the bed becomes a turbulent mass of rising and recirculating bubbles. As the velocity is increased further, the bed reaches a point where large plugs of gas are formed, which cause the bed level to fluctuate about some mean value. In general, the curves show that the finer porous discs give the lower bed densities.

The effect of liquid velocity (Fig. 2) is to lower the bed density, presumably by reducing the terminal velocity of rise of bubbles in the bed, thus causing more bubbles to be held in suspension. However, increases in liquid velocity above 0·144 ft/sec seem to cause the bed density to increase again. This may be caused either by slight frictional or contractional effects across the bubbler, or by the effect of liquid velocity on the size or number of bubbles produced by the disc. However, at no point do the bed

densities at the higher liquid velocities differ by more than 10 per cent from the values for the stationary liquid. The accuracy of the bed levels computed from the bed-density curves is estimated to be about ± 2 per cent for gas velocities lower than 0·15 ft/sec and ± 5 per cent for higher velocities.

The effect of the properties of the liquid on the size and distribution of bubbles in fluidized and foam beds will be described in a further communication [3].

Carry-Over

Any given bubble will rise with a certain terminal velocity of rise in water; and if the water is given a downward velocity equal to the terminal velocity of rise, the bubble will remain stationary with respect to the column. Further increase in liquid velocity will carry the bubble in the same direction as the liquid. Hence, too great a liquid velocity will carry bubbles out of the exit-water pipe suspended in the water. Carry-over in the region of the bubbler may be caused by the sudden acceleration of the water in the annular space between the bubbler and the 3 in. pipe, an effect actually observed in the glass column. The overall effect of carry-over is an apparent loss of gas, revealed by a decrease in the material balance around the plant. This balance is based upon analytical determination of the carbon dioxide in the inlet and outlet streams and liquid. However, the liquid-sampling technique at the water outlet ignores the presence of suspended bubbles in the liquid stream. With no bubble "carry-over" the carbon dioxide balance around the plant should be close to 100 per cent; for operation of the plant without bubble "carry-over" the overall average material balance for 50 runs was 99·4 $\pm$ 1·3 per cent, possibly indicating some small consistent error in analytical technique. The effect of increased relative gas-liquid superficial velocity on the material balance is shown in Fig. 3. As the relative velocity is increased beyond 0·3 ft/sec there is a drop in the material balance corresponding to "carry-over". Hence, with the particular bubbler used, the sum of the superficial liquid and gas velocities should not exceed 0·3 ft/sec.

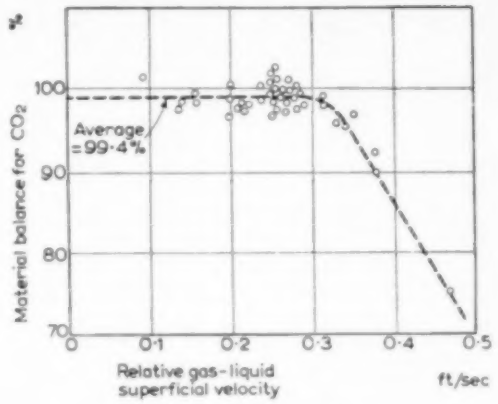

Fig. 3. Effect of carry-over.

Equilibrium Curve for Carbon Dioxide in Water

For calculating the mean driving forces it is necessary to have accurate values for the solubility of carbon dioxide in water over a wide range of temperatures and pressures. The present authors have summarized [4] the compressibility, fugacity, and water-solubility of carbon dioxide for pressures up to 36 atm and temperatures in the range 0-100°C. The equilibrium relationships are almost linear up to a partial pressure of 10 atm for carbon dioxide, and Henry's law is obeyed with a maximum deviation of about 10 per cent at 10 atm and at all temperatures in the range 0–100°C.

Operating Line

Since as much as 90 per cent of the carbon dioxide entering the plant may be absorbed, the composition of the gas in a typical run may change from (say) 85 per cent down to 30 per cent carbon dioxide. Consequently, the *operating line* may have a pronounced curvature, while the *equilibrium curve* may be almost straight. Operating lines for various changes in gas composition are plotted in Fig. 4. Inspection shows that the curvature becomes less pronounced as the change in gas composition between inlet and outlet becomes smaller. It was therefore decided to determine the point at which the curvature of the operating line was so small that the logarithmic mean concentration-gradient could be used to calculate

VOL. 7 1957/58

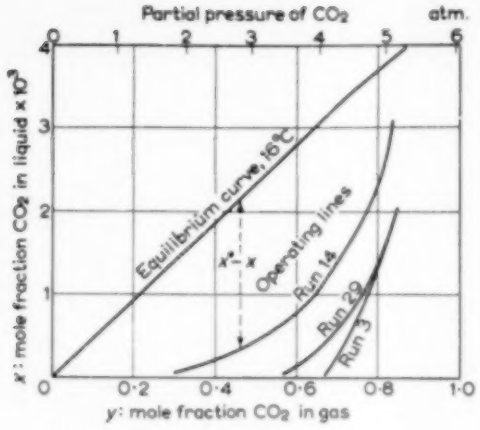

FIG. 4. Operating lines.

the $(H.T.U.)_{OL}$ and K_La values. In addition the method of CAREY and WILLIAMSON [5] was investigated; this allows for the curvature of the operating line by determining the driving force midway between the inlet and outlet liquid compositions and then correcting the arithmetic mean driving force, based on the inlet and outlet compositions, for the much larger driving force in the middle. Comparison of the logarithmic mean driving force, the driving force obtained by the CAREY and WILLIAMSON method, and the driving force obtained by graphical integration is shown in Table 2. The results are expressed for convenience in terms of the number of transfer units.

A comparison of the CAREY and WILLIAMSON method with the graphical integration method shows that the two agree within a maximum deviation of better than 4 per cent. The logarithmic mean driving force deviates from the driving force calculated by graphical integration by less than 4 per cent, 8 per cent and 16 per cent for gas-composition changes less than 18 per cent, 28 per cent and 40 per cent respectively. (The change in gas composition is here merely the difference in composition between the inlet and outlet gas.) As a result of the comparisons in Table 2, the logarithmic mean driving force was used for gas-composition changes less than 18 per cent, the CAREY and WILLIAMSON three-point method for composition changes less than 40 per cent and greater than 18 per cent, and graphical integration for all composition changes greater than 40 per cent.

It must be pointed out that in the computation of mean driving forces it is assumed that a fluidized bubble-bed operates under true counter-current conditions. It is shown later (Fig. 12) that in actual practice the liquid may be completely mixed for distances up to 1·5 ft from the gas inlet. Hence, the mean concentration gradient computed from the inlet and outlet liquid concentrations may be higher than that obtained in practice.

Table 2. Calculation of $(N.T.U.)_{OL}$

Inlet velocity (ft/sec)		*Gas composition* (per cent CO_2)		$(N.T.U.)_{OL}$				
				Graphical integration	*Log mean*		*Three-point method* [5]	
Gas	*Liquid*	*In*	*Out*		$(N.T.U.)_{OL}$	*dev.* (per cent)	$(N.T.U.)_{OL}$	*dev.* (per cent)
0·116	0·144	84·3	67·7	0·607	0·626	+ 3·1	0·607	0
0·119	0·142	83·7	28·9	2·070	3·250	+ 57	2·04	− 1·5
0·062	0·153	77·5	22·8	0·591	0·780	+ 32	0·614	+ 3·9
0·075	0·170	82·8	38·0	0·614	0·723	+ 7·8	0·609	− 0·8
0·110	0·170	84·8	56·8	0·809	0·870	+ 7·5	0·811	+ 0·3
0·082	0·200	84·5	45·1	0·534	0·619	+ 16	0·539	+ 0·9
0·116	0·200	83·9	42·1	0·811	0·925	+ 14	0·782	− 3·6

VOL. 7 1957/58

Expression of Absorption Rates

Absorption rates can be expressed by an overall absorption efficiency E_A based on the inlet gas (equation 3), by an overall efficiency E'_A based on the outlet gas (equation 4), by the $(H.T.U.)_{OL}$ (equation 5), or by the K_La concept (equation 6), thus :

$$E_A = \frac{x_2 - x_1}{x_2^{\bullet} - x_1} \tag{3}$$

$$E'_A = \frac{x_2 - x_1}{x_1^{\bullet} - x_1} \tag{4}$$

$$(H.T.U.)_{OL} = h/(N.T.U.)_{OL} \tag{5}$$

$$K_La = B/hA \,.\, \Delta x_M \tag{6}$$

However, it must be noted that the gas velocity through the unit may change considerably, since as much as 90 per cent of the incoming carbon dioxide may be absorbed. For instance, in a typical run where 80 per cent of the incoming gas was absorbed, the inlet superficial gas velocity was 0·11 ft/sec and the outlet gas velocity only 0·044 ft/sec. Consequently, the values of $(H.T.U.)_{OL}$ and K_La calculated from equations (5) and (6) are overall average values, since the corresponding instantaneous values at any point in the column may vary considerably from the inlet to the outlet.

The overall absorption efficiencies E_A and E'_A have advantages over the $(H.T.U.)_{OL}$ and K_La concepts for correlating the data from counter-current bubble-absorption plants where large amounts of gas are absorbed. E_A is more convenient in design calculations, since it avoids the computation of mean concentration gradients by graphical integration, or by the three-point method [5]. In addition, E_A can be used directly in calculating the power requirements for pressure absorbers ; in this respect, it is more useful than E'_A since the latter may have values considerably greater than 100 per cent for counter-current operations.

It is important to realise that absorption from rising bubbles is a complex physical phenomenon, and that the rate coefficients E_A, $(H.T.U.)_{OL}$, and K_La are more in the nature of empirical correlation variables than rate constants of exact physical significance. These rate constants by themselves may have very little practical significance, since high absorption-rates do not necessarily indicate high absorption ; on the contrary, exceedingly high absorption rates may occur under conditions where very little material is absorbed. The designer of absorption equipment is more often faced with the problem of attaining a practical operating condition, where high rates of absorption are coupled with large amounts of material absorbed by the plant.

Effects of Superficial Gas and Liquid Velocities on E_A

To determine the effect of superficial velocities on the absorption efficiency, experiments were conducted under conditions of constant bed height, inlet partial pressure of carbon dioxide, total absorber pressure, and temperature. An attempt was made to hold the bed height constant at 1·5 ft for the various runs, in spite of changes (due to absorption) in the velocity of the gas through the bed. After a period of steady-state operation the inlet and outlet gas-velocities were obtained from the flowmeters. The bed density, and the corresponding sight-glass level required to give a bed height of 1·5 ft, could then be computed at the average of the inlet and outlet gas-velocities, using the experimental data for the glass column (Fig. 2). Bed levels at various sight-glass levels, calculated thus, could also be checked by locating the gas-liquid interface by means of the pet-cocks. Errors in computing the bed level by this procedure are probably less than $\pm$ 10 per cent. Further, it will be shown later that the absorption efficiency E_A is relatively insensitive to changes in bed height, being proportional to the cube root of bed height ; hence a 10 per cent change in bed level will affect the absorption efficiency by only about 3 per cent. A plot of E_A vs. inlet superficial gas-velocity (u_G) is shown in Fig. 5, using the superficial liquid-velocity as a parameter. The results are corrected to an inlet partial pressure of carbon dioxide of 75 lb/in^2 abs., a bed height of 1·5 ft, and a temperature of 15°C. Since the gas velocity changes considerably as absorption proceeds it is difficult to decide whether the inlet, outlet, or average gas velocities should be used

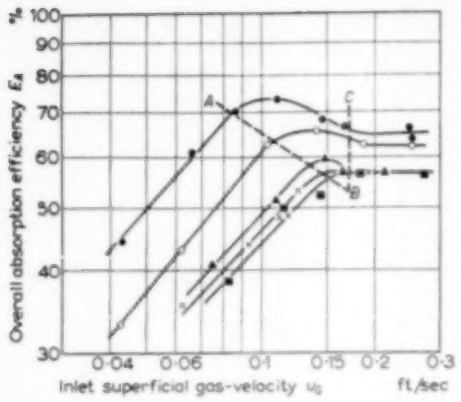

FIG. 5. Effect of liquid and gas velocities on absorption efficiency.

(Temp. 15°; partial pressure of CO_2 75 lb/in^2 abs; bed height 1·5 ft; fine porous disc.)

Liquid velocity
- ● u_L = 0·052 ft/sec
- ○ = 0·100
- × = 0·144
- ▲ = 0·170
- ■ = 0·200

to correlate the data; consequently, the data were plotted using each of the variables separately. The inlet and average superficial gas velocities correlated the data equally well; it was decided to use the inlet superficial gas-velocity as the correlating variable since it is more convenient for design purposes.

At constant liquid-velocity the absorption efficiency increases with rising gas-velocity until a constant absorption-efficiency is obtained, independent of further increase in gas velocity. At the lower liquid velocities, 0·052 and 0·100 ft/sec, the absorption efficiency rises to a maximum before reaching a constant value. In all cases, a constant absorption-efficiency is attained at $u_G > 0{\cdot}17$ ft/sec. An explanation of this phenomenon can be obtained by referring to Fig. 2. It will be noted that the bed density decreases to a constant value at a gas velocity of about 0·17 ft/sec, so that the initial rise in absorption efficiency with gas velocity is probably due to an increase in the amount of gas in the bed, absorption efficiency becoming constant when bed density becomes constant. Experiments to be presented in a later communication [3] show that the average bubble-volume in the bed does not change much with gas velocity, but that as the latter increases the number of bubbles per unit volume of bed increases. The initial rise of absorption efficiency with gas velocity can therefore be explained as an increase in gas hold-up, which increases the surface area for absorption. Hence, the region where absorption efficiency increases with gas velocity will be referred to as the "rising hold-up" region; the region where efficiency becomes independent of velocity will be termed the "constant hold-up" region. Between the two there is a "transition" region. In the rising hold-up region, and at constant liquid velocity, the absorption efficiency is proportional to $u_G^{0{\cdot}61}$.

The effect of liquid velocity is also illustrated by Fig. 5. At constant gas velocity the effect of increasing the liquid velocity is to decrease the absorption efficiency up to a liquid velocity of 0·144 ft/sec. At this point further increases in liquid velocity up to 0·200 ft/sec have a relatively small effect upon the absorption efficiency, particularly in the constant hold-up region. No particular significance can be attached to the fact that in Fig. 5 the curve for $u_L = 0{\cdot}170$ ft/sec is higher than those for $u_L = 0{\cdot}144$ ft/sec and $u_L = 0{\cdot}200$ ft/sec in the rising hold-up region. This small difference is most probably due to experimental errors (particularly in computing bed level) although it is possible that the liquid velocities within the range 0·144–0·200 ft/sec constitute a transition region where absorption efficiency depends upon the flow pattern developed in the bubble bed. In the rising hold-up region, absorption efficiency is directly proportional to $u_L^{-0{\cdot}48}$; in the constant hold-up region, it is proportional to $u_L^{-0{\cdot}15}$ at constant gas-velocities.

Fig. 6 shows the effect of liquid velocity in both the rising and constant hold-up regions. Liquid velocity has a greater effect upon absorption efficiency in the former than in the latter region.

Figs. 7 and 8 show the effect of liquid and gas velocities on the average K_La and $(H.T.U.)_{OL}$ values. The rising and the constant hold-up regions are also apparent in the plot of these

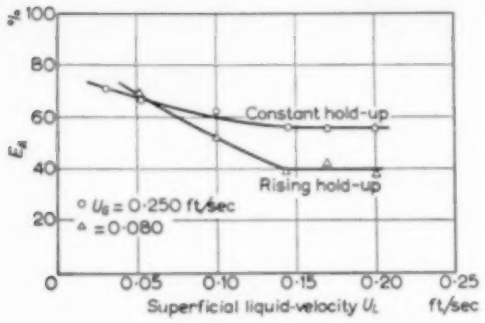

FIG. 6. Effect of liquid velocity.
(Temp. 15°; partial pressure of CO_2 75 lb/in² abs; bed height 1·5 ft; fine porous disc.)

variables, as is the relatively small effect of liquid velocity on absorption coefficient where $U_L > 0{\cdot}144$ ft/sec. This latter effect has been noticed in packed towers by VAN ARSDEL [6], who found that an increase in liquid velocity

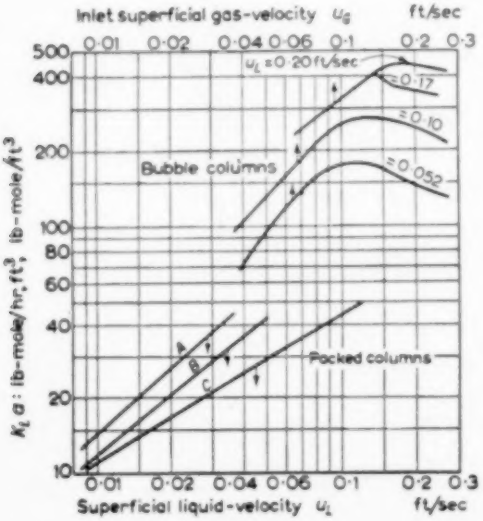

FIG. 7. $K_L a$ for packed and bubble columns.
Curve *A* after SIMMONS and OSBORN [8]. 0·73 in. glass balls; u_G 0·018–0·1 ft/sec CO_2.
Curve *B* after ADAMS and EDMONDS [9]. 1 in. coke; u_G 0·17–0·42 ft/sec CO_2
Curve *C* after CANTELO, SIMMONS, GILES and BRILL [10]. Small glass rings; u_G 0·036 ft/sec CO_2
Bubble column: Present data
Bed height = 1·5 ft
CO_2 pressure = 5·1 atm
Temperature = 15°C

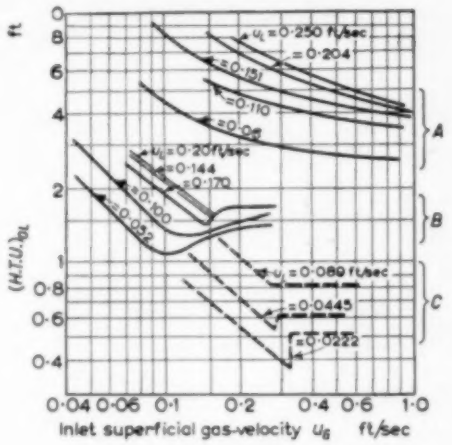

FIG. 8. $(H.T.U.)_{OL}$ for packed and bubble columns.
Curves *A* after COOPER, CHRISTL and PEERY [11]. Packed column, 2 in. steel rings; temp. 18°; pressure of CO_2 1 atm.
Curves *B* from present work. Bubble column; temp. 15°; pressure of CO_2 5·1 atm; bed height 1·5 ft.
Curves *C* after SHULMAN and MOLSTAD [1]. Bubble column; temp. 15°; total pressure 1 atm; bed height 1·0 ft.

relative to gas flow caused an increase in absorption coefficient until a critical velocity was reached, after which further increases had little effect.

EFFECT OF BED HEIGHT

The effect of bed height on absorption efficiency was investigated by holding all other variables constant. Fig. 9 illustrates the effect of bed height on E_A, $(H.T.U.)_{OL}$, and average $K_L a$ when the partial pressure of carbon dioxide is 75 lb/in² abs. and the temperature is 15°C, at various liquid and gas velocities.

In the rising hold-up region the overall absorption efficiency is proportional to $h^{0{\cdot}33}$, while in the constant hold-up region the efficiency is proportional to $h^{0{\cdot}22}$ for bed heights between 0·4 and 5·5 ft. However, each plot of E_A vs. bed height exhibits a slight curvature, attributed to the effect of the ratio of bed height to column diameter at large bed heights.

Change in bed height increases the average $(H.T.U.)_{OL}$ proportionally to $h^{0{\cdot}5}$ in the rising hold-up region and to $h^{0{\cdot}64}$ in the constant hold-up region.

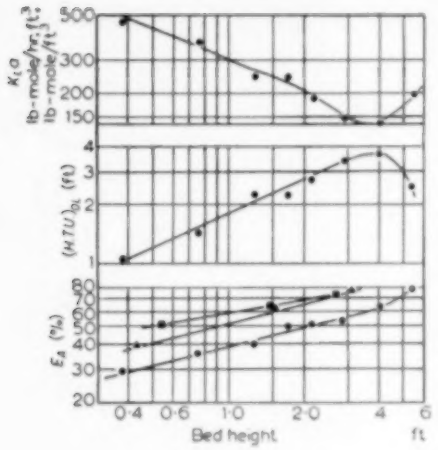

FIG. 9. Effect of bed height.
(Temp. 15°; partial pressure of CO_2 75 lb/in² abs.; fine porous disc).
● u_L 0·144 ft/sec, u_G 0·106 ft/sec;
▲ u_L 0·052 ft/sec, u_G 0·065 ft/sec;
■ u_L 0·052 ft/sec, u_G 0·253 ft/sec).

Average $K_L a$ decreases with increase in bed height according to $h^{-0.5}$ in the rising hold-up region, and to $h^{-0.37}$ in the constant hold-up region. However, at bed heights greater than 4·0 ft, an increase in average $K_L a$ and a corresponding decrease in average $(H.T.U.)_{OL}$ are observed, indicating that for long columns (i.e. almost complete absorption) there is a region at the top which does not behave as a fluidized bed. In this region it might be expected that the residual bubbles are so small that they rise independently with very little recirculation.

EFFECT OF TOTAL PRESSURE

Total pressure was investigated by making measurements at constant bed height and temperature. The results (Fig. 10) are corrected to a bed height of 1·5 ft and a temperature of 15°C. The effect of pressure on the overall absorption efficiency is the same in both rising and constant hold-up regions, and is virtually independent of gas and liquid velocities over the ranges studied. For inlet partial pressures of carbon dioxide in the range 2·5–14·0 atm. the absorption efficiency is proportional to $p^{-0.33}$.

In the rising hold-up region, average $K_L a$

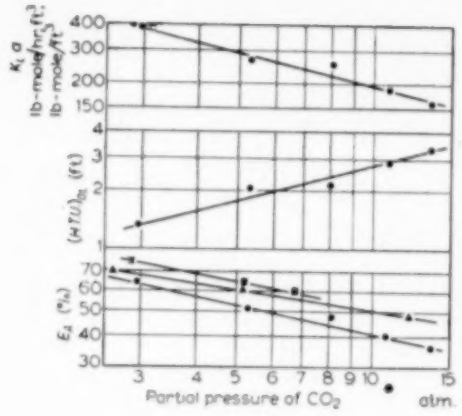

FIG. 10. Effect of pressure.
(Temp. 15°; bed height 1·5 ft; fine porous disc.)
● u_L 0·144 ft/sec, u_G 0·113 ft/sec;
▲ u_L 0·052 ft/sec, u_G 0·063 ft/sec;
■ u_L 0·052 ft/sec, u_G 0·248 ft/sec).

decreases with increasing partial pressure of carbon dioxide according to $p^{-0.5}$, while in the constant hold-up region the effect of pressure is much greater, being proportional to $p^{-1.4}$.

The average $(H.T.U.)_{OL}$ was found to be proportional to $p^{0.5}$ in the rising hold-up region and $p^{0.68}$ in the constant hold-up region.

EFFECT OF TEMPERATURE

The effect of temperature on E_A, average $(H.T.U.)_{OL}$, and average $K_L a$ is shown in Fig. 11. They are corrected to a bed height of 1·5 ft and an inlet partial-pressure of carbon dioxide of 75lb/in² abs.

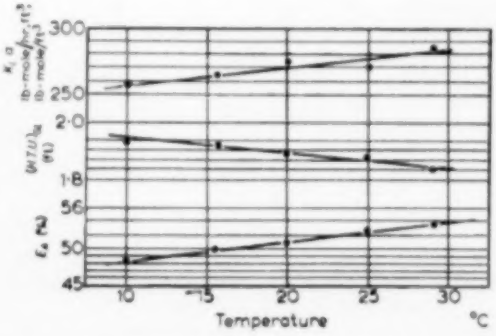

FIG. 11. Effect of temperature.
(Bed height 1·5 ft; partial pressure of CO_2 75 lb/in² abs.; u_L 0·144 ft/sec; u_G 0·127 ft/sec; fine porous disc.)

VOL. 7 957/58

The effect of temperature is to increase the absorption rate in both the rising and constant hold-up regions. However, the effect is slight, being proportional to $t^{0.1}$ for E_A and $t^{-0.1}$ for average $(H.T.U.)_{OL}$ in both regions, for temperatures in the range 10–30°C. The temperature effect is independent of gas and liquid velocities in both regions. Temperature has a slightly greater effect on K_La, since the exponent of t was found to be 0·15 for both regions.

General Correlation Equations

For the rising hold-up region the overall absorption efficiency is given with an average deviation of ± 6 per cent from the experimental value by the equation :

$$E_A = 0{\cdot}86 \cdot \frac{u_G^{0.61}}{u_L^{0.48}} \cdot \frac{h^{0.33}\, t^{0.1}}{p^{0.33}} \qquad (7)$$

Equation (7) can be used for superficial liquid-velocities in the range 0·052–0·200 ft/sec, superficial gas-velocities in the range 0·04–0·15 ft/sec, bed heights in the range 0·4–5·5 ft, partial pressures of carbon dioxide from 2·5 to 14·0 atm, and temperatures in the range 10–30°C.

Equation (7) can be used only if the calculated value of E_A does not exceed the value of E_A calculated from the equation below :

$$E_A = \frac{0{\cdot}30}{u_G^{0.40}} \cdot \frac{h^{0.33}\, t^{0.1}}{p^{0.33}} \qquad (8)$$

Equation (8) defines the limits of the rising hold-up region and is the equation of the broken line AB shown in Fig. 5 for varying bed height, temperature, and partial pressure of carbon dioxide.

For the constant hold-up region the absorption efficiency is independent of the superficial gas velocity and is given by the equation :

$$E_A = \frac{0{\cdot}52}{u_L^{0.15}} \cdot \frac{h^{0.22}\, t^{0.1}}{p^{0.33}} \qquad (9)$$

Equation (9) gives values of E_A with an average deviation of ± 4·0 per cent from experimental values, and applies to all liquid velocities in the range 0·030–0·200 ft/sec, and to all gas velocities greater than 0·17 ft/sec (i.e., for all gas velocities to the right of the vertical line BC in Fig. 5).

For the transition region the absorption efficiency is best obtained by using equation (9), which gives calculated values of E_A within ± 5 per cent of the experimental results.

Equations (7) and (9) show that the absorption efficiency can be made to approach 100 per cent by increasing the bed height or by decreasing the pressure. Obviously, absorption efficiencies of 100 per cent or greater are impossible ; and where values above 100 per cent are calculated from equations (7) and (9) it may be assumed that the water leaving the absorber is almost saturated at the partial pressure of carbon dioxide in the incoming gas.

Concentration Gradients in Fluidized Beds

Concentration changes through the bubble-bed were determined by analysing liquid samples taken at various distances above the gas distributor. The results (Fig. 12) indicate that there

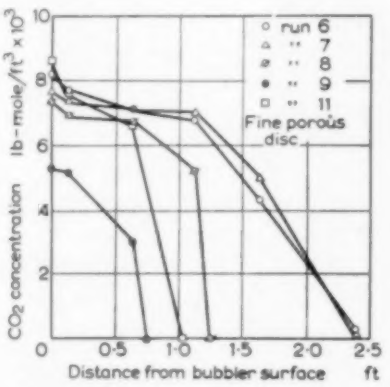

Fig. 12. Concentration gradients.

are three concentration regions in a fluidized bubble-bed :

(a) *A region of about* 1·5 in. *close to the distributor, where there is a sharp drop in concentration.* A similar end effect has been discussed by Geankoplis and Hixon [7] for a countercurrent spray-type extraction column.

(b) *A region of about* 1 ft *above the distributor, where the concentration does not change much with distance.* This region probably corresponds to the completely fluidized region where the bubbles and liquid are continually recirculated in the direction of flow. This will result in complete mixing and a liquid of uniform composition.

(c) *A region where the gas leaves and the water enters, where there is a sharp change in concentration.* This may be caused by a stratified layer of water which has not been mixed into the fluidized region. In addition, the bubble size may be reduced, as absorption proceeds, to a point where the bubbles rise independently of each other without recirculation, so that this region of the bed is no longer fluidized. This non-fluidized region would lead to the development of a concentration gradient in the liquid, particularly at large bed heights. This sharp break in concentration is observed for bed heights of about 1·5 ft or less, but for heights greater than this the concentration change is not so sharp though still quite steep.

EFFECT OF PLATE POROSITY

To ascertain the effect of plate porosity, measurements were made of E_A, average $(H.T.U.)_{OL}$, and average K_La (using seven different gas distributors with widely differing porosities) at constant liquid and gas velocities, and the results corrected to a bed height of 1·5 ft, a partial pressure of carbon dioxide 75 lb/in^2 abs., and a temperature of 15°C.

The results (Table 3) show no significant effect of porosity up to average pore diameters of 3180 μ. The results for the two arrangements of indented strip are identical, even though one arrangement has more than twice as many holes per unit area as the other. The results from the indented strip are identical with those from the porous disc, even though the area of the former was only 0·0214 ft^2 as compared to 0·0307 ft^2 for the latter, indicating that the area of the bubbler is not important.

To determine the point at which the number and size of the holes in the bubbler significantly affects the absorption rate, discs with four medium-sized holes, and with a single larger hole, were investigated. The disc with four holes (diam. 0·125 in.), spaced 0·875 in. apart at the corners of a square, gave a value of E_A which differed by only 4·5 per cent from the value of E_A obtained for the indented strip, while the single hole (diam. 0·375 in.) gave values which differed by only 13·3 per cent.

It is concluded from this investigation that the size, number, and distribution of pores or holes, and the area of the bubbler plate, can be varied over a wide range without a profound effect on the absorption rate.

COMPARISON OF COUNTER-CURRENT BUBBLE-TYPE ABSORBERS WITH PACKED TOWERS

Fig. 7 compares absorption rates for packed towers (using data available in the literature) with absorption rates now obtained for bubble-type absorbers. For the latter, average K_La values range from 75 to 500 lb-mole/hr, ft^3, lb-mole/ft^3 while the operating values for packed towers lie in the range 4-75 lb-mole/hr, ft^3, lb-mole/ft^3 depending upon the liquid velocity, gas velocity, and type of packing [8, 9, 10].

Fig. 8 compares the data of COOPER, CHRISTL and PEERY [11], for the absorption of carbon dioxide in water in a packed tower, with the data now available for its absorption by counter-

Table 3. Effect of porosity on absorption rate

$h = 1·5$ ft
$p = 5·1$ atm CO_2
$t = 15$°C
$u_L = 0·144$ ft/sec
$u_G = 0·125$ ft/sec

Distributor	*Area* (ft^2)	*Porosity* (μ)	E_A (per cent)	$(N.T.U.)_{OL}$ (average)	K_La (average)
Fine bronze	0·0307	72	53·0	1·80	286
Medium bronze	0·0307	408	55·4	1·61	325
Coarse bronze	0·0307	634	55·3	1·67	317
Indented strip *A*	0·0214	1150	52·9	1·77	266
Indented strip *B*	0·0214	810	53·1	1·75	227
4 × $\frac{1}{8}$ in. diam. holes	—	3180	49·4	2·06	254
1 × $\frac{1}{8}$ in. diam. hole	—	9540	40·8	2·66	198
1 × $\frac{1}{4}$ in. diam. hole	—	9540	40·4	2·49	208

current bubble-type absorbers. The $(H.T.U.)_{OL}$ values for the latter lie in the range 0·75–3·5 ft at an inlet partial pressure of 75 lb/in² abs., while for packed towers they lie in the range 2·75–9 ft.

Shulman and Molstad [1] have measured the absorption rates of carbon dioxide by water in a glass bubble-column (diam. 2 in.) at atmospheric pressure and for three liquid rates. Their results at 1 atm total pressure and a bed height of 1 ft are compared with the present average $(H.T.U.)_{OL}$ values at an inlet partial pressure of 5·1 atm of carbon dioxide and a bed height of 1·5 ft (Fig. 8) The present results are somewhat higher than those of Shulman and Molstad [1] because of the higher partial pressure and bed height, and because the present values are average $(H.T.U.)_{OL}$ values between the inlet and outlet gas velocities.

In general, it may be concluded that bubble-type absorption towers give absorption rates which are from three to ten times greater than those of packed towers.

VOL. 7 957/58

Summary and Discussion

The objective of this work has been to determine the effects of various operating variables on the behaviour of bubble-type water scrubber for carbon dioxide under conditions where large quantities of soluble gas are absorbed. The results show that the bubble-type scrubber is superior to the packed tower for the absorption of carbon dioxide in water, where the liquid-film resistance is believed to control the rate of absorption. The reason is undoubtedly connected with the rate of renewal of the liquid film. When a bubble rises it must displace its own volume of liquid as it rises through its own diameter. It may therefore be expected that the liquid film around a bubble is renewed each time it moves through one diameter. In general, it may be expected that the volume of a bubble-type tower will be about one third to one tenth of the volume of a packed tower for the same amount of absorption, depending on the operating pressure. The bubble tower has the additional advantages of (i) better mixing through fluidization, and (ii) relative independence of performance and mechanism of bubble formation and distribution. Investigations on the effect of the porosity of the gas distributor show that absorber performance is insensitive to changes in the number, size, and distribution of the holes in the gas bubbler, over a wide range. The reason is that the bubbles in the fluidized bed result from the coalescence of two or more bubbles, either in the fluidized bed itself or in the region of the gas distributor. A recent paper by Helsby and Tuson [12] shows how two or more bubbles leaving a jet may coalesce under viscous solutions of glycerol in water. Evidence will be presented in a later paper [3] to show that the bubbles in a fluidized bed follow a probability size-distribution, and result from the coalescence of two or more bubbles.

The effect of gas velocity is to increase the absorption rate in the rising hold-up region. The reason has been found [3] by photographing bubble-beds and measuring the number and size of the bubbles as the gas is increased. For water, the average bubble-volume increases only slightly with gas velocity; but the number of bubbles per unit volume increases more rapidly, thus causing a rise in the surface area for absorption. The point at which absorption becomes independent of gas velocity corresponds to the point at which the bubble-bed holds the maximum possible amount of gas, and further increases in gas velocity cause the formation of plugs or large bubbles of gas. Observations in glass columns show that there is much turbulence and recirculation at low gas-velocities in the rising hold-up region, so that it may be incorrect to refer to this region as "streamline", a term used by Shulman and Molstad [1].

The effect of liquid velocity upon absorption rate is best illustrated by its effect on the average K_La. This quantity increases with rise in both gas and liquid velocities. The effect of increasing the liquid velocity should be to increase the eddy diffusivity in the liquid film moving round the bubble. Although greater liquid velocities increase the absorption rate, the overall effect is to decrease E_A and increase $(H.T.U.)_{OL}$. The reason is that both these quantities are functions of a liquid-rate term other than that involved in the effect of liquid rate on absorption rate.

For instance, $(H.T.U.)_{OL}$ is related to K_La as follows :

$$(H.T.U.)_{OL} = L/\rho_L K_L a \qquad (10)$$

The average K_La in Fig. 7 varies with liquid velocity in proportion to $u_L^{0.52}$; hence $(H.T.U.)_{OL}$ should increase with liquid velocity according to $u_L^{0.48}$.

The decrease in absorption-rate coefficients with increase in bed height can be explained on the theory that in columns where the ratio of bed height to diameter is large, the surface area per unit volume for absorption changes as the distance from the bubbler plate increases. As a bubble rises its volume decreases owing to absorption; hence, the surface area decreases. If the rate of bubble recirculation in the bed is less than the rate of absorption, there will be a gradual change in bubble volume and surface area for absorption with distance from the bubbler.

An increase in inlet partial pressure of carbon dioxide decreases the absorption rate (Fig. 10). If the absorption of carbon dioxide in water is completely liquid-film controlled, the effect of pressure could be explained by supposing that the diffusion coefficient of dissolved carbon dioxide is influenced by concentration. However, it is to be expected that under the highly turbulent conditions in a fluidized bed the static diffusion coefficient is negligible compared with the eddy diffusivity ; and it is difficult to visualize how the concentration of dissolved carbon dioxide could influence the eddy diffusivity. Another explanation is that under these turbulent conditions the absorption process is partially controlled by the gas-film resistance, and the effect of pressure is to increase this resistance.

Increase in temperature increases the absorption rate, in both rising and constant hold-up regions, as would be expected for a diffusion-controlled mechanism in both regions. However, Shulman and Molstad observed a negative temperature coefficient at atmospheric pressure for low gas-velocities. It may be that higher pressures increase the proportion of the gas-film resistance enough to reverse the temperature coefficient.

The concentration data (Fig. 12) show that the " end effect " is large at the water inlet and small at the gas bubble-plate. The end effect at the water inlet can be explained by the presence of a stratified layer of fresh water, incompletely mixed into the fluidized bed. To ascertain the reason for the end effect at the gas bubble plate, experiments were conducted in a glass column of the same dimensions at the pressure unit. In the glass unit a layer of bubbles was observed just below the gas distributor, so that absorption would still continue to a slight extent after the liquid had passed the bubbler. The sampling point for the water leaving the column was 10 in. below the surface of the bubbler ; the so-called end effect in this case could therefore be attributed to a small amount of absorption in this region. It was not possible to obtain samples closer to the bubble plate than about 4 in., since large quantities of gas issued with the liquid from the sampling point and it was impossible to obtain constant material balances.

To sum up, the bubble-type absorber has proved successful for the absorption of large quantities of carbon dioxide from gas mixtures where most of the gas consists of carbon dioxide. The percentage absorbed can be made to approach 100 per cent by (i) increasing the bed height in the region 0·5–6 ft, (ii) decreasing the partial pressure of carbon dioxide in the range 2·5–14 atm, (iii) increasing the liquid-to-gas velocity ratio in the range 0·2–2·5, and (iv) decreasing the temperature.

Acknowledgement—The authors thank the Admiralty for permission to publish this paper.

Notation

A = cross-sectional area of column, ft².
B = gas absorbed, lb-mole/hr.
d = pore diameter, μ.
E_A = absorption efficiency ; fraction of saturation based on inlet gas.
E'_A = absorption efficiency ; fraction of saturation based on outlet gas.
h = bed height, ft.
h_L = water level in sight-glass above porous disc, ft.
$(H.T.U.)_{OL}$ = height of overall liquid-phase transfer unit, ft.
K_La = overall liquid-film coefficient, lb-mole/hr, ft³, lb-mole/ft³.

L = mass velocity of liquid, lb/hr, ft^2.
$(N.T.U.)_{OL}$ = number of overall liquid-phase transfer units.
ΔP_0 = back pressure across porous disc at zero gas flow, dyn/cm^2.
p = partial pressure of carbon dioxide in inlet gas, atm.
t = temperature, °C
u_G = inlet superficial gas velocity, ft/sec.
u_L = superficial liquid velocity, ft/sec.
x_1 = mole fraction carbon dioxide in inlet liquid.
x_2 = mole fraction carbon dioxide in outlet liquid.
x_1^* = mole fraction carbon dioxide in equilibrium with outlet gas.
x_2^* = mole fraction carbon dioxide in equilibrium with inlet gas.
Δx_M = mean driving force.
γ' = surface tension, dyn/cm.
ρ_B = bed density, g/ml.
ρ_L = water density, g/ml.

References

[1] Shulman H. L. and Molstad M. C. *Industr. Engng. Chem.* (*Industr.*) 1950 **42** 1058.
[2] Howard J. R. *Trans. Inst. Chem. Engrs., Lond.* Symposium on Gas Absorption, 1954 **32** 146.
[3] Houghton G., McLean A. M. and Ritchie P. D. To be published.
[4] *Idem. Chem. Engng. Sci.* 1957 **6** 132.
[5] Carey W. F. and Williamson G. J. *Proc. Inst. Mech. Engrs.* 1950 **163** (W.E.P. No. 56) 41.
[6] Van Arsdel W. B. *Trans. Amer. Inst. Chem. Engrs.* 1921-22 **14** 391.
[7] Geankoplis C. J. and Hixon A. N. *Industr. Engng. Chem.* (*Industr.*) 1950 **42** 1141.
[8] Simmons C. W. and Osborn H. B. *Ibid.* 1934 **26** 529.
[9] Adams F. W. and Edmonds R. G. *Ibid.* 1937 **29** 447.
[10] Cantelo R. C., Simmons C. W., Giles E. M. and Brill F. A. *Ibid.* 1927 **19** 989.
[11] Cooper C. M., Christl R. J. and Peery L. C. *Trans. Amer. Inst. Chem. Engrs.* 1941 **37** 979.
[12] Helsby F. W. and Tuson K. R. *Research* 1955 **8** 270.

VOL. 7 1957/58

Chemical Engineering Science, 1957, Vol. 7, pp. 40 to 50. Pergamon Press Ltd.

Mechanism of formation of gas bubble-beds

G. Houghton, A. M. McLean and P. D. Ritchie

Technical Chemistry Department, Royal College of Science and Technology, Glasgow

(*Received* 18 *January* 1957)

Abstract—Data are presented on the size, number, and size-distribution of bubbles in fluidized bubble-beds and foam beds. These types of bed differ in that bubble diameter and bubble density (i.e. the number of bubbles per ml) tend to become constant for the former as the superficial gas velocity is increased, whereas bubble density tends to decrease and bubble diameter to increase for the latter. Also, foam beds are sensitive to the size, number, and distribution of the pores in the gas distributor, whereas fluidized beds are not.

Résumé—Les auteurs présentent des données sur la dimension, le nombre et la répartition suivant la grosseur, des bulles dans les " lits fluidisés par bulles " et dans les lits de mousses. Ces deux types de lits diffèrent, car le diamètre des bulles et leur concentration (c'est-à-dire le nombre de bulles par cm^3) tendent à devenir constants pour les premiers quand la vitesse superficielle du gaz augmente, tandis que pour les seconds, le diamètre des bulles tend à augmenter et leur concentration tend à diminuer.

Par ailleurs, les lits de mousse sont sensibles à la dimension, au nombre et à la répartition des pores du distributeur de gaz, alors que les lits fluidisés ne le sont pas.

Zusammenfassung—Für die Grösse, Zahl und Grössenverteilung von Blasen in fluidisierten Blasenbetten und in Schaumbetten werden Zahlenwerte mitgeteilt. Diese beiden Bett-Typen unterscheiden sich in folgendem: Blasendurchmesser und Blasendichte (Anzahl der Blasen je ml) werden im ersteren Falle konstant mit steigender Gasgeschwindigkeit, bezogen auf den Bett-Querschnitt, im zweiten Falle nimmt die Blasendichte ab und der Blasendurchmesser zu. Schaumbetten sind auch empfindlich gegenüber der Grösse, Zahl und Verteilung der Poren des Anströmbodens, in Gegensatz zu den fluidisierten Betten.

Introduction

Recent work shows that in certain cases the rates of absorption from moving bubbles are greater than those from moving liquid-films such as are present in packed towers.

Shulman and Molstad [1] have described a method for the absorption and desorption of carbon dioxide in dilute mixtures, where the gas is bubbled counter-current to the liquid at atmospheric pressure; and Houghton, McLean and Ritchie [2] have discussed the operation of a bubble column for carbon dioxide at high partial pressures of carbon dioxide, where most of the soluble gas is removed. In both cases, the absorption medium may suitably be described as a " fluidized bubble-bed." It was concluded that rates of absorption are higher in bubble columns than in packed towers when the rate of absorption is controlled by the liquid-film resistance.

Several authors have discussed the use of foams, in contrast to fluidized bubble-beds, for the absorption of gases. Pozin, Mukhlenov, Tumarkina and Tarat [3] have discussed absorption from a foam which flowed across a sieve-plate through which the gas was forced. Helsby and Birt [4] have described an apparatus for the absorption of carbon dioxide from dilute mixtures in aqueous ethanolamine solutions, where the liquid velocity was so low (0·0005 ft/sec) that a foam was produced. Dixon and Kiff [5] have discussed the use of perforated and porous plates for the formation of bubbles and foam from 30 per cent monoethanolamine, and also the rate of absorption of carbon dioxide in ethanolamine solutions, in relation to the number, size, and distribution of holes in the perforated-plate gas distributor.

Little work has been done, however, on the mechanism of formation and operation of

fluidized and foam beds. VERSCHOOR [6] measured the densities of various bubble beds as a function of gas velocity, using water, methanol, and a glycerine–water mixture. He observed that small bubbles emerging from a porous plate in water and organic liquids show coalescence, and that in water this can be suppressed by the addition of small quantities of acetic acid. The coalescence of bubbles near jets has recently been confirmed photographically by HELSBY and TUSON [7]. However, no published work has been found on the size, number, and distribution of bubbles in the bubble bed itself in relation to the formation of fluidized and foam beds for absorption of gases.

EXPERIMENTAL

The apparatus (Fig. 1) consists of a glass column (internal diam. 3·14 in.) containing the liquid to be studied, into which gas is bubbled through porous metal or glass discs. The gas flow-rate is held constant by the flowmeter

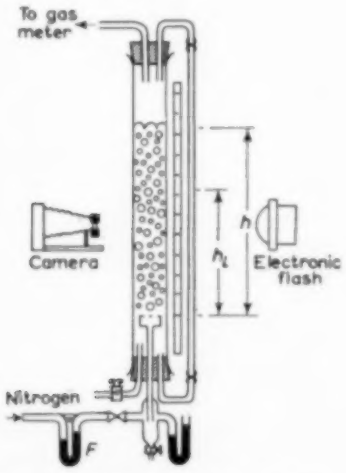

FIG. 1. Diagram of equipment.

F, and the flow of gas leaving the column is accurately measured by a gas meter. The bed height (h) and the manometer reading (h_L) are read on the same scale, so that the bed density can be computed from the following equation, where ρ_L is the density of the liquid being studied :

$$\rho_B = h_L \rho_L / h \qquad (1)$$

In this way the bed density can be determined over a range of superficial gas velocities.

To determine the size, shape, and distribution of the bubbles, the column was photographed using a plate camera and electronic flash.

The liquids studied were water, acetone, ethyl acetate, monoethanolamine, glycerine, glycerine – water mixtures, and solutions of acetic acid in water; the gases were nitrogen, oxygen, and carbon dioxide.

POROSITY OF GAS DISTRIBUTORS

Gas distributors of two different types were used : (a) porous discs of sintered glass or sintered bronze, with porosities varying over a wide range, and (b) the packed indented strip described by HELSBY and BIRT [4].

The pressure drop (ΔP) across the gas distributor is obtained by subtracting the hydrostatic pressure (due to the bubble bed) from the back pressure, read on manometer **M**, thus :

$$\Delta P = h_m \rho_m - h\rho_B \qquad (2)$$

The resulting pressure-drop is the sum of the friction and contraction pressure-drops due to flow of gas through the porous plate (ΔP_f), and the maximum bubble-pressure required for the formation of bubbles at the plate surface (ΔP_0), thus :

$$\Delta P = \Delta P_0 + \Delta P_f \qquad (3)$$

It is well known that during formation of a bubble at a jet the pressure first increases until the bubble is a hemisphere whose radius is equal to that of the jet, and thereafter decreases as the bubble grows. Consequently, if ΔP is plotted against gas velocity and the resulting line extrapolated to zero gas-flow, the intercept will be the maximum bubble-pressure (ΔP_0) which is independent of gas velocity. The average pore-diameter (d) can then be calculated from the equation :

$$d = 4\gamma'/\Delta P_0 \qquad (4)$$

Fig. 2 shows typical plots of ΔP against superficial gas-velocity (u_G), and it is apparent that they can be divided into three regions :

(1) *A region at very low gas-velocities where ΔP increases rapidly with increase in superficial gas-velocity.* This can be attributed to an increase in maximum bubble-pressure as smaller pores come into operation.

(2) *A region where ΔP increases less rapidly with gas velocity.* This region can perhaps be ascribed to either

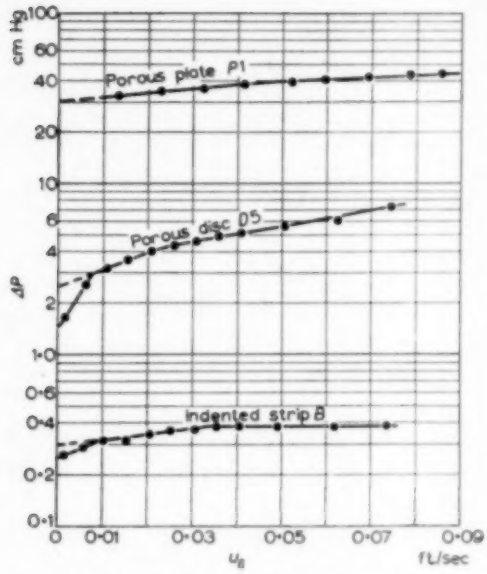

Fig. 2. Pressure drop (porous plate *P*3) across gas distributors.

streamline or turbulent flow of gas through the pores. Since the number of pores in effective operation is unknown, the Reynolds number cannot be computed for a single pore in order to ascertain the nature of the flow in this region. Further, it is evident that since the porous plates are quite thin the contraction and expansion losses for the gas entering and leaving the disc may also be appreciable.

(3) *A region where further increases in gas velocity have very little effect upon* ΔP. The explanation of this region of constant pressure-drop may be that for high pressure-drops a large number of fine pores inside the disc becomes progressively freed of liquid, thus producing a larger area for flow. However, the authors regard the present experiments on pore size as preliminary in nature; and it is intended to make further comparisons of the pressure-drops across the same discs both wet and dry.

It was found that if the line for region (2) is extrapolated to zero gas-velocity, the pressure-drop obtained (ΔP_0) can be used to calculate the average pore-size, with good reproducibility. Values obtained in this way for the sintered glass discs agreed with the manufacturers' published data to within $\pm$ 15 per cent; and the porosities for the indented strip agreed well with those measured geometrically. The pore diameter obtained will be an average value for the case where the maximum number of pores operates for the particular liquid used.

Table 1. *Porosities of gas distributors (measured in water)*

Distributor		*Thickness* (in.)	*Area* (ft^2)	*Porosity* (μ)
Porous glass	*P*1	0·160	0·029	7·3
	*P*2	0·160	0·026	81
	*P*3	0·160	0·030	114
Porous bronze	*D*1	0·123	0·0307	1330
	*D*2	0·123	0·0307	634
	*D*3	0·126	0·0307	408
	*D*4	0·126	0·0307	364
	*D*5	0·121	0·0307	72
	*D*6	0·121	0·0307	170
Indented strip	*A*	1·00	0·0214	1150
Indented strip	*B*	1·00	0·0214	810

Table 2. *Effect of liquid on porosity measurements*

Liquid	*Surface tension* (dyn/cm)	*Porosity* (μ)	
		*P*2	*P*3
Pure water	72·9	81	114
Sea water	58·7	75	107
Acetone	26·2	82	76
Acetic acid	27·8	49	56
Ethyl acetate	24·6	45	74
23 wt. per cent glycerine	72·3	80	93
37 wt. per cent glycerine	71·3	83	88
49 wt. per cent glycerine	70·0	81	89
58 wt. per cent glycerine	69·0	80	89

Table 1 summarizes the measured porosities of six sintered-bronze discs and three sintered-glass plates, for water, and Table 2 the porosities of plates *P*2 and *P*3 for various other liquids and solutions. These show that the average pore-size depends upon the physical properties of the liquid used, in particular the surface tension; in general, the lower the surface tension of the liquid the lower the average pore-size for the same porous plate. However, acetone appears to be an exception, since it gives an average pore-diameter in agreement with that obtained by using pure water, even though the respective surface tensions are 26 as compared with 72 dyn/cm.

It may be inferred that the pore diameters vary over a wide range, and that in general there is a tendency for the largest pores to operate during bubble formation. However, smaller pores may be brought into action by using liquids of lower surface tension.

BED DENSITIES

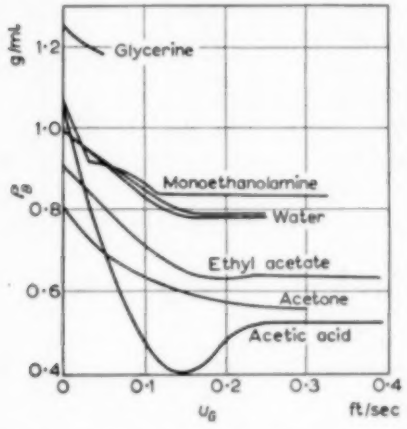

FIG. 3. Bed densities of pure liquids (porous plate *P*3).

Fig. 3 shows the variation of bed density with superficial gas-velocity for various pure liquids. All the curves have the same general shape; the bed density decreases and the gas hold-up increases as the superficial gas-velocity increases, until a more or less constant value is reached over the range studied. At this point, plugs of gas are formed which cause the bed level to rise and fall as they are discharged at the surface. With acetic acid and ethyl acetate, plug formation causes the bed density to rise from a minimum value to a constant average value between the maximum and mininum levels. It was ascertained at the beginning of the investigations that the curve was independent of the gas used (O_2, N_2 or CO_2) for any given porous plate and liquid.

The bed densities of various glycerine solutions are shown in Fig. 4. Addition of glycerine to water (up to ca. 68 wt. per cent) lowers the bed-density curve; at 84 wt. per cent the curve lies between those of pure glycerine and pure water, and it is evident that the bed densities of glycerine solutions bear very little relationship to those of the pure components.

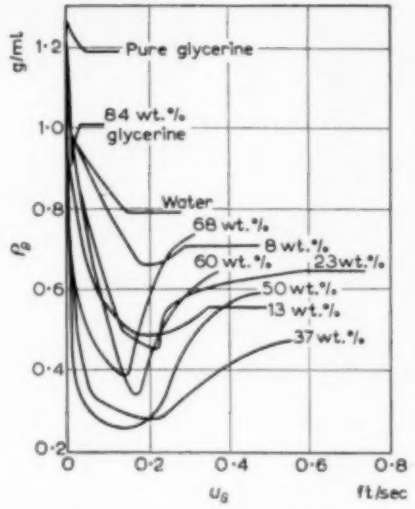

FIG. 4. Bed densities for glycerine solutions (porous plate *P*3).

Solutions containing from 13 to 68 wt. per cent of glycerine have good foaming properties. At low gas-velocities, bubbles rise to the surface to form stable bubble-rafts above a fluidized bubble-bed containing mainly liquid; as the gas velocity is increased, the raft increases in volume until at a certain velocity the whole bed becomes a mass of foam where the gas is the main constituent. Fig. 5 (1) shows a fluidized bubble-bed consisting mainly of liquid, with a foam raft consisting mainly of gas: this may suitably be termed a "two-phase" bubble-bed.

Fig. 6 compares the behaviour of acetic acid solutions with that of pure water and pure acetic acid. Clearly, the behaviour of the solutions is quite out of proportion to the amount of acetic acid present: for concentrations as low as 0·04 – 0·42 wt. per cent, it is comparable with that of glycerine solutions (13 – 68 wt. per cent). Further increases in acetic acid concentration (0·42 – 3·6 wt. per cent) have no noticeable effect upon the bed density. With acetic acid solutions at low gas-velocities, a "two-phase" region is observed between the fluidized and the foam regions.

Fig. 7 compares the effect of gas velocity on bed density for sea-water and freshwater, for two porous plates. Sea–water is clearly more akin in its behaviour to glycerine – water and acetic acid –

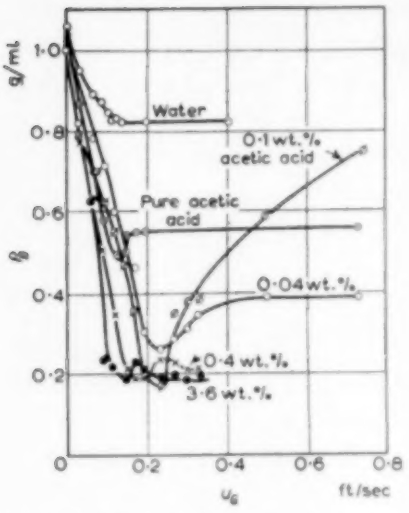

Fig. 6. Bed densities for acetic acid solutions (porous plate *P*2).

water foams than to the fluidized beds produced by pure liquids. The sea-water curves exhibit a pronounced minimum, and bed densities as low as 0·85 g/ml are observed. The sea-water (chlorinity 16; obtained from Firth of Clyde near entrance to Loch Long) had a surface tension of 58·7 dyn/cm at 20°C, indicating the presence of surface-active agents, probably produced by decay of animal and plant organisms. Fig. 7 also

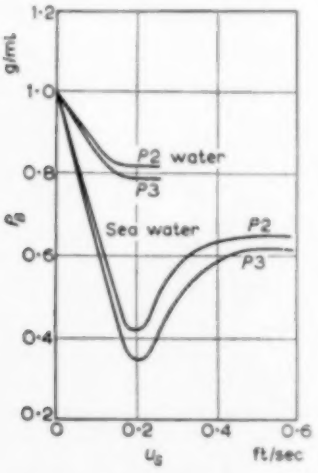

Fig. 7. Bed densities for fresh and sea-water.

shows that variations in bed density with gas velocity can be used to detect differences in porosity. The porous-glass plates *P*2 and *P*3 have average pore-diameters which differ by about 15 per cent, which is reflected by a 5 per cent difference in bed density for sea-water. A similar effect is observed for different liquids over a wide range of porous plates. In general the more porous plates produce the higher bed-densities; but this is not necessarily so, since the bed density is a function of both bubble-size and the number of bubbles per unit volume of bed.

It is evident that for pure liquids there is (a) a region of *rising hold-up*, where the bed density decreases with increases in gas velocity, and (b) a region of *constant hold-up*, where the bed already holds the maximum amount of gas and further increases in gas flow produce large bubbles or plugs of gas which cause the bed level to rise and fall. For solutions, gas bubbles form stable bubble-rafts at the surface, instead of bursting, so that the fluidized bed passes through a " two-phase " region to form a complete mass of foam; further increases in gas velocity cause plugs to form in the foam.

Plug Formation

Optimum conditions for plug formation are those in which the rate of bubble formation is very high and the velocity of bubble rise is low. In this respect pure glycerine was found to be the ideal liquid. Fig. 5 (2 – 9) illustrates the mechanism of plug formation, and shows eight successive stages corresponding to gradually increasing gas-velocity. At low velocities only a few pores operate in the centre of the porous plate; at higher velocities a greater proportion of the plate area becomes effective, and small bubbles collect in groups of approximately the same shape as the large bubble which finally results. These groups coalesce to produce a large bubble or plug which, as it rises, collects in its wake other smaller bubbles which may or may not combine with the larger one before the plug breaks the surface. Helsby and Tuson [7] have observed a similar phenomenon in the formation of bubbles at jets under glycerine solutions; here, during bubble formation at single jets, two or more

VOL. 7
957/58

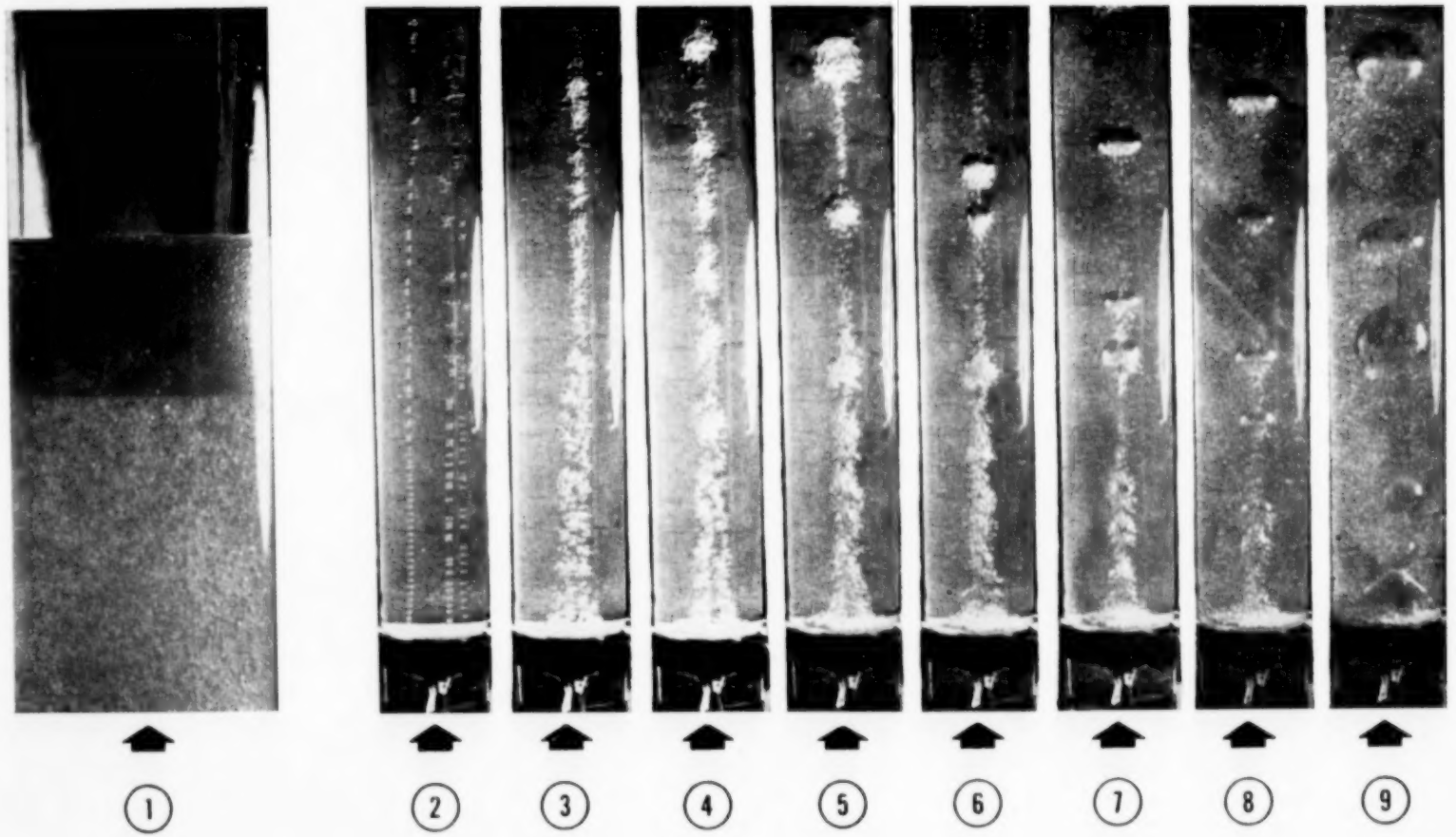

FIG. 5. (1) Typical fluidized bubble-bed, consisting mainly of liquid, with a foam raft above it consisting mainly of gas.
(2—9) Eight successive stages in plug formation (glycerine).

VO
7
1957

bubbles may coalesce to produce a single bubble within a short distance of the jet at high gas-rates. It is evident that coalescence takes place on a large scale in a bubble bed during plug formation.

Bubble Shapes

The variation of bubble shape with bubble size was determined by photographing bubble beds at various stages of their development. In general, most of the observed bubbles in the fluidized and foam beds were oblate spheroids; and Fig. 8 is a log – log plot of the major axis b against the minor axis a for bubbles of nitrogen in six different liquids. (Each point is an average for at least 30 bubbles, the accuracy of measuring the axes being ca. $\pm$ 5 per cent). For liquids of

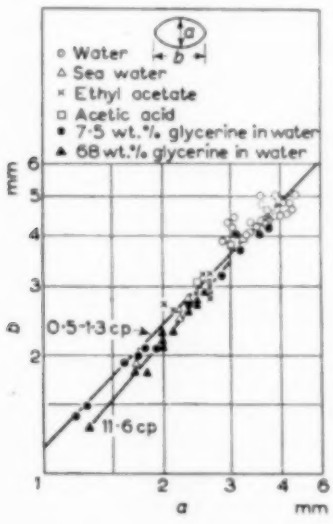

Fig. 8. Shape of bubbles.

viscosity 0·5–1·3 cP the plot is linear, indicating that bubble shape is insensitive to viscosity in this range; but for glycerine solutions of viscosity 11·6 cP the plot shows that the bubbles tend to becomes more spherical as viscosity increases.

For viscosities in the range 0·5–1·3 cP, a and b are related thus:

$$b = 1{\cdot}2\,a \qquad (5)$$

For correlation purposes, the equivalent spherical diameter (D_e) has some advantages over either a or b, and is the variable most often used in the literature; it is the diameter of a sphere equal in volume to the oblate spheroid, and is given by:

$$D_e = (ab^2)^{1/3} \qquad (6)$$

Substitution of equation (4) into equation (5) gives the relationship:

$$D_e = 1{\cdot}13\,a$$

Bubble-size Distribution

Enlarged photographs of both fluidized and foam beds show that the bubble sizes are not uniform; and by examining a large number of bubbles the bubble-size distribution in a bed can be determined (Fig. 9, which refers to a bed of nitrogen bubbles in pure water). The bubble sizes follow a typical probability distribution about the most probable value, which was found to vary with plate porosity, gas velocity, and the properties of the liquid phase. The relationship between bubble size and the cumulative percentage of bubbles of a size smaller than this, when plotted on log-probability paper, is a linear one, which confirms the presence of a probability function.

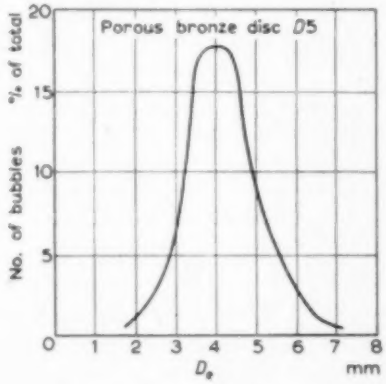

Fig. 9. Bubble-size distribution.

Observed bubbles *smaller* than the most probable size may have been formed at very small pores, or may have been broken off from other bubbles by the action of the container wall or by collision with other bubbles; those *larger* than the most probable size could be be produced either by larger pores or by coalescence. Coalescence seems less probable in the

VOL. 7 957/58

main body of the liquid than close to the bubbler plate, since most bubbles seem to coalesce by being sucked upwards into the slip stream of the bubble ahead. Coalescence of bubbles moving in opposite directions appears unlikely, since the moving films of liquid around the front and sides would tend to repel them.

Effect of Liquid Properties on Average Bubble-Diameter

Fig. 10 illustrates the effect of superficial gas-velocity upon average bubble-diameter for various pure liquids. Each point represents an average of the diameters of 30 bubbles in the bed.

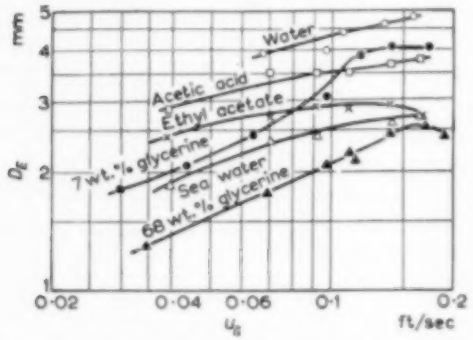

Fig. 10. Effect of liquid properties on bubble size (porous plate *P2*).

Increasing the gas velocity increases the average bubble-size, but the effect is very much less for pure liquids than for glycerine solutions and sea water. In ethyl acetate, for example, the equivalent spherical diameter changes only from 2·42 to 2·95 mm as the velocity increases from 0·0386 to 0·16 ft/sec, whereas the bubble diameter in 68 wt. per cent glycerine changes from 1·3 to 2·5 mm in the same range, a much larger effect.

The largest bubbles from plate *P3* are produced under water, and the smallest under 68 wt. per cent glycerine, although the respective surface tension (72 and 68 dyn/cm) show a difference of only 4 units.

A comparison of ethyl acetate, acetic acid, and water (surface tensions 24·6, 27·8, and 72 dyn/cm respectively), shows that bubble size increases with surface tension, though not proportionately. Table 2 shows that the average pore-size for acetic acid and ethyl acetate is about half of that for water (Plate *P2*) so that the smaller average bubble-sizes at the lower surface tensions is probably due to the effective operation of smaller pores.

Fig. 10 shows that superficial gas-velocity has a much more profound effect upon bubbles in foams from 7 wt. per cent and 68 wt. per cent solutions of glycerine than in fluidized beds from pure liquids. The reason for variation of foam bubble-size with gas velocity may be that the porous plate produces larger bubbles as the amount of liquid available becomes less, or that there is a greater rate of coalescence in foams. Observations on single bubbles in a foam show that foam bubbles, once formed, are very stable and resistant to coalescence. Hence, the most probable explanation for the variation of diameter with gas velocity is that as the gas-to-liquid ratio increases in the foam, the film of liquid over the porous plate becomes thinner and a large bubble is then formed from gas issuing from several adjacent pores.

Fig. 10 also shows that the bubble size in sea-water beds increases with gas velocity. This indicates that such a bubble bed behaves more as a foam than as a fluidized bed, a fact confirmed by the much lower bed densities observed with sea water as compared with fresh water.

Effect of Plate Porosity on Average Bubble-Diameter

Fig. 11 illustrates the effect of plate porosity on average bubble-size. With pure liquids

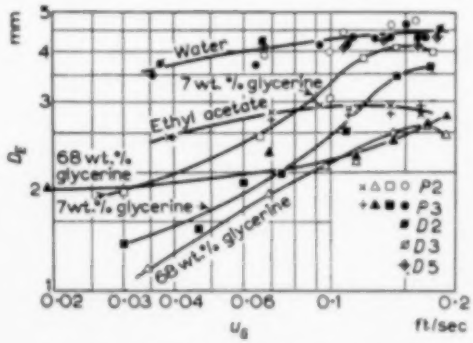

Fig. 11. Effect of porosity on bubble size.

(water and ethyl acetate) there is no detectable effect within the limits of experimental error, for plates *P2* and *P3*. For foams of 7 wt. per cent and 68 wt. per cent glycerine, the bubble sizes produced by plates *P2* and *P3* differ considerably in the same solution. However, as superficial gas-velocity is increased the average bubble-sizes produced by the two plates tend to approach the same value for each solution.

The conclusion is that foams are more sensitive to changes in plate porosity than are fluidized bubble-beds. This sensitivity to the number and size of the holes in the distributor plate may become a serious drawback in the use of foam scrubbers, where the pores may become blocked by deposits from solution.

VOL. 7 957/58

Effect of Liquid Properties on Bubble Density

The bubble density is defined as the number of bubbles per ml of bubble bed, and can be calculated from bed density and average bubble-volume. Plots of bubble density against superficial gas-velocity are given in Figs. 12 and 13.

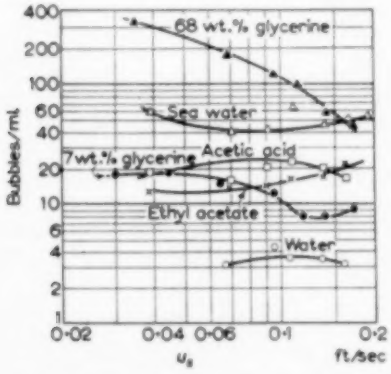

Fig. 12. Effect of liquid properties on bubble density (porous plate *P2*).

Fig. 12 illustrates the effect of liquid properties on bubble density. The foaming glycerine solutions (7 wt. per cent and 68 wt. per cent) show a decrease in bubble density with increase in gas velocity; the 68 wt. per cent solution shows a very high bubble-density (between 50 and 300 bubbles/ml). The decrease in bubble density with increase in velocity in foaming media is probably caused by the initial formation of much larger bubbles at the porous plate as the gas-to-liquid ratio becomes higher.

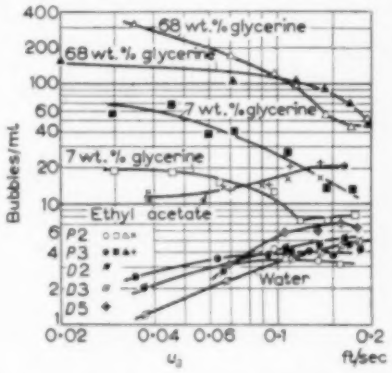

Fig. 13. Effect of porosity on bubble density.

Figs. 12 and 13 show that at low gas-velocities, in pure liquids, an increase in velocity increases the bubble density to a constant value at gas velocities greater than about 0·1 ft/sec. In the isolated case of porous plate *P2* the gas velocity has very little effect upon bubble density. It will be noted that the number of bubbles per ml of bed for water is of the order 1 – 7 (very much lower than for foam beds).

Effect of Plate Porosity on Bubble Density

Fig. 12 shows that, for pure liquids, plate porosity has very little effect upon the number of bubbles per ml of bed. The porous-bronze discs and porous-glass plates give low bubble-densities (1 – 7 bubbles/ml) and show a slight variation of bubble density with porosity.

For glycerine solutions which form foams, even the 15 per cent difference in porosity of plates *P2* and *P3* can have an appreciable effect on bubble density.

Velocity of Rise in Bubble Beds

The average velocity of rise of bubbles in a bubble bed can be expressed thus:

$$u_B = u_G(\rho_L/\rho_L - \rho_B) \qquad (8)$$

In Fig. 14, u_B is plotted against equivalent spherical bubble-diameter, so that the velocity

of rise in bubble beds may be compared with that of single free-rising bubbles. It must be remembered, however, that the motion of bubbles in a fluidized or foam bed is hindered by the close proximity of other bubbles, so that here the velocity of rise is not constant for a particular bubble-size but varies with the density of bubbles in the bed.

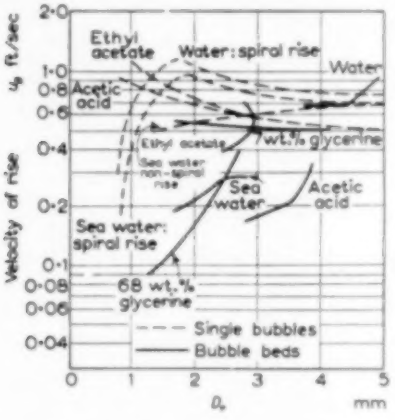

Fig. 14. Velocities of rise (porous plate $P2$).

The broken lines in Fig. 14 represent the velocities of rise of single free-rising bubbles in an infinite liquid as a function of bubble diameter. For acetic acid and ethyl acetate, these velocities were obtained from the data of Peebles and Garber [8]. For pure water and sea-water they have been determined by Houghton, Ritchie and Thomson [9] by timing the rise of bubbles produced singly at a jet; and it was found that bubbles may rise in sea-water either with or without a spiral motion, even though their diameters are identical. Spiral motion is usually observed when the jet is vibrated at the moment of bubble detachment. Spiral and non-spiral motions are observed only for bubbles whose diameters lie within the range 1 – 4 mm. (A similar effect has been observed by Stuke [10] for oxygen bubbles rising in caproic acid solutions.) Apparently certain dissolved impurities suppress the spiral type of rise; and occasionally the non-spiral rise of a single bubble in tap water has been observed under conditions where the normal motion was spiral. The curves for spiral and non-spiral motion are plotted in Fig. 14; the velocity of spiral rise is somewhat less in sea-water than in pure water, by an amount which cannot be accounted for by the small differences in density and viscosity. The surface tension of the sea-water employed was 58·7 dyn/cm, as compared with 72 dyn/cm for pure water, so that the differences in velocities of rise are almost certainly connected with the presence of surface-active agents.

Velocities of rise in fluidized and foam beds are in general lower than the corresponding velocities for single bubbles (which agrees with the previous picture of hindered rise of bubbles in a bed).

For sea-water bubble-beds, the velocities are less than half of those of single bubbles, which bears out the previous conclusion that sea-water beds are allied more closely to foams than to fluidized beds.

It is an interesting fact that sometimes the velocity of rise in a bubble bed can be greater than the velocity of rise of a single free-rising bubble, which is not in accordance with the theory of hindered rise. For instance (Fig. 14), the velocities of rise in ethyl acetate and water beds are greater than those of single bubbles. In other experiments an average bubble-velocity of 1·7 ft/sec was observed in water and 2·7 ft/sec in ethyl acetate under conditions where the bubble density was very high. Velocities of rise in bubble beds greater than those of single bubbles of the same diameter can be explained by the formation of plugs of gas in the liquid such that u_G in equation (8) becomes large while the bed density ρ_B remains approximately the same. This is confirmed by the observation that high bubble-velocities in beds are always observed in the region of "bumping," where plugs of gas cause the bed level to rise and fall about an average value.

Discussion

The bed density at any superficial gas-velocity is a function of the number of bubbles/ml, and of their average volume. In these respects, fluidized and foam beds have been found to behave differently. In the former the bed density decreases and the gas hold-up increases, because the number of bubbles/ml increases while the average bubble-size remains constant and independent of gas velocity. At higher gas-velocities the number of bubbles per ml and the bubble diameter both tend to become constant. It may therefore be concluded that in the region

of rising hold-up the increase in absorption rate with gas velocity is caused by an increase in surface area for absorption, and that this area becomes constant in the region of constant hold-up.

In general, foams show a wider variation of bed density with gas velocity than do fluidized beds. The former usually contain a much larger number of bubbles/ml than the latter, and the bubbles are smaller; the effect of increasing the gas flow-rate with foams is to decrease the number of bubbles/ml and to increase the average bubble-size, a behaviour quite different from that of fluidized bubble-beds.

Foams are sensitive to the porosity of the gas distributor, while fluidized beds are relatively insensitive to the number, size, and distribution of the pores.

It is of interest to discuss here the stages in the formation of a foam from a fluidized bed. At low gas-velocities the bubbles rise more or less independently through the liquid, and the bed may be termed "dilute". At higher velocities the bed expands further; the bubbles can no longer rise independently, being hindered by the motion of other bubbles. The bed soon becomes a turbulent mass of rising and recirculating bubbles, to which the term "fluidized" may now correctly be applied. Further increase in gas flow-rate causes plug formation, with consequent bumping.

The conversion of a fluidized bed to a foam bed is closely linked with the behaviour of the bubbles when they reach the surface. For pure liquids, the bubbles are observed to burst immediately, while in the initial stages of foam formation the bubbles collect on the surface in the form of rafts which appear quite stable. The rate at which bubbles burst is very much lower for foams than for fluidized beds. If the bursting rate is lower than the rate at which the bubbles reach the surface, the foam raft will expand until the rate of bubble formation equals the bursting rate at the surface. The volume of foam increases with the gas flow until the two-phase region becomes entirely foam. When the amount of liquid available at the porous-plate surface becomes low, plugs of gas form in the foam.

Obviously, the essential difference between fluidized and foam beds is bound up with the stability of bubbles at the liquid surface. It would appear that bubbles are more stable at a liquid surface when they are formed in solutions rather than in pure media.

Gibbs [11] has ascribed the stability of bubbles in solutions to the "elasticity" of the liquid film which encloses them. It would appear that in solutions the bubble film is more elastic, and more resistant to bursting, than in pure liquids.

Acknowledgement—The authors thank the Admiralty for permission to publish this paper.

Notation

a = minor axis of oblate spheroid, mm.
b = major axis of oblate spheroid, mm.
d = pore diameter, cm or μ
D_e = equivalent spherical diameter, mm.
h = bed height, ft.
h_L = manometer height, ft.
h_m = height of manometric fluids, ft.
ΔP = total pressure-drop across porous plate, mm Hg.
ΔP_f = pressure drop across porous plate due to frictional and contractional losses alone, mm Hg.
ΔP_0 = maximum bubble-pressure, mm Hg.
u_B = average bubble-velocity in bed, ft/sec.
u_G = average superficial gas-velocity through bed, ft/sec.
γ = surface tension, dyn/cm.
ρ_B = bed density, g/ml.
ρ_L = liquid density, g/ml.
ρ_m = density of manometric fluid, g/ml.

References

[1] Shulman H. L. and Molstad M. C. *Industr. Engng. Chem.* (*Industr.*) 1950 **42** 1058.
[2] Houghton G., McLean A. M. and Ritchie P. D. *Chem. Engng. Sci.* 1957 **6** 132.
[3] Pozin M. E., Mukhlenov I. P., Tumarkina E. S. and Tarat E. Y. *Zh. Prikl. Khim., Leningr.* 1954 **27** No. 1, 12.
[4] Helsby F. W. and Birt D. C. P. *J. Appl. Chem.* 1955 **5** 347.
[5] Dixon B. E. and Kiff P. R. *Ibid.* 1955 **5** 390.
[6] Verschoor H. *Trans. Inst. Chem. Engrs., Lond.* 1950 **28** 52.

VOL. 7 957/58

[7] Helsby F. W. and Tuson K. R. *Research, Lond.* 1955 **8** 270.

[8] Peebles F. N. and Garber H. J. *Chem. Engng. Progr.* 1953 **49** 88.

[9] Houghton G., Ritchie P. D. and Thomson J. A. *Chem. Engng. Sci.* 1957 **7** 111.

[10] Stuke B. *Naturwissenschaften* 1952 **39** 325.

[11] Gibbs J. W. *Collected Papers*. Vol. I. p. 300 ff. Longmans, Green, London, 1920.

Chemical Engineering Science, 1957, Vol. 7, pp. 51 to 59. Pergamon Press Ltd.

Concentration changes in an aerosol

J. F. Richardson and E. R. Wooding*
Department of Chemical Engineering, Imperial College, S.W.7

(*Received* 22 *March* 1957)

Abstract—Optical methods have been developed for measuring particle size and concentration in an aerosol. In a small sample of monodisperse aerosol, the concentration of particles has been measured as a function of vertical position and time, and the results have been used to verify the differential equation defining the concentration distribution in a system of particles subjected to the combined effects of Brownian Motion and gravitation.

Résumé—Des méthodes optiques ont été développées pour mesurer le diamètre des particules et leur concentration dans un aerosol. Dans un petit échantillon d'aérosol monodispersé la concentration des particules a été mesurée en fonction de la position verticale et du temps, et les résultats ont été utilisés pour verifier l'équation différentielle déterminant la distribution des concentrations dans un système de particules soumises aux effets combinés du mouvement Brownien et de la gravitation.

Zusammenfassung—Zur Messung der Teilchengrösse und der Konzentration in einem Aerosol wurden optische Methoden entwickelt. In einer kleinen Probe eines monodispersen Aerosols wurde die Konzentration der Teilchen als Funktion der senkrechten Höhe und der Zeit gemessen. Mit den Messergebnissen wurde die Differentialgleichung für die Konzentrationsverteilung in einem System von Teilchen bestätigt, wie sie sich aus dem Zusammenwirken der Brownschen Bewegung und der Gravitation ergibt.

VOL.
7
957/58

Introduction

An aerosol confined in such a way that convection currents are absent undergoes changes in concentration as a result of the diffusion of particles to the walls of the container, settling under the influence of gravity, and coagulation. The effect of diffusion in a field of force is described by a relation derived by Smoluchowski [1a]. The rate of coagulation was calculated by the same author [1b] and it has been shown [2] how this rate is affected by a potential barrier around the particles.

In the experiments now described, the concentration changes at various positions in a small volume of a monodisperse aerosol have been followed by optical methods. At low concentrations where individual particles could be detected, a photographic technique has been used. For aerosols of higher concentrations, a photometer has been used to determine particle size and concentration from measurements of the light scattered in a particular direction. The sample of aerosol was contained in a shallow cell so that the vertical boundaries were small in area compared with the horizontal boundaries which were assumed to be completely absorbing. The concentrations were sufficiently low for coagulation to be negligible, though the photometric method was shown to be applicable at high concentrations.

From the results obtained in the present work, it has been found possible to provide an experimental verification of Smoluchowski's equation for the diffusion of a particle in a field of force. It is hoped at a later date to extend the work using aerosols of higher concentrations in order to study the effects of collisions between particles.

Theory

The equation derived by Smoluchowski [1a] for diffusion in a field of force has been discussed in a review by Chandrasekhar [3]. In the

*Now in the Department of Physical Chemistry, University of Sheffield.

gravitational field the numerical concentration (n) of a cloud of particles is given as a function of vertical position (z) and time (t) by :

$$\frac{\partial n}{\partial t} = D\frac{\partial^2 n}{\partial z^2} - v\frac{\partial n}{\partial z} \tag{1}$$

where D is the diffusivity of the particles

$$\left(= \frac{kTF}{6\pi\mu r}\right) \tag{2}$$

and v is the sedimentation velocity

$$\left(= \frac{2}{9}\frac{r^2 g}{\mu}(\rho - \rho_0)F.\right) \tag{3}$$

In the derivation of equation (1), coagulation of particles is neglected. When it is appreciable, an additional term must be added to equation (1) as follows :

$$\frac{\partial n}{\partial t} = D\frac{\partial^2 n}{\partial z^2} - v\frac{\partial n}{\partial z} - Kn^2 \tag{4}$$

where K is the Smoluchowski coagulation factor $= 8\pi Dr$.

No solution has been obtained for equation (4) but equation (1) has been solved for various boundary conditions. Mason and Weaver [4] considered the upper and lower surfaces to be perfectly reflecting, so that the total number of particles remained constant. Davies [5] obtained a solution for two cases : in the first, the upper and lower surfaces were completely absorbing, and in the second, the upper surface was free and the lower one completely absorbing. Smoluchowski [1a] also solved equation (1) for two cases : first, where both surfaces were free, and secondly, where the upper surface was free and the lower surface completely reflecting.

Previous experimental investigations have been limited to those of Perrin [6] and Fürth [7] who determined the probability density distribution of a particle of gamboge or mercury suspended in water. The present investigation was carried out with an aerosol of many thousands of particles enclosed between two horizontal plane surfaces. It was assumed that all particles colliding with these surfaces were removed from the aerosol, and that the experimental conditions therefore corresponded to the first case considered by Davies.

Experimental Method

To verify equation (1) experimentally, conditions were chosen so that each of the terms was of the same order of magnitude. A considerable increase in the significance of experimental results was achieved by using a monodisperse aerosol, which was formed in a generator of the type first proposed by Sinclair and La Mer [8]. Particle sizes between 0·1 and 1 μ could most readily be obtained. A preliminary examination of the magnitudes of the quantities in equation (1) then showed that the depth of the observation cell should be about 2 mm, and to make the loss of particles at the vertical boundaries relatively negligible a diameter of about 10 mm was chosen.

The apparatus and technique were so designed that phenomena other than Brownian motion and sedimentation had a negligible effect on the aerosol. To suppress convection currents the cell was constructed from a large block of brass and all leaks were sealed. The aerosol must be formed from a liquid of very low vapour pressure in order to minimize evaporation of the particles during the observation, and dinonyl phthalate was selected as a suitable material both because of its low vapour pressure (2×10^{-9} cm Hg at 20°C), and because of its stability at the maximum temperature to which it was subjected in the generator (250°C). It was calculated that, for a particle of 1 μ radius, evaporating into vapour in equilibrium with a plane liquid surface a 10 per cent decrease in radius would occur only after 3×10^7 sec. The corresponding figure for a 0·1 μ particle was 3×10^5 sec.

Optical methods of analysis of the aerosol were chosen since they do not cause appreciable interference with the motion of the particles. A photographic technique was used at low concentrations, and a photometer was employed at high concentrations where the individual particles could not be identified. The observation cell was designed so that the aerosol could be illuminated and observed in various directions, and the particle size and concentration could be determined as a function of time and vertical height.

The generator and observation cell and the two methods of measurement are described below, but a detailed description of the photographic technique has been published elsewhere [9].

Production of a monodisperse aerosol. The aerosols were produced in a generator similar to that used by SINCLAIR and LA MER [8], but modified to prevent the entry of stray condensation nucleii, and to give a more uniform temperature gradient in the condensation tube (Fig. 1).

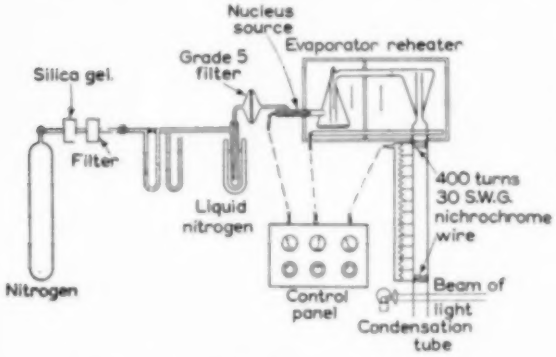

FIG. 1. Generator for monodisperse aerosols.

The gas used was nitrogen, containing only 10 p.p.m. of oxygen, and it was dried and carefully filtered. It was then thoroughly mixed with the condensation nucleii which were formed from analytical quality sodium chloride evaporated from an alumina-covered heater. The sodium chloride vapour was cooled rapidly so that the majority of the nuclei were about 0·005 μ in radius, as seen from electron micrographs.

The liquid was held at a constant temperature and the mixture of nuclei and nitrogen flowed over its surface at a constant velocity. After further mixing and removal of any liquid spray, the gas stream passed down a condensation tube where temperature gradients of between 1 and 5°C per cm could be maintained by graded heater coils wound round the tube. A radial temperature gradient was found to exist in the tube, and consequently the aerosol was taken only from a region within 5 mm of the axis. The apparatus was found capable of producing aerosols with particle radii between 0·1 and 4 μ in concentrations of up to 10^9 particles per cm^3. The mass concentrations could be increased by raising the temperature of the evaporator. At a given mass concentration, the numerical concentration was increased, and hence the particle size reduced, by raising the temperature of the nucleus source and increasing the cooling rate, though at high rates of cooling the dispersion of the aerosol increased. Those parts of the apparatus which were subjected to high temperatures were made entirely of borosilicate glass and were frequently cleaned by chemical means to remove products of decomposition.

The cell and illumination. The observation cell, 2 mm deep and 10 mm diameter (Fig. 2) was constructed from a block of brass 7 cm in diameter, and the interior surfaces were blackened to prevent stray reflections. The aerosol could pass

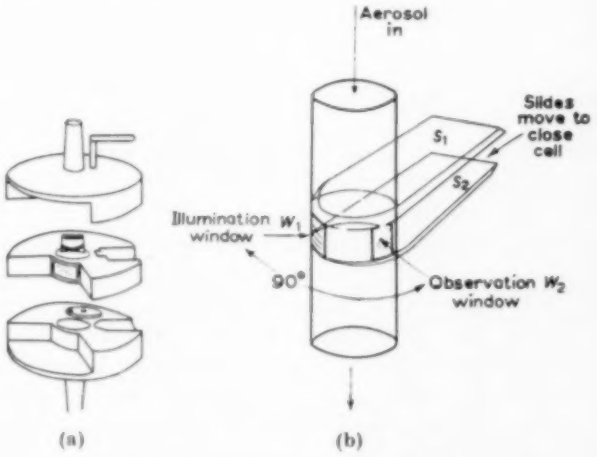

FIG. 2. The observation cell (*a* and *b*).

unimpeded downwards through the cell, and a sample was isolated by the simultaneous operation of slides S_1 and S_2. The sample was illuminated through the window W_1, and observed through a second window W_2, set at an angle of 90° to the first. The windows were made from thin mica, carefully sealed to prevent leakage, and the apparatus operated at a pressure slightly above atmospheric to reduce the risk of the entry of air.

Light from the source A (Fig. 3) was focussed on to a slit S_1 and an image of this slit was formed at the centre of the cell C by means of a 25 mm microscope objective 0_1, the beam being

limited in width by the stop E. A set of Chance ON 20 heat absorbing filters F removed all but 10^{-5} per cent of the infra-red energy. The whole illumination system was mounted on an optical bench, and either the camera K or the photometer was mounted on the arm R which could be rotated about the vertical axis of the cell.

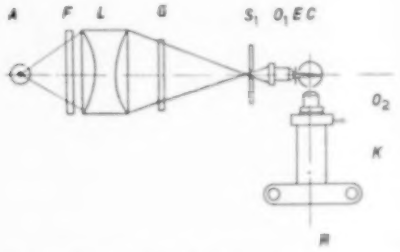

Fig. 3. Illumination and photography of aerosol (horizontal section).

Photographic method of analysis. For concentrations below 10^4 particles per cc, the photographic method already described [9] was used for the determination of numerical concentration and particle size, using light from a 250 W compact mercury-arc. Concentration was determined by photographing a known volume of aerosol using an exposure time of about 0·5 sec, and counting the number of particles. Determination of particle size was effected by using a longer exposure (about 5 sec) and measuring the vertical displacement of the particles; the radius was then calculated using the Stokes-Cunningham relation (3) for the sedimentation velocity.

Photometric method of analysis. For the determination of concentrations above about 10^4 particles per cm^3, a photometric method was employed in which the light scattered by the aerosol at a given angle was measured. Illumination was provided by a near-monochromatic source (the mercury yellow lines 5770 and 5791 A) and a parallel beam was produced by introducing an additional lens between the objective O_1 and the slit S_1. The beam was interrupted at a frequency of 600 c/s by means of a rotating shutter.

The light scattered at a given angle was focussed by means of a 25 mm objective O_2 (Fig. 4) in the plane of a horizontal slit S_4 which restricted the depth of cell from which light was received. By means of the cylindrical lens L_3 an image of the slit was formed on the cathode of the photomultiplier P (RCA 931A). By adjustmen of the vertical position of the slit S_4 it was possible to measure the light scattered at 10 different depths in the cell. The photomultiplier moved with the slit so that the light was always received on the same element of the cathode. Vertical slits S_2 and S_3 limited the angle of acceptance in the horizontal plane to 20 minutes of arc.

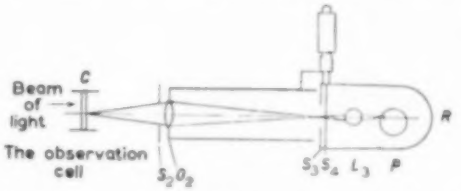

Fig. 4. Optical system for photometer (vertical section).

The photomultiplier current was passed through a 1 megohm resistor, and the resulting potential difference was amplified by an A.C. amplifier, whose output was indicated on an ammeter. The amplifier was tuned to 600 c/s by means of a parallel-Tee filter [10]. The signal-to-noise ratio, and hence the sensitivity of the photometer, was increased by reducing the band-width. The equipment was found to be insensitive to small amounts of daylight and to slow variations of the arc. Fluctuations in the mains supply and movement of the arc affected the intensity of the illumination and it was necessary to take the mean of several readings to minimize the error so caused. The response of the photometer was shown to be linear by measuring the light transmitted by a neutral filter wedge of known density.

In each experiment, concentration was measured at various levels in the cell over a period of 30-40 min and sufficient readings were obtained to determine an accurate average value. In all cases the spatial resolution was adjusted so that the light falling on the photomultiplier was that scattered by particles in a volume of depth equal to 0·08 of the total depth of the cell. The maximum sensitivity of the photometer was such that a single particle of 1 μ radius caused a deflection of 10 divisions on the ammeter and a

particle of 0·1 μ a deflection of 0·1 division (full scale = 100 divisions).

(*a*) *Determination of particle size.* When a suspension of small spheres of isotropic dielectric material is illuminated by a beam of parallel unpolarized light, the intensity of the light scattered at an angle γ to the direction of the transmitted light is given by [8] :

$$I_\gamma = \frac{\lambda^2}{8\,\pi^2\,R^2} I_0\,(i_1 + i_2) \qquad (5)$$

where λ is the wavelength of the light,

R is the distance of the point of observation from the sphere,

i_1 and i_2 are functions of λ, γ, r and the refractive index, and have been tabulated by Lowan [11], and

I_0 and I_γ are the intensities of the incident and scattered light.

The intensity of the scattered light was measured at intervals of 10° and the position of maximum intensity determined. From the tables of i_1 and i_2, the position and number of the maxima were plotted as functions of particle radius for given wave-lengths and refractive indices. Hence the particle size could be determined.

(*b*) *Determination of initial concentration.* If a parallel beam of intensity I_0 is incident on a system of n particles per unit volume of radius r, the intensity of the transmitted light is given [8] by the relation

$$\frac{I}{I_0} = \exp\left[-\,nK(r)\,\pi\,r^2\,.\,x\right] \qquad (6)$$

where $K\,(r)$ is the scattering coefficient which has been tabulated by Lowan [11], and is a function of $(2\pi\,r/\lambda)$, and

x is the length of the path through the aerosol.

A reading proportional to the intensity of the incident light, I_0, was obtained when the photometer received the light passing directly through the empty cell. The cell was then filled with aerosol and a value proportional to the intensity of the transmitted light I was obtained immediately. Since the radius r had been determined, n could then be directly calculated from the ratio I/I_0.

(*c*) *Determination of relative concentration.* The concentration changes were determined by setting the photometer at an angle γ corresponding to one of the maxima of the intensity distribution, and observing the reading at suitable intervals until the deflection had fallen to about 1 per cent of its original value. For a given particle size and at low concentrations, the amount of light scattered is proportional to the number of particles present, and therefore the ratio of any reading to the initial reading (after correction for background illumination) is equal to the relative concentration c at that time. This procedure was repeated at various depths of the cell and the concentration determined as a function of time and position. In making the measurement it has been assumed that secondary scattering in the aerosol is negligible. Comparisons of photographic and photometric measurements are made in Fig. 7. The concentration was 10^5 to 10^6 particles cm^{-3}.

Results

Experiments were carried out with samples of monodisperse aerosols of numerical concentrations in the range 10^2 to 10^7 particles per cm^3, and particle radii from 0·05 – 2 μ. The numerical concentration was found to be affected by random. density fluctuations in the cell. Consequently the results were tabulated as a function of time and vertical position and were smoothed by using the general formula :

$$n_{j_s} = 1/3\,(n_{j-1} + n_j + n_{j+1}) \qquad (7)$$

where n_{j_s} is the smoothed value at position or time j, and n_{j-1}, n_j, n_{j+1} are the measured values at positions or times $j-1$, j, $j+1$.

Smoothing was effected first in the direction of z decreasing and then of t increasing. The smoothed values of relative concentration, $c = n/n_0$, were then plotted as a function of the distance z from the top of the cell, with t as parameter.

Evaluation of the results. Equation (1) can be obtained in dimensionless form by writing equation [5]

$$\left.\begin{aligned} t &= \tau \cdot \frac{L}{v} \\ n &= n_0\, c \\ z &= ZL \end{aligned}\right\} \qquad (8)$$

where L is the depth of the cell.

$$\text{Then} \quad \frac{\partial c}{\partial \tau} = \alpha \frac{\partial^2 c}{\partial Z^2} - \frac{\partial c}{\partial Z}, \qquad (9)$$

$$\text{where} \quad \alpha = \frac{D}{vL}. \qquad (10)$$

Equation (9) has been solved by Davies [5] to obtain the relative concentration c as a function of α, Z and τ. It is not possible from his solution to obtain α explicitly in terms of c, Z and τ. A numerical value of α may be obtained, however, if equation (9) is expressed in finite difference form by writing :—

$$\left.\begin{aligned} \frac{\partial c}{\partial \tau} &= \frac{c_2 - c_4}{2H} \\ \frac{\partial c}{\partial Z} &= \frac{c_1 - c_3}{2h} \\ \frac{\partial^2 c}{\partial Z^2} &= \frac{c_1 + c_3 - 2c_0}{h^2} \end{aligned}\right\} \qquad (11)$$

where c_1, c_2, etc. represent the relative concentrations in the aerosol in the $Z-\tau$ plane as shown in Fig. 5, and

$$\left.\begin{aligned} h &= \Delta Z \\ H &= \Delta\tau = \Delta t \frac{v}{L} \end{aligned}\right\} \qquad (12)$$

Here h is the interval between the levels at which observations are made, but H can only be evaluated when the value v is known. The terms in equation (11) are subject to errors of the order H^2 or h^2 respectively (approximately 1 per cent).

Equation (9) then becomes :

$$0 = \alpha \frac{c_1 + c_3 - 2c_0}{h^2} - \frac{c_1 - c_3}{2h} - \frac{c_2 - c_4}{2H} \qquad (13)$$

which may be written :

$$a_1 y_1 + a_2 y_2 = b \qquad (14)$$

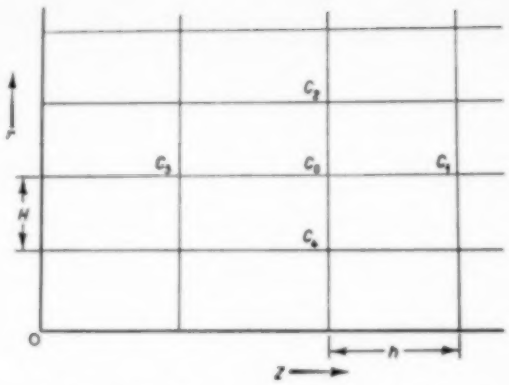

Fig. 5. Relative concentrations in $Z - \tau$ plane.

where $a_1 = (c_1 + c_3 - 2c_0)$, $b = \frac{h}{2}(c_1 - c_3)$,

$$a_2 = -\frac{h^2}{2}(c_2 - c_4), \quad y_1 = \alpha, \quad y_2 = \frac{1}{H} \qquad (15)$$

Now, from the experimental results obtained it is possible to evaluate a_1, a_2 and b in terms of the relative concentration c and the interval h. Hence α and H may be determined by solving two such equations similtaneously.

Since a single experiment results in over 100 values of c, at least 64 equations such as equation (14) could be obtained. To avoid edge effects the values of c near the boundaries of the cell and the initial values were discarded. Then the mean values of α and H were determined from about 20 values of c. Several values of the parameter α are plotted in Fig. 6 against the

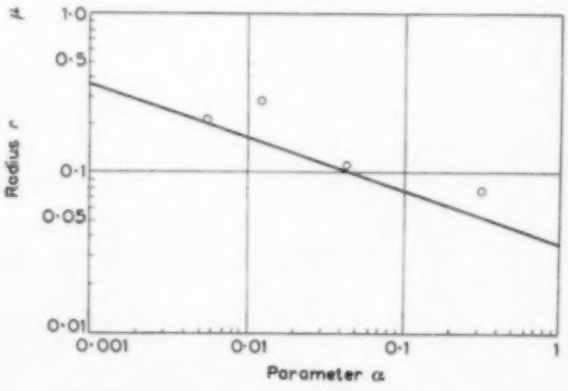

Fig. 6. Parameter α as a function of particle radius.

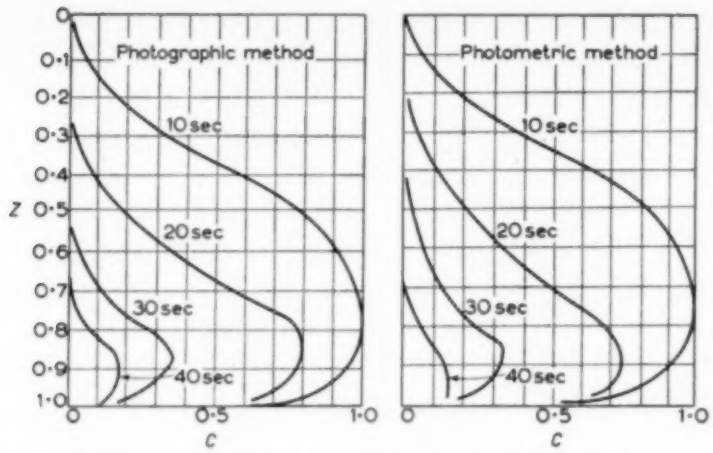

FIG. 7. Relative concentration as a function of time and position. Comparison of two methods for aerosol consisting of particles of 0·80 μ radius in concentrations of 10^6 particles cm^{-3} initially.

VOL. 7 957/58

radius measured by the photographic method. The line drawn is the one which would fit the equation $\alpha = D/vL$, for measured values of r.

Accuracy of the results. The accuracy of the photographic measurements has been discussed in an earlier paper [9]. The errors for the upper and lower limits of particle radius which could be measured can be expressed as $0{\cdot}1 \pm 0{\cdot}001\ \mu$ and $2{\cdot}0 \pm 0{\cdot}04\ \mu$. In order to obtain some indication of the accuracy of the photometric measurement, several particle radii were determined by both methods and a comparison is made in Table 1.

Table 1

	Photometric measurement	*Photographic measurement*
	Radius (μ)	*Radius* (μ)
1	0·7	0·64
2	0·6	0·51
3	0·55	0·56
4	0·45	0·42

The relative concentration at various times was also determined by both methods and a comparison is made in Fig. 7. The standard error of the determination of relative concentration is also indicated in Fig. 8. The influence of the experimental errors on the parameter α may be estimated as follows.

From equations (2), (3) and (10), it can be shown that :

$$\alpha = \frac{3\,kT}{4\,\pi\,L\,r^3\,g\,(\rho - \rho_0)}\ \alpha\ r^{-3} \qquad (16)$$

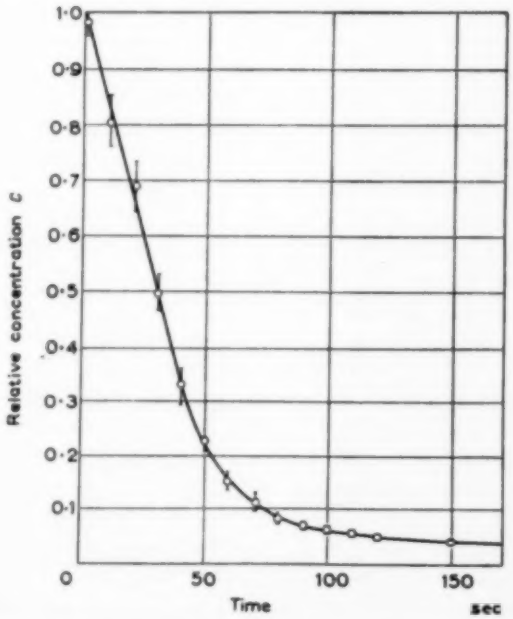

FIG. 8. Change in relative concentration with time (particle radius 0·80 μ, initial concentration 10^6 particles cm^{-3}).

Equation (16) is represented by the solid line in Fig. 6, which therefore gives the expected value of α for an aerosol whose particle radius has been calculated from measured values of sedimentation velocities. The value of α obtained by the numerical method is an average value for a large number of particles and depends on the mean value of r^{-3}. Hence there is a divergence between the two values of α if the aerosol is not monodisperse since the arithmetic mean and the root mean cube values of r will then differ. The magnitude in the error in the parameter α is indicated by the scatter in Fig. 6.

The values of the intervals used in the finite difference evaluation were sufficiently small for the errors in the value of α to be less than 1 per cent.

Conclusions

Two experimental methods of determining particle size and concentration in a monodisperse aerosol have been developed; a photographic technique for use at low concentrations and a photometric method for high concentrations. Together, they may be used to measure radii 0·1 and 5 μ and concentrations up to 10^7 particles per cm^3. For concentrations between 10^5 and 10^6 particles per cm^3, determinations of particle size have been made by both methods and satisfactory agreement has been obtained.

Concentration changes have been measured in a sample of aerosol contained in a shallow cell with absorbent horizontal boundaries and the experimental results have been used to calculate values of the parameter α in the equation for motion of a system of diffusing particles in a gravitational field. Other factors giving rise to movement of particles have been almost entirely eliminated. Reasonable agreement is obtained with the theoretical values.

The photometric method is shown to be applicable at high concentrations when the effects of coalescence following collisions between particles would be expected to be large, and the work is therefore capable of extension in order to obtain information on the rate of coalescence of particles.

Acknowledgements—The authors are indebted to the British Shipbuilding Research Association who sponsored the work described in this paper. They are grateful to Prof. D. M. Newitt for general supervision of the work, and to Dr. J. H. Burgoyne for his helpful suggestions and interest. The apparatus was constructed in the departmental workshop and the authors would like to convey their thanks to the staff for their co-operation. Imperial Chemical Industries very kindly offered advice on suitable liquids to use and generously provided a sample of dinonyl phthalate.

Symbols

$a_1 = c_1 + c_3 - 2c_0$ (See Fig. 5)

$a_2 = -\frac{h^2}{2}(c_2 - c_4)$ (See Fig. 5)

$b = \frac{h}{2}(c_1 - c_3)$ (See Fig. 5)

c = Relative concentration n/n_0
D = Diffusivity
F = Slip factor
g = Acceleration due to gravity
H = ΔZ
h = $\Delta\tau$
I = Intensity of transmitted light
I_0 = Intensity of incident light
I_γ = Intensity of light scattered at angle γ to transmitted light
i_1, i_2 = Function of r, λ, γ and refractive index
K = Smoluchowski coagulation factor ($= 8\pi Dr$.)
k = Boltzmann's constant
L = Depth of cell
n = Numerical concentration of particles
n_0 = Initial numerical concentration of particles
R = Distance of point of observation from sphere
r = Particle radius
T = Absolute temperature
t = Time
v = Sedimentation velocity
x = Length of optical path through aerosol
y_1 = Parameter α
y_2 = $1/H$
Z = Reduced vertical coordinate z/L
z = Vertical distance from top of cell
α = Parameter D/vL
γ = Angle between scattered and transmitted light
λ = Wavelength of light
μ = Viscosity of gas
ρ = Density of material of particle
ρ_0 = Density of gas
τ = Reduced time co-ordinate (vt/L)
$K(r)$ = Scattering coefficient

References

[1a] Smoluchowski M. v. *Ann. Phys.* 1915 **48** 1103-1112.

[1b] Smoluchowski M. v. *Z. Phys. Chem.* 1917 **92** 129-168.

[2] Wooding E. R. *Proc. Phys. Soc.* B 1957 **70** 65-70.

[3] Chandrasekhar *Rev. Mod. Phys.* 1943 **15** 1.

[4] Mason M. and Weaver W. *Phys. Rev.* 1924 **23** 412-426.

[5] Davies C. N. *Proc. Roy. Soc.* A 1949 **200** 100-113.

[6] Perrin J. *Atoms.* 1916 Constable, London.

[7] Fürth R. *Ann. Phys.* 1917 **53** 177-213.

[8] Sinclair D. and La Mer V. K. *Chem. Rev.* 1949 **44** 245-267.

[9] Richardson J. F. and Wooding E. R. *J. Photogr. Sci.* 1956 **4** 73-78.

[10] Sturtevant J. M. *Rev. Sci. Instrum.* 1947 **18** 124.

[11] Lowan A. W. Tables of scattering functions for spherical particles. *Nat. Bur. Stand.* (Applied Mathematics Series 4) 1949 U.S. Govt. Printing Office, Washington.

VOL.
7
957/58

Chemical Engineering Science, 1957, Vol. 7, pp. 60 to 65. Pergamon Press Ltd.

Condensation of vapours from gas–vapour mixtures. An approximate method of design

B. HULDÉN

Ekono Association for Power and Fuel Economy, S. Esplanadgatan 14, Helsinki, Finland

(*Received* 18 *April* 1957)

Abstract—By using a hypothetical driving force, the well known COLBURN-HOUGEN [6] analysis may be applied graphically, without trial and error, to solve condenser design problems. The method, as compared with the original calculation in [6], is rapid and the result agrees within 1 per cent.

The graphical method is approximate and includes the assumption [6] of latent heat transfer overbalancing sensible heat transfer as pointed out by SMITH [10]. It is believed that reasonable surface estimates may be obtained even for initially superheated mixtures, as shown for the example of BRAS [1]. The method has the advantage of giving a clear overall view of the design procedure in analogy to the enthalpy driving force methods.

Résumé—Par l'emploi d'un gradient fictif, il est possible d'utiliser l'analyse de Colburn-Hougen (6) sous forme graphique, sans itération, pour résoudre les problèmes de calcul des condenseurs. La méthode, comparée au calcul original (6), est rapide et donne des résultats en accord à I pour cent près.

La méthode graphique est approchée, et suppose (6) que l'échange de chaleur latente l'emporte sur l'échange de chaleur sensible, comme l'a indiqué Smith (10). Il est admis qu'une évaluation normale de la surface peut être obtenue, même pour des mélanges préalablement surchauffés, comme le montre l'exemple de Bras (I). La méthode à l'avantage de donner une vue d'ensemble claire, en comparaison avec les méthodes utilisant les gradients d'enthalpie.

Zusammenfassung—Das bekannte Verfahren von COLBURN und HOUGEN [6] zur Berechnung von KONDENSATOREN kann durch Einführung hypothetischer treibender Kräfte graphisch ohne schrittweise Verbesserung verwendet werden. Diese Methode führt schnell zu Ergebnissen, die, verglichen mit der Original-Methode [6], nicht mehr als 1% Abweichung aufweisen.

Die graphische Methode ist ein Näherungsverfahren und enthält die ANNAHME [6], dass die zu übertragenden latenten Wärmen gross sind gegenüber den fühlbaren Wärmen, wie es von SMITH [10] näher ausgeführt wurde. Sogar für anfänglich überhitzte Mischungen, wie bei dem Beispiel von BRAS [1], erhält man vernünftige Abschätzungen der Oberfläche. Die Methode hat den Vorteil, eine klare Übersicht über das Berechnungsverfahren zu geben in Analogie zu jenen Methoden, die mit der Enthalpie als treibender Kraft arbeiten.

INTRODUCTION

THEORETICALLY, the simultaneous transfer of heat and mass across a phase boundary is an extremely complicated process. For the cooling of a saturated mixture of a condensing vapour and an inert gas, COLBURN and HOUGEN [6] have presented a straighforward, stepwise, trial-and-error method of calculation, later refined by SMITH [10]. CAIRNS [3] has presented experimental evidence for the validity of the uncorrected original COLBURN-HOUGEN method. However, the application of it is time-consuming. The same is true for a general graphical method proposed by BRAS [1]. For the special case of water vapour and air mixtures the simple enthalpy driving force method has been successfully applied (MICKLEY [8], BROWN [2]). An interesting extension of MICKLEY's method has recently been published by CRIBB and NELSON [7], who use a corrected enthalpy transfer potential for the system moist coal gas-water.

The aim of this paper is to show that by introducing a new hypothetical driving force concept, the basic COLBURN-HOUGEN analysis may be applied with little time-consumption and good accuracy. The writer has used the

method successfully for some years in engineering practice.

Theory

By introducing a hypothetical potential of the form

$$\theta = t - F \ln (1 - p/P) \quad (1)$$

or

$$\theta = t + F \ln (1 + x) \quad (2)$$

for the total heat transferred, the rate of heat transfer at any point of a condensate surface will be proportional to the difference $\theta_g - \theta_c$.

Assuming that diffusion and heat transfer occur independently of each other according to the rate equations

$$dq_s/dA = h\,(t_g - t_c) \quad (3)$$

$$dq_c/dA = L \cdot M_v \cdot k \cdot \ln \left(\frac{P - p_c}{P - p_g}\right) \quad (5)$$

and applying the semi-empirical relation suggested by Chilton and Colburn [4].

$$\frac{h}{c_m G} (Pr)^{2/3} = \frac{k}{G/M_m} (Sc)^{2/3} \quad (6)$$

it follows that

$$dq_s/dA + dq_c/dA = dq/dA = h\,(\theta_g - \theta_c) \quad (7)$$

with

$$F = L \cdot M_v \frac{k}{h} = \frac{L \cdot M_v}{c_m M_m} \left(\frac{Pr}{Sc}\right)^{2/3} \quad (8)$$

As can be seen from equations (1), (7) and (8) the potential θ and the factor F have the dimension of temperature. Thus, θ could be considered an "effective" temperature for a sensible heat transfer rate equivalent to the total heat transfer rate.

Now, generally, the value of the factor F will vary with gas composition and temperature. For purposes of engineering design, however, good approximations may be obtained by using a mean, constant value of F throughout the whole condenser.

The solution of a design problem requires knowledge of the relation between the potential θ and the enthalpy i of the gas-vapour mixture. The enthalpy of a condensate-free mixture may be expressed as

$$i = c_m M_m (1 + x)\, t + L_0 M_v \cdot x \quad (9)$$

or

$$i = L_0 M_v \left[\frac{c_m M_m}{L_0 M_v} (1 + x)\, t + x\right] \quad (10)$$

Using equations (2) and (8), the expression (10) may be written

$$i = L_0 M_v \left[\frac{1 + m\,(t/F)}{\exp (t/F)} \exp (\theta/F) - 1\right] \quad (11)$$

or

$$i = L_0 M_v \left[a \cdot \exp (\theta/F) - 1\right] \quad (12)$$

with the notation

$$m = \frac{L}{L_0} \left(\frac{Pr}{Sc}\right)^{2/3} \quad (13)$$

$$a = \frac{1 + m\,(t/F)}{\exp (t/F)} \quad (14)$$

Keeping the temperature factor F constant, the factor a is a function of the temperature t and the ratio m. If, however, (t/F) is small as compared with unity, the factor a may be taken as approximately constant and ratios between enthalpy differences of the gas mixture may be approximated using only values of θ, i.e.

$$\frac{i_1 - i_2}{i_3 - i_4} \approx \frac{\exp (\theta_1/F) - \exp (\theta_2/F)}{\exp (\theta_3/F) - \exp (\theta_4/F)} \quad (15)$$

For small values of (θ/F), the relation (15) takes the form

$$\frac{i_1 - i_2}{i_3 - i_4} \approx \frac{\theta_1 - \theta_2}{\theta_3 - \theta_4} \quad (16)$$

but the approximation may be poor unless we have simultaneously

$$\frac{L}{L_0} \left(\frac{Pr}{Sc}\right)^{2/3} \approx 1 \quad (17)$$

As this is the case for a mixture of water-vapour and air, the expression (16) thus confirms the enthalpy driving force approximation for small values of (θ/F), i.e. for low partial pressures of steam.

In a condenser with constant cross-section for gas flow, the sensible heat transfer coefficient h will usually decrease towards the cold end due

to a decreasing mass velocity. As the mass velocity is proportional to the factor $(1 + x)$, the relation between θ and h may by the use of equation (2) be approximated using the proportionality

$$\frac{h_1}{h_2} = \left[\frac{\exp\left(\frac{\theta_1 - t_1}{F}\right)}{\exp\left(\frac{\theta_2 - t_2}{F}\right)}\right]^n \tag{18}$$

with n denoting the mass velocity exponent of h. If t is small as compared with θ, the proportionality may be approximated by the simpler expression

$$\frac{h_1}{h_2} = \left[\frac{\exp(\theta/F)}{\exp(\theta/F)}\right]^n \tag{19}$$

This last expression will be used even when t is not small as compared with θ because, to some extent it takes into account the temperature dependency of h.

These approximations enable a rapid graphical evaluation of a sufficient number of condensate interface temperatures in a $\theta - t$ – diagram for the saturated gas mixture in question, a subsequent integration giving the required condenser surface. The technique is analogous to that used in connection with the enthalpy potential, with tie-lines from the operating line giving interface conditions [7], [8] and [9].

APPLICATION

The use of the method may best be shown by applying it to the carefully calculated example given in reference [6], as recommended by COLBURN [5].

The problem consisted in designing a counter-flow condenser for a saturated mixture of steam and nitrogen at one atmosphere pressure and saturated at 95°C. The mixture is to be cooled to 40°C with water entering at 25°C and leaving at 60°C.

An accurate calculation of the F-value is not justified, since even rough approximations give good accuracy.

The mean value of the factor F for a steam-nitrogen mixture will thus be taken as

$$F = 1500°\text{C}$$

which is close to the arithmetic mean of the end values as is seen from Table 1.

The value of the potential θ can then be evaluated and plotted against t. The operating line, generally, will not be a straight line but an exponential curve, which is constructed as

Table 1. *Summary of calculations*

Point		1	3	4	5	7	9
t_g	°C	95	90	85	75	55	40
$(1\text{-}p_g/P)$ from [6]		0·165	0·305	0·430	0·622	0·844	0·927
Mean F-value used	°C	1500	1500	1500	1500	1500	1500
Proper F-value inherent in [6]	°C	1355	1470	1505	1550	1620	1630
$\theta = t_g - 1500 \ln (1 - p_g/P)$	°C	2798	1871	1351	787	309	154
$\exp(\theta/1500)$		6·457	3·481	2·461	1·690	1·229	1·108
t_w	°C	60	40·5	33·8	28·8	25·8	25
t_w from [6]	°C	60	42·3	35·8	30·5	26·6	25
h P.c.u./(hr) (ft^2)	(°C)	34·5	23·8	19·3	15·4	12·7	12·0
h from [6] P.c.u./(hr) (ft^2)	(°C)	34·5	23·0	18·0	14·5	12·0	11·7
t_c	°C	93·6	84·4	72·9	53·5	33·4	27·7
t_c from [6]	°C	93·6	84·3	73·0	54·4	34·6	27·8
$t_c - t_w$	°C	33·6	43·9	39·1	24·7	7·6	2·7
LMTD	°C		38·4	41·5	31·4	14·5	4·8
ΔA	ft^2	0	233	76	82	134	165
ΔA from [6]	ft^2		226·4	81·0	85·4	134·1	168·1
A	ft^2	0	233	309	391	525	690
A from [6]	ft^2		226·4	307·4	392·8	526·9	695

follows (Fig. 1). With the end values given, the water temperature corresponding to e.g. 90°C gas temperature is calculated from a heat balance using the analogy (15), (neglecting condensate cooling)

$$\frac{60 - t_w}{60 - 25} = \frac{\exp(2798/1500) - \exp(1871/1500)}{\exp(2798/1500) - \exp(154/1500)}$$

giving

$$t_w = 60 - (60 - 25)\frac{6{\cdot}457 - 3{\cdot}481}{6{\cdot}457 - 1{\cdot}108} = 40{\cdot}5°\text{C}$$

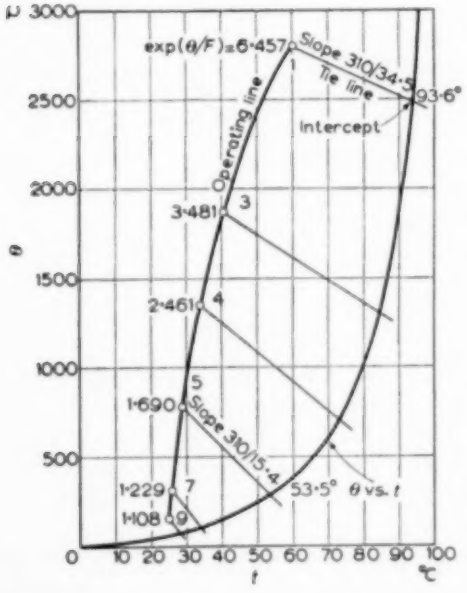

FIG. 1. Approximate graphical solution of condenser problem given by COLBURN and HOUGEN [6]. Saturated mixture of steam and nitrogen at a total pressure $P = 1$ atmosphere. Temperature factor $F = 1{,}500$°C. Hypothetical temperature $\theta = t - 1{,}500 \ln (1 - p_g/P)$°C.

Similarily, the water temperatures corresponding to 85, 75 and 55°C gas temperatures respectively are calculated, (see Table 1) and the resulting points of the operating line are plotted in the $\theta - t$ – graph. Now, a "tie-line" from any point of the operating line having a negative slope equal to ratio of the heat transfer coefficients h_0/h gives an immediate graphical solution of the COLBURN-HOUGEN rate balance equation

$$h\,(t_g - t_c) + L \cdot M_v \cdot k \cdot \ln\left(\frac{P - p_c}{P - p_g}\right) = h_0\,(t_c - t_w) \qquad (20)$$

because, by definition, the left side of the equation (20) equals $h\,(\theta_g - \theta_c)$ and consequently

$$\frac{\theta_g - \theta_c}{t_c - t_w} = \frac{h_0}{h} \qquad (21)$$

Using the hot end values given in [6], viz.

$$\frac{h_0}{h} = \frac{310}{34{\cdot}5} = 9{\cdot}0$$

a straight line from point 1 on the operating line with a slope of $-9{\cdot}0$ gives a condensate interface temperature intercept of 93·6°C.

In the same way, the interface temperatures corresponding to points 3, 4, 5, 7 and 9 are calculated. For this purpose the relation (19) is used, with the mass velocity exponent n taken as 0·6. Thus, the value of h for e.g. point 3 is

$$h = 34{\cdot}5\,(3{\cdot}481/6{\cdot}457)^{0{\cdot}6} = 23{\cdot}8$$

(see Table 1). The neglecting of condensate cooling introduces an error in the position of the operating line and consequently also in the interface temperatures. A correction for this error could certainly be made, but considering that the error is usually comparatively small and the method approximate, a more accurate but time-consuming procedure seems not justified.

With the interface temperatures thus calculated, the required surface between the points can be evaluated e.g. from the water-interface temperature differences. In this calculation the heat due to condensate cooling must not be neglected, or a considerable error will be introduced, because this amount of heat is clearly transferred with a smaller mean temperature difference than the rest of the heat.

From the data given, the total heat of condensate cooling amounts to an additional 10 per cent. To simplify calculations, all condensate is assumed to be formed at the gas inlet point 1. The error thus introduced partly compensates the error made in approximating the operating line.

The evaluation of the surface required between points 1 and 3 will accordingly run

Total heat transferred without condensate cooling, from [6]	4,899,000 P.c.u./hr
Heat from condensate cooling, [6]	493,000 P.c.u./hr
Combined heat transfer coefficient, [6]	310 P.c.u./(hr) (ft^2) (hr)
Exp ($\theta/1500$), point 1	6·457
Exp ($\theta/1500$), point 9	1·108
Exp ($\theta/1500$), point 3	3·481
Temperature difference point 1, from graph	33·6°C
Temperature difference point 3, from graph	43·9°C
Log. mean temperature difference, points 1-3	38·4°C

Surface required between points 1-3, without condensate cooling

$$\left(\frac{6{\cdot}457 - 3{\cdot}481}{6{\cdot}457 - 1{\cdot}108}\right)\left(\frac{4{,}899{,}000}{310 \cdot 38{\cdot}4}\right) = 229\ ft^2$$

Additional surface for condensate cooling points 1-3

$$\left(\frac{95 - 90}{95 - 40}\right)\left(\frac{493{,}000}{310 \cdot 38{\cdot}4}\right) = 3{\cdot}7\ ft^2$$

totalling

$$229 + 3{\cdot}7 = 232{\cdot}7\ ft^2$$

Similarily, between points 3-4, the required surface is

$$\left(\frac{3{\cdot}481 - 2{\cdot}461}{6{\cdot}457 - 1{\cdot}108}\right)\left(\frac{4{,}899{,}000}{310 \cdot 41{\cdot}5}\right) + \left(\frac{90 - 85}{95 - 40}\right)\left(\frac{493{,}000}{310 \cdot 41{\cdot}5}\right)$$

$$= 72{\cdot}6 + 3{\cdot}5 = = 76{\cdot}1\ ft^2$$

As a result, the total surface between points 1 and 9 adds up to 690 ft^2 as compared to the accurate figure of 695 ft^2.

A summary of the calculations is given in Table 1. Use of logarithmic mean values for the temperature differences is not theoretically justified but has been made since it gives slightly conservative results.

In view of the many approximations made, the final result is in surprisingly good agreement with the accurate calculation, the deviation being less than 1 per cent.

DISCUSSION

An analysis of errors shows that small relative errors in the position of the operating line and in the factor F should be divided by the factor

$$E = 1 + \frac{d\theta/dt}{h_0/h}$$

in order to obtain the resulting relative errors in the temperature difference. As the accuracy decreases with E, the mean value of F used should approach the proper value at the cold end in cases of a large variation in F between the hot and cold end.

Preliminary checks of the method against the examples given in [9] and [3] show also good agreement with the calculations.

Although not intended for initially superheated mixtures, the method is believed to give reasonable surface estimates even in such cases. It is then necessary to assume saturation at the cold end. Depending upon the position of dew-point relative to intercept temperature, the method makes possible a quick determination of the onset of condensation, before which the surface calculation must be based on sensible heat transfer only.

Using an F-value of 1500°C, the method was applied to the example given by BRAS [1]. The problem was to design a condenser for moist converter gases at one atmosphere pressure entering at 136·4°C with a dew-point of 54·4°C and to be cooled to 29·3°C with water having an average temperature of 21°C throughout the condenser. The terminal conditions indicated a constant average tie-line slope of about − 11·0. As the $\theta - t$ – plot showed only a slight curvature in the equilibrium line and the operating curve was a straight vertical line, the required surface

was evaluated using the end points only. The resulting surface was 14 per cent larger than that given by BRAS. With one intermediate point between the end points, an excess surface of only 7 per cent was obtained. The intercept temperatures showed good agreement with those given, although the F-values inherent in the calculations at entrance and outlet were 1680 and 1600°C respectively.

NOTATION

A = surface
a = factor
c = specific heat ; c_m mean specific heat of gas mixture
E = factor
F = factor, temperature units
G = molar mass rate
h = coefficient of sensible heat transfer ; h_0 combined heat transfer coefficient
i = enthalpy of gas mixture on inert gas basis
k = molar mass transfer coefficient
L = latent heat of vaporization ; L_0 at enthalpy reference temperature
M = molecular weight ; M_m mean molecular weight of gas mixture ; M_v molecular weight of vapour
m = factor
n = mass velocity exponent of h
p = partial pressure of vapour ; p_g in bulk stream of gas mixture ; p_c at condensate interface
P = total pressure of gas mixture
Pr = Prandtl number
q = rate of total heat transfer ; q_s sensible heat transfer rate ; q_c heat transfer rate due to diffusion
Sc = Schmidt number
t = temperature ; t_g bulk temperature of gas stream ; t_c temperature at condensate interface ; t_w cooling water temperature
x = molar "humidity" : moles of condensing vapour per mole of inert gas
θ = hypothetical temperature for combined heat transfer

VOL. 7
957/58

REFERENCES

[1] BRAS G. H. *Chem. Engng.* 1953, 223-226, 238-240.
[2] BROWN G. *Trans. Roy. Inst. Tech.* 1954 No. 77 Stockholm.
[3] CAIRNS R. C. *Chem. Engng. Sci.* 1953 **2** 127-138.
[4] CHILTON T. H. and COLBURN A. P. *Industr. Engng. Chem.* (*Industr.*) 1934 **26** 1183-1187.
[5] COLBURN A. P. *Inst. Mech. Engrs. Proc. Disc. Heat Transfer London* 1951 James Clayton Lecture.
[6] COLBURN A. P. and HOUGEN O. A. *Industr. Engng. Chem.* (*Industr.*) 1934 **26** 1178-1182.
[7] CRIBB G. S. and NELSON E. T. *Chem. Engng. Sci.* 1956 **5** 20-33.
[8] MCADAMS W. H. *Heat Transmission* (2nd Ed.) 1942 pp. 285-292. McGraw-Hill, New York.
[9] MICKLEY H. S. *Chem. Engng. Progr.* 1949 **45** 739-745.
[10] SMITH J. C. *Industr. Engng. Chem.* (*Industr.*) 1942 **34** 1248-1252.

Chemical Engineering Science, 1957, Vol. 7, pp. 66 to 72. Pergamon Press Ltd.

The vapour pressure of di-*n*-butylphthalate, di-*n*-butylsebacate, lauric acid and myristic acid

EGIL HAMMER and AKSEL L. LYDERSEN
The Technical University of Norway, Chemical Engineering Laboratory, Trondheim, Norway

(*Received* 23 *May* 1957)

Abstract—The vapour pressures of di-*n*-butylphthalate, di-*n*-butylsebacate, lauric acid and myristic acid were measured in the pressure range of 0·1 to 13 mm Hg. The results were adequately covered by the equation

$$\log p = A - \frac{B}{T} - \frac{C}{T^2}$$

with the constants A, B and C as reported in Table 7.

For di-*n*-butylphthalate the results were in good agreement with previous measurements for pressures higher than 1·5 mm Hg. Previous measurements for di-*n*-butylsebacate are only reported for pressures below 0·063 mm Hg [19], [16].

The vapour pressure determinations for the fatty acids were in very good agreement with the data obtained by DUSSEL [7], WITGERT [25] and POOL and RALSTON [17].

The latent heat of vaporization calculated from the vapour pressure data by means of the Clausius-Clapeyron equation are reported in the Tables 2-5.

Résumé—Les auteurs ont mesuré les pressions de vapeur du di-n-butylphthalate, di-n-butylsebacate, de l'acide laurique, et de l'acide myrislique dans l'intervalle de pression de 0, 1 à 13 mm Hg. Les résultats sont traduits d'une façon convenable par l'équation :

$$\log p = A - \frac{B}{T} - \frac{C}{T^2}$$

où les constantes A, B, C, ont les valeurs indiquées dans le tableau 7.

Pour le di-n-butylphthalate les résultats concordent bien avec les mesures précédentes, pour les pressions supérieures à 1, 5 mm Hg.

Les mesures antérieures pour le di-n-butylsebacate ne sont indiquées que pour les pressions inférieures à 0,063 mm Hg (19) (16).

Les déterminations des tensions de vapeur des acides gras sont en accord avec les données obtenues par DUSSEL (7), WITGERT (25) et POOL-RALSTON (17).

Les chaleurs latentes de vaporisation, calculées à partir des données de tension de vapeur au moyen de l'équation de CLAUSIUS-CLAPEYRON sont indiquées dans les tableaux 2 à 5.

Zusammenfassung—Die Dampfdrücke von Di-*n*-butylphthalat, Di-*n*-butylsebacat, Laurinsäure und Myristinsäure wurden im Druckbereich von 0,1 bis 13 Torr gemessen. Die Ergebnisse wurden hinreichend durch die Gleichung.

$$\log p = A - \frac{B}{T} - \frac{C}{T^2}$$

beschrieben, deren Konstanten A, B und C in Tafel 7 wiedergegeben sind.

Für Di-*n*-butylphthalat waren die Ergebnisse in guter Übereinstimmung mit früheren Messungen für Drücke oberhalb 1,5 Torr. Frühere Messungen für Di-*n*-butylsebacat waren nur im Druckbereich unterhalb 0,063 Torr bekannt [19], [16].

Die Dampfdruckbestimmungen für die Fettsäuren waren in guter Übereinstimmung mit den Werten von DUSSEL [7], WITGERT [25] sowie von POOL und RALSTON [17].

Die aus den Dampfdruckwerten mit Hilfe der Clausius-Clapeyron-Gleichung berechneten Verdampfungswärmen sind in den Tafeln 2 bis 5 wiedergegeben.

VOL. 7 957/58

Introduction

The vapour pressure measurements reported in this paper were carried out in order to obtain accurate data on materials suitable for the calibration of vacuum columns with only few theoretical plates. Di-*n*-butylphthalate and di-*n*-butylsebacate were chosen because the mixtures are easy to analyse by refractive index, the fatty acids because they are commercially important.

Materials

The materials were purified by fractional destillation in a vacuum column operated with a reflux ratio 10 : 1 at a pressure of approximately 2 mm Hg. 20-30 per cent was removed overhead, and a middle fraction of constant refractive index was collected. The fatty acids were also purified by repeated crystallization in ethyl alcohol and benzene until the melting point remained unchanged.

The purified esters and acids were colourless and had the properties listed in Table 1.

Experimental

The vapour pressure measurements were carried out with a new low pressure vapour-liquid equilibrium still to be described in a later communication on vapour-liquid equilibria.

The pressure drop through the still became detectable at pressures below 1 mm Hg. For pressures above 1 mm Hg, the final readings were taken after the individual temperature readings at the lower, the central and the top part of the still, were within 0·07°C of the average reading. The temperature for pressures between 0·5 and 1·0 mm Hg are based only on the readings in the central and the top part of the still, whereas below 0·5 mm Hg only the readings at the top part close to the connection to the McLeod gauge was used.

Results

The experimental data are given in the Tables 2-5, together with the pressures read from the smooth curves of the Figs. 1 and 2 and the calculated values of the enthalpy of vaporization.

Table 1. *Properties of purified materials. The values in parentheses refer to the corresponding properties given in the literature. Reference* [14] *refers to a commercial grade, reference* [15] *to 99·5 per cent*

	*Di-*n*-butyl –*		*Fatty acid*	
	phthalate	*sebacate*	*lauric*	*myristic*
Molecular weight	278·34	314·45	200·31	228·37
Refractive indices for esters n_D^{25}	1·4908 (1·4925 [12] 1·4928 [23]	1·4405 (1·4397 [21] 1·4423 [14])	1·4263 (1·4267 [6])	1·4307 (1·4310 [6])
for acids n_D^{60}	1·4926 [14])			
Density, for esters d_4^{25}, for acids d_4^{70} g/cm³	1·0427 (1·045 [12] 1·043 [2] 1·048 [14])	0·9340 (0·9321 [21] 0·9326 [1] 0·935 – 0·942 [14])	0·8562* (0·8544 [18])	0·8523* (0·8528 [18])
Melting point, °C		−9·2 (−9·2 [21] −11 [14])	43·7 – 43·9 (44·2 [24] 43·9 [15])	54·0 – 54·2 (53·9 [24] 54·1 [18] 54·4 [8] 53·8 [15])

* The density at 60°C was 0·8631 g/cm³ for lauric, 0·8600 g/cm³ for myristic acid.

Tables 2 and 3. Experimental and smoothed vapour pressure in mm Hg and calculated enthalpy of vaporization λ for

Di-n-butylphthalate					*Di-n-butylsebacate*				
Run No.	*Temp.* °C	*Vapour pressure*		λ kcal/kg	*Run No.*	*Temp.* °C	*Vapour pressure*		λ kcal/kg
		Exp.	*Smoothed*				*Exp.*	*Smoothed*	
24	125·70	0·240	0·240	75·2	30	128·45	0·102	0·104	72·6
25	131·55	0·368	0·351	74·4	31	134·20	0·151	0·156	71·8
17	139·21	0·554	0·567	73·3	32	141·21	0·250	0·249	70·8
23	147·02	0·90	0·90	72·2	33	146·41	0·350	0·348	70·1
18	156·70	1·54	1·55	71·0	34	155·41	0·603	0·603	69·0
29	158·39	1·71	1·70	70·8	38	160·04	0·790	0·790	68·4
22	162·12	2·08	2·07	70·3	35	164·67	1·025	1·028	67·8
26	172·76	3·60	3·56	69·9	36	175·36	1·85	1·834	66·5
21	180·18	5·03	5·04	68·1	37	186·02	3·16	3·15	65·3
19	180·36	5·00	5·11	68·1	39	194·98	4·80	4·82	64·4
27	186·87	6·91	6·89	67·4	40	208·14	8·69	8·70	63·0
20	195·88	10·15	10·25	66·4					
28	202·05	13·04	13·27	65·7					

Tables 4 and 5. Experimental and smoothed vapour pressure in mm Hg and calculated enthalpy of vaporization λ for

Lauric acid					*Myristic acid*				
Run No.	*Temp.* °C	*Vapour pressure*		λ kcal/kg	*Run No.*	*Temp.* °C	*Vapour pressure*		λ kcal/kg
		Exp.	*Smoothed*				*Exp.*	*Smoothed*	
78	106·37	0·167	0·167	111·6	64	111·88	0·105	0·113	104·8
82	111·50	0·250	0·248	110·4	65	124·75	0·173	0·177	103·4
79	117·37	0·377	0·382	109·1	70	129·30	0·250	0·247	102·4
83	122·20	0·542	0·538	108·0	66	133·68	0·335	0·338	101·4
80	130·95	0·956	0·971	106·1	71	139·90	0·520	0·519	100·1
84	136·76	1·43	1·41	105·0	67	145·40	0·75	0·748	98·9
81	142·30	1·97	1·98	103·8	72	149·58	0·97	0·977	98·1
85	149·23	3·02	2·99	102·5	61	149·60	1·00	0·978	98·1
86	157·83	4·86	4·86	100·9	68	156·25	1·47	1·47	96·8
87	164·05	6·85	6·79	99·8	62	161·75	2·03	2·04	95·8
88	171·05	9·78	9·73	98·5	75	162·50	2·15	2·13	95·5
89	175·85	12·42	12·67	97·7	69	169·80	3·22	3·22	94·2
					73	178·35	5·10	5·09	92·6
					74a	185·10	7·20	7·19	91·5
					74	185·50	7·32	7·34	91·4
					76	185·82	7·26	7·46	91·3
					77	191·90	10·05	10·04	86·0

VOL. 7 957/58

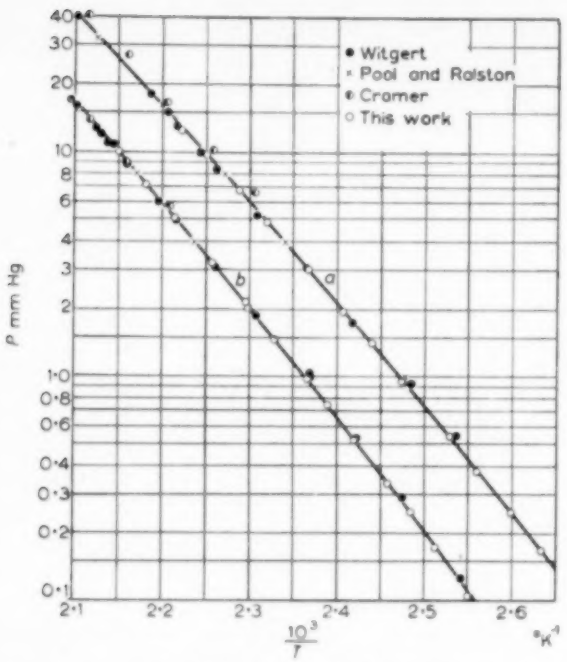

FIG. 1. Vapour pressure p mm Hg for esters vs. the reciprocal of the temperature $10^3/T$ °K^{-1}.

a = curve for di-*n*-butylphthalate,

$$\log p = 6{\cdot}439 - \frac{1011}{T} - \frac{720\,000}{T^2}$$

b = curve for di-*n*-butylphthalate according to equation by SMALL *et al.* [19].

c = curve for di-*n*-butylsebacate,

$$\log p = 6{\cdot}459 - \frac{984{\cdot}4}{T} - \frac{804\,000}{T^2}$$

d = curve for di-*n*-butylsebacate according to equation by SMALL *et al.* [19].

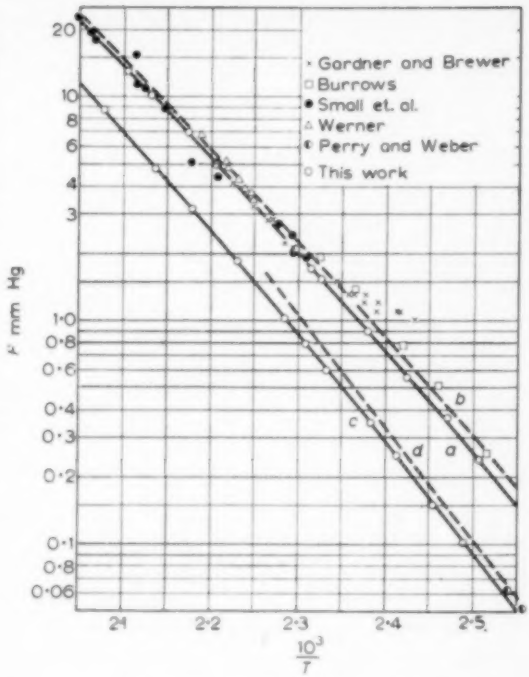

FIG. 2. Vapour pressure p mm Hg for fatty acids vs. the reciprocal of the temperature, $10^3/T$ °K^{-1}.

a = curve for lauric acid, $\log p = 6{\cdot}9247 - \frac{960}{T} - \frac{745\,000}{T^2}$

b = curve for myristic acid, $\log p = 6{\cdot}533 - \frac{637{\cdot}2}{T} - \frac{900\,000}{T^2}$

COMPARISON WITH PREVIOUS MEASUREMENTS

Measurements in the same pressure region by other investigators are plotted together with the results from the present work in the Figs. 1 and 2.

GARDNER and BREWER [9], BURROWS [3], SMALL *et al.* [19], and WERNER [22] measured the vapour pressure of di-*n*- butylphthalate. GARDNER and BREWER seem to have got too high vapour pressures in the region 1·0 to 1·5 mm Hg. BURROWS used a technical phthalate without any further purification, and got vapour pressures approximately 25 per cent higher than determined in this work. The broken line *b* in Fig. 1 corresponds to an equation by SMALL *et al.* [19]. The lower part of this curve gives 25 per cent, and the upper part 5 per cent higher pressures than measured by the present authors.

Previous measurements with di-*n*-butylsebacate are only published by SMALL *et al.* in the pressure range 0·0002 to 0·013 mm Hg [19] and by PERRY and WEBER [16] in the pressure range from 0·0007 to 0·063 mm Hg. The broken line *d* in Fig. 1 corresponds to an equation by SMALL *et al.* [19], which, however, should probably not be extrapolated into the pressure range of Fig. 1.

The measurements for the fatty acids are plotted in Fig. 2 together with the previous measurements by DUSSEL [7], WITGERT [25], POOL and RALSTON [17] and CRAMER [5]. All measurements are in very good agreement, with the exception of values given in the recent publication by CRAMER for lauric acid which are

Table 6. Smoothed saturation temperature data of lauric and myristic acid in °C as reported by different investigators

Pressure, mm Hg	0·1	0·2	0·5	1·0	2·0	5·0	10·0	*Acid*
DUSSEL [7]						158·6	172·0	
WITGERT [25]	99·2	108·2	120·5	130·8	142·6	159·1	172·4	
POOL and RALSTON [17]				130·2	141·8	158·2	171·9	C_{12}
CRAMER [5]						155·0	168·2	
This work		108·7	119·9	131·4	142·4	158·4	171·6	
WITGERT [25]	117·3	126·2	138·4	148·8	161·2	178·6	192·6	
POOL and RALSTON [17]				149·2	161·1	179·1	192·3	C_{14}
CRAMER [5]						177·8	191·6	
This work	117·4	126·4	139·3	150·0	161·4	178·0	191·8	

approximately 12 per cent higher than found by any of the others.

Table 6 lists the saturation pressures for the fatty acids as reported by different investigators.

The agreement between the data reported in Table 6 makes it reasonable to believe that the saturation pressure data for lauric and myristic are well established.

VAPOUR PRESSURE EQUATIONS

The relation between the vapour pressure and the enthalpy of vapourization is expressed by the Clausius-Clapeyron equation, which in a complete form can be written

$$\frac{dp}{dT} = \frac{p \cdot \lambda}{R\,(z'' - z')\,T^2} \qquad (1)$$

$(z'' - z')$ = difference between the compressibility factor for saturated vapour and saturated liquid. $(z'' - z') = 1{\cdot}00$ in the low pressure range where our measurements were carried out (see [13], p. 63).

For a narrow range with λ almost constant, integration of equation (1) gives

$$\log p = \frac{A}{T} + B \qquad (2)$$

corresponding to a straight line in the plots of Figs. 1 and 2. The complete vapour pressure curve from the critical point to the triple point has an *s*-shaped curvature, and SONDAK and THODOS [20] recommend an equation of the form

$$\log p = \frac{A}{T} + B \log T + \frac{C}{T^2} + D \qquad (3)$$

For sub-atmospheric pressures only three terms are necessary as in the KIRCHHOFF equation [11].

$$\log p = A - \frac{B}{T} - \frac{C}{T^2} \qquad (4)$$

Another empirical vapour pressure equation suitable for our purpose was suggested by HENGLEIN (10) and recommended by CORNELISSEN and WATERMAN [4].

Table 7. The constants of the equations (4) and (5)

Compound	*A*	*B*	*C*	*D*	*E*	*x*
Di-*n*-butylphthalate	6·4390	1011	720 000	5·9800	235 000	1·75
Di-*n*-butylsebacate	6·4590	984·4	804 800	6·0960	255 000	1·75
Lauric acid	6·9247	960	745 000	6·5560	239 300	1·75
Myristic acid	6·5330	637·2	900 000	6·4100	342 400	1·8

$$\log p\ D - \frac{E}{T^x} \qquad (5)$$

The equations (4) and (5) both have 3 empirical constants which easily can be adjusted to fit the curves of the Figs. 1 and 2. The constants corresponding to the plotted curves are given in Table 7.

The smoothed values of the vapour pressure reported in the Tables 2-6 are calculated from equation (4) with the constants of Table 7.

The curves are only slightly influenced by a minor change in x. For all the compounds in question, x seems to be in the range 1·75-1·8. CORNELISSEN and WATERMAN [4] found values of x from 1·2 to 1·7 for the compounds they investigated. The higher value in our case may be due to the large size of the molecules and the low pressures.

VOL. 7 957/58

LATENT HEAT OF VAPORIZATION

Combining equation (1) with equation (4) gives the enthalpy or latent heat of vaporization,

$$\lambda = 2{\cdot}3026\ R\,(z'' - z')\left(B + \frac{2C}{T}\right) \qquad (6)$$

In the low pressure region with $(z'' - z') \sim 1{\cdot}00$ and with the proper conversion factors to give λ in kcal/kg, equation (6) becomes

$$\lambda = \frac{4{\cdot}575}{M}\left(B + \frac{2C}{T}\right) \text{ kcal/kg} \qquad (7)$$

where M = the molecular weight.

Equation (7) with the molecular weights of Table 1 and the constants of Table 7 gives the latent heats reported in the Tables 2-5.

Heats of vaporization of fatty acids are given by CRAMER [5] as 97 kcal/kg for lauric acid at 164°C and 93 kcal/kg for myristic acid at 182°C. The corresponding figures according to this work are 99·8 and 91·5 kcal/kg.

Acknowledgement—The authors are indebted to the Royal Norwegian Council for Scientific and Industrial Research for a grant which has made this work possible.

NOTATION

A, B, C, D and E = constants of the vapour pressure equations

R = the universal gas constant, 848 m kg/kmole °K

T = absolute temperature °K

p = vapour pressure, in the equations (4) and (5) in mm Hg

x = constant of equation (5)

λ = enthalpy or latent heat of vaporization, in the equations (1) and (6) m kg/kmole; in question (7) kcal/kg

$(z'' - z')$ = difference between the compressibility factor (defined by $pV = zRT$, where V is the volume of 1 mole) of saturated vapour and saturated liquid.

REFERENCES

[1] BEILSTEIN F. K. *Handb. Org. Chem.* 4 Ausg. **2** 719.

[2] BRIED E. M. *et al. Industr. Engng. Chem.* (*Industr.*) 1947 **39** 484-91.

[3] BURROWS G. *J. Soc. Chem. Ind.*, 1946 **65** 360-5.

[4] CORNELISSEN J. and WATERMAN H. I. *Chem. Engng. Sci.* 1956 **5** 141-60.

[5] CRAMER J. S. N. *Rec. Trav. Chim.* 1943 **62** 605-10.

[6] DORINSON A., MCCORKLE M. R. and RALSTON A. W. *J. Amer. Chem. Soc.* 1942 **64** 2739-41.

[7] DUSSEL K. 1930 Dissertation, Hamburg.

[8] FRANCIS F. and PIPER S. H. *J. Amer. Chem. Soc.* 1939 **61** 577-81.

[9] GARDNER G. S. and BREWER J. E. *Industr. Engng. Chem.* (*Industr*). 1937 **29** 179-81.

[10] HENGLEIN F. A. *Z. Phys. Chem.* 1921 **98** 1-13.

[11] KIRCHHOFF G. *Ann. Phys. Chem.* 1858 **104** 612-21.

[12] LANGE *et al. Handbook of Chemistry* (7th Ed.) 1949.

[13] LYDERSEN A. L., GREENKORN R. A. and HOUGEN O. H. *Generalized Thermodynamic Properties of Pure Fluids* Report No. 4, Univ. of Wisc., Engng. Expt. Station, 1955.

[14] *Modern Plastics* Encyclopedia Issue, Sept. 1954. Plastics Catalogue Corp.

[15] PAQUOT *Bull. mens. Inst. techn. ét et rech. corps gras* 1952 **6** 174-8.

[16] PERRY E. S. and WEBER W. H. *J. Amer. Chem. Soc.* 1949 **71** 3726-30.

[17] POOL W. O. and RALSTON A. W. *Industr. Engng. Chem.* (*Industr.*) 1942 **34** 1104-5.

[18] RALSTON A. W. *Fatty acids and Their Derivatives* 1948.

[19] SMALL P. A., SMALL K. W. and COWLEY P. *Trans. Faraday Soc.* 1948 **44** 810-16.

[20] SONDAK N. E. and THODOS G. *Amer. Inst. Chem. Engrs. J.* 1956 **2** 347-53.

[21] STAHL W. and PESSEN H. *J. Amer. Chem. Soc.* 1952 **74** 5487-9.

[22] WERNER A. C. *Industr. Engng. Chem.* (*Industr*) 1952 **44** 2736-40.

[23] WILLIAMS F. E. *Ibid.* 1947 **39** 779-82.

[24] WILLIAMS F. C. and OSBORN J. O. *J. Amer. Oil Chem. Soc.* 1949 **26** 663-8.

[25] WITGERT H. 1933 Dissertation, Achen.

VC
7
1957

Chemical Engineering Science, 1957, Vol. 7, pp. 73 to 82. Pergamon Press Ltd.

The effect of fine material on the structure and resultant pressure drop of a bed charged against an uprising gas stream

G. C. GARDNER*

Development Department, Imperial Smelting Corporation Limited, Avonmouth, Glos., England

(*Received* 4 *February* 1957)

Abstract—Experiments were performed in which mixtures of up to 20 volume per cent of small sized material in large sized material—from 3 to 6 times the size of the small material—were charged against an uprising gas stream to form a bed. Measurements of the pressure drop and bed bulk density were taken at completion of charging and with the air stream volume flow rate maintained at the charging value. Plots of the recorded pressure drops versus the charging air velocity gave maxima, which, for different percentages of fine material, showed little variation in magnitude but which occurred at different air velocities. The maxima were much smaller than the pressure drop required for fluidization.

The limitation of the pressure drop was due to the mobility of the fine material in the bed during the charging procedure, with consequent alterations to the bed structure, which were reflected quantitatively by changes in the bed voidage and by the friction factor deviations—defined by equation (3). Changes in the bed voidage could account for most of observed pressure drop phenomena.

The beds formed in the presence of an air flow were stable, in so far as a reproducible pressure drop curve could be obtained by reducing the air flow to zero and then increasing it once more to the charging value.

The results are of particular application to blast furnaces, whose operation the experiments were meant to simulate.

Résumé—L'auteur fait passer, dans ses expériences un courant gazeux ascendant à travers un lit constitué par des matériaux de dimensions diverses : chaque lit est un mélange à 20% en volume de petites particules dans un ensemble de grandes particules (ces dernières ayant taille de 3 à 6 fois celle des petites). Les mesures de pertes de charge et de densité en vrac ont été faites à charge complète de l'appareillage et en maintenant le courant d'air à son débit en volume du point de charge. Les courbes des pertes de charge en fonction des vitesses de l'air présentent des maxima qui, pour des matériaux contenant des pourcentages variés de fines, ne diffèrent que légèrement en grandeur mais se produisent pour des vitesses de l'air différentes selon le matériau utilisé. Ces maxima sont très inférieurs aux pertes de charges requises en fluidisation.

La limitation de la perte de charge est due à la mobilité des fines dans le lit durant son chargement, à cause des altérations qui en résultent pour la structure du lit ; ceci se traduit quantitativement par des variations du vide dans le litet par des déviations du facteur de friction défini par l'équation (3). Les variations du % de vide du lit ont leur importance pour la plupart des phénomènes de pertes de charges observés.

Les lits formés en présence d'un courant d'air sont stables dans la mesure où l'on peut obtenir des courbes de pertes de charge reproductibles en réduisant à zéro le débit d'air et en le faisant croître à nouveau jusqu'au point de charge.

Les résultats s'appliquent en particulier aux hauts-fourneaux dont les expériences avaient pour but de simuler le fonctionnement.

Zusammenfassung—Zur Bildung einer Schüttschicht wurden Mischungen von bis zu 20 Volumenprozent eines feinkörnigen Materials in grobkörnigem Material – mit 3 bis 6 fachem Durchmesser gegenüber den feinen Körnerngegen aufwärtsströmende Luft aufgegeben. Nach

*Present address : U.S. Steel Corp., Research Center, Monroeville, Pa., U.S.A.

Beendigung der Aufgabe wurden – bei unverändertem Luftvolumenstorm – Druckabfall der Luft und Dichte der Packung gemessen. Der gemessene Druckabfall zeigte in Abhängigkeit von der Luftgeschwindigkeit Maxima, deren Höhe wenig vom Anteil an feinem Korn abhing, die jedoch bei verschiedenen Luftgeschwindigkeiten lagen. Die Maxima waren bedeutend geringer als der zum Fluidisieren erforderliche Druckabfall.

Die Begrenzung des Druckabfalls wurde durch die Beweglichkeit der feinen Teilchen innerhalb des Bettes während der Beladung bewirkt wodurch sich auch die Strucktur des Bettes veränderte. Dies zeigte sich quantitativ an den Veränderungen des Zwischenkornvolumens und den Abweichungen der Widerstandszahl, definiert nach Gl. (3).

Änderungen im Zwischenkornvolumen konnten zur Deutung der meisten Beobachtungen über den Druckabfall herangezogen werden.

Die in Gegenwart des Luftstroms gebildeten Schüttschichten waren insoweit stabil, als ein reproduzierbarer Druckabfall erhalten wurde, wenn man den Luftstrom abstellte und ihn dann wieder auf den alten Wert brachte.

Die Versuchsergebnisse lassen sich z.T. auf den Hochofen anwenden, dessen Arbeitsweise durch die Versuche nachgeahmt werden sollte.

INTRODUCTION

IN THE operation of a blast furnace, fresh charge is periodically dumped on to the top of existing burden, while maintaining the blast volume constant. The experiments reported here simulated this procedure by loading a fixed bed, consisting of materials of two different sizes, against a constant uprising air stream and then taking a back pressure measurement when charging was complete. It would normally be expected under these circumstances that the pressure drop at the charging air velocity would vary approximately proportionally to the square of the velocity until a pressure drop was achieved equal to that required for fluidization. However, it will be shown that only small amounts of material, fine enough to have a degree of mobility in the air stream in the bed whilst charging, are required to alter this relation and to limit back pressures to values far below those which would be obtained if the bed were charged in the absence of the rising air stream. The beds of modified structure, formed by the presence of fine material and the use of an air flow while charging, are stable, as demonstrated by the fact that the air velocity can be reduced to zero after charging, left for a while and then increased to the charging value again, when the back pressure returns to that which was observed initially.

The investigation was originally prompted by the observation that the burden back pressure of a non-ferrous blast furnace remained substantially constant when the blast volume was varied during a month's operation in the range from 3·8 to 5·4, expressed in arbitrary units. This furnace's charge contained one constituent which, as charged, had much fine material and which was friable, and would therefore produce further fine material in the furnace itself. Later an opportunity was obtained to get similar measurements for a furnace in which all constituents charged were mechanically strong and where no material of less than 1in. size was used. In this case the back pressure of the burden increased approximately proportionally to the square of the blast volume, as expected.

APPARATUS

The apparatus employed is shown diagrammatically in Fig. 1. Air was supplied by a fan and was metered by a venturi. It entered the base of a 5½ in. diameter windbox through a 3 in. diameter pipe and the windbox was filled to a height of 1 ft with ¼ in. to ½ in. granite chips for distribution purposes. A 2½ ft tall, 5½ in. inside diameter Perspex tube was flanged to the top of the windbox and a 36 mesh copper gauze was set between the flanges to act as a charge support. There were piezometric rings 3 in. and 9 in. above the charge support to take a differential pressure measurement. The tube could be unloaded through a small door, which was flush with the inside surface of the Perspex tube just over the charge support. The door was held in place by a strong rubber band and was gasketed with rubber sheet to ensure that it was leak proof.

The top of the Perspex tube was occupied by a rather complicated charge distributor which was found necessary to ensure even distribution of differently sized materials. A funnel led to a vertical 1¼ in. inside diameter pipe which discharged on to the charge scatterer. This consisted of nine planes of ½ in. diameter wooden balls with a 1¼ in.

spacing between planes and with 10 to 12 balls per plane. The balls were arranged to approximate a hexagonal close-packing, except that some balls near the walls were displaced to compensate for wall effects. Balls in a plane were supported on a frame of $\frac{1}{8}$ in. diameter brass wire and the frames were supported on a central vertical $\frac{1}{4}$ in. diameter brass rod.

The scatterer mixed the charge effectively, but particles left the bottom at various angles to the vertical and tended to pile close to the walls in forming the bed. To avoid this a straightener was placed underneath the scatterer. It comprised a honeycomb of square cells of $1\frac{1}{4}$ in. side and $3\frac{1}{2}$ in. deep. It was set 2 in. from the bottom plane of wooden balls and, as an additional corrective to the wall effect, a ring of $5\frac{1}{8}$ in. outside diameter and $5\frac{1}{4}$ in. inside diameter was fixed to its top.

The performance of the complete distributor was tested by collecting samples of its discharge in test tubes standing on the charge support. It was found to deliver the same weight of a mixed charge, containing a constant proportion of fine material, to every part of the Perspex tube's cross-section if the bottom of the straightener was set 4 in. to 6 in. from the top of the bed. To maintain this distance during charging the distributor was suspended from a wire running over a pulley with a balance weight on the other end.

VOL. 7 957/58

Packing Materials

It was considered desirable to perform some experiments with spherical packings, whose pressure drop characteristics in beds containing material of one size are well known. For cheapness the following materials were chosen: divinyl benzene (D.V.B.) spheres—an oversize fraction of moulding powder—mustard seed and dried peas. Granite chips were chosen as an irregular material.

The properties of the materials are given in the following table. The terminal velocities of the D.V.B. spheres and mustard seed, which were used as the smaller constituents of charges, were calculated. The shape factor and the effective surface diameter will be explained in a later section. The apparent density was measured by displacement in a suitable fluid and in the case of peas and mustard seed it was measured by displacement in water, diacetone alcohol and a silicone fluid to check that no absorption occurred. The volume diameter is the diameter of a sphere with the same volume as that of a particle and was calculated from the apparent density and the weights of not less than three separate lots of 100 particles.

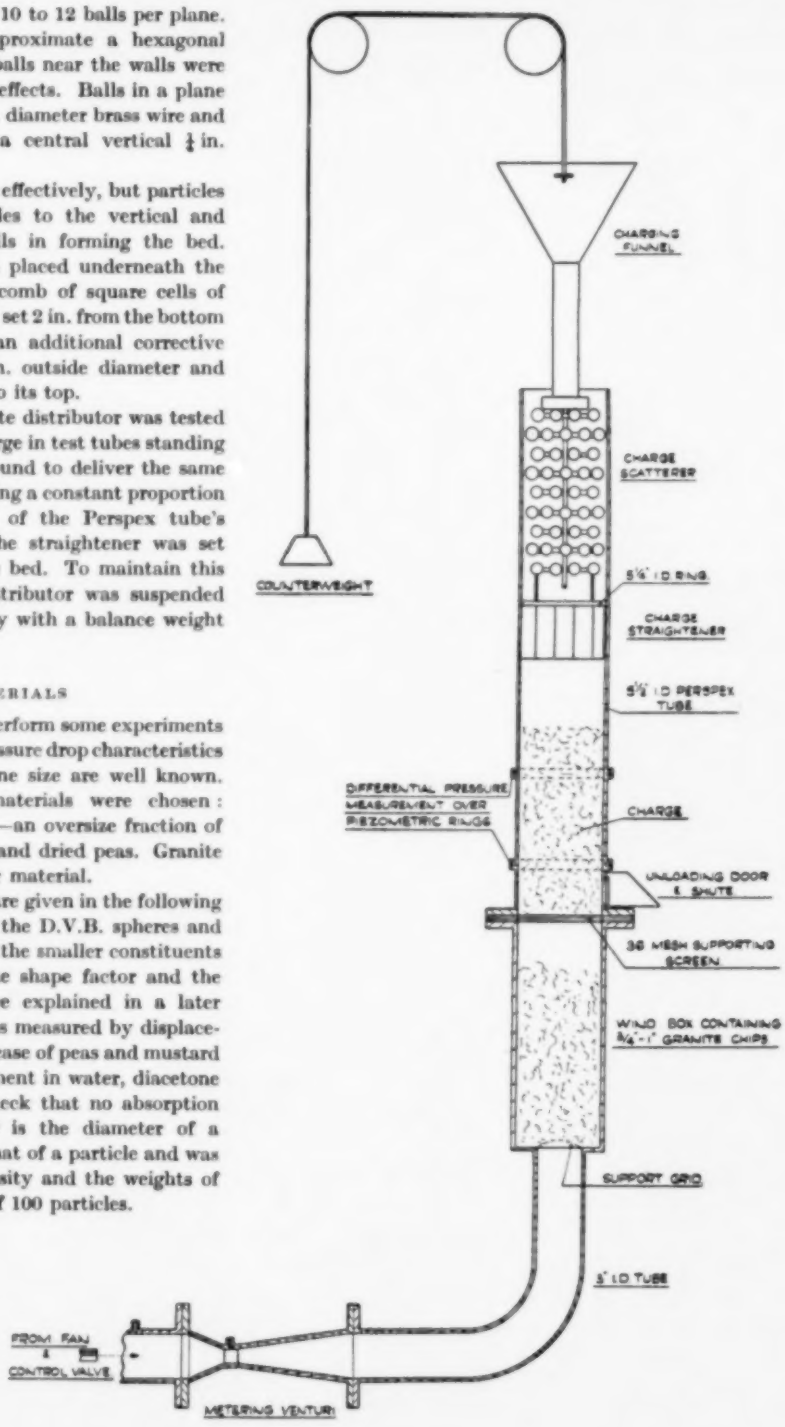

Fig. 1.

Properties of packing materials

Material	*Apparent density* (g/cm^3)	*Volume diameter* (*ft*)	*Shape factor*	*Effective surface diameter* (*ft*)	*Terminal velocity in air at 18°C* (*ft/sec*)
D.V.B. spheres	1·05	0·0044	6·0	0·0044	17·0
Mustard seed	1·21	0·0074	6·0	0·0074	26·8
Peas	1·40	0·0242	6·0	0·0242	
$\frac{1}{4}$–$\frac{3}{8}$ in. granite chips	2·57	0·0265	11·0	0·0145	
$\frac{3}{8}$–$\frac{1}{2}$ in. granite chips	2·54	0·0407	11·0	0·0222	

EXPERIMENTAL METHOD

The two packing materials to be used in the experiment were weighed separately in bulk. Two small vessels were filled from these bulk supplies, one containing about 300 cm^3 of the larger material and the other the required volume of the smaller material. The constituents of the charge were tipped evenly and together into the funnel of the charge distributor. The procedure was repeated until a bed of about 1 ft depth had been formed, care being taken that the proportions of fine to coarse material were not altered and also making sure that the base of the charge distributor was maintained at the requisite 4 in. to 6 in. from the top of the bed.

During charging the air volume passing through the bed was kept at a constant value to simulate conditions existing in a blast furnace. If the volume was sufficient, some of the fine material would float to the top of the bed and was sucked off when charging was completed and added to the bulk quantity of fine material. The unloaded bulk materials were weighed and the proportion of fine material in the charge was calculated as a volume percentage of the total solid volume charged.

On completion of charging the air flow rate, the pressure drop over the 6 in. between piezometric rings, and the bed height were measured. The height of the bed was determined at six points round the perimeter and an average value was recorded.

To test the stability of the structure of beds charged against a rising air stream, a number of experiments were performed in which the air volume was successively increased or decreased after charging, and measurements of pressure drop and bed height were made for each change. If, on increase of the air volume, fine material migrated to the top of the bed, it was extracted and the volume per cent of fine material remaining in the bed and the bed voidage were recalculated.

At the end of the experiment, the bed was unloaded and the two constituents were separated by sieving and weighed to check the prevous weighings.

TREATMENT OF RESULTS

The experimental results of pressure drop at the charging air velocity versus the square of the charging air velocity, given in Figs. 3 to 7, have been treated to show how far the limitation of the pressure drop can be attributed to changes in the voidage. The criterion has been to calculate the friction factor, in the manner described below, and to see how far it deviates from a reference friction factor curve determined experimentally for beds of material of one size. As the friction factor makes what is normally a sufficient allowance for changes in the voidage of the bed, deviation of the friction factor from the reference curve will indicate how far other effects are of importance and thus, indirectly, how far the voidage changes have influenced the back pressure. The other effects can be attributed to those changes of structure in the bed which give the air a more streamlined or less tortuous passage, or which tend to hide surface area which would normally exert a drag.

To obtain the reference friction factor curve, individual materials were charged against a zero air flow. Then measurements were taken of pressure drop with respect to air flow rate and the results were put in the form of friction factor ψ and Reynold's number Re and were plotted in Fig. 2. The two parameters are defined by

$$\psi = \frac{\Delta h}{L}\,\frac{2g}{V^2}\,\frac{\epsilon^3\, d}{\phi\,(1-\epsilon)},\quad Re = \frac{V\rho\, 4d}{\mu\phi\,(1-\epsilon)} \qquad (1)$$

Here V is the superficial air velocity or the volume of air per unit time divided by the tube cross-sectional area, d is the volume diameter or the diameter of a sphere which has the same volume as a particle forming the bed, ϵ is the fractional

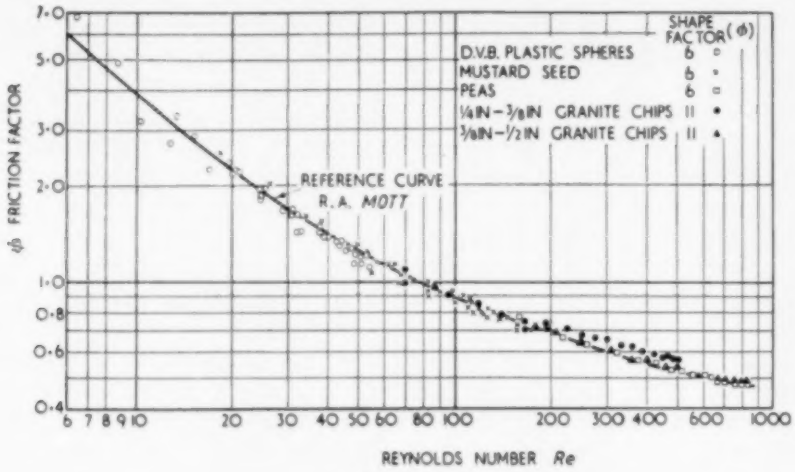

FIG. 2.

VOL. 7 957/58

bed voidage and ϕ is a shape factor. ϕ is 6 for spheres and Fig. 2 shows that this value correlates the results for D.V.B. spheres, mustard seed and peas with the curve given by MOTT [3] for spherical materials. It was found necessary to use a value of $\phi = 11{\cdot}0$ for granite chips and again Fig. 2 shows that the results correlate well with MOTT's curve [3] which was used as the reference curve.

To utilize equations (1) for beds containing material of two different sizes, a hypothetical bed is defined, containing spherical particles of diameter d_E for which the pressure drop and all other factors in equations (1), except, of course, d/ϕ, remain the same as for the experimental bed. There is much evidence (see references [1] and [4]) to show that the hypothetical bed will have the same surface area per unit volume as the experimental bed, so long as the particles in the latter are compact in form and have no plane surfaces. Hence d_E is called the "effective surface diameter," which for a particular material is $6d/\phi$, and is shown in the table of properties of packing materials. Applying this reasoning to beds containing two materials, where v_S and v_L are the fractions of the solid volume which are composed of small and large material respectively.

$$\frac{1}{d_E} = \left(\frac{\phi}{6d}\right)_S v_S + \left(\frac{\phi}{6d}\right)_L v_L \qquad (2)$$

d_E from equation (2) was used in equations (1), with $\phi = 6$, in place of the volume diameter d. ROSE and RIZK [4] and ERGUN [1] among others have used the same principle with success for correlating pressure drops through beds containing mixtures of materials.

The friction factor deviation is now defined as

$$\frac{\psi - \psi_R}{\psi_R} \times 100\% \qquad (3)$$

where ψ_R is the friction factor value on the reference curve at the same Reynold's number value as that calculated for the experimental system and ψ is the friction factor calculated from the experimental results.

The friction factor deviations are plotted in Figs. 8 to 12. Figs. 13 to 17 are presented to show the voidages of the beds but, instead of plotting the actual voidages, the fraction of the bed volume due to voids plus fines is given, or the voidage if the fine material was removed. This parameter avoids confusion, since the various curves are well separated, and it also shows clearly what happens to the large material, which can be considered to form the basic structure of the bed.

Finally, it must be noted that all the curves presented are cross-plots from curves of the ordinate versus the volume percentage of fine material for different superficial air velocities, for it was experimentally impossible to predict beforehand the quantity of fine material that would be retained by the bed. It should also be

remembered, when looking at the figures, that the abscissa is always the square of the charging air velocity.

DISCUSSION OF THE RESULTS

The pressure drop results will be described and discussed first and then an attempt will be made to explain the phenomena they exhibit by examining the friction factor deviations and the bed voidages. It is clear that a relationship between pressure drop and charging air velocity, such as that shown by Figs. 3 to 7, can be explained by changes in the structure of the bed as the charging velocity is increased; a study of the friction factor deviations and the bed voidages will give some insight into the nature of the changes of structure and their cause. It must be emphasized, however, that the picture presented will not be complete and will be indefinite, though it is hoped that further work, using other techniques, will shed greater light on the mechanisms involved.

(1) *Pressure drop at the charging air velocity*

All the families of curves in Figs. 3 to 7 show one most obvious characteristic, a substantially constant upper limit to the pressure drop, irrespective of the quantity of fine material, as long as a certain amount is present. However, the minimum quantity required may be as low as 2 per cent when the size of ratio coarse to fine material is large (6 : 1). The maximum pressure drop will, of course, occur at lower velocities the greater the amount of fine material, but at high air velocities the system with the greater amount of fine material will have the lower back pressure.

From examination of the curves, it is quite possible to imagine a blast furnace, operating over a range of blast velocities and with small variations in the amount of small material in the burden, having a substantially constant back pressure.

The level of the maximum pressure drop is less than that which would be required to fluidize the charge. This does not mean that the charge could not be fluidized if a sufficient air velocity were used, but that, before these conditions were achieved, it would be impossible to retain the fine material in the bed. Due to differences in the densities of their constituents, systems containing peas would require about 11 in. W.G./ft bed height to fluidize, and those containing granite chips would require 17 in. W.G./ft, whereas the figures show that the pressure drop can be limited to less than 4 in. W.G./ft bed height.

Comparison of Figs. 3 and 4 or 6 and 7 show that the maximum pressure drop that can be obtained is largely determined by the properties of the small material present and its size in relation to the size of the large material. Changing the shape and density of the coarse material has little effect upon the maximum back pressure, though it does affect the charging air velocity at which it is attained for a given volume percentage of fine material. The maximum pressure drop that can be attained increases as the size of the small material increases with respect to the large material.

It is apparent that the properties of the small material are of major importance in controlling the pressure drop characteristics because the small material has the ability to move about within the charge. In this respect it is important to note that the effect of changes in the density and shape of the fine particles has not yet been studied. If, for instance, a system using D.V.B. spheres, with a density of 1·05 g/cm^3, had been changed to one using lead shot of the same size as the D.V.B. spheres, higher maximum pressure drops should have been attained, since much higher air velocities would be required to move the lead shot to the same degree. The shape of the small material might also have an effect, but one impossible to forecast.

(2) *Friction factor deviations*

It remains to enquire what has happened in the bed to limit the back pressure. Since the pressure drops in Figs. 3 to 7 have been plotted against the square of the charging velocity, approximately straight lines would be expected if the voidage or structure of the bed did not alter. Inspection shows that none of the friction factor deviations, given in Figs. 8 to 12, are sufficient to account for more than a small part of the

VOL. 7 957/58

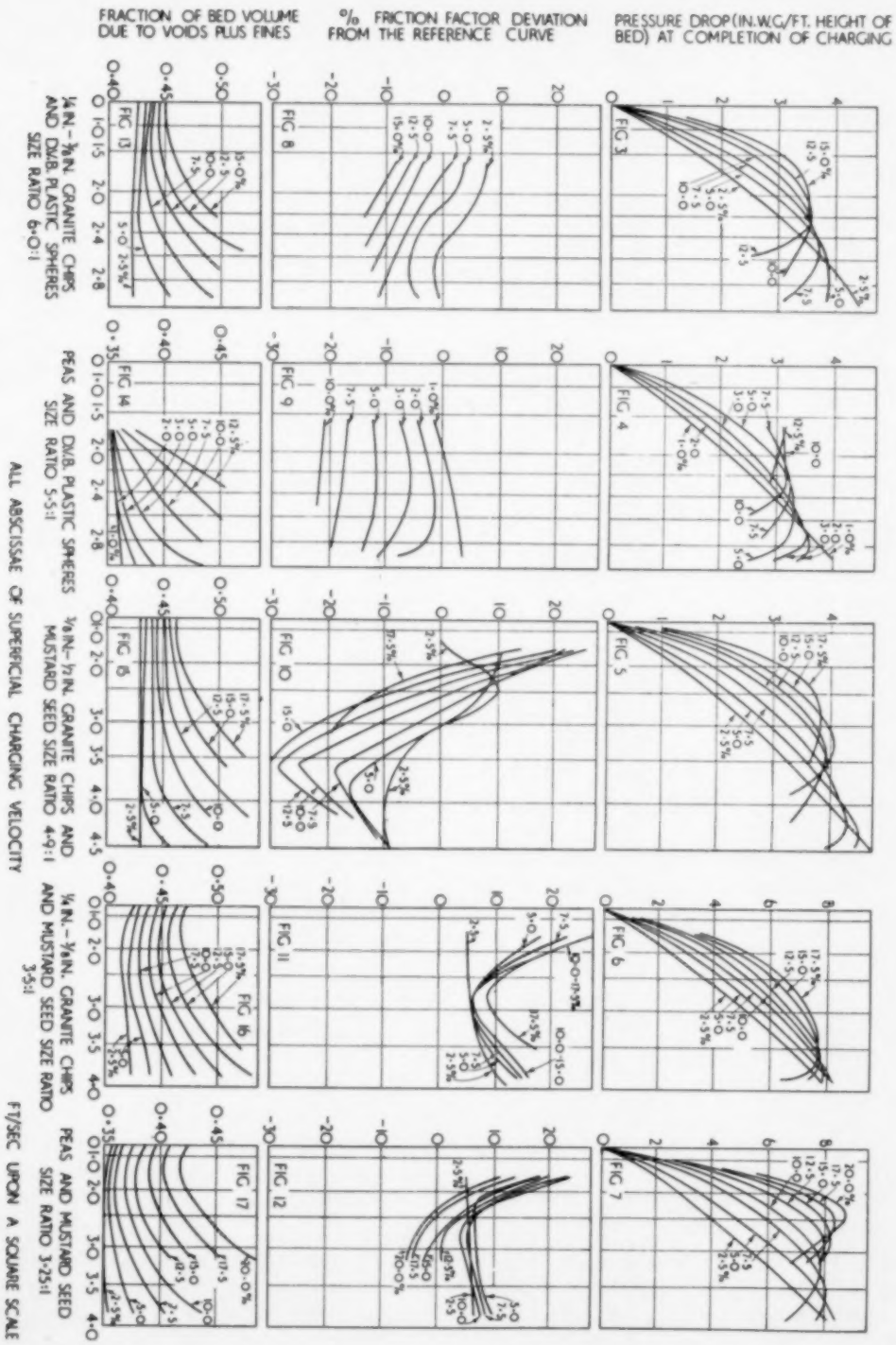
FRACTION OF BED VOLUME DUE TO VOIDS PLUS FINES
% FRICTION FACTOR DEVIATION FROM THE REFERENCE CURVE
PRESSURE DROP (IN. W.G./FT. HEIGHT OF BED) AT COMPLETION OF CHARGING
¼ IN. – ⅜ IN. GRANITE CHIPS AND DM/B. PLASTIC SPHERES SIZE RATIO 6·0:1
PEAS AND DM/B. PLASTIC SPHERES SIZE RATIO 5·5:1
⅜ IN. – ½ IN. GRANITE CHIPS AND MUSTARD SEED SIZE RATIO 4·9:1
¼ IN. – ⅜ IN. GRANITE CHIPS AND MUSTARD SEED SIZE RATIO 3·5:1
PEAS AND MUSTARD SEED SIZE RATIO 3·25:1
ALL ABSCISSAE OF SUPERFICIAL CHARGING VELOCITY FT/SEC UPON A SQUARE SCALE

deviation of the pressure drops from a straight line and, in fact, many of the friction factor deviations are positive. Therefore, it must be concluded that small material influences the back pressure mostly due to its ability to increase the voidage of the bed, as will be discussed in the next sub-section. However, the friction factor deviations show trends which are worth studying.

If Figs. 11 and 12, in which the size ratios are 3·5 : 1 and 3·25 : 1, are examined, they show a strong similarity between one another, both as regards the shape of the friction factor deviation curves and their magnitude. The only difference of note between the two systems is the shape and density of the coarse material, which is granite chips in the one case, and peas in the other. The curves fall rapidly from high positive deviation values of the order of 20 per cent to values in the region of 5 per cent and thereafter tend to remain unaltered or to increase slightly with increasing air velocity. A few exceptions may be noted in Fig. 12 where the friction factor deviation drops to near zero before levelling off. The magnitude of the deviations does not show any significant change as the proportion of fine material is increased. A mechanism which agrees with these facts, though there may be others, is that small material at low charging velocities falls into position where the gas velocity is relatively high, but that higher charging velocities forces it into positions where it makes a more normal contribution to the back pressure. However, if more fine material is added to the system, it does not increase the back pressure proportionally, because if it did, the friction factor deviations would increase as well.

Figs. 8 and 9, in which the size ratios are 6·0 : 1 and 5·5 : 1, also show great similarity with one another when the only difference of note is again the shape and density of the coarse material. However, where the fine material is smaller in relation to the coarse material, the friction factor deviations are mostly negative; they show much less or no variation with respect to charging air velocity and they have increasingly greater negative values as the amount of fine material in the charge is increased. Observations through the Perspex walls of the bed indicate that the fine material tends to form clusters, which grow in size or increase in number as the proportion of fine material increases. Since clusters would form in suitable positions on the top of coarse particles and thus out of the air stream and as, in any case, only a small part of the surface area of particles in a cluster would be exposed to the main air stream, the observations support the friction factor deviations and suggest that only a part of the surface area of the small material is useful in creating the back pressure though, it must be remembered, other structural modifications, discussed in the next subsection, may contribute to the deviations.

One family of curves in Fig. 10, in which the size ratio is 4·9 : 1, remains to be noted. The shape of the curves resembles that for a size ratio of 3·5 : 1 or 3·25 : 1, but large negative as well as large positive deviations are attained and they are a striking family to be found sandwiched between Figs. 9 and 11. There is, however, insufficient information to justify an explanation and they are presented without comment.

(3) *Fraction of the bed volume due to voids plus fines*

It has been shown that the limitation of the pressure drop that can be attained with fine material in the charge must be largely due to increased voidage of the bed. It is also apparent that the increased voidage must be almost solely due to the presence of the fine material and its mobility, as the lifting forces involved, which are shown quantitatively by the back pressure, are insufficient to move the coarse material. Figs. 13 to 17 are given to show how the structure of the coarse material was opened out.

There are three ways in which the voidage of the coarse material could be increased. Firstly, if it is present in sufficient quantities, the fine material would itself form the matrix for the coarse material to rest in, but that was not the case in these experiments. Secondly, as charging proceeds, fine material may be trapped between one coarse particle and another in line vertically, horizontally or in any other direction. Thirdly, if the charging velocity is sufficient, fine material will be blown

into positions where it offers the least resistance to air flow, or on top of large particles, so that the following coarse particle will be separated from the first.

Where fine material is layered between succeeding coarse particles it will tend to make an incomplete contribution to the pressure drop and it may even have a stream-lining effect upon the air passages. If, on the other hand, it gets jammed between large particles in line in a horizontal plane or if it lies at the bottom of naturally occurring pockets formed by the coarse particles, it will tend to have an excessive effect upon the back pressure, as it will be in a position where the air is flowing faster than at its average velocity.

Examination of the graphs shows that the bed is opened out to a considerable degree as the charging velocity increases. The amount of expansion can exceed the volume of the fine material.

The larger the fine with respect to the coarse material, the greater is the expansion of the coarse material at zero charging velocity for a given volume percentage of fines. This is understandable. However, as the charging velocity is increased, the bed containing the smaller fine material will tend to expand more, and the voidage of its coarse material will tend to become greater than for a bed with a larger fine material, at a given air velocity.

(4) *Variation of the air flow rate after charging*

Before the main work was performed, exploratory experiments were made with a system of D.V.B. spheres and peas, in which the bed was loaded against an air flow and then the air volume was decreased by small decrements to zero, increased to close to the fluidization point, decreased to zero and finally increased to close to the fluidization point again. The experiments were abandoned as the behaviour shown was very complex and, from the blast furnace point of view, interest was largely confined to the initial loading conditions. However, the general features of the results are worth presenting.

Fig. 18 is a friction factor—Reynold's number plot, which shows most of the phenomena that occurred, for a system of D.V.B. spheres and peas, in which D.V.B. spheres were 5 per cent of the total solid volume. Decreasing the air volume from the loading conditions gave a curve, *AB*, which at first tended to approach the reference curve and then to run parallel to it. The same curve, *BA*, was followed when the volume was increased again, but it continued with its negative slope beyond the loading conditions until a break point *C* was reached. Here the friction factor rose sharply, *CD*, and then levelled off to a constant value, *DE*. In the range *CD* much fine material rose to the bed surface and had to be extracted and weighed. Decreasing the air volume once more resulted in another curve, *EF*, which again tended to approach and then run parallel to the reference curve, but this time above it. The same curve was followed, though it might run closer to the reference curve at the higher flow rates, if the air velocity was increased for the last time.

If the bed were charged against an air volume flow-rate less than that corresponding to the

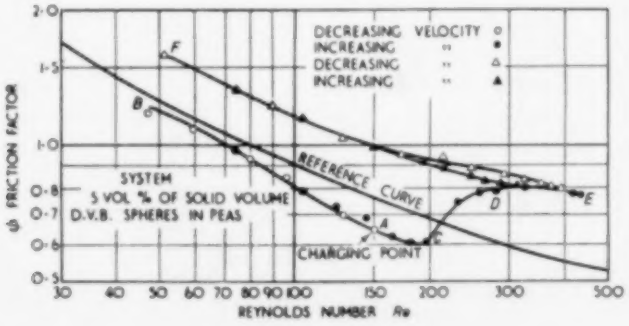

FIG. 18.

point *C*, the break point always occurred at approximately the same superficial air velocity. The bed could be charged, however, against a rising air flow-rate greater than that represented by the normal break point *C*, when much fine material floated to the top of the bed as charging proceeded and was not assimilated by the bed as fresh charge was added. The break point then occurred at an air velocity slightly greater than the charging air velocity, even if the air flow-rate was decreased first to zero before it was increased again.

Up to the break point, only slight or no motion of the smaller constitutent of the charge was observed, once any material that was going to had floated to the top of the bed during the charging procedure. Such motion as there was occurred with a few small particles, that appeared to be in a state of unstable equilibrium, and which teetered about a fixed point. At and after the breakpoint, however, vigorous eddying and jigging of the small material took place and some of the fine material migrated to the top of the bed and was extracted and weighed to make an allowance in the calculations. It is important to note that the remarks of this paragraph were true whatever the position of the breakpoint. Thus, if a high charging air flow-rate was used, so that the breakpoint air velocity was high, little motion of small material was noted until the breakpoint for that specific charging condition was reached.

The behaviour described was generally true for the systems studied. There were always two friction factor curves which could be travelled up and down, though in some cases both curves ran above the reference curve and not astride it as in the example.

The phenomena will not be discussed in detail but it may be noted that two stable configurations of the bed appear to be possible. In the first case the fine material can be assumed to be evenly distributed throughout the bed, either as individual particles or in clusters. In the second case, however, the opportunity has arisen for segregation of the fine material due to its movement within and through the bed. Perhaps certain flow channels are blocked and only a reduced number remain for the passage of air. It is also possible that the presence of fine material has imposed a certain structure on the coarse material, which tends to give a greater back pressure than the normal random structure, and removal of some of the fine material—in the example the experiment finished with 3 per cent D.V.B. spheres instead of the original 5 per cent—allows this effect to be felt. MARTIN, MCCABE, and MONRAD [2] carried out some interesting experiments on the resistance of different arrangements of spheres, which are relevant to this argument. Nevertheless these are merely conjectures at present.

Acknowledgements—The author is indebted to the Imperial Smelting Corporation Limited for permission to print this work. He also wishes to thank Mr. R. JAMES and Mr. G. COURTNEY for their aid in carrying out the experimental part and Mr. P. A. T. KEEPING for help and discussions throughout.

NOTATION

d = Diameter of the sphere with the same volume as the particle.
d_E = The effective surface diameter of a particle or mixture of particles; defined by equation (2).
g = Gravitational constant.
Δh = Pressure drop over a bed of particles expressed as head of air flowing.
L = Height of bed corresponding to the pressure drop measurement.
v_S, v_L = Volume fraction of solid material which is small material and large material respectively.
V = Superficial air velocity calculated using the empty tube's cross-section.
ϵ = Fractional voidage of the bed.
μ = Viscosity of the air.
ρ = Density of the air.
ϕ = Shape factor.
ψ = Friction factor.
ψ_R = Reference friction factor.

REFERENCES

[1] ERGUN S. *Industr. Engng. Chem.* 1953 **45** 477.
[2] MARTIN J. J., MCCABE W. L. and MONRAD C. C. *Chem. Engng. Prog.* 1951 **47** 91.
[3] MOTT R. A. Inst. of Physics *Some Aspects of Fluid Flow*. Conference at Leamington Spa. Arnold, 1950.
[4] ROSE H. E. and RIZK A. M. A. *Proc. Instn. Mech. Engrs.* 1949 **160** 493.

Chemical Engineering Science, 1957, Vol. 7, pp. 83 to 88. Pergamon Press Ltd.

Interfacial resistance, adsorption and interfacial tension in single drop liquid–liquid extraction

B. J. MELHUS* and S. G. TERJESEN

The Technical University of Norway, Chemical Engineering Laboratory, Trondheim, Norway

(*Received* 21 *January* 1957)

Abstract—The theory proposed by LINDLAND and TERJESEN [3] for interfacial resistance in liquid–liquid extraction, based on proportionality between interfacial resistance and the fraction of the interface covered by surface active molecules, results in an adsorption isotherm which has been compared with information about interfacial tension derived from measurements of deformation of falling drops. Although no general correlation was found between interfacial tension and drop deformation, the results have been shown by means of the thermodynamic equation of Gibbs to lead to an effective cross-sectional area of 39 Å^2 per molecule of sodium oleyl-*p*-anisidinesulphonate adsorbed at the interface between water and carbon tetrachloride. This value is of the order of magnitude to be expected.

It has also been shown that the results of GARNER and HALE [6] with Teepol as surface active agent are in qualitative agreement with the theory.

It is concluded that interfacial resistance and interfacial tension are two different manifestations of adsorption, unrelated to each other except for the fact that they are both functions of adsorption.

Résumé—LINDLAND et TERJESEN [3] ont proposé une théorie de la résistance interfaciale dans l'extraction liquide–liquide, basée sur la proportionnalité entre cette résistance et la fraction d'interface recouverte par des molécules à surface active. Leur théorie conduit à une adsorption isotherme qui a été comparée avec les données sur la tension interfaciale obtenues par la mesure de déformation des gouttes au moment de leur chute. Bien qu-ils n'aient pas trouvé de corrélation générale entre la tension interfaciale et la déformation, les résultats ont conduit par l'équation thermodynamique de Gibbs à une aire effective de section droite de 39 Å^2/molécule de sodium oleyl-*p*-anisidine-sulphonate adsorbé à l'interface entre l'eau et le CCl_4. Cette valeur est de l'ordre de grandeur attendu.

Les résultats obtenus por GARNER et HALE [6] avec du Teepol comme agent de surface actif, sont en accord qualitatif avec la théorie.

Les auteurs concluent que la résistance interfaciale et la tension interfaciale sont deux manifestations différentes de l'adsorption.

Zusammenfassung—Die von LINDLAND und TERJESEN [3] vorgeschlagene Theorie für den Grenzflächenwiderstand bei der Flüssig–flüssig Extraktion, die auf der Proportionalität zwischen Grenzflächenwiderstand und dem von oberflächenaktiven Molekülen besetzten Anteil der Grenzfläche beruht, führt zu einer Adsorptions-Isotherme, die mit solchen Werten der Grenzflächenspannung verglichen wurde, die aus Messungen der Deformation fallender Tropfen erhalten wurden. Obwohl keine allgemeine Beziehung zwischen Grenzflächenspannung und Tropfendeformation gefunden wurde, lässt sich mit Hilfe der thermodynamischen Gleichung von Gibbs zeigen, dass die Ergebnisse zu einem wirksamen Querschnitt von 39 Å^2 je Molekül-Natrium-oleyl-*p*-anisidinsulfonat führen, das an der Grenzfläche Wasser-Tetrachlorkohlenstoff adsorbiert ist. Dieser Wert ist von der erwarteten Grössenordnung.

Die Ergebnisse von GARNER und HALE [6] mit Teepol als oberflächenaktivem Stoff sind mit der Theorie in guter Übereinstimmung.

Die Verfasser kommen zu dem Schluss, dass Grenzflächenwiderstand und Grenzflächenspannung zwei verschiedene Auswirkungen der Adsorption sind, zwischen denen keine Beziehungen bestehen ausser der Tatsache, dass beide Funktionen der Adsorption sind.

*Present address: Gullaug Kjemiske Fabrikker A/S, Lillestrøm, Norway.

VOL. 7 957/58

Introduction

In previous papers [1] Holm and Terjesen [2] and Lindland and Terjesen [3] have shown that minute additions of the surface active agent sodium oleyl-*p*-anisidinesulphonate have the effect of greatly reducing the rate of transfer of iodine from an aqueous solution to droplets of carbon tetrachloride. The latter authors found that the results expressed as an interfacial resistance coefficient R_i sec/cm within the limits of experimental error obeyed the equation

$$C_S = 5{\cdot}4 \times 10^{-9} \frac{R_i}{\left(1 - \frac{R_i}{7400}\right)^{0{\cdot}1}} \qquad (1)$$

where C_S is the concentration of surface active agent in g/100 ml aqueous phase. This equation was derived on the basis of the assumptions that the interfacial resistance-coefficient is proportional to the fraction of the interface covered by adsorbed surface active molecules $A_0\Gamma$, and that the adsorbed film is of the vapour expanded type exhibiting strong cohesive forces. The corresponding adsorption isotherm was also given :

$$C_S = 4{\cdot}0 \times 10^{-5} \frac{A_0\Gamma}{(1 - A_0\Gamma)^{0{\cdot}1}} \qquad (2)$$

The isotherm has been derived from mass transfer measurements with falling drops. Under these conditions it cannot safely be assumed that an adsorption equilibrium is established on the drop surface. The isotherm therefore describes a stationary state rather than a true equilibrium [3]. The equilibrium isotherm is assumed to be of the general form derived earlier [3] viz :

$$C_S = K \frac{A_0\Gamma}{(1 + A_0\Gamma)^n} \qquad (3)$$

By eliminating C_S from equation (3) and the thermodynamic equation of Gibbs

$$\Gamma = -\frac{1}{RT} \frac{d\gamma}{d \log_e C_S} \qquad (4)$$

the equation of state for the adsorbed film results:

$$\Delta\gamma = \frac{RT}{A_0} \left[n \log_e (1 - A_0\Gamma) - (1 - n) A_0\Gamma \right] \qquad (5)$$

The constant K in the adsorption isotherm does not appear in the equation of state. The equation of state is a relationship between surface concentration and surface pressure and must therefore be assumed to be independent of the method of establishing this surface concentration. An equation of state applicable to equilibrium conditions will therefore apply to stationary states also. This requires that n in equations (3) and (5) must be invariant, and in this case have the value of 0·1. The lack of adsorption equilibrium is expressed by the value of K only, whereas n remains unaffected.

With the present system at 25°C equation (5) gives

$$a_0 = \frac{412}{\Delta\gamma} \left[0{\cdot}1 \log_e (1 - A_0\Gamma) - 0{\cdot}9 A_0\Gamma \right] \qquad (6)$$

where a_0 is the effective cross-section in Å^2 of an adsorbed surface active molecule. This equation is applicable to non-equilibrium conditions provided corresponding non-equilibrium values of $\Delta\gamma$ and $A_0\Gamma$ are used.

By means of equation (6) and a knowledge of the reduction in interfacial tension $\Delta\gamma$ as a function of the bulk concentration of surface active agent C_S an independent check on the previously found isotherm (2) can be provided. The procedure will be to calculate $A_0\Gamma$ from the isotherm (2) and then obtain the area a_0 from the equation of state (6). The isotherm must be considered to have passed the test if the resulting cross-sectional area of an adsorbed surface active molecule is of the order of magnitude found for similar molecules by other investigators using conventional methods.

It was the intention to derive the reduction in the interfacial tension from measurements of the size, the velocity of fall and the deformation of the drops using a method similar to that proposed by Spilhaus [4] and further developed by Hughes and Gilliland [5] for liquid drops falling freely in air. Although about 800 drops were observed and photographed it has unfortunately so far not been possible to find a reliable correlation along these lines. The observations have, however, given an indication of the concentration at which the shape of the drops becomes unstable

corresponding to zero interfacial tension, and this can be used with equation (6).

GARNER and HALE (6) have compared the reduction in the rate of transfer of diethylamine from toluene drops to water caused by small additions of the surface active agent "Teepol" with the reduction in the static interfacial tension. They concluded that the resistance to transfer is not primarily due to the area occupied by the surface active molecules. Their results will be reconsidered in light of the theory of interfacial resistance proposed earlier [3].

EXPERIMENTAL

The shape of the falling drops of carbon tetrachloride was recorded by a photographic technique similar to that described by HAUSER, EDGERTON, HOLT AND COX [7] and by EDGERTON, HAUSER and TUCKER [8]. The drops were photographed by transmitted light as silhouettes as they passed through a chamber with parallel glass walls similar to that used by LEWIS, JONES and PRATT [9]. Two sharply pointed iridium needles were placed in the chamber and photographed together with the drops. With a knowledge of the distance between the points the magnification of the photographs could be determined accurately.

The source of light was a gas-filled discharge lamp giving a flash of about 5 μsec duration. The discharge was triggered by a photoelectric cell through a suitable amplifier when a drop appeared in view of the camera and in focus. The camera was focussed on the needles mentioned above.

For drop sizes less than 5 mm^3 the photoelectric cell did not function satisfactorily, and was not used. Instead, a cloud of small drops was allowed to fall through the chamber with the discharge lamp flashing at a frequency of about 600 per min and with the camera shutter set to give an exposure of 0·1 sec. By this procedure a large number of the drops were photographed out of focus, but only those giving a sharp image were taken into account.

In order to ensure the establishment of a stationary adsorption state before the drops reached the chamber they were allowed to descend in a spiral path through a 1·5 m long glass tube fitted with a rotating glass rod. This arrangement as well as the method of forming the drops has been described previously [3]. The materials used are also described in the earlier communications. The temperature was 20°C.

The image of the drops on the negative corresponded to a magnification of about 1·6 : 1. The horizontal and vertical axis of the smaller drops were measured from the negative by means of a "Hilger Projector" with micrometer reading, whereas for the larger drops they were measured on enlarged prints with a graduated ruler. The ratio of the vertical axis to the horizontal was taken as a measure of the deviation from sphericity. The drop volume was calculated on the assumption that the drops were oblate spheroids formed by the rotation of an ellipse about its minor axis, $V = 4/3\ \pi a^2 b$, where a and b are the major and minor semiaxis respectively. For drops under 19 mm^3 the volumes thus calculated agreed within $\pm$ 5 per cent with those determined from direct measurement of the volume of a counted number of collected drops.

RESULTS

The results are shown in Fig. 1 where the ratio of the short to the long axis of the drops has been plotted against drop volume for experiments carried out in the absence of surface active agent and with additions of 6×10^{-5} and 4×10^{-4} g sodium oleyl-*p*-anisidinesulphonate per 100 ml of the aqueous phase. With drops larger than about 19 mm^3 the scatter was too great probably due to oscillations of the drops, and these results are not included. Of the 253 observations falling within the range plotted 13 were omitted as they strayed so far from the others as to be obviously irrelevant.

In spite of the poor reproducibility of the individual measurements, Fig. 1 shows clearly that the deformation of the drops due to the surface active agent is very small at a concentration of 6×10^{-5} g/100 ml which, according to previous work [3] is sufficient to develop fully the interfacial resistance. Much larger additions which resulted in no further increase in the interfacial resistance produced large deformations. The relationship between these two phenomena is therefore not a direct one.

A very large number of experiments carried out with additions of 10^{-3} g/100 ml resulted in ratios of the short to the long axis which were distributed over a range of 0·4–1·0, even for drops with volumes less than 0·2 mm^3. With this addition of surface active agent the shape of the drops has clearly become unstable, but without any breaking up of the drops occurring. This indicates that the interfacial tension has been reduced practically to zero.

According to DONAHUE and BARTELL [10] the interfacial tension for the system carbon tetrachloride – water is $\gamma = 43{\cdot}7$ dyn/cm at 25°C. Although the present investigation was carried

VOL. 7 957/58

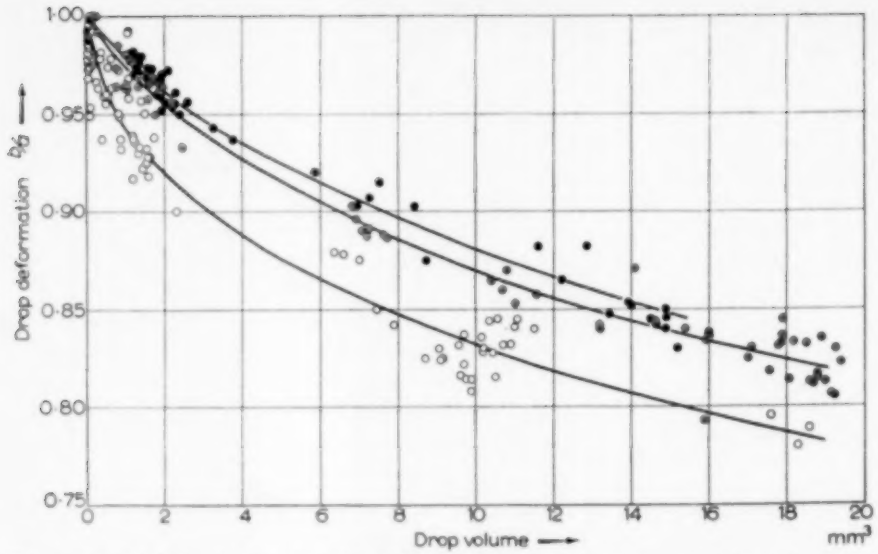

Fig. 1. Drop deformation as a function of drop volume for different concentrations of sodium oleyl-*p*-anisidine-sulphonate.

● No addition ⊕ 6×10^{-5} g/100 ml ○ 4×10^{-4} g/100 ml

out at 20°C the value for 25°C will be used since the isotherm relates to this temperature. The effect of a temperature difference of 5°C is small, estimated to be about 1 per cent for the interfacial tension. The value of $\Delta\gamma = 43{\cdot}7$ dyn/cm at $C_S = 10^{-3}$ g/100 ml gives with the equations (2) and (6) an effective cross-sectional area of each adsorbed surface active molecule of $a_0 = 39$ Å^2. A comparison with a few selected molecular areas for adsorbed films reproduced in Table 1 from Adam [11] shows that the value found for the film of sodium oleyl-*p*-anisidinesulphonate is of the correct order of magnitude.

The molecular area estimated above can be used in conjunction with the isotherm (2) and the equation of state (6) to calculate the reduction in interfacial tension $\Delta\gamma$ as a function of the bulk concentration of surface active agent C_S. The result can be seen in Fig. 2 where $\Delta\gamma$ for convenience has been plotted on semilogarithmic paper together with the isotherm. As the curves in Fig. 1 are nearly parallel for drop volumes between 5 and 15 mm^3 the expression $(b/a)_{C_S=0} - (b/a)_{C_S}$ has been selected as a measure of the additional deformation of the drops caused by the presence of the surface active agent. Only two values are available viz.

$$(b/a)_{C_S=0} - (b/a)_{C_S=6\times10^{-5}} = 0{\cdot}0105$$

$$(b/a)_{C_S=0} - (b/a)_{C_S=4\times10^{-4}} = 0{\cdot}0482$$

Table 1. *Molecular areas of adsorbed films according to* Adam [11]

	Å^2
Three dimensional crystals	
Carbon chains	18·4
Condensed films at zero compression	
Vertically oriented carbon chains	20·5
Simple *p*-substituted benzene compounds	24·0
Liquid-expanded films at low compression	
Saturated aliphatic acids on dilute HCl	48
Resorcinols on 0·1 N NaOH	58
Phenols on 0·1 N NaOH	39
Gaseous films	
Aliphatic chains laying flat	120
Dibasic esters at higher compression	85
Oleic acid at 16 dyn/cm	48
Caproic acid at 40 dyn/cm	28·6

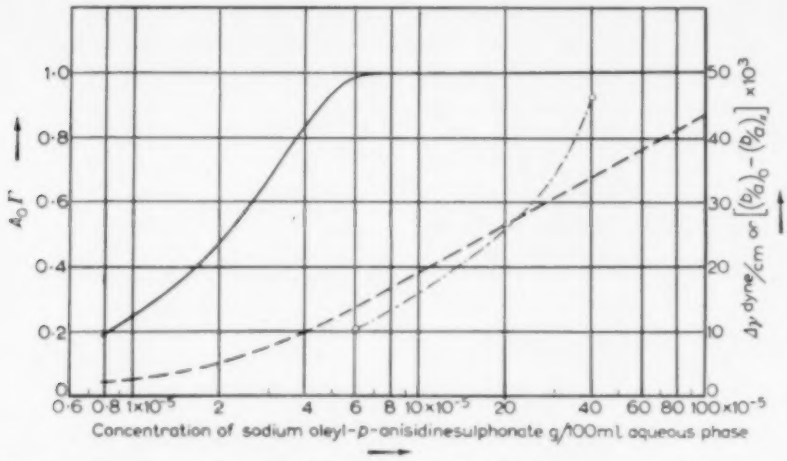

FIG. 2. Comparison between adsorption, interfacial pressure and drop deformation.

— · — 0 — · — $(b/a)_0 - (b/a)_x$ = Additional deformation caused by the surface active agent
———— $A_0\,\Gamma$ = Fraction of surface covered
– – – – – – – – – $\Delta\,\gamma$ = Calculated surface pressure

VOL. 7 957/58

These are also shown in Fig. 2 connected with a dotted line which has no other significance than to show that the two points are of the same category.

Fig. 2 emphasizes the completely different character of the curves representing the reduction in interfacial tension $\Delta\,\gamma$ on the one hand, and the fraction of the interface covered with adsorbed surface active molecules $A\Gamma$ on the other. This lack of parallelism between adsorption and surface pressure is indicative of the strong cohesive forces associated with vapour expanded films. Fig. 2 also shows the direct effect of interfacial tension on drop deformation.

The Results of Garner and Hale

The only other published results to which it is profitable to apply the theory of interfacial resistance are those of Garner and Hale [6]. Their experimental material is, however, somewhat limited, and the lack of observations in the region of low interfacial resistance made a derivation of an adsorption isotherm too uncertain. The following alternative procedure was therefore adopted: By means of Gibbs' equation (4) the adsorption under static conditions was derived from a logarithmic plot of their measurements of static interfacial tension. The interfacial resistance was assumed to be proportional to the adsorption thus calculated, and the factor of proportionality so adjusted that the resulting curve gave the best possible fit with the interfacial resistances calculated from the extraction coefficients given in their paper. It can be seen from Fig. 3 that the equation

$$R_{i(0)} = -\,28100\,\frac{1}{RT}\,\frac{d\gamma}{d\log_e C_S}\ \text{sec/cm} \qquad (7)$$

holds within the limits of experimental error. The equation is even capable of reproducing the

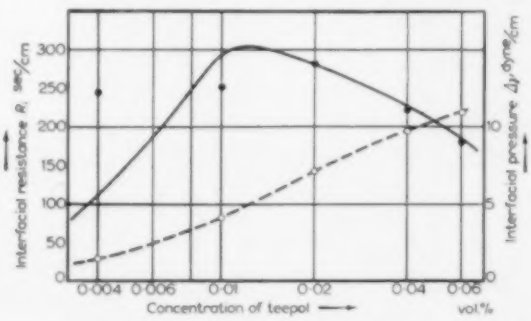

FIG. 3. The results of Garner and Hale [6].

— — 0 — — Experimental interfacial pressure
● Experimetal interfacial resistance
———— $R_i = -\,28100\,\frac{1}{RT}\,\frac{d\gamma}{d\log_e C_S}$

surprising maximum in the interfacial resistance observed by Garner and Hale [6]. This maximum appears as a consequence of the inflection point exhibited by the curve for interfacial tension when plotted against the logarithm of the bulk concentration in Fig. 3. It is most likely explained by the fact that Teepol is a mixture of a number of surface active compounds rather than a pure substance.

Conclusions

It has been shown that the present results and those of Garner and Hale [6] are in agreement with the supposition that the interfacial resistance caused by additions of surface active molecules is proportional to the fraction of the interface covered by adsorbed molecules. Interfacial resistance and interfacial tension are two different manifestations of adsorption, and they are not related to each other except for the fact that they are both functions of adsorption which is the primary and more fundamental phenomenon.

The nature of interfacial resistance will be discussed in a subsequent paper.

Acknowledgements—The authors are indebted to the Royal Norwegian Council for Scientific and Industrial Research for a grant which has made this work possible.

Notation

A	= Interfacial area	cm^2
A_0	= Effective cross-sectional area of adsorbed surface active molecules	cm^2/ mole
a_0	= Effective cross-sectional area of adsorbed surface active molecules	A^2/molecule
a	= Major semiaxis of oblate ellipsoid	mm
b	= Minor semiaxis of oblate ellipsoid	mm
C_S	= Bulk concentration of surface active agent	g/100 ml or vol. %
N	= Avogadro's number $6{\cdot}02 \times 10^{23}$ molecules/mole	
R	= Gas constant $8{\cdot}3144 \times 10^7$ dyn cm/mole °K	
$R_{i(t)}$	= Interfacial resistance on a solvent and time basis	sec/cm
T	= Absolute temperature	°K
V	= Drop volume	mm^3
γ	= Interfacial tension	dyne/cm
$\Delta\gamma$	= Reduction in interfacial tension caused by the surface active agent	dyne/cm
Γ	= Surface concentration of surface active agent	mole/cm^2

References

[1] Holm A., Lindland K. P. and Terjesen S. G. *Ber. 8 Nordiske Kjemikermøte*, Oslo, 14-17 June 1953.

[2] Holm A. and Terjesen S. G. *Chem. Engng. Sci.* 1955 **4** 205.

[3] Lindland K. P. and Terjesen S. G. *Chem. Engng. Sci.* 1956 **5** 1.

[4] Spilhaus A. F. *J. Met.* 1948 **5** 108.

[5] Hughes R. R. and Gilliland E. R. *Chem. Engng. Progr.* 1952 **48** 497.

[6] Garner F. H. and Hale A. R. *Chem. Engng. Sci.* 1953 **2** 157.

[7] Hauser E. A., Edgerton H. E., Holt B. M. and Cox J. T., Jr. *J. Phys. Chem.* 1936 **40** 973.

[8] Edgerton H. E., Hauser E. A. and Tucker W. B. *J. Phys. Chem.* 1937 **41** 1017.

[9] Lewis J. B., Jones I. and Pratt H. R. C. *Trans. Instn. Chem. Engrs., Lond.* 1951 **29** 126.

[10] Donahue D. J. and Bartell F. E. *J. Phys. Chem.* 1952 **56** 480.

[11] Adam N. K. *The Physics and Chemistry of Surfaces* (3rd ed.) Oxford, London 1941.

Chemical Engineering Science, 1957, Vol. 7, pp. 89 to 96. Pergamon Press Ltd.

On the efficiency in separating mixtures of two constituents

K. Rietema

Koninklijke/Shell-Laboratorium, Amsterdam,* Netherlands

(*Received* 7 *March* 1957)

Abstract—The definition of efficiency in a process of separation is discussed, and the various requirements that should be fulfilled by such a definition are enumerated. The formulae so far proposed in literature for expressing the separation efficiency are reviewed in the light of these requirements. A formula put forward by the author is found to satisfy them all. Its application is illustrated by means of two examples.

Résumé—La définition du rendement d'un procédé de séparation est discutée, et les différentes exigences auxquelles doit répondre une telle définition sont énumérées. Les formules proposées jusqu'à présent dans la littérature exprimant le rendement de séparation sont considérées tenant compte de ces exigences. Une formule mis au point par l'auteur s'est montré satisfaisante sous tous les aspects. Deux exemples sont donnés pour illustrer l'application de la formule.

Zusammenfassung—Es wird die Definition der Wirksamkeit eines Trennprozesses diskutiert und es werden die verschiedenen Forderungen aufgeführt, denen eine solche Definition genügen muss. Unter diesem Gesichtspunkt werden die in der Literatur vorgeschlagenen Gleichungen betrachtet. Es zeigt sich, dass eine vom Autor mitgeteilte Formel alle aufgestellten Forderungen erfüllt. Ihre Anwendung wird an zwei Beispielen erläutert.

VOL.
7
957/58

1. Introduction

In every form of industry – a word here used in its widest sense – we are concerned with efficiency, or with the approach to ideality of operation. In some cases we may be interested in the efficient operation of a whole industry or process; in other cases our interest may be centred only on a part of an industry, sometimes even on a specific piece of apparatus or on a machine.

The term " efficiency " is frequently ill-defined and is then used in a qualitative sense only. In chemical and physical technology, however, there usually exists the possibility of defining this concept more closely. Thus in the case of a heat engine we can define the efficiency of heat conversion as the ratio of the useful mechanical energy produced to the total energy consumed.

Physical separation processes carried out in stages may be described in terms of a so-called stage efficiency, which defines the efficiency of a single stage as the ratio between the number of ideal stages necessary for a certain degree of separation and the number of actual stages required for the same result. The use of this stage efficiency is confined to physical separation methods such as distillation and extraction, which are based on mass transfer through or to an interface between two phases.

In order to calculate the final result of the separation from the stage efficiency it is necessary to know which separation method has been used and how many real stages were involved. The figure for the stage efficiency does not provide any information as to whether the separation has been effective or not. In extreme cases, for instance when distilling an azeotropic mixture, no separation is obtained even with an ideal stage efficiency.

A different type of efficiency definition is that based entirely on the final result of the separation. Several definitions of this class have been proposed by various authors, especially in the field of screen analysis and dust separation. The

*N.V. De Bataafsche Petroleum Maatschappij.

figures so obtained are claimed to describe the more or less ideal operation of the separating apparatus discussed.

A critical investigation into the value of the definitions of the latter type, has, however, never been published. It is the aim of this study to fill up this gap and to come to a proposal for a generally applicable definition of separation efficiency.

Although such a method of expressing efficiency will be primarily of interest in the field of phase separations, it can be applied in any case where a mixture is split up into two quantities, in order to describe the degree to which ideal separation is approached. It should be remarked, however, that such an efficiency cannot be a substitute for the stage efficiency mentioned before.

2. Purpose of an Efficiency Number for Separations

If two components or phases are to be separated and a high degree of separation is required, the yield j and also the quality q of the final products should be as high as possible with respect to the original mixture. The case in which both the yield and the quality are maximum might be considered as the ideal separation. In actual operation it is practically impossible to arrive at this ideality because of hold-back or entrainment. The purpose of an efficiency number, therefore, will be to give an objective measure for indicating the difference between the separation actually achieved and the ideal separation.

Such an efficiency number can also be a suitable means for comparing, from a technical point of view :

(a) different operating conditions,
(b) different feed mixtures,
(c) different methods of separation,
(d) improvements in the separating apparatus.

It should be realized, however, that a single efficiency number can never be capable of fully describing the result of the separation, except in the theoretical case of ideal separation. For a complete description at least two quantities (e.g. the yield and the quality) should be available if the feed composition is known, and even three quantities if this feed composition is unknown. This follows immediately from the fact that in the separation of a two-component mixture four flow rates are involved (viz. the two split flows of both components); of these, however, only the mutual ratios are needed and it is hence but necessary to know three independent ratios.

Sometimes it is suggested that such a figure for efficiency can be used as a means to describe the increase in economic value of the mixture by the separation. Since, however, the economic value may also be determined by many other factors than the physical or chemical composition, it must be clear that such a parallel between efficiency and economic value cannot be expected to exist.

3. Requirements for a Suitable Efficiency Number for Phase Separation

The requirements to be satisfied by a generally valid definition of efficiency will now be summarized and discussed as far as necessary.

(1) The definition should be unambiguous.

(2) An improved quality of the final product at constant yield should be reflected in a higher efficiency number.

(3) An increased yield at constant quality should also give a higher efficiency number.

(4) The lowest value should be zero.

(5) The highest value should be unity (or one hundred when expressed as a percentage).

(6) This highest value should be reached only when both phases or components are obtained completely pure after separation.

(7) If one constituent is obtained *pure*, the efficiency should be equal to the ratio of the amount separated of this constituent to the total amount of this constituent originally present.

(8) If the feed is split up into two streams having the same composition as the feed, the efficiency number should be zero.

(9) The efficiency should remain the same if the two components or phases, or the two outgoing streams are interchanged.

(10) When distributions of certain parameters x and y are present in each phase or component, so that the separation is different for different values of these parameters, a fractional separation efficiency E_{xy} can be defined in the same way as the overall efficiency $\overline{E}$. If $g(x)$ and $h(y)$ are the above mentioned distribution functions, the overall efficiency $\overline{E}$ should be related to the fractional separation efficiency by: $\overline{E} = \int\int g(x)\, h(y)\, E_{xy}\, dx\, dy$. In other words, there should exist an "additivity of fractional efficiencies."

(11) The definition should be simple.

Most of these requirements are self-evident. (2) and (3) arise from the demand that an improved separation should be reflected by a higher efficiency number.

(4) and (5) are necessary for normalization.

(9) is required for a generally valid definition of efficiency, since when applied to the separation of a mixture of two components, the efficiency should be the same if calculated for the one component (stream) or for the other.

If requirement (10) is satisfied it increases the applicability of the efficiency definition and facilitates calculations involving the efficiency. Requirement (10), and also (11), are not strictly necessary, but highly desirable.

4. Discussion of Various Efficiency Formulae

Suppose that the mixture to be separated consists of the two components or phases g and h, the flow rate for each component or phase being G_0 and H_0 respectively in the feed, and after separation G_1 and H_1 in the one stream and G_2 and H_2 in the other.

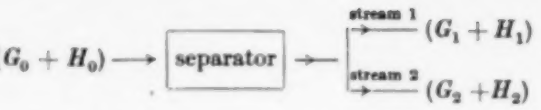

Suppose further that:

a = percentage of g in the feed $= 100\, \dfrac{G_0}{G_0 + H_0}$

b = percentage of g in stream 1 $= 100\, \dfrac{G_1}{G_1 + H_1}$

c = percentage of g in stream 2 $= 100\, \dfrac{G_2}{G_2 + H_2}$

o = percentage of h in the feed $= 100 - a$

p = percentage of h in stream 1 $= 100 - b$

j = amount of stream 1 as a percentage of the feed $= 100\, \dfrac{G_1 + H_1}{G_0 + H_0}$

E = efficiency number (ranging from 0 to 1)

$\eta = 100\, E$

Various definitions of separation efficiency found in the literature will now be compared on the basis of the requirements discussed previously. In the adjoined table these efficiency formulae are given in the notation defined above.

It can be shown by rearrangement that several efficiency formulae are identical. For this rearrangement use is made of the formula $j = 100\, \dfrac{a - c}{b - c}$ which can easily be derived from a material balance of one of the two components or phases.

Although several of the formulae are undoubtedly useful for certain applications (particularly formula VI, [2, 5, 6], the value of which is identical with that of formula IX [7] except for its sign) it is evident from the table that only formula IX satisfies all the requirements summed up in the foregoing.

It would appear necessary to give the proof that requirement (10) is satisfied in the case of formula I, II and IX [1, 7], the first two only after rearrangement to $E = G_1/G_0$ since concentrations are not defined in combination with size distributions.

If $g(x)$ and $h(y)$ are the normalized distribution

Table 1

No.	*Efficiency formula*	*After rearrangement*	*Requirements satisfied*	*References*
I	$\eta = j\frac{b}{a}$	$E = G_1/G_0$	(1), (2), (3), (4), (5), (7), (10) (11)	
II	$\eta = 100\frac{b(a-c)}{a(b-c)}$	$E = G_1/G_0$	(1), (2), (3), (4), (5), (7), (10) (10) only after rearrangement	[1]
III	$\eta = 100^2\frac{a-c}{a(100-c)}$	$\eta = 100\,j\frac{b-c}{a(100-c)}$	(1), (2), (3), (4), (5) Also (7) if $H_1 = 0$	[2]
IV	$\eta = b - c$		(1), (2), (3), (4), (5), (6), (8), (9) If the absolute value is taken, also (10)	[3]
V	$\eta = 100\frac{(b-a)(a-c)}{a(100-a)}$	$\eta = j\frac{(b-a)(b-c)}{a(100-a)}$	(1), (2), (3), (4), (5), (6), (8), (9)	[4]
VI	$\eta = 100\,j\frac{b-a}{a(100-a)}$	$E = \frac{G_1}{G_0} - \frac{H_1}{H_0}$	(1), (2), (3), (4), (5), (6), (8), (10) (10) only after rearrangement	[2, 5, 6]
VII	$\eta = 100^2\frac{(a-p)(a-c)}{a(100-c-p)}$			
VIII	$\eta = j\frac{b-a}{100-a} + (100-j)\frac{a-c}{a}$			
IX	$E = \left\lvert\frac{G_1}{G_0} - \frac{H_1}{H_0}\right\rvert = \left\lvert\frac{G_2}{G_0} - \frac{H_2}{H_0}\right\rvert$		(1), (2), (3), (4), (5), (6), (7), (8), (9), (10), (11)	[7]

functions of the components g and h over their respective parameters x and y, then according to definition IX :

$$E_{xy} = \left| \frac{G_1\, g_1(x)}{G_0\, g_0(x)} - \frac{H_1\, h_1(y)}{H_0\, h_0(y)} \right|,$$

where $\int g(x)\,dx = 1$ and $\int h(y)\,dy = 1$.

Integration over the distribution functions gives

$$\begin{aligned}
&\int\int E_{xy}\, g_0(x)\, h_0(y)\, dx dy \\
&\quad = \int h_0(y) \left(\int E_{xy}\, g_0(x)\, dx \right) dy \\
&\quad = \int h_0(y) \left| \frac{G_1}{G_0} \int g_1(x)\, dx - \frac{h_1 H_1}{h_0 H_0} \right| dy \\
&\quad = \int h_0(y) \left| \frac{G_1}{G_0} - \frac{h_1 H_1}{h_0 H_0} \right| dy \\
&\quad = \left| \frac{G_1}{G_0} \int h_0(y)\, dy - \frac{H_1}{H_0} \int h_1(y)\, dy \right| \\
&\quad = \left| \frac{G_1}{G_0} - \frac{H_1}{H_0} \right| = \text{overall efficiency } E^*.
\end{aligned}$$

5. Interpretation of Efficiency Formula

We will now further discuss the efficiency according to formula IX or according to the absolute value of formula VI :

$$E = \left| \frac{G_1}{G_0} - \frac{H_1}{H_0} \right| = \left| \frac{G_2}{G_0} - \frac{H_2}{H_0} \right| = \left| j\frac{b-a}{a(100-a)} \right|$$

From the last presentation it can be seen that this efficiency can be conceived as the product of the yield j and the quality increase $(b - a)$, which

*The interchange of sequence of integration and taking absolute values is permissible since the sign of the two quantities between the " absolute " lines does not change.

VOL. 7 957/58

product, because of normalization. is divided by the product of the yield and quality increase in the case of ideal separation.

There is also a physical interpretation of this definition : E is equal to the fraction of the feed mixture which would be fed to an imaginary separation apparatus operating ideally, while the fraction $1 - E$ would not be separated at all, but be distributed in an arbitrary ratio over the two outgoing streams.

Suppose that the fraction going to the ideally operating separator is equal to α and that the fraction $(1 - \alpha)$ is divided into two parts $\beta(1 - \alpha)$ and $(1 - \beta)(1 - \alpha)$.

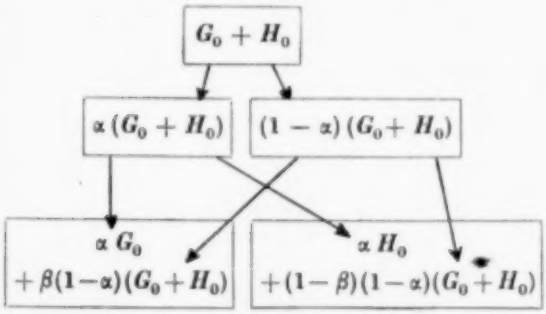

The efficiency of this separation now becomes

$$E = \left|\frac{G_1}{G_0} - \frac{H_1}{H_0}\right| =$$

$$\left|\frac{\alpha G_0 + \beta(1-\alpha) G_0}{G_0} - \frac{\beta(1-\alpha) H_0}{H_0}\right| = \alpha$$

which proves the above statement.

6. Examples of the Application of Efficiency Formula IX

As has already been remarked, this efficiency formula can be used for any separation of a mixture of two phases or components. It was used, for instance, for liquid extraction by Tepe and Woods [6] (VIII), for separation of water-oil emulsions in a hydrocyclone by J. van Rossum [7] (IX) for describing the effect of screening by Newton and Newton [2, 5, 6] (VII). (For references see table).

A purely hypothetical example will be given here to describe the classification of a powder into a fine and a coarse fraction. Whether this classification is carried out in the dry state on a screen or in the wet state in a hydrocyclone or in some other type of classifier is of no importance.

In such a case, for a given feed powder and a given separation curve (which is the plot of the percentage separated of each fraction of a certain particle size against this size), the separation efficiency depends on the required separation diameter d_s if the two components are defined in such a way that the fines include all particles smaller than d_s and the oversize fraction includes all particles coarser than d_s.

In an ideal separation one outgoing stream contains all the fines and the other all the oversize material.

Further it is assumed that the powder to be separated conforms to the so-called log-probability size distribution and that the separation curve of the classifier also gives a straight line on a log-probability grid.

In Fig. 1 the cumulative size distribution of the feed powder is given, as well as two separation curves (type I and type II) on a log-probability grid. The two separation curves shown have an equal 50 per cent separation diameter (d_{50}), viz. of 50 μ, and are supposed to belong to two different types of classifiers,.the first type making a less sharp separation than the second. It is also assumed that these classifiers can be so adjusted that the separation curves shift in parallel to the drawn curves and the 50 per cent separation diameter becomes respectively 50, 62·5, 80, 100 and 125 μ.

The separation efficiency according to formula IX [7] has been calculated and has been plotted against d_s for the separation curves of type I in Fig. 2 and for those of type II in Fig. 3.

It follows that the more selective separation curves of type II give a higher efficiency (which is not surprising) and that to obtain the highest separation efficiency, at a certain slope of the separation curve and at a certain value of d_s the 50 per cent diameter should not be equal to d_s, but smaller if d_s is larger than the average diameter $\bar{d}$ of the feed powder and larger if d_s is smaller than $\bar{d}$.

In the second example a valuable liquid is to be freed from suspended solids by means of a

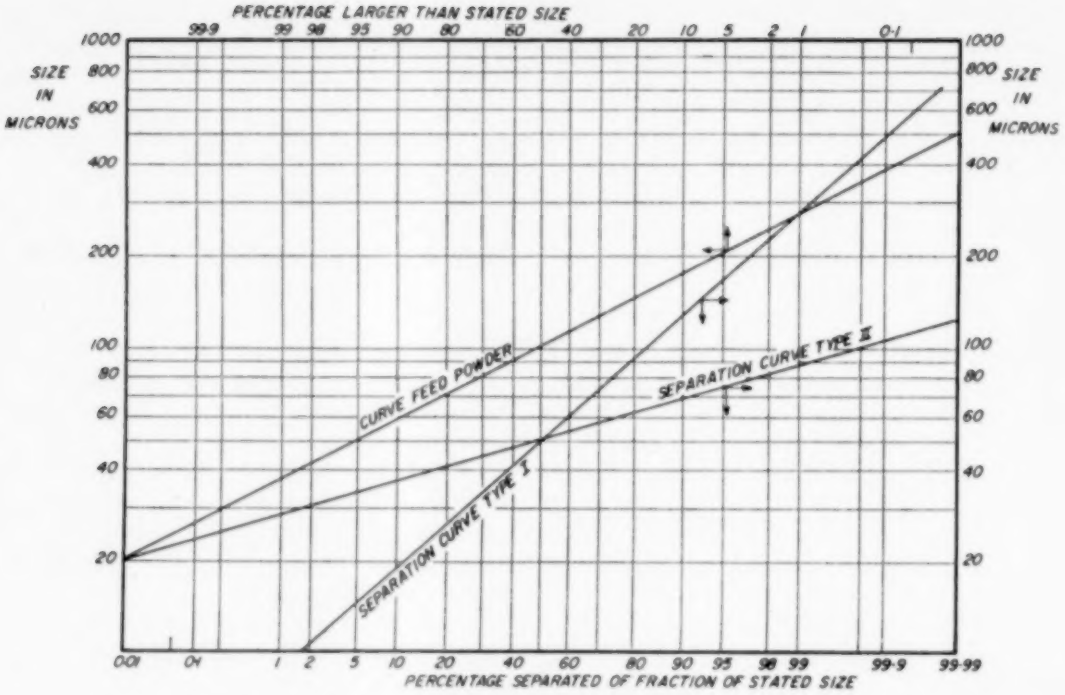
PERCENTAGE LARGER THAN STATED SIZE
99·9 99 98 95 90 80 60 40 20 10 5 2 1 0·1
SIZE IN MICRONS
1000 800 600 400 200 100 80 60 40 20
CURVE FEED POWDER
SEPARATION CURVE TYPE II
SEPARATION CURVE TYPE I
0·01 0·1 1 2 5 10 20 40 60 80 90 95 98 99 99·9 99·99
PERCENTAGE SEPARATED OF FRACTION OF STATED SIZE

FIG. 1. Cumulative size distribution of feed powder and plot of separation curves belonging to hypothetical case, discussed in section 6.

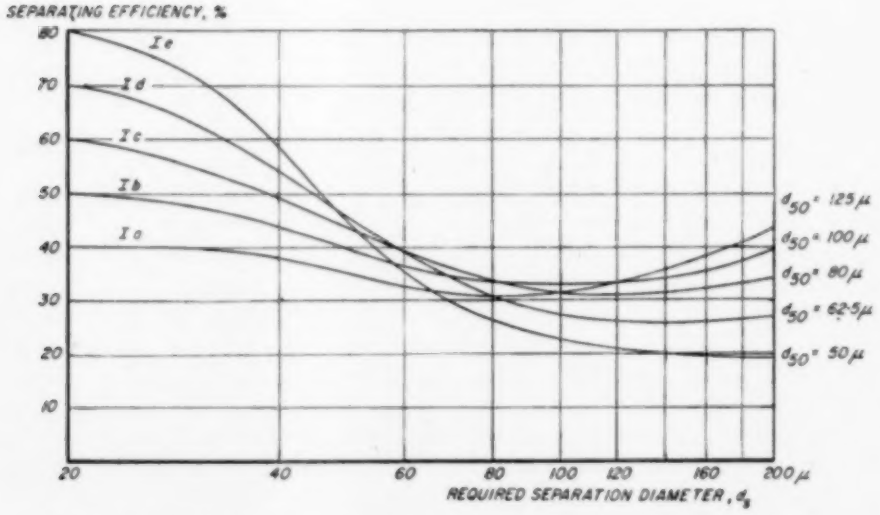

FIG. 2. Separation efficiency as function of wanted separation diameter d_s with, as parameter, the diameter of particles separated for 50 per cent in classifier of type I.

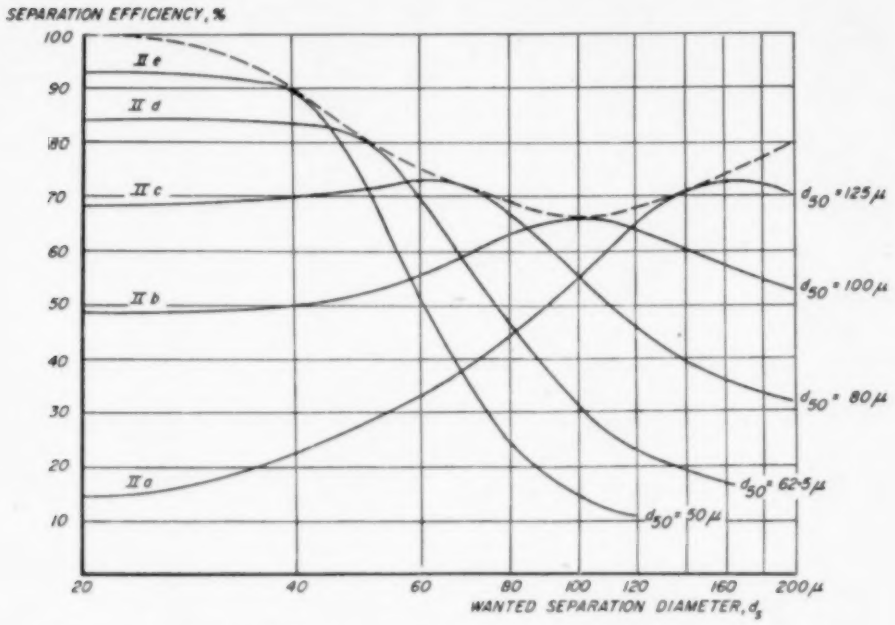

FIG. 3. Separation efficiency as function of wanted separation diameter d_s with, as parameter, the diameter of particles separated for 50 per cent in classifiers of type II.

hydrocyclone. For a given hydrocyclone there are still two variables: the throughput and the ratio of underflow to throughput. If the throughput increases, the pressure drop also increases and the separation usually improves while the separation curve shifts to smaller particle sizes. The ratio of underflow to throughput also influences the separation efficiency for two reasons:

(1) if this ratio is very small and the concentration of solids in the feed is high, the capacity of the underflow may be too small to remove all solids. In this case the solids concentration in the cyclone increases and the solids are entrained partly with the overflow. The minimum total amount of underflow necessary is equal to the amount of solids separated plus the total amount of liquid which is entrained in the pores between the solids even when these solids are closely packed. From this it follows that the optimum efficiency obtainable is limited by $E = \frac{U(1-\epsilon)}{S} - \frac{U\epsilon}{Q-S}$, in which U = the underflow rate, S = volume rate of solids in the feed, ϵ = the minimum porosity of the concentrated solids and Q = the throughput of the cyclone.

(2) if the cyclone does not separate at all, a certain amount of solids are removed by the underflow in a ratio equal to that of underflow to throughput. This means that in operating a hydrocyclone there always exists a by-pass in a quantity equal to the amount of original feed corresponding to the liquid in the underflow. Therefore, as follows from the physical interpretation in Section 5, the optimum efficiency which can be obtained with a hydrocyclone is also limited by: $E = 1 - \frac{U-S}{Q-S}$.

Because of these two effects the efficiency cannot increase above the two straight lines in Fig. 4. (The slope of the left line is determined by the concentration of the solids in the feed, the higher this concentration, the smaller the slope). Three different curves are indicated for different throughputs (Q_1, Q_2, Q_3).

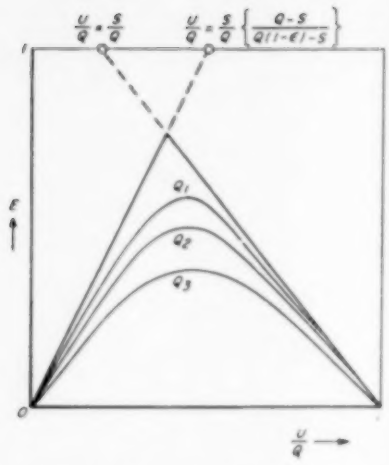

FIG. 4. Efficiency of a hydrocylone as a function of the ratio of underflow to throughput.

U = underflow
Q = throughput
S = total volume rate of solids in feed
ϵ = minimal porosity of solids separated

In this example the overall efficiency can be calculated by integration of the fractional separation efficiency over the particle size distribution, as explained in Section 4 and also by direct estimation of the solids content of the overflow.

Acknowledgements—The author is very grateful to Dr. G. H. REMAN, Dr. A. KLINKENBERG, IR. L. A. PELETIER and Mr. R. D. DOBSON for discussions and fruitful suggestions which stimulated this work and to the management of the Koninklijke/Shell-Laboratorium, Amsterdam, for permission to publish the results.

NOTATION

a = percentage of component g in the feed
b = percentage of component g in outlet stream 1
c = percentage of component g in outlet stream 2
d = particle diameter
d_s = required separation diameter
d_{50} = 50 per cent separation diameter
E = efficiency number
E_{xy} = efficiency number at two specific parameters x and y
$g(x)$ = distribution function over parameter x in component g
G_0 = feed rate of component g
G_1 = flow rate of component g in outlet stream 1
G_2 = flow rate of component g in outlet stream 2
$h(y)$ = distribution function over parameter y in component h
H_0 = feed rate of component h
H_1 = flow rate of component h in outlet stream 1
H_2 = flow rate of component h in outlet stream 2
j = amount of stream 1 as a percentage of the feed
o = percentage of h in the feed
p = percentage of h in stream 1
Q = throughput of separation apparatus
S = volume rate of solids in feed of cyclone
U = total underflow rate (by volume) of cyclone
ϵ = minimum porosity of concentrated solids
η = 100 E

REFERENCES

[1] STURTEVANT ENGNG. CO. Publication 8701 p. 8, 1946.
[2] TAGGART A. F. *Handbook of Mineral Dressing* (4th Ed.) Vol. I. pp. 19-190, 1950.
[3] PELETIER Ir. L. A. Publication M5. Bureau van Tongeren N.V., Heemstede, Holland, 1954.
[4] DOBSON R. D. Publication MB110. Bureau van Tongeren N.V., Heemstede, Holland, 1954.
[5] NEWTON H. W. and NEWTON W. H. *Rock Products* 1932 **35** 26.
[6] TEPE J. B. and WOODS W. K. Technical Information Division, Ore, Oakridge, Tennessee. Report AECD-2864.
[7] RIETEMA K. as cited by VAN. ROSSUM J. *De Ingenieur* 1953 No. 40 ; *Chemische Techniek* p. 8.

Chemical Engineering Science, 1957, Vol. 7, pp. 97 to 101. Pergamon Press Ltd.

Binary vapour–liquid equilibria of the systems : Methyl ethyl ketone–*cyclo*hexane and acetone–*cyclo*hexane

K. V. KURMANADHARAO and C. VENKATA RAO

Chemical Engineering Laboratories, Andhra University, Waltair, India

(*Received* 3 *December* 1956 ; *in revised form* 22 *March* 1957)

Abstract—Vapour-liquid equilibrium data for the systems : methyl ethyl ketone-*cyclo*hexane and acetone-*cyclo*hexane are determined at 760 mm Hg. It is found that methyl ethyl ketone-*cyclo*hexane system forms a minimum boiling azeotrope at 52·7 mole per cent *cyclo*hexane and 71·6°C at 760 mm. This is in close agreement with the recently published data of DONALD and RIDGWAY, [1] but shows some disagreement with that of LECAT [2]. Acetone-*cyclo*hexane system forms an azeotrope at 25·0 mole per cent *cyclo*hexane and 53·0°C at 760 mm. This is in close agreement with the azeotropic data reported in literature [3]. Thermodynamic consistency for both the systems has been tested by the method of REDLICH and KISTER [4] and the area condition is well satisfied showing that the experimental data are thermodynamically sound. The activity coefficients of the two systems are satisfactorily correlated by the Margules 3-suffix equations of WOHL [5].

Résumé—Des données concernant l'équilibre liquide-vapeur des systèmes : méthyl cétone–*cyclo*hexane et acétone–*cyclo*hexane, sont obtenues sous 760 mm Hg.

On trouve que les systèmes méthyl éthyl cétone–*cyclo*hexane présentent un azéotrope (minimum) pour 52,7% molaires de *cyclo*hexane bouillant à 71,6°C sous 760 mm.

Ce résultat est en complet accord avec les données récemment publiées par DONALD et RIDGWAY [1], mais présente quelque écart avec les travaux de LECAT [2]. Les systèmas acétone–*cyclo*hexane présentent un azéotrope pour 25,0% molaires de *cyclo*hexane bouillant à 53,0°C sous 760 mm. Ce résultat concorde parfaitement avec les données azéotropiques de la littérature (3).

La valeur des propriétes thermodynamiques des deux systèmes a été vérifiée par la méthode de REDLICH et KISTER (4) qui a montré que les résultats expérimentaux sont thermodynamiquement valables. Les coefficients d'activité des 2 systemès sont vérifiés de façon satisfaisante par les équations aux 3 indices de Margules et WOHL (5).

Zusammenfassung—Dampf-Flüssigkeits-Gleichgewichte sind für die Systeme : Methyläthylketon-*Cyclo*hexan und Aceton-*Cyclo*hexan bei 760 Torr bestimmt worden. Danach besitzt das System Methyläthylketon-*Cyclo*hexan ein zaeotropes Siedeminimum bei 52,7 Molprozent *Cyclo*hexan und 71,6°C bei 760 Torr. Dieses Ergebnis ist in guter Übereinstimmung mit den kürzlich veröffentlichten Werten von DONALD und RIDGWAY [1], zeigt jedoch einige Abweichungen zu denen von LECAT [2]. Das System Aceton-*Cyclo*hexan bildet ein Azeotrop bei 25,0 Molprozent *Cyclo*hexan und 53,0°C bei 760 Torr. Diese Werte stimmen gut mit den azeotropischen Daten der Literatur [3] überein. Die thermodynamische Konsistenz für beide Systeme wurde nach der Methode von REDLICH und KISTER [4] nachgeprüft. Die Flächenbedingung ist gut erfüllt, woraus hervorgeht, dass die Versuchsergebnisse thermodynamisch korrekt sind. Die Aktivitätskoeffizienten der beiden Systeme lassen sich befriedigend durch eine Margules-Gleichung vom " Drei-Suffix-Typ " nach WOHL [5] wiedergeben.

INTRODUCTION

A FAIRLY complete knowledge of the vapour–liquid relationships is essential for the development of distillation processes and for the design of necessary equipment, especiallý for non-ideal systems. With the development of azeotropic and extractive distillation techniques as potential methods of separation of liquid mixtures the need for such type of data is further increasing.

The purpose of the present investigation is to

evaluate the vapour–liquid equilibrium characteristics of the binary systems: methyl ethyl ketone–*cyclo*hexane and acetone–*cyclo*hexane.

Materials. The chemicals used in this investigation have been obtained in a sufficiently pure condition and further purified by fractional distillation. The physical properties of the purified chemicals show close agreement with the literature values as shown below:

Name of the chemical	*Ref. Index* n_D^{30}		*Density at 30°C*		*b.p.°C*
	Exp.	*Lit.*	*Exp.*	*Lit.*	
1. Methyl ethyl ketone	1·3742	1·37412	0·7945	0·79452	79·6
2. *Cyclo*hexane	1·4210	1·42088	0·7693	0·76928	80·8
3. Acetone	1·3540	1·3541	0·7793	0·77933	56·2

ANALYSIS

The refractive index is used as the basis of analysis of the liquid solutions. Mixtures of known composition are prepared at intervals of approximately 5 mole per cent and their refractive indices are determined at 30°C using ABBE's precision refractometer and sodium vapour lamp. Prism jackets of the refractometer are maintained at 30°C ± 0·05 by circulating water from TOWNSON and MERCER's constant temperature bath. The refractive indices can be accurately measured up to the third decimal place and the fourth place can be obtained by approximation. By plotting refractive index vs. composition, a calibration curve is obtained which permits evaluation of the composition of any sample. The accuracy of analysis in this method is believed to be 0·5 mole per cent.

Vapour pressure data. Vapour pressures required for the calculation of activity coefficients are computed from the following equations given in the literature [7, 8].

Methyl ethyl ketone $\log P^\circ = 7{\cdot}222 - (1343{\cdot}6/t + 230)$

*Cyclo*hexane $\log P^\circ = 7{\cdot}1329 - (1505{\cdot}15/272{\cdot}18 + t)$

Vapour pressures of acetone, taken from the literature [6] and plotted as $\log P$ vs. $1/t + 230$, give straight line which can be represented by the following equation:

$$\log P^\circ = 7{\cdot}1438 - (1220/t + 230)$$

Vapour pressures of acetone at the equilibrium boiling temperatures are calculated using the above equation.

Apparatus and experimental procedure. For the determination of vapour-liquid equilibria, an equilibrium still of COLBURN type [9] with slight modifications is employed. While all the features described by the authors have been incorporated, the present still differs mainly in certain mechanical details. One of them is with regard to the still capacity which is increased up to 2·5 l. as suggested by Prof. PIGFORD [10]. This enables vapour samples to be taken without altering the liquid composition. The second one is that two thermometer pockets are provided both at the top of the vapour column and a little ahead of the flash boiler. The introduction of these two thermometers greatly improves the working of the still and affords a very precise control on the operating conditions of the still and eliminates the dependency on the visual observation of the liquid drops in the flash boiler to avoid superheating. Conditions can be adjusted such that as soon as the condensate enters the flash boiler, the liquid flashes into vapour. The vapour is then led to the still by means of a tube at the end of which is a perforated bulb. This perforated bulb dips well below the liquid surface and serves to distribute the vapour, ensures good agitation and provides for the accurate measurement of the equilibrium temperatures. A mercury seal is provided in the condensate return line and serves the essential function of smoothing the flow of liquid into the

boiler and preventing undue fluctuations in vaporization rate during minor adjustments of the heat input. A diagrammatic sketch of the still is given in Fig. 1.

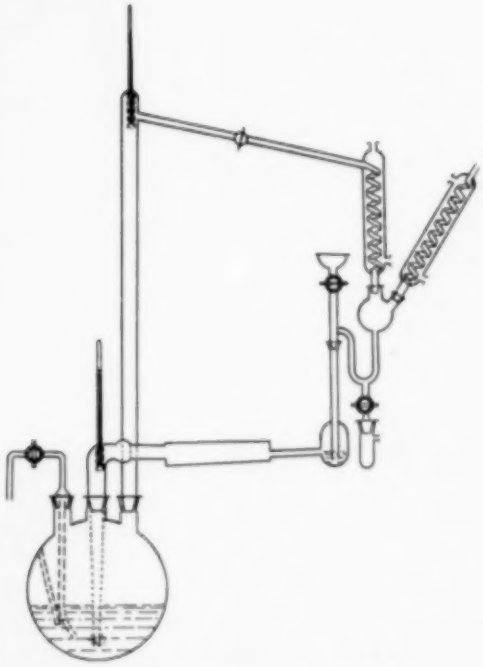

FIG. 1. Modified COLBURN still.
Still capacity = 2·5 l.

The full details regarding the operation of the above still are the same as those described in an earlier paper [11].

RESULTS

*System : Methyl ethyl ketone–*Cyclo*hexane*

The vapour-liquid equilibrium data for the system : methyl ethyl ketone–*cyclo*hexane are given in Table 1. This system forms an azeotrope at 52·7 mole per cent *cyclo*hexane and 71·6°C at 760 mm. This is in excellent agreement with the recently published data of DONALD and RIDGWAY [1], but shows some disagreement with that of LECAT [2].

Activity coefficients are calculated from experimental data and are presented in Table 1.

Table 1.
Experimental : T-x-y and Activity coefficient data
System : Cyclo*hexane* (1) *and Methyl ethyl ketone* (2) *at* 760 mm

Temperature °C	x_1	y_1	γ_1	γ_2
79·6	0·00	0·00		
77·8	3·00	9·50		0·978
76·7	5·50	14·00	2·855	0·997
75·1	12·00	21·50	2·103	1·030
73·6	19·50	30·50	1·916	1·049
72·2	32·00	41·00	1·635	1·105
7·18	40·25	45·50	1·459	1·177
71·6	56·25	52·00	1·200	1·426
71·7	60·50	54·50	1·166	1·491
72·0	66·50	59·00	1·138	1·568
72·3	71·00	60·50	1·084	1·727
72·8	75·00	63·25	1·058	1·833
73·2	78·00	65·00	1·033	1·958
73·65	80·50	67·00	1·018	2·051
75·15	82·00	69·50	1·010	2·020
74·9	85·00	72·50	1·007	2·131
75·3	86·50	74·00	0·998	2·210
75·8	88·00	75·50	0·987	2·304
76·7	90·50	79·00	0·979	2·421
77·6	92·50	82·90	0·979	2·425
78·0	94·25	85·10	0·976	2·720
78·6	94·50	88·00	0·989	2·247
80·8	100·00	100·00		

The thermodynamic consistency of the experimental results has been tested by the method of REDLICH and KISTER [4] who have shown that the criterion for thermodynamic consistency may be expressed in the form

$$\int_0^1 \log \frac{\gamma_1}{\gamma_2}\, dx_1 = 0.$$

According to this equation, if $\log \frac{\gamma_1}{\gamma_2}$ is plotted against x_1, the area above and below the abscissa must be equal. In the case of the present system, the area condition is well satisfied and hence the data are thermodynamically sound.

Correlation of data. Fig. 2 shows a plot of log γ vs. x_1. From this plot it is evident that this is almost a symmetric system. Hence either

VAN LAAR 2-suffix or MARGULES 3-suffix equations will give nearly identical results as discussed by WOHL [5]. But since the present system forms part of the ternary system : acetone methyl ethyl ketone–*cyclo*hexane and since the ternary VAN LAAR equations have got certain limitations,

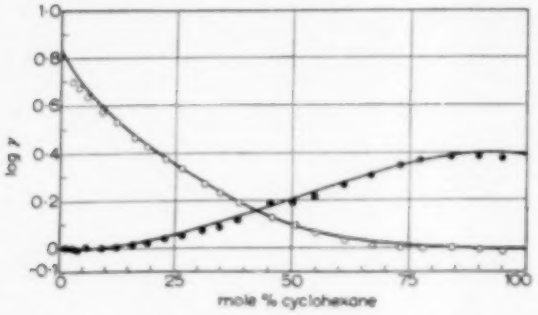

FIG. 2. Activity coefficients of methyl ethyl ketone *cyclo*hexane at 760 mm.

——— calculated Margules 3-Suffix.
○] ●] Experimental.

the binary data of the present system are correlated by the 3-suffix MARGULES equations. The constants A and B in the 3-suffix MARGULES equations are calculated at various compositions using the relationships given by CARLSON and COLBURN [12]

$$A = \frac{\log \gamma_1}{x_2^2} + 2x_1\left(\frac{\log \gamma_2}{x_1^2} - \frac{\log \gamma_1}{x_1^2}\right)$$

$$B = \frac{\log \gamma_2}{x_1^2} + 2x_2\left(\frac{\log \gamma_1}{x_2^2} - \frac{\log \gamma_2}{x_1^2}\right)$$

The average values of these constants are found to be $A = 0{\cdot}404$ and $B = 0{\cdot}501$. These constants check well with the values of A and B calculated with the above relationships, using azeotropic data. In Fig. 2 the solid lines represent the calculated values of the activity coefficients and the points lying on the curves represent experimental data. From this plot it is evident that close agreement is obtained between the experimental and calculated activity coefficients showing that the 3-suffix MARGULES equations are quite satisfactory.

System : *Acetone*–cyclo*hexane*

The vapour-liquid equilibrium data for the system : Acetone – *cyclo*hexane are given in Table 2. This system forms an azeotrope at 25·0 mole per cent *cyclo*hexane and 53·0°C at 760 mm. This is in close agreement with the azeotropic data reported in literature [3].

Table 2. *Experimental : T-x-y and Activity coefficient data*

System : Cyclo*hexane* (1) – *Acetone* (2) at 760 mm

Temperature °C	x_1	y_1	γ_1	γ_2
56·2	0·00	0·00		
55·6	1·25	2·50	4·235	1·007
55·1	2·50	5·75	4·949	1·004
54·8	3·75	8·25	4·781	0·999
54·3	5·75	11·25	4·320	1·004
53·85	9·00	15·00	3·737	1·012
53·45	12·50	18·75	3·411	1·020
53·20	16·00	20·50	2·932	1·049
53·15	19·00	22·50	2·714	1·063
53·1	22·75	23·80	2·404	1·097
53·1	26·50	25·25	2·190	1·131
53·1	31·00	25·50	1·891	1·201
53·1	34·50	26·00	1·732	1·257
53·3	38·50	26·50	1·569	1·320
53·8	45·50	27·50	1·356	1·445
54·2	50·25	28·75	1·267	1·533
54·5	54·75	29·00	1·162	1·662
55·0	61·00	30·50	1·079	1·856
56·0	67·00	32·50	1·014	2·058
57·6	73·00	37·00	1·007	2·223
59·2	77·50	41·00	1·000	2·366
63·0	84·00	50·50	1·009	2·462
68·0	89·75	62·50	0·998	2·480
73·8	94·75	77·50	0·996	2·426
80·8	100·00	100·00		

Activity coefficients are calculated from experimental data and are presented in Table 2. Thermodynamic consistency of the data is tested by the method of REDLICH and KISTER as discussed earlier. The area condition is well satisfied, showing that the data are thermodynamically sound.

Correlation of data. Fig. 3 shows a plot of log γ vs. x_1. From this plot it is seen that the

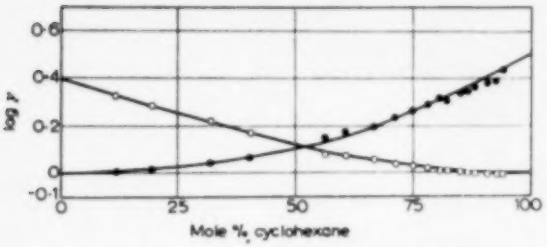

FIG. 3. Activity coefficients of acetone and *cyclo*hexane at 760 mm.
——— Calculated Margules 3-Suffix.
°] Experimental.

ratio of A to B is slightly more than 2 and the log γ_2 curve is showing a maximum at about 95·0 mole per cent *cyclo*hexane. VAN LAAR equations fail to represent such type of behaviour whereas 3-suffix MARGULES equations can handle such situations. Hence an attempt is made to utilize these equations for correlation of the present data. The constants in the three suffix MARGULES equations are evaluated at various liquid compositions and the average values are found to be $A = 0{\cdot}842$ and $B = 0{\cdot}401$. In Fig. 3 the solid lines represent calculated activity coefficient data while the points lying on the curves represent actual experimental data. It is found that the experimental and calculated results agree well showing that the 3-suffix MARGULES equations are quite satisfactory in the case of this system. The values of A and B calculated from azeotropic data for this system are in agreement with the average values of A and B given above.

CONCLUSIONS

Vapour–liquid equilibrium data are presented for the binary systems : methyl ethyl ketone-*cyclo*hexane and acetone–*cyclo*hexane, at 760 mm. Both the systems form minimum boiling azeotropes. The experimental data are tested by the method of REDLICH and KISTER and found to be thermodynamically consistent. The activity coefficient data of the two systems can be satisfactorily correlated by the 3-suffix MARGULES equations.

This work has been carried out as part of an investigation of the acetone–methyl ethyl ketone–*cyclo*hexane ternary system, the results of which will be published in due course.

NOMENCLATURE

γ = Activity coefficient
P° = Vapour pressure of pure component
x = Mole fraction in liquid
y = Mole fraction in vapour

REFERENCES

[1] DONALD M. B. and RIDGWAY K. *Chem. Engng. Sci.* 1956 **5** 188.
[2] LECAT *Ann. Chim.* 1947, **2** No. 12, 158-202.
[3] LECAT *Ann. Soc. Sci. Bruxelles* 1925 **45** No. 1, 228.
[4] REDLICH O. and KISTER A. T. *Industr. Engng. Chem.* 1948 **40** 345.
[5] WOHL K. *Trans. Amer. Inst. Chem. Engrs.* 1946 **42** 215, *Chem. Engng. Prog.* 1953 **49** 218.
[6] TIMMERMANS J. *Physico Chemical Constants of Organic Compounds.*
[7] DREISBACH R. R. and MARTIN R. A. *Industr. Engng. Chem.* 1949 **41** 2875.
[9] JONES C. A., SHOENBORN E. M. and COLBURN A. P. *Industr. Engng. Chem.* 1943 **35** 666.
[10] PIGFORD R. L. Private communication to Prof. C. V. RAO.
[11] RAJARAO M., KURMANADHARAO K. V. and VENKATARAO C. Paper communicated to *J. Appl. Chem.* (London).
[12] CARLSON H. C. and COLBURN A. P. *Industr. Engng. Chem.* 1942 **34** 581.

Chemical Engineering Science, 1957, Vol. 7, pp. 102 to 110. Pergamon Press Ltd.

Ternary liquid equilibria

Systems : acetone - water - esters

A. Venkataratnam, R. Jagannadha Rao, and C. Venkata Rao
Department of Chemical Technology, Andhra University, Waltair

(*Received* 30 *April* 1957)

Abstract—Mutual solubility and tie-line data are presented for six ternary liquid-liquid systems containing acetone, water, and the esters methyl acetate, ethyl acetate, propyl acetate, amyl acetate, ethyl propionate and ethyl butyrate at 30°C. For comparison, equilibrium data for the system acetone–water–*n*-butyl acetate reported in literature has been plotted on the mutual solubility, equilibrium distribution and selectivity diagrams. The tie-line data for the six systems have been correlated satisfactorily by the methods of Hand and Othmer and Tobias and the plait points are located by the method of Treybal, Weber and Daley. From the comparative plot of the distribution of acetone between the ester and aqueous layers for the various systems, it is found that acetone favours the ester layer in all the cases. The system, propyl acetate–acetone-water is observed to exhibit solutropy. Among the various esters studied, amyl acetate is observed to be the most selective of all the solvents.

Résumé—Les auteurs donnent les solubilités réciproques et les conodales pour 6 systèmes ternaires liquide – liquide contenant Acétone – eau – ester acétate de méthyle – acétate d'éthyle – de propyle – d'amyle – d'éthyle et butyrate d'éthyle à 30°C. Par comparaison, les données d'équilibre pour le système acétone – eau – n – butyl acétate, données dans la littérature ont été portées sur les diagrammes, de solubilité réciproque, de distribution d'équilibre et de sélectivité. Les conodales pour les 6 systèmes ont été déterminées de façon satisfaisante par les méthodes de Hand et Othmer et Tobias et les points de démixtion situés par la méthode de Treybal, Weber et Daley. A partir du tracé comparatif de la distribution de l'acétone entre l'ester et les couches aqueuses pour les divers systèmes les auteurs ont trouvé que l'acétone se dissout dans la couche d'ester dans tous les cas. Le système acétate de propyl – acétone – eau est étudié pour montrer la solutropie. Parmi les différents esters étudiés l'acétate d'amyle est le plus sélectif de tous les solvants.

Zusammenfassung—Für sechs ternäre Flüssig-flüssig-Gemische, enthaltend Azeton, Wasser und die Ester Methylazetat, Äthylazetat, Propylazetat, Amylazetat, Äthylpropionat und Äthylbutyrat bei 30°C, werden die gegenseitige Löslichkeit und die Konnoden-Daten mitgeteilt. Zum Vergleich werden Literaturwerte des Gleichgewichts für das System Azeton – Wasser – *n* – Butylazetat in Diagrammen der gegenseitigen Löslichkeit. der Gleichgewichtsverteilung und der Selektivität dargestellt. Die Konnoden-Daten für die sechs Systeme lassen sich befriedigend nach den Methoden von Hand und Othmer und Tobias korrelieren, die " Plait-points "* sind nach der Methode von Treybal, Weber und Daley bestimmt. Aus dem Vergleichsdiagramm der Verteilung von Azeton zwischen dem Ester und den wässerigen Schuchten für die verschidenen Systeme ergibt sich, dass Azeton in allen Fällen die Esterschicht bevorzugt. Das System Propylazetat – Azeton – Wasser zeigt, wie beobachtet wurde, Solutrope)**. Unter den verschiedenen Eastern wurde Amylazetat als der am meisten selektive gefunden.

Introduction

In recent years, liquid extraction, as a means of separation, has found increased application in industry and much attention has been bestowed for its development. The successful design of a suitable equipment for any liquid extraction process necessitates a thorough understanding and a complete knowledge of the solubility and equilibrium relationships. The present investigation is confined to the study of the liquid phase equilibrium relationships of the ternary systems, acetone-water-esters and to assess the feasibility

* d.i. die Stelle der Binodalkurve, an der die Konnoden zu einem Punkt zusammenlaufen.
**d.i. gleiche Löslichkeit in beiden Phasen.

of the use of the esters for the extraction of acetone from its aqueous solution which finds extensive application in industry.

The esters chosen in the present study are methyl acetate, ethyl acetate, propyl acetate, amyl acetate, ethyl propionate and ethyl butyrate. For comparison, data for the system, acetone-water-*n*-butyl acetate at 30°C reported in reference [1] are taken and plotted as shown in Figs. 1, 2 and 4.

Materials Used

Acetone of analytical grade supplied by the British Drug House Ltd., is directly used. Of the esters, methyl acetate and propyl acetate are of the laboratory reagent grade supplied by the British Drug House Ltd., and are subjected to fractionation and the fractions collected at their indicated boiling points are used. The other esters are of analytical grade and directly used. Distilled water free from carbon dioxide is used throughout the work.

The physical constants of the materials used in this study are listed in Table 1.

Experimental Procedure

The experimental procedure followed for the determination of the binodal curve data and tie-line data is the method described earlier by Othmer *et al.* [2]. The end wings of the binodal curve are determined by titrating known mixtures of ester–acetone and water–acetone with the third component to the point of appearance of permanent turbidity and the middle portion is

VOL. 7
957/58

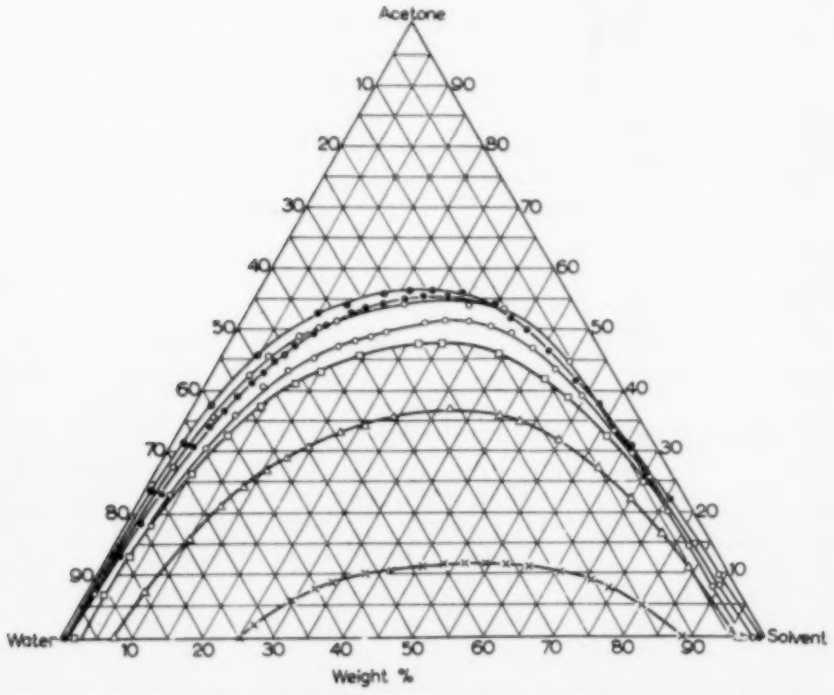

Fig. 1. Comparison of mutual solubility curves for acetone-water-esters systems at 30°C.

Legend :
- Acetone–water–methyl acetate . ×
- Acetone–water–ethyl acetate . . △
- Acetone–water–propyl acetate . □
- Acetone–water–*n*–Butyl acetate . ○
- Acetone–water–amyl acetate . . ⊗
- Acetone–water–ethyl propionate ⊖
- Acetone–water–ethyl butyrate . ●

Table 1. *Physical constants of the materials used*

Material	*Density at* 30°C	*Refractive index at* 30°C	*Boiling point at* 760 mm Hg
Acetone (B.D.H.)	0·7791	1·3541	56·1°C
Methyl acetate (B.D.H.)	0·9234	1·3570	57·3°C
Ethyl acetate (B.D.H.)	0·8885	1·3680	77·1°C
Propyl acetate (B.D.H.)	0·8773	1·3800	101·6°C
n-Butyl acetate (B.D.H.)	0·8710	1·3916	126·0°C
Amyl acetate (May and Baker)	0·8630	1·3937	95 per cent between 120° and 150°C
Ethyl propionate (Naarden)	0·8790	1·3812	99·1°C
Ethyl butyrate (Naarden)	0·8685	1·3880	121·5°C

Table 2. *Mutual solubility and tie-line data for the system: methyl acetate–aceto newater at* 30°C
(*Wt per cent*)

Mutual solubility data

S.no.	*Methyl acetate*	*Acetone*	*Water*	*S.no.*	*Methyl acetate*	*Acetone*	*Water*
1	25·4	0·0	74·6	12	57·3	11·8	30·9
2	26·2	1·9	71·9	13	61·0	11·5	27·5
3	29·8	6·1	64·1	14	65·9	10·5	23·6
4	32·0	8·0	60·0	15	71·0	9·0	20·0
5	34·2	8·8	57·0	16	74·0	8·0	18·0
6	38·0	10·3	51·7	17	80·5	5·0	14·5
7	41·6	11·0	47·4	18	84·0	3·0	13·0
8	45·8	11·6	42·6	19	88·6	0·0	11·4
9	48·3	12·0	39·7				
10	51·5	11·9	36·6				
11	54·5	11·9	33·6				

Tie-line data

	Solvent layer			*Water layer*		
S.no.	*Methyl acetate*	*Acetone*	*Water*	*Methyl acetate*	*Acetone*	*Water*
1	86·5	1·5	12·0	26·0	1·3	72·7
2	83·1	3·4	13·5	27·0	2·7	70·3
3	76·0	7·6	16·4	28·3	5·0	66·7
4	68·0	10·0	22·0	32·4	8·1	59·5

built up by titrating known heterogeneous mixtures of water and ester with acetone to the point of disappearance of turbidity. For determining the tie-line data, different mixtures of the three components of known composition within the two phase region are prepared in separating funnels and maintained at a constant temperature of 30°C by keeping them in a Fischer's unitized constant temperature bath and allowed to settle for 4 hr with intermittent shaking. The layers are then separated and weighed on a Mettler balance. The concentration

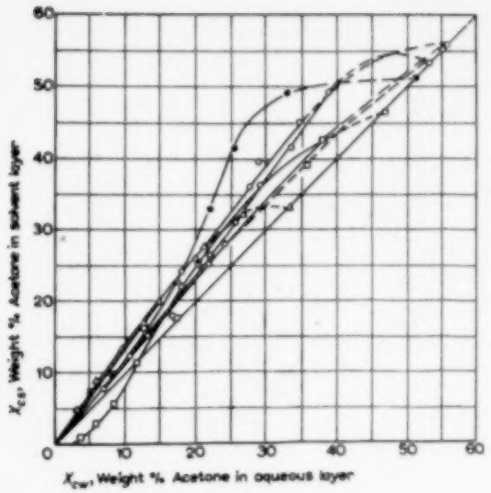

FIG. 2. Weight per cent acetone in aqueous layer. ← Abscissa (x-axis) ordinate → weight per cent acetone in solvent layer. Equilibrium distribution diagram. Legend : same as in Fig. 1.

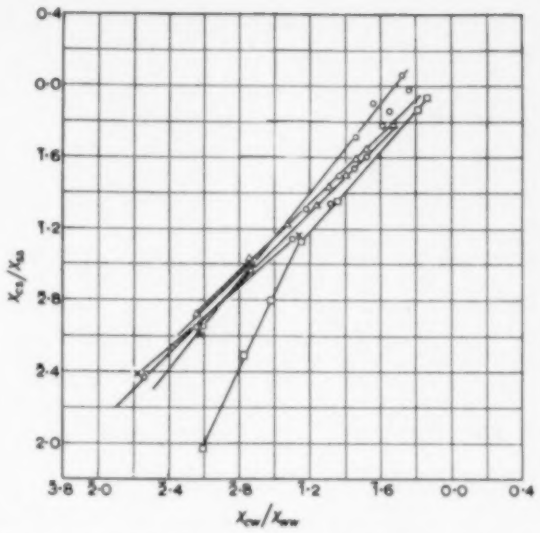

FIG. 3. HAND's plot of tie-line correlation. Legend : same as in Fig. 1.

Table 3. Mutual solubility and tie-line data for the system : ethyl acetate–acetone–water at 30°C (Wt per cent). Mutual solubility data

S.no.	*Ethyl acetate*	*Acetone*	*Water*	*S.no.*	*Ethyl acetate*	*Acetone*	*Water*
1	7·4	0·0	92·6	11	29·0	36·0	35·0
2	8·0	7·6	84·4	12	30·7	37·0	26·3
3	9·9	16·1	74·0	13	44·4	36·1	19·5
4	11·9	21·1	67·0	14	47·6	35·0	17·4
5	13·6	24·3	62·1	15	55·0	32·0	13·0
6	15·5	27·0	57·5	16	62·5	27·5	10·0
7	17·4	29·2	53·4	17	70·0	22·4	7·6
8	19·2	31·1	49·7	18	77·0	17·0	6·0
9	24·0	33·4	42·6	19	83·7	11·2	5·1
10	25·5	34·6	39·9	20	96·5	0·0	3·5

Tie-line data

	Solvent layer			*Water layer*		
S.no.	*Ethyl acetate*	*Acetone*	*Water*	*Ethyl acetate*	*Acetone*	*Water*
1	91·0	4·8	4·2	8·3	3·2	88·5
2	85·6	9·4	5·0	8·0	6·0	86·0
3	80·5	13·5	6·0	8·3	9·5	82·2
4	77·2	16·6	6·2	9·2	12·8	78·0
5	73·0	20·0	7·0	9·8	14·8	75·4
6	70·0	22·4	7·6	10·2	17·5	72·3
7	65·0	26·0	9·0	12·2	19·8	68·0
8	62·0	27·8	10·2	11·8	21·2	67·0
9	54·0	32·6	13·4	15·0	26·4	58·6

VOL. 7 957/58

Table 4. *Mutual solubility and tie-line data for the system : propyl acetate–acetone–water at* 30°C
(*Wt per cent*)
mutual solubility data

S.no.	*Propyl acetate*	*Acetone*	*Water*	*S.no.*	*Propyl acetate*	*Acetone*	*Water*
1	1·8	0·0	98·2	11	26·8	47·7	25·5
2	2·2	7·0	90·8	12	30·0	47·9	22·1
3	3·0	13·1	83·9	13	39·0	46·3	14·7
4	3·4	18·3	78·3	14	47·7	42·3	10·0
5	4·8	26·7	68·5	15	52·7	39·1	8·2
6	6·8	33·0	60·2	16	61·4	32·7	5·9
7	9·2	37·5	53·3	17	70·8	25·2	4·0
8	12·4	41·5	46·1	18	82·5	14·6	2·9
9	14·8	43·3	41·9	19	89·8	8·0	2·2
10	19·2	45·8	35·0	20	98·4	0·0	1·6

Tie-line data

	Solvent layer			*Water layer*		
S.no.	*Propyl acetate*	*Acetone*	*Water*	*Propyl acetate*	*Acetone*	*Water*
1	97·3	0·9	1·8	2·0	3·7	94·3
2	94·5	3·5	2·0	2·0	5·8	92·2
3	92·3	5·7	2·0	2·1	8·4	89·5
4	85·9	11·6	2·5	2·7	11·7	85·6
5	79·0	17·8	3·2	3·0	17·5	79·5
6	70·8	25·0	4·2	4·0	20·5	75·5
7	52·5	39·0	8·5	8·0	35·5	56·5
8	47·1	42·6	10·3	9·3	37·5	53·2

Table 5. *Mutual solubility and tie-line data for the system : amyl acetate–acetone–water at* 30°C
(*Wt per cent*)
Mutual solubility data

S.no.	*Amyl acetate*	*Acetone*	*Water*	*S.no.*	*Amyl acetate*	*Acetone*	*Water*
1	0·2	0·0	99·8	11	24·5	56·5	19·0
2	0·5	13·5	86·0	12	29·1	55·9	15·0
3	0·8	23·6	75·6	13	34·6	53·9	11·5
4	1·3	31·5	67·2	14	41·5	50·0	8·5
5	2·4	37·6	60·0	15	46·1	46·8	7·1
6	3·4	42·4	54·2	16	37·7	37·7	4·6
7	4·9	46·0	49·1	17	65·7	31·0	3·3
8	10·1	52·6	37·3	18	75·9	22·0	2·1
9	13·4	54·3	32·3	19	89·1	9·7	1·2
10	18·1	55·6	26·3	20	99·6	0·0	0·4

Tie-line data

	Solvent layer			*Water layer*		
S.no.	*Amyl acetate*	*Acetone*	*Water*	*Amyl acetate*	*Acetone*	*Water*
1	95·0	4·3	0·7	0·5	3·5	96·0
2	86·6	12·1	1·3	0·5	11·0	88·5
3	80·0	18·0	2·0	0·5	17·0	82·5
4	72·8	25·1	2·1	0·7	21·9	77·4
5	69·2	28·1	2·7	1·0	24·2	74·8

Table 6. Mutual solubility and tie-line data for the system : ethyl propionate–acetone–water at 30°C
(Wt per cent)

Mutual solubility data

S.no.	*Ethyl propionate*	*Acetone*	*Water*	*S.no.*	*Ethyl propionate*	*Acetone*	*Water*
1	2·7	0·0	97·3	11	25·9	51·2	22·9
2	2·9	13·2	83·9	12	28·7	51·6	19·7
3	3·6	23·0	73·4	13	35·4	50·8	13·8
4	5·0	30·4	64·6	14	43·5	46·9	9·6
5	6·4	36·1	57·5	15	48·6	43·6	7·8
6	8·3	40·3	51·4	16	54·6	39·2	6·2
7	10·4	43·4	46·2	17	62·0	33·4	4·6
8	13·0	45·5	41·5	18	71·2	25·5	3·3
9	17·6	48·2	34·2	19	82·9	14·9	2·2
10	21·3	49·8	28·9	20	98·2	0·0	1·8

Tie-line data

	Solvent layer			*Water layer*		
S.no.	*Ethyl propionate*	*Acetone*	*Water*	*Ethyl propionate*	*Acetone*	*Water*
1	89·1	9·0	1·9	2·8	6·5	90·7
2	81·4	16·5	2·1	2·9	12·8	84·3
3	73·1	23·7	3·2	3·1	18·0	78·9
4	58·8	36·0	5·2	3·9	27·5	68·6
5	54·4	39·4	6·2	4·0	28·8	67·2
6	46·4	45·1	8·5	4·9	34·4	60·7

of acetone in each layer is estimated by the method of MARASCO [3].

RESULTS AND CORRELATIONS

The experimental mutual solubility and tie-line data at 30°C for the six ternary systems, viz., methyl acetate–acetone–water, ethyl acetate–acetone–water, propyl acetate–acetone–water, amyl acetate–acetone–water, ethyl propionate–acetone–water and ethyl butyrate–acetone–water are presented in Tables 2 to 7. The binodal curve data for the above six systems are compared along with the data for the system *n*-butyl acetate–acetone–water reported in reference [1] at 30°C and the comparative plot is shown in Fig. 1. The equilibrium distribution of acetone

Table 7. Mutual solubility and tie-line data for the system: ethyl butyrate–acetone–water at 30°C (Wt per cent)

Mutual solubility data

S.no.	Ethyl butyrate	Acetone	Water	S.no.	Ethyl butyrate	Acetone	Water
1	0·8	0·0	99·2	11	16·6	53·8	29·6
2	1·0	7·2	91·8	12	23·7	55·5	20·8
3	1·5	13·3	85·2	13	29·0	54·9	16·1
4	2·0	18·6	79·4	14	38·2	51·5	10·3
5	2·3	23·3	74·4	15	46·6	46·1	7·3
6	2·6	27·4	70·0	16	51·9	42·1	6·0
7	3·8	34·0	62·2	17	62·1	33·8	4·1
8	5·2	39·0	55·8	18	71·4	25·7	2·9
9	7·3	44·9	47·8	19	83·2	15·0	1·8
10	10·9	49·5	39·6	20	90·3	8·1	1·6
				21	99·4	0·0	0·6

Tie-line data

	Solvent layer			Water layer		
S.no.	Ethyl butyrate	Acetone	Water	Ethyl butyrate	Acetone	Water
1	96·6	2·3	1·1	0·7	1·8	97·5
2	94·7	4·2	1·1	0·9	3·7	95·4
3	90·3	8·4	1·3	1·1	6·7	92·2
4	82·0	16·0	2·0	1·6	13·1	85·3
5	63·0	33·0	4·0	2·1	21·8	76·1
6	52·5	41·8	5·7	2·3	25·2	72·5
7	42·0	49·0	9·0	3·1	32·6	64·3

Table 8. plait point data (Wt per cent)

System	Solvent	Acetone	Water
Methyl acetate–acetone–water	38·8	10·4	50·8
Ethyl acetate–acetone–water	27·2	35·6	37·2
Propyl acetate–acetone–water	22·4	46·8	30·8
Amyl acetate–acetone–water	19·5	55·5	25·0
Ethyl propionate–acetone–water	19·2	55·7	25·1
Ethyl butyrate–acetone–water	13·0	51·4	35·6

between water and the different esters for all the seven systems is shown in Fig. 2.

The tie-line data for all the systems are correlated fairly well by the methods of Hand [4] and Othmer and Tobias [5] except for the solutropic system propyl acetate–acetone–water, in which case two straight lines are obtained. The Hand's plot of tie-line correlation is presented in Fig. 3 which shows single straight lines for all the systems, but two straight lines for propyl acetate–acetone–water. The plait points are located by the method of Treybal, Weber and Daley [6] and their compositions are given in Table 8.

To assess the selectivity of the esters studied, a selectivity diagram is drawn by plotting the weight fraction of acetone in the solvent layer against the weight fraction of acetone in the

Table 9.
Dielectric constant data (ϵ) *of liquids used at* 20°C

Liquid	*Dielectric constant*
Acetone	21·40
Methyl Acetate	7·30
Ethyl Acetate	6.40
Propyl Acetate	6.30
n-Butyl Acetate	5·14
Amyl Acetate	5·07
Ethyl Propionate	5·76
Ethyl Butyrate	5·19
Water	81·00

aqueous layer both on solvent-free basis and the plot is shown in Fig. 4.

Discussion

It is seen from Fig. 1, that the region of heterogeneity bounded by the binodal curve increases from methyl acetate to amyl acetate as also from ethyl propionate to ethyl butyrate in the order of increasing molecular weight. This behaviour of esters exhibited by the increase in the zones of heterogeneity from the lower to the higher esters has been explained earlier by Raja Rao and Venkata Rao [7] and by Jagannadha Rao and Venkata Rao [8] by attributing to the close similarity of the esters in their chemical structure and the concept of polarity which exercises a major influence on their solubility. Also, similar behaviour of the esters has been noticed by Murti *et al.* [1] and Jayarama Rao and Venkata Rao [9]. From the dielectric constant data [10] which is a measure of the polarity, recorded in Table 9, it is seen that the decrease in polarity as evidenced by the decrease in the dielectric constant in succession from methyl acetate to amyl acetate and from ethyl propionate to ethyl butyrate may account for the corresponding increase in the zones of heterogeneity from the lower to the higher ester.

The equilibrium distribution of acetone between water and the esters shown in Fig. 2 reveals that acetone favours more the ester phase than the aqueous phase in all the systems with the exception of propyl acetate–acetone–water which exhibits solutropy at about 12 per cent by weight of acetone. In chemical structure, acetone resembles closely the esters and the fact that the polarity of acetone being closer to the esters than to water explains its favouring the ester phase.

For the solutropic system propyl acetate–acetone–water, equilibrium data is represented on Hand's plot of tie-line correlation (Fig. 3) by two straight lines with different slopes, the point of intersection of the two lines coinciding with the solutropic point. The selectivity diagram reveals that amyl acetate is the most selective of all the solvents studied.

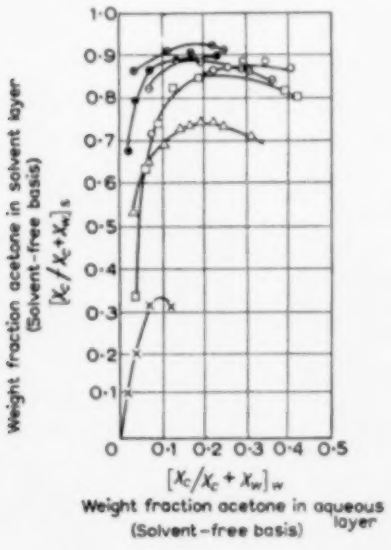

Fig. 4.
x-axis :—Weight fraction acetone in aqueous layer (solvent free basis).
y-axis :—Weight fraction acetone in solvent layer (solvent free basis).
Selectivity diagram. Legend : same as in Fig. 1.

Notation

X_{cs} = weight fraction of solute in solvent layer
X_{cw} = weight fraction of solute in water layer.
X_{ss} = weight fraction of solvent in solvent layer.
X_{ww} = weight fraction of water in water layer.
Subscripts
c = solute
s = solvent
w = water

References

[1] Murti P. S., Venkataratnam A. and Venkata Rao C. *J. Sci. Industr. Res.* B1954 **13** 392.

[2] Othmer D. F., White R. E. and Trueger E. *Industr. Engng. Chem.* (*Industr.*) 1941 **33** 1240.

[3] Marasco M. *Industr. Engng. Chem.* (*Industr.*) 1926 **18** 701.

[4] Hand D. B. *J. Phys. Chem.* 1930 **34** 1961.

[5] Othmer D. F. and Tobias P. E. *Industr. Engng. Chem.* (*Industr.*) 1942 **34** 693.

[6] Treybal R. E., Weber L. D. and Daley J. F. *Industr. Engng. Chem.* (*Industr.*) 1946 **38** 817.

[7] Raja Rao M. and Venkata Rao C. *J. Sci. Industr. Res.* B1955 **14** 204.

[8] Jagannadha Rao R. and Venkata Rao C. *J. Appl. Chem.* Accepted for publication in November 1956.

[9] Jayarama Rao G. and Venkata Rao C. *J. Sci. Industr. Res.* B1955 **14** 444.

[10] *International Critical Tables* (1st Ed.) Vol. VI, p. 83. McGraw-Hill, New York, 1928.

VOL 7 1957

VOL. 7 957/58

Velocity of rise of air bubbles in sea-water, and their types of motion

(*Received* 23 *May* 1957)

POPE [1] and SOUTHWARD [2], commenting upon the foaming properties of sea-water, suggested the possible presence of surface-active substances to account for these properties, though they were unable to detect such materials. STUKE [3] has shown that long-chain fatty acids (e.g. caproic and capric) in low concentrations of the order $1{\cdot}5 \times 10^{-4}$ molar, can reduce the velocity of rise of oxygen bubbles in water. A similar effect on the velocity of rise of air bubbles in sea-water has now been observed; again, the presence of surface-active agents in sea-water may be inferred.

The method used was to time the rise, in a column of water 100 cm long, diam. 5 cm, of bubbles produced singly at a jet. The velocity of rise was measured with an accuracy better than $\pm$ 5 per cent. A micrometer syringe was designed to produce single bubbles whose volumes could be measured with an accuracy better than $\pm$ 0·5 per cent. Although small bubbles were timed singly, it was found necessary to measure the volume of a number of bubbles to achieve the desired accuracy.

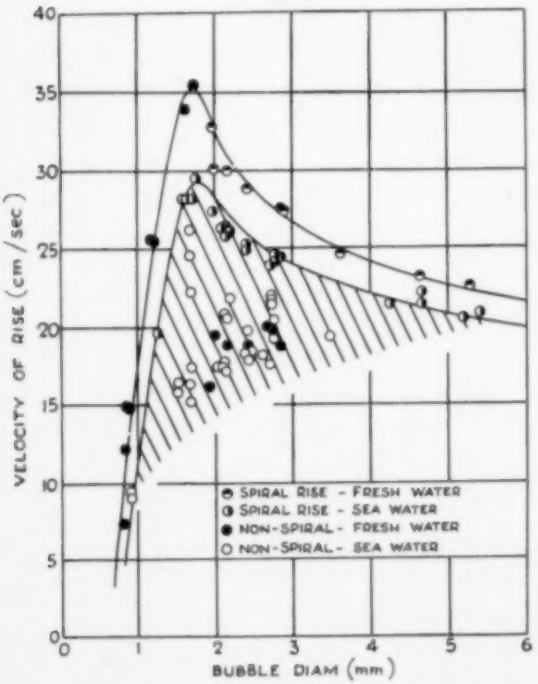
VELOCITY OF RISE (cm/sec)
BUBBLE DIAM (mm)
SPIRAL RISE - FRESH WATER
SPIRAL RISE - SEA WATER
NON-SPIRAL - FRESH WATER
NON-SPIRAL - SEA WATER

FIG. 1. Velocity of rise of bubbles in fresh water and sea-water.
(Transition region shaded)

Single bubbles in sea-water usually rose with a fast spiral motion; but occasionally a single bubble would be produced, having the same volume, but showing a much lower velocity of rise and a non-spiral motion. Velocities of rise between these two extremes were also observed, and in these intermediate cases the spiral motion was of smaller diameter. It was noted that once spiral motion had started for any one bubble, the spiral was propagated with a radius which increased as the bubble rose. The results for sea-water are shown in Fig. 1. The shaded area represents a transition region between spiral and non-spiral motion. The incidence of each type of motion seems to be a matter of chance, no doubt affected by vibration of the jet or by vortices in the liquid. Possibly one reason why non-spiral motion has been observed is that the micrometer syringe can generate bubbles at any desired interval, so that vortices formed in the liquid by the rise of a bubble may have time to decay before the passage of the next bubble. The approximate frequency of occurrence of spiral motion as compared with that of intermediate and non-spiral motions is shown in Table 1.

Table 1

Bubble diam. (mm)	*Bubbles generated (%)*	
	With spiral motion	*With intermediate and non-spiral motion*
0·8	0	100
1·0	0	100
1·5	80	20
2·0	80	20
2·5	80	20
3.0	60	40
3·5	20	80
4·5	0	100

For comparison, the experimental results for air bubbles rising in pure water are also shown in Fig. 1, and the data agree remarkably well with those of STUKE [3]. The occurrence of non-spiral rise was much less frequent than in sea-water, only about 1 bubble in 50 being observed to rise non-spirally. It was also observed that for the fastest spiral motion the velocity of rise is always greater in fresh than in sea-water. The explanation is probably the presence of small amounts of surface-active agents in the latter.

The sea-water samples used had a chlorinity of 16 and were obtained from the Firth of Clyde near the entrance to Loch Long. Their surface tension at 19·8°C was found to be 58·7 dyn/cm, as compared with 71·8 dyn/cm for a sample of freshwater. The freshwater used for comparison was Glasgow City water. The lower surface tension of sea-water further confirms the presence of surface-active agents.

The present results may also throw some light on the discrepancies between the values obtained by various authors for the velocity of rise in pure water of bubbles whose diameters lie between 0·8 and 4·0 mm. Benfratello [4] has summarized the literature available on velocity of rise in pure water, and inspection of his curves shows that a bubble with a diameter of (for example) 2 mm has been reported to rise with a velocity in the range 17 – 34 cm/sec. The explanation may be that the diameter range 0·8 – 4·0 mm is a transition region where spiral, non-spiral, and intermediate types of rise can occur, and where the velocity of rise and the incidence of non-spiral motion are sensitive to dissolved impurities.

Acknowledgement—The authors thank the Admiralty for permission to publish this note.

Technical Chemistry Department G. Houghton
Royal College of Science and Technology P. D. Ritchie
Glasgow J. A. Thomson

References

[1] Pope E. C. *Nature, Lond.* 1953 **171** 913.
[2] Southward A. J. *Ibid.* 1953 **172** 1059.
[3] Stuke B. *Naturwissenschaften* 1952 **39** 325.
[4] Benfratello G. *Energia elett.* 1953 **30** 80, 486.

Some considerations on heat transfer in spiral plate heat exchangers

(*Received* 17 *May* 1957)

Introduction

The spiral plate heat exchanger is finding many applications today. Thus far no data has been made available, within the limits of our knowledge, from which heat transfer coefficients may be calculated. Those determined on the basis of equations for rectangular ducts [1] show variations of the order of 30 per cent, and indicate the need for a specific study of this type of heat exchanger. A brief opportunity was afforded to the authors of studying a Rosenblad Spiral Plate Exchanger, installed at Glenochil Research Station, by the courtesy of the Distillers Company.* Facilities were restricted to the use of water for both channels.

Equipment

The heat exchanger was in the form of a disc approximately 5 ft in diameter by 1 ft thick, made up from two 104ft long stainless steel ducts wrapped round a central header in the form of a spiral. The dimensions and the general form are shown in Figs. 1 and 2. The sides of the disc were enclosed by heavy steel doors fitted with gaskets which isolated the spirals. A hot water stream passed in at the centre and travelled outwards through one of the ducts, leaving at the periphery. Cooling water flowed countercurrent in the adjacent duct, leaving by another central header. Provision was made for recording inlet and outlet temperatures to within ± 0·5°F and for measuring flow rates to ± 1 per cent.

* Distillers Company Ltd., Glenochil Research Station, Menstrie, Clackmannan, Scotland.

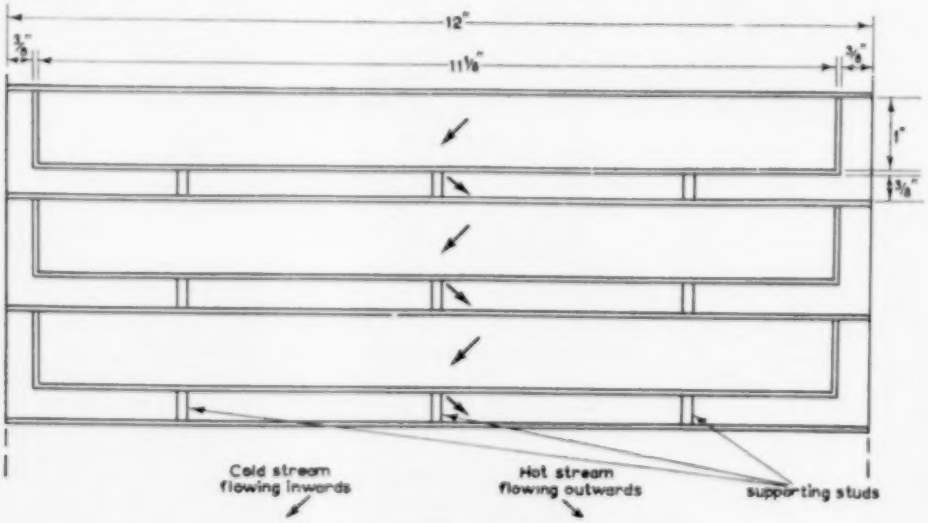

Fig. 1. Section of typical ducts.

VOL.
7
957/58

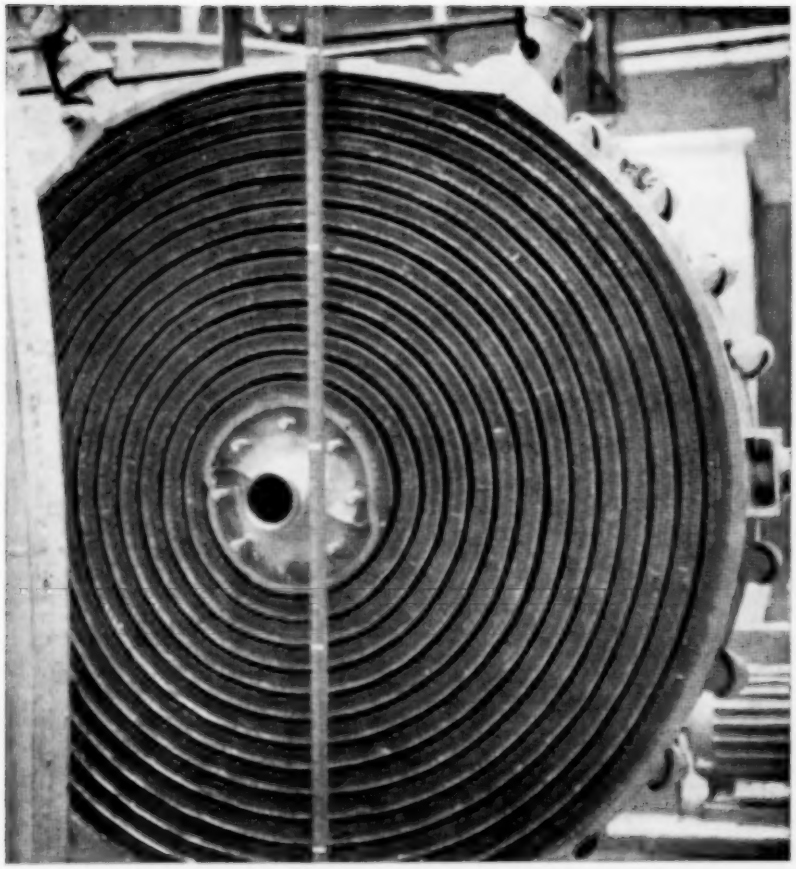

FIG. 2.

VO
7
1957

VOL. 7 957/58

Discussion

Considering only counter-current flow, any element of the cooling duct will receive heat first from its inner heat transfer surface, A_u ($A - B - C - D$ of Fig. 1) under a certain temperature difference ΔT_u from the adjacent element of hot fluid. This element of hot fluid will in due course pass through one revolution outwards and again be in a position to transfer heat to the same element of cooling duct, this time on its outer surface A_p ($A - D$, Fig. 1). Since it has lost a certain amount of heat, the second transfer is under a lower temperature drop, ΔT_p.

It will not therefore be desirable to assess heat transfer on the basis of the entire area available, and the apparent Log Mean Temperature Difference from end conditions, as given by $Q = U_a A \Delta T_M$ (1)

If it is assumed that individual heat transfer coefficients are functions of the Reynolds and Prandtl Numbers, which may be assumed to remain constant in the course of one revolution of the spiral, then the overall heat transfer coefficients over A_u and A_p may be taken as the same. Then

$$Q = U(A_u \Delta T_u + A_p \Delta T_p) \quad (2)$$

In any given exchanger A_u and A_p are constant, and $A_p = K'' A_u$. Since U is constant, likewise $\Delta T_p = K' \Delta T_u$ where $K' < 1{\cdot}0$. Hence

$$A_p \Delta T_p = K' K'' A_u \Delta T_u = K \cdot \Delta T_u \cdot A_u \quad (3)$$

whence

$$Q = U A_u (1 + K) \Delta T_u \quad (4)$$

Since K must vary with A_p/A_u and with the radius and number of the spirals, it cannot be expected that the Dittus-Boelter [2] or Colburn [3] equations will fit the data obtained.

Evaluation of K'. Consider Fig. 3 in which is represented the temperature variation with length of spiral for the heating and the cooling streams. A definite assumption has been made that temperature change is approximately linear with spiral length throughout.

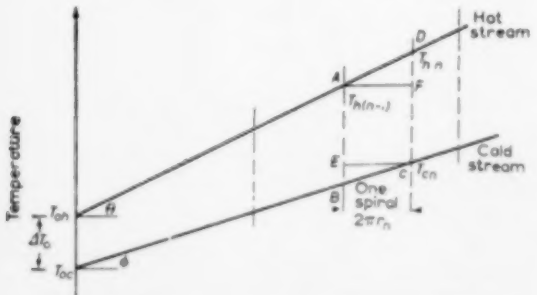

Fig. 3.

Cold fluid at C (nth spiral) receives heat from the hot fluid at D under ΔT represented by D–C, an instantaneous value of ΔT_u, and at A ($n - 1$ spiral) under ΔT of A–E ($= F - C$) an instantaneous value of ΔT_p.

Now the length of the spiral up to any radius r_n is given by

$$L_n = \frac{\pi (r_2^2 - r_n^2)}{t} \quad (5)$$

where t is the increment in radius per lap, r_2 the radius of the outermost spiral, and r_n the n^{th} spiral from the outside. The length of duct between the n^{th} and the $n - 1^{\text{th}}$ spiral approximates to $2\pi r_n$.

Then

$$K' = \frac{\Delta T_p}{\Delta T_u} = \frac{FC}{DC} = \frac{T_{h,n-1} - T_{c,n}}{T_{h,n} - T_{c,n}}$$

$$= \frac{[T_{h,0} + L. \tan\theta - 2\pi r_n \tan\theta] - [T_{c,0} + L. \tan\phi]}{[T_{h,0} + L. \tan\theta] - [T_{c,0} + L. \tan\phi]}$$

$$= \frac{(T_{h,0} - T_{c,0}) + L(\tan\theta - \tan\phi) - 2\pi r_n \tan\theta}{(T_{h,0} - T_{c,0}) + L(\tan\theta - \tan\phi)}$$

But $T_{h,0} - T_{c,0} = \Delta T_0$, the temperature difference between two streams at the spiral periphery.

$$\therefore K' = 1 - \frac{2\pi r_n \tan\theta}{\Delta T_0 + L(\tan\theta - \tan\phi)}$$

$$= 1 - \frac{2\pi r_n}{\dfrac{\Delta T_0}{\tan\theta} + L\left(1 - \dfrac{\tan\phi}{\tan\theta}\right)}$$

Now $\dfrac{\tan\phi}{\tan\theta}$ is determined by the relative heat masses of the two streams. If these be $F_c c_{sc}$ and $F_h c_{sh}$ respectively,

$$\frac{dT_h}{dT_c} = \frac{F_c C_{s.c}}{F_h C_{s.h}} = \frac{dT_h/dL}{dT_c/dL} = \frac{\tan\theta}{\tan\phi} = \frac{\Delta T_h}{\Delta T_c}$$

Then $K' =$

$$1 - \frac{2\pi r_n}{\dfrac{\Delta T_0}{\Delta T_h} \cdot L + L\left(1 - \dfrac{\Delta T_c}{\Delta T_h}\right)} \text{ since } \tan\theta = \frac{\Delta T_h}{L}$$

$$= 1 - \frac{2\pi r_n \Delta T_h}{L(\Delta T_0 + \Delta T_h - \Delta T_c)} \quad (6)$$

It will be appreciated that K' must vary across the spiral of the exchanger. In the correlation r_n has been taken as the radius at the mean spiral length $L/2$ and from this

$$r_n = \sqrt{(r_2^2 - L.\, t/2\pi)} \quad (7)$$

For the exchanger used in this work $r^n = 1{\cdot}63$ft, while r_2 was 2·16 ft, and r_1 was 0·76 ft. For a typical case this gave a value of K' of 0·963 at the core and 0·83 at the periphery, with a mean value (from equation 7) of 0·870.

Evaluation of K''. K'' is the ratio of the inner and outer surfaces of the cooling water duct at the mean wall thickness. Were this to be of simple spiral ribbon rectangular section, then for any one turn of radius r and increment t the ratio would be $(r + t)/r$. In the actual unit, as seen from Fig. 1, the ratio is more complex; the actual value of r is not so directly concerned and the form of the channel gives a fixed value for K'' of 0·835. The total area A was 202 ft^2 while A_u was 115·5 ft^2.

Evaluation of heat transfer coefficient. The value of K in equation (3) can be derived from values of K' and K''. For any test, the value of the total heat flow Q can be calculated from the mass flow and temperature change of either the heating or the cooling streams. In passing, it may be noted that a heat balance over the two streams always checked to within 5 per cent of the total heat flow. The mean value of ΔT_u is clearly (Fig. 3) the Log. Mean Value from end to end of the exchanger, i.e. $\Delta T_u = \Delta T_m$. The area A_u is the area of the inner surface of the duct ($A - B - C - D$) in Fig. 1. Then for any one experiment, the value of U may be derived from equation (4).

Now U is made up from three individual coefficients, as in

$$\frac{1}{U} = \frac{1}{h_{f.h}} + \frac{1}{h_{fc}} + \frac{1}{h_{\text{wall}}}$$

The film coefficients will be determined by some form of standard dimensional equation. This implies variation with the Reynolds and Prandtl Numbers of the fluid streams. If the Prandtl number variation is small compared to the Reynolds Number variation, it may be stated that for any one film coefficient, h_f varies as R_e^a and the combined film resistance $R\left(= \frac{1}{h_{f.h}} + \frac{1}{h_{f.c}}\right)$ varies as $\left(\frac{1}{R_{e.h}^a} + \frac{1}{R_{e.c}^a}\right)$. Now if the combined film resistance results (derived from U by correction for wall effects) are plotted on a graph with the Reynolds Numbers of the heating and cooling streams as the $X - Y$ axes, it is possible to join together a series of experimental points to show lines of equal film resistance, as in Fig. 4. In this chart, which forms a graphical summary of all the experimental data, individual points are reciprocals of the combined film resistances, i.e. values for the overall heat transfer coefficient corrected for metal wall effects. The dotted lines show estimated positions for constant film resistance values with varying Reynolds Numbers in the two streams. On an $X = Y$ line in the diagram of Fig. 4, the Reynolds Numbers of the two streams will be equal, and $R_{e.h} = R_{e.c}$

$$\text{and } a = \frac{\log_e R_1 - \log_e R_2}{\log_e Re_1 - \log_e Re_2}$$

where 1 and 2 are selected points in Fig. 5.

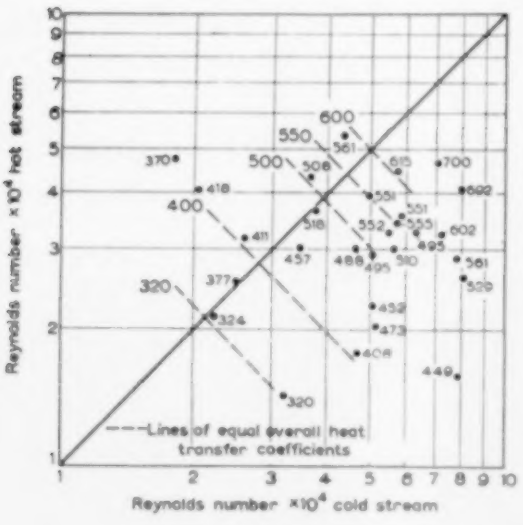

Fig. 4.

Experimental Results

In a series of experimental runs, the Reynolds Numbers for either stream were varied from 9000 to 78000. Fig. 4, though comprised of scattered data, was capable of fairly precise interpretation, and independent interpolation by three observers gave the same result when expressed in the form of Fig. 5. The value of a shown by this is 0·75.

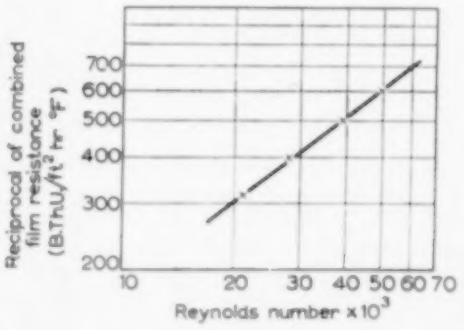

Fig. 5.

The Prandtl Numbers of the fluid streams varied from 4 to 10, and since the exponent could not be accurately assessed, it was held to be the same as in the Dittus Boelter relation. This suggests a final expression for the various film coefficients of

$$\frac{h_f \cdot d}{k} = C\,(R_e)^{0.75}\,P_r^{0.3} \text{ (or } P_r^{0.4} \text{ for stream losing heat.)}$$

The constant C remains to be determined. Insertion of experimental values into the equation $Q = U \cdot A_u\,(1 + K)\,\Delta T_u$ suggested a mean value of 0·055 giving the final expression for film coefficients in the exchanger as

$$\frac{h_f d}{k} = 0{\cdot}033\ R_e^{0{\cdot}75}\ Pr^{0{\cdot}3}\ (P^{0{\cdot}4}) \qquad (8)$$

Now the apparent value of the overall coefficient U_a is based on the relation $Q = U_a \cdot A \cdot \Delta T_m$ (1)

For any single experiment

$$U_a \cdot A \cdot \Delta T_m = U \cdot A_u (1 + K)\ \Delta T_u$$

or, as $\Delta T_m = \Delta T_u$, $U_a = U \cdot \dfrac{A}{A_u (1 + K)}$ (9)

Values for U can be calculated from the film coefficients (8), with correction for the metal wall, and used to give values for U_a by substitution in equation (9). These have been plotted against the values for U_a as derived from equation (1), and are set out in Figure (6). As will be seen, except for certain abnormal results, the spread of points is small, and the mean deviation for all figures is 8 per cent.

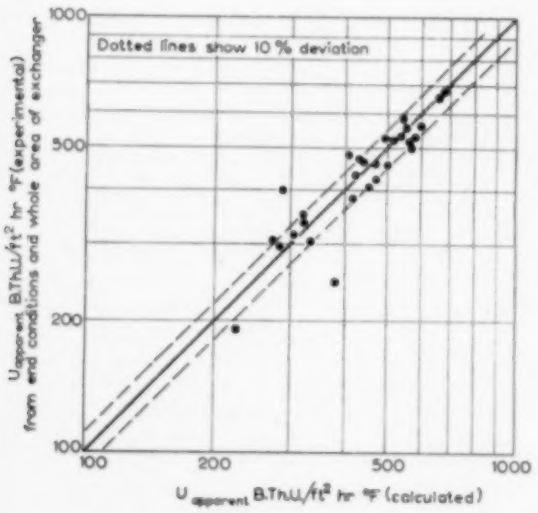
Dotted lines show 10 % deviation
U apparent B.Th.U./ft² hr °F (experimental) from end conditions and whole area of exchanger
U apparent B.Th.U./ft² hr °F (calculated)
100
200
500
1000

Fig. 6.

Conclusions

A correlation based upon dimensional equations for film coefficients has been derived which fits the experimental data with a mean deviation of 8 per cent. This is regarded as being close enough to justify the two major assumptions made, namely that the temperature change through the length of the spiral is linear, and that the mean spiral radius can be taken as the radius at mean length of the spiral.

The correlation takes into account variations in spiral diameter and number of turns, and the modifying effects of two heat transfer surfaces working at different temperature differences. It has not yet been possible to check the validity of the expression for spirals of different size or configuration.

M. H. I. Baird
W. McCrae
F. Rumford
C. G. M. Slesser

Nomenclature

θ, ϕ = slope of hot and cold fluid streams, Fig. 3
ΔT = temperature difference – (°F)
A = Area – ft²
c_s = specific heat – B.T.U./lb.
D = equivalent diameter of duct – $\left(\dfrac{4 \times \text{cross-sectional area}}{\text{wetted perimeter}}\right)$
F = mass flow—lb/hr
h_f = film heat transfer coefficient – B.T.U./ft² °F. hr.
k = thermal conductivity – B.T.U./ft. hr.°F.
C, K, K', K'' = constants
L_n, L = length of spiral at n^{th} revolution; total length of spiral – ft.
Pr = Prandtl number
Q = heat transferred – B.T.U./hr
R = combined film resistance
Re = Reynolds number
r_1, r_2 = inner and outer radii of spiral – ft
r_n = radius of spiral at n^{th} revolution – ft
t = increment in radius between spirals – ft
U = Overall heat transfer coefficient – B.T.U./ft² hr °F

Subscripts

u = inner heat transfer surface
p = outer heat transfer surface
(for areas)
c, h = hot and cold streams (for temperature)
0 = temperature conditions at periphery

References

[1] Perry J. H. *Chemical Engineers Handbook* (3rd Ed.) 1930 p. 470.
[2] Dittus F. W. and Boelters *University of California, Publications in Engineering* 1930 **2** 443.
[3] Colburn A. P. *Trans. Amer. Inst. Chem. Engrs.* 1933 **29** 174.

VOL. 7 957/58

Measurement of Molecular homogeneity in a mixture

(*Received* 14 *June* 1957)

I HAVE suggested elsewhere [1] how the degree of mixing of two fluids on the molecular scale (or its converse, the degree of segregation) could be determined by observing the rate of a second-order reaction in the mixture. This method gives essentially the mean square concentration of component A in a non-homogeneous mixture of A and B.

The method to be described here appears to be more powerful, in that it will give the actual distribution of deviations from the mean concentration in the mixture. It is also experimentally simpler.

The mixture consists of two aqueous solutions, A and B. A contains m molal NaOH, while B contains mx molal HCl. In any portion of the mixture in which A and B are mixed on the molecular scale in proportions a, $(1 - a)$ the local composition will be

alkaline if $a > x(1 - a)$, or $a > \dfrac{x}{1 + x}$;

acid if $a < x(1 - a)$, or $a < \dfrac{x}{1 + x}$.

Phenolphthalein or some other suitable indicator is added to one or the other or both of the solutions. Thus three cases may be considered:

(1) *Phenolphthalein in concentration n added to solution A.* The solution will be red in the alkaline regions; in an alkaline region in which the proportion of A is a, the concentration of phenophthalein in the red form will be na. Thus if the fraction of the volume of the mixture in which the porportion of A lies between a and $(a + da)$ is $f(a)\,da$, the average concentration of phenolphthalein in the red form will be

$$n_R = n \int_{x/1+x}^{1} a f(a)\, da \tag{1}$$

$$\therefore \frac{1}{n}\frac{dn_R}{dx} = -\frac{x}{1+x} \cdot f\left(\frac{x}{1+x}\right) \cdot \frac{d}{dx}\left(\frac{x}{1+x}\right). \tag{2}$$

$$\therefore \frac{(1+x)^3}{nx}\frac{dn_R}{dx} = -f\left(\frac{x}{1+x}\right). \tag{3}$$

Thus by varying x, the ratio of the strengths of the two solutions, and measuring the corresponding colour-density of the mixture, it is possible in principle to determine the fraction of the volume of the mixture which contains A and B mixed on the molecular scale in any given proportion. In a mixture with a high intensity of segregation, consisting mostly of undiluted A and B, $f(a)$ will have high values at $a = 0$ and $a = 1$, and will be low at intermediate values of a. When the segregation is small and mixing on the molecular scale nearly complete, $f(a)$ will be small at $a = 0$ and $a = 1$, and will pass through a maximum at a value of a corresponding to the volume fraction of A in the mixture as a whole. The "intensity of segregation" as previously defined [1] can be calculated if $f(a)$ is known.

(2) *Phenolphthalein in concentration n added to solution B.* By a similar argument,

$$n_R = n \int_{x/1+x}^{1} (1 - a) \cdot f(a) \cdot da, \tag{4}$$

and

$$\frac{(1+x)^3}{n}\frac{dn_R}{dx} = -f\left(\frac{x}{1+x}\right). \tag{5}$$

In this case also (a) can be determined by varying x. However, the colour is developed only in the regions in which molecular mixing has taken place, so that it may be easier to make the requisite colour measurements with sufficient accuracy in case (b) than in case (a). Case (b) will also provide a better visual demonstration of the progress of molecular mixing, particularly when $x = 0$ – that is, when B contains phenophthalein but no acid – since the whole region of molecular intermixing will then be coloured.

(3) *Both solutions contain phenophthalein in concentration n.* Then

$$n_R = n \int_{x/1+x}^{1} f(a) \cdot da, \tag{6}$$

and

$$\frac{(1+x)^2}{n}\frac{dn_R}{dx} = -f\left(\frac{x}{1+x}\right). \tag{7}$$

In this case there is a sharp boundary separating regions in which $a > \dfrac{x}{1+x}$ and the concentration of red phenolphthalein is uniformly equal to n, from regions in which $a < \dfrac{x}{1+x}$ and the solution is colourless. The arrangement is thus particularly suitable for the study of macroscopic mixing processes, since it emphasises the outlines of the blobs and streaks of the components in an inhomogeneous mixture.

It is interesting to consider the application of the various versions of the method to a specific case, such as the mixing of a central jet into a coaxial stream in a pipe. In case (a), if solution A were the central stream, it would form a solid red jet which, for a given flow-ratio, would either dwindle and vanish downstream or spread to fill the whole tube, depending on the value of x. If solution B were the central stream, red and white would be reversed. In case (b) the central jet would be colourless and surrounded by a red shell, which would either vanish or fill the whole tube downstream, depending on the value of x. Case (c) will be similar to case (a), except that the

boundary of the central jet will be more sharply defined; if conditions are such that the central jet disappears downstream, it will offer a close analogy to a flame. In all cases the time-average concentration of colour at any point can be determined by taking a time-exposure photograph of the system. The mathematical problem of determining the radial concentration distribution from such a photograph will be discussed elsewhere.

There are three assumptions involved in the arguments leading to equations (3), (5) and (7) which are probably justified in many circumstances, although they must be borne in mind. These are that the full colour-change of phenolphthalein occurs over a very small increment of a; that acid, alkali, phenolphthalein and water can be regarded as being affected to the same degree by processes leading to molecular mixing; and that the colour-change of phenophthalein can be regarded as an instantaneous reaction.

P. V. Danckwerts

Reference

[1] Danckwerts P. V. The effect of incomplete mixing on homogeneous reactions. Paper presented at the first European Symposium on chemical engineering, *Chemical Reaction Engineering*. Amsterdam, May, 1957.

VOL.
7
957/58

Book reviews

J. M. Smith: **Chemical Engineering Kinetics.** McGraw-Hill, 1956. ix + 402 pp. 60s.

In the preface to his new book, Prof. Smith remarks that progress in methods of design has been much slower for the operations which involve chemical reactions than for the purely physical processes. What is to be hoped for is to "bring reactor design closer to the stage of development achieved in the unit operations." The book has been written at a level suitable for the degree student in his final year, but it will clearly be of help to a much broader group of readers and will be a valuable addition to any chemical engineering library.

The first three chapters present a general introduction to the field of study, and a review of thermodynamics and chemical kinetics. The thermodynamics review is too short to be of real value and is best regarded as a summary of the equations relevant to chemical equilibria. (There is a misprint in the important equation 2.44, where the first term on the R.H.S. should contain the gas constant).

The substance of the book commences at Chapter IV where the author gives a preliminary account of the design theory for batch processes, and for tubular reactors and continuously stirred tank reactors, as applied to homogeneous reactions. The theory is elaborated in the two following chapters and there are numerous examples relating to isothermal and non-isothermal conditions. For tubular reactors the plug-flow assumption is used throughout the book and there is hardly any discussion of the range of its validity. With regard to continuouly stirred tank reactors, the point is not made as clearly as it might be that these reactors operate at lower mean concentrations than batch or tubular reactors, and it is for this reason that it is normal to operate with two or more of them in series. A quantitative comparison of the reaction volume required for one, two, etc., such tanks in series, and with the volume required for a tubular reactor, would have been of value. There is also insufficient discussion on the relative merits of the various types of process – batch, tubular and C.S.T.R. – in cases where there are side reactions or degradation reactions. An important factor in the choice of the process is that it should suit the kinetic conditions of the particular reaction.

Semi-batch reactions and the transients of the C.S.T.R. are briefly discussed in Chapter VII. This is followed by a survey over the field of catalysis and adsorption, and a discussion on the rate-limiting factors in catalytic reactions, including diffusion up to the surface of the catalyst and diffusion within its interior.

Chapter X is concerned with heat and mass transfer in reactors and includes a discussion on the effective thermal conductivity and diffusivity of packed beds. This is a necessary preliminary to the final chapter which is on the design of gas-solid catalytic reactors. The first design method which is described here is the relatively simple one in which the whole of the temperature difference is assumed to be located at the wall of the reactor. The author then proceeds to the more elaborate methods which allow for the variation of temperature and concentration in the radial, as well as in the longitudinal, direction. The book concludes with a brief treatment of fluidized bed reactors, and two appendices.

A serious omission is the absence of any discussion of optimum temperature sequences, so important in ammonia synthesis and several other industrial reactions. The study of residence-time distributions is also not included. These omissions may be due to the fact that the author has based his work mainly on American references; British, Continental and Russian work is poorly represented.

The book is clearly written and is packed with an immense amount of useful data, much of it in the form of worked examples. There are also a considerable number of problems for the student to solve for himself.

K. G. Denbigh.

W. H. Corcoran, J. B. Opfell and B. H. Sage: **Momentum Transfer in Fluids.** Academic Press Inc., New York, 1956. pp. 394, $9.00 or 72s.

According to the preface, the purpose of this book, which consists of seven chapters and four appendices, is to describe a portion of fluid mechanics of special interest to chemical engineers; in particular viscous flow, boundary-layer theory and turbulence. A large number of topics are discussed incorporating both the older analyses and the more modern theories, the result being a useful handbook once the general lay-out has been understood. Unfortunately the chapter titles are not very helpful in this respect, and the chapter sections could possibly have been arranged more systematically. The material is presented on the assumption that the reader is familiar with the calculus and the principles of differential equations. Although tensor methods are not incorporated in the main body of the text, a long Appendix is included in which tensors are briefly described and various useful formulae developed. A number of interesting examples illustrate the theory, and there is a comprehensive list of references at the end of each chapter. The authors have produced a book that should be of interest to applied mathematicians as well as to the advanced engineering student.

The most serious criticism the reviewer has to offer concerns the style of writing adopted by the authors and their thoughtlessness of composition. Grammatical errors

and badly-chosen phrases appear frequently. It is possible that these things are considered to be of little importance in such a book but sentences like "The intensive properties of the fluid will be considered to be independent of state" (p. 11), and "The restriction homogeneous is used so that the equations to be developed are mathematically correct inasmuch as the analyses will be confined to regions where all functions of interest are continuous and differentiable" (p. 114) are surely meaningless to most people. It seems a pity that a book on which a great deal of time and energy has obviously been spent should be marred by such carelessness.

G. POWER

Fortschritte der Verfahrenstechnik, Band 2, 1954/55, (Progress in Process Engineering in 1954/55). Edited by H. MIESSNER and U. GRIGULL, Verlag Chemie, G.m.b.H., Weinheim, 1956. 720 pp. D.M. 53.

VOL. 7 957/58

THIS is the second volume of the series published by the Farben-Fabriken Bayer A. G., Leverkusen, reviewing and summarizing the literature on chemical engineering and process techniques. Compared with the first volume more room is given to chemical engineering principles; new chapters on heat transfer, mass transfer and thermodynamics are added. Of the usual unit operations drying, extraction, gas absorption, adsorption and ion exchange, distillation and rectification, crystallization and many of the mechanical operations, disintegration, classification, flotation, mixing, feeding and liquids solids separation are well treated; the techniques involved in the use of high and low temperatures, high pressures and vacua, electroheat, measurement and control of process variables and the surveys of materials of construction, corrosion and chemical reaction engineering form the contents of the other specialized chapters.

Each of the 30 sections is again written by one or more specialists of reputation in their respective fields.

Extensive bibliographies are added in which the references are listed in order of discussion; a very complete author and subject index makes the references readily accessible.

This second volume is again well written as a whole.

The different sections vary in style and quality, which is quite natural in view of the many co-operators, but nearly all of the sections are very readable, have been written critically and are not simply a collection of abstracts.

This book is a welcome counterpart to the reviews of unit principles, unit operations, unit processes and materials of construction published by *Industrial and Engineering Chemistry* and in some respects more successful.

D. W. VAN KREVELEN.

International News

FRANCE

THE *Annales du Génie Chimique*, sponsored by the Institut du Genie Chimique, University of Toulouse, will shortly commence publication. The *Annales* are intended to make available the results of the work achieved in the Research Department of this institution. This new periodical, published annually will be devoted to original and complete studies of chemical engineering problems.

The first volume, to be published in 1957, analyses a new method for the production of sulphur trioxide entirely designed and developed to the pilot plant stage in the Research Department, in Toulouse.

Futher particulars can be obtained from the Institut du Genie Chimique, 17 rue Sainte-Catherine, Toulouse.

SOME CURRENT PAPERS IN OTHER JOURNALS

Chemical Engineering Progress

O. J. M. Smith : Closer control of loops with dead time 217

T. J. Williams and R. T. Harnett : Automatic control in continuous distillation .. 220

R. Aris and N. R. Amundson : Stability of some chemical systems under control .. 227

I. O. Winsch and L. Burris : Magnesium extraction process separates Pu from uranium 237

R. J. Hengstebeck and D. W. Schubert : Graphical method for calculating multi-component distillation 243

F. G. Hammitt : Considerations for selecting liquid metal pumps 249

E. L. Piret, N. F. Schulz and S. R. B. Cooke : Energy-new surface relationship in crushing of solids 254

EDITORIAL ANNOUNCEMENT

Chemical Engineering Science will, in future, publish two forms of short communications :

1. *Letters to the Editors* which should be concerned with comments on papers previously published and

2. *Preliminary Communications*, giving details about the results of work in progress and which will later be written up at length.

Items under both these headings will be given rapid publication and the delay should normally not exceed 60 days from the time of acceptance.